DEVELOPMENT OF IN SITU NON DESTRUCTIVE ANALYTICAL METHODOLOGIES FOR THE CONSERVATION DIAGNOSIS OF URBAN BUILT HERITAGE

Olivia Gómez Laserna

Julio 2015

eman ta zabal zazu

Universidad del País Vasco

Euskal Herriko Unibertsitatea

Universidad del País Vasco Euskal Herriko Unibertsitatea

Department of Analytical Chemistry

Development of in situ non destructive analytical methodologies for the conservation diagnosis of urban built heritage

Report to compete for the International PhD degree

Olivia Gómez Laserna

July 2015

"If you wish to control the future,

study the past"

Confuncius

INDEX

CHAPTER 1: INTRODUCTION

1.1. Built heritage and its cultural message

Built heritage is one of the most important cultural assets. Its unique and irreplaceable architecture along with its historic background play an indispensable role in the development of our society, as a recognition engine of our own values. It describes our origins and informs our understandings of who we are, defining our sense of place and identity as community.

As evidence of cultural development, it represents the historical layers of our built environment with not just beautiful and impressive buildings but it also includes small constructions that can reflect any social condition. Thus, it can be composed of both old and modern buildings of historic importance such as palaces, houses, churches, castles, and military fortifications as well as, by other areas of heritage value, village squares, harbours or even cemeteries. All of them merit preservation for the future generations since they are the key to understand the past and enrich the daily lives rebuilding our shared history[1-2].

During the last decade, the value of built heritage in relation to the rest of the spheres of the life has completely changed. In addition to its concept as expression of cultural richness and testimony of contribution to the civilization, its social performance has been especially highlighted. Not only its symbolic value is maintained but also, its

1 A. Kadluczka, G. Cristinelli, M. Zádor. Carta de Cracovia 2000: Principios para la conservación y restauración del Patrimonio Construido. Buenos Aires, Argentina: Conferencia Internacional sobre Conservación "Cracovia 2000"; 2000.

2 C. Bákula Budge. Documentos fundamentales para el Patrimonio Cultural. Textos internacionales para su recuperación, repatriación, conservación, protección y difusión. Perú: Instituto Nacional de Cultura; 2007.

value has gained importance acting as link with the past, enhancing our quality of life and strengthening our cultural identity[3].

1.2. Built heritage preservation in its environment as a socio-economic resource

Nowadays, the economic potential of the built heritage preservation is widely recognized due to its status as essential resource for cultural tourism and its revalorization for educational use. Strategies to increase return on equity that just a few years ago were unthinkable, represent for the current society necessary policies to achieve a balanced and sustainable development.

Although from the beginning tourism has been linked to heritage, just recently cultural tourism has been recognized as a distinct sector of leisure tourism. Such is its importance that in the last decade, approximately 37% of global travels had cultural motivations, of which 30 to 50% were historical and heritage visits. Therefore, at present, tourism has become one of the world's largest industries, highlighting the importance of its preservation from a new economic point of view[4].

Unfortunately, the first maintenance works were carried out without any prior diagnostic study and thus, it did not allow organizing suitable methods, tools and media for its assessment. The derived damages from these actions are innumerable and irreversible. For that reason, the consequences of this way of working have been strongly criticized, requiring a more scientific and respectful methodology with the monument. To achieve this, not only must the physical preservation be sought but also, natural and human components of the landscape should be viewed as a vital set to maintain its cultural identity, without impeding development of current needs since, eventually, the most significant elements of this century will form part of the heritage of later generations[5-6].

3 G. Wijesuriya, J. Thompson, C. Young. Gestión del Patrimonio Mundial Cultural: Manual de referencia. París, Francia: Organización de las Naciones Unidas para la Educación, la Ciencia y la Cultura; 2014.

4 A. Azkarate, M. J. Ruiz de Ael, A. Santana. El Patrimonio Arquitectónico. Vitoria, País Vasco: Departamento de Arquitectura y Vivienda del Gobierno Vasco; 2003.

5 L. Rubio Medina, G. Ponce Herrero. Gestión del Patrimonio Arquitectónico, Cultural y Medioambiental. Enfoques y casos prácticos. Alicante, España: Biblioteca Virtual Miguel de Cervantes; 2013.

6 M. A. Troitiño Vinuesa. Territorio, patrimonio y paisaje: desafíos de una ordenación y gestión inteligentes. Ciudad y Territorio - Estudios Territoriales; 2011; 169: 561-569.

1.3. Heritage science field

As the valorization of built heritage is booming, the need to carry out scientific studies has gained special relevance. However, its development is really complex as it requires the involvement of different areas of knowledge such us engineering, chemistry, geology, biology and so on. Besides, the decisions proposed have to be in accordance with the experience of restorers, architects and art historians. Therefore, the research of this field is a great effort made by all the scientific community to preserve efficiently our inheritance.

In this way, the preservation decisions have to be adopted through a multidisciplinary approach (Fig. 1.1), which must take into account several factors such as the selection of compatible materials and its durability, the assessment of the socioeconomic impact and sustainability considerations. Hence, its effective protection demands a wide study in which the structure of the building and the materials, the integrated diagnostic study, and the assessment of the performance of conservation materials, as well as interventions, should be included[7-8].

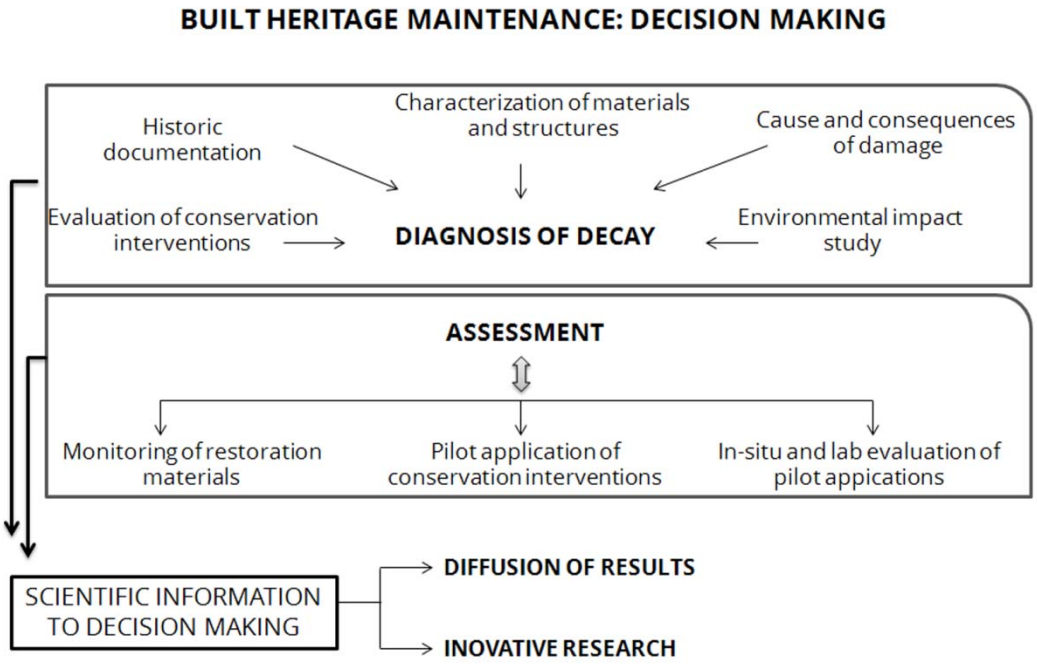

Figure 1.1. Requirements of a correct multidisciplinary approach to make decisions of built heritage conservation.

7 A. Moropoulou, K. C. Labropoulos, E. T. Delegou, M. Karoglou, A. Bakolas. Non-destructive techniques as a tool for the protection of Built Cultural Heritage. Constr. Build. Mater.; 2013; 48: 1222-1239.

8 L. Binda, A. Saisi, C. Tiraboschi. Investigation procedures for the diagnosis of historic masonries. Constr. Build. Mater.; 2000; 14: 199-233.

In order to have all the necessary information, an integrated diagnosis study should include historic documentation, characterization and origin of the materials, evaluation of previous interventions and assessment of the environmental impact. In addition to this, it has to contain a monitoring of the environment factors, studies of conservation state of materials as well as the cause and consequences of the pathologies suffered[9]. For that, the identification of the decay products, mechanism and severity of damage and its correlation with the weathering agents is crucial to take proper conservation decisions.

However, understanding what is causing the deterioration is not an easy task. Sometimes the source of damage is clear but other times several unknown causes can act at the same time, producing a synergic effect difficult to find out. Besides, the process of stone decay can be sudden and fast, gradual or go completely unnoticed (Fig. 1.2), damaging the building irreversibly[10-11].

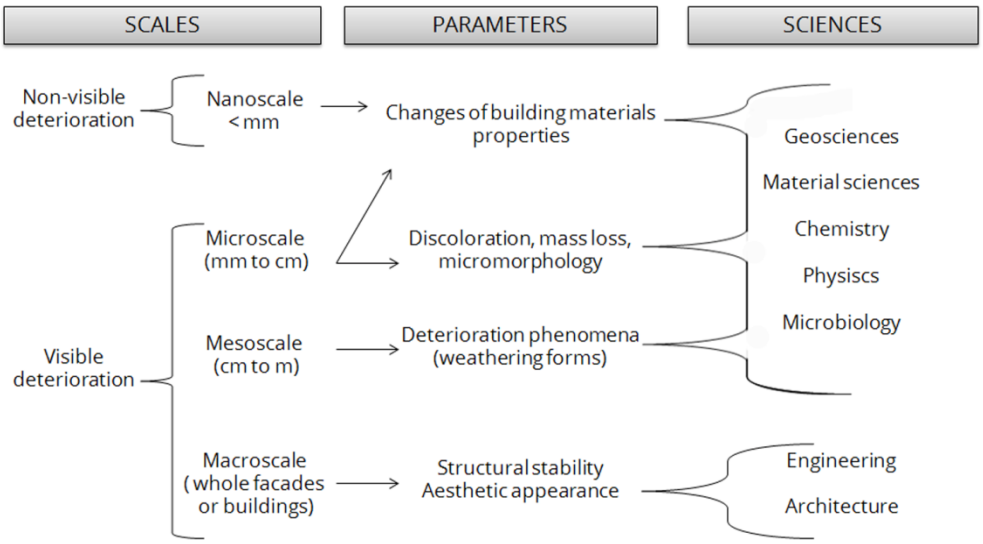

Figure 1.2. Scales and parameters of stone deterioration[12]

9 A. Moropoulou, A. Kioussi, M. Karoglou, A. Bakolas, G. Georgousopoulos, M. Chronopoulos. Innovative protocols for integrated diagnosis on historic materials and structures. Edinburgh, Scotland: Structural Faults & Repair; 2012.

10 E. Doehne, C. Price. Stone conservation, an overview of current research. Los Angeles: The Getty conservation Institute; 2010.

11 H. A. Viles, D. Camuffo, S. Fitz, B. Fitzner, O. Lindquist, R. A. Livingston, P. V. Maravellaki, C. Sabbioni, T. Warscheid. What is the state of our knowledge of the mechanisms of deterioration and how good are our estimates of rates of deterioration: Report of the Dahlem Workshop on "Saving our architectural heritage: the conservation of historic structures". Berlin: John Wiley & Sons; 1997.

12 B. Fitzner. Diagnosis of weathering damage on stone monuments. Conference of weathering damage on stone monuments bacteria, Macla; 2014; 18: 21-27.

Therefore, the following sections attempt to explain the main causes of the stone decay and, how the different damages can be identified and studied.

1.4. Causes of stone decay

Our built heritage is mainly made by stone and thus, it is prone to decay by natural and irreversible processes. Moreover, materials are also exposed to an anthropogenic environment, in which there are many factors that can accelerate its deterioration rate. Due to this fact, before proposing any solutions to its maintenance, preservation or revitalization, the study of building materials requires a wide knowledge of several intrinsic and extrinsic factors[13] that have a strong influence in their decay (Fig. 1.3).

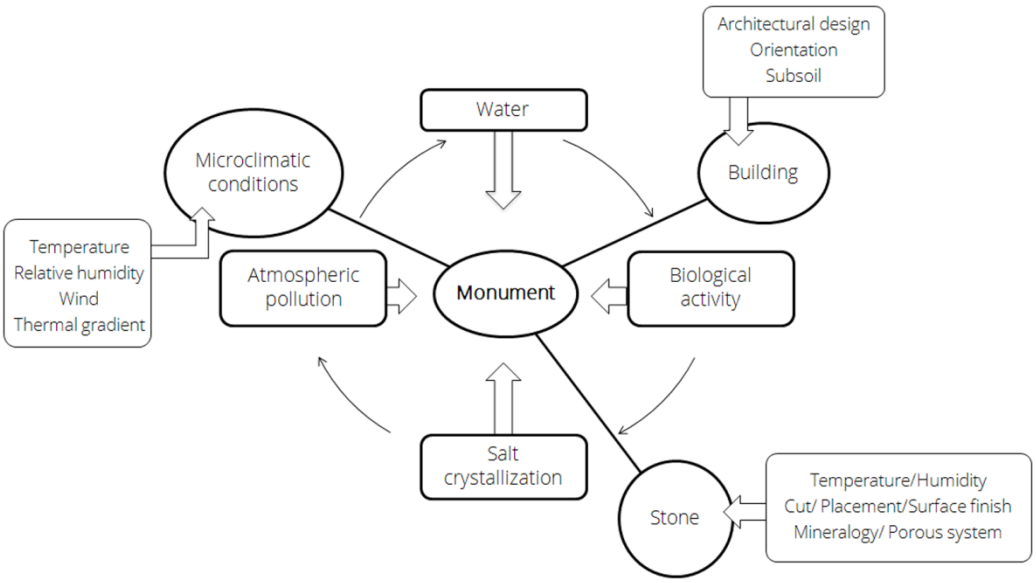

Figure 1.3. Scheme of the main factors related to the maintenance, preservation and revitalizations of built heritage.

1.4.1. Intrinsic and extrinsic factors

Decay can be defined as degradation of material properties and characteristic suffered over time, considering any change of the materials that differ from their

13 S. Siegesmund, T. S. Weiss, A. Vollbrecht. Natural Stones, Weathering Phenomena, Conservation Strategies and Case Studies. London: Geological Society of London Special Publication; 2002.

original design[14]. Thereupon, the analysis of the main influencing factors is necessary to carry out a correct assessment of the current conservation state.

In this way, the extrinsic factors largely determine the transformations undergone by the materials that constitute the building. However, the structure itself and the materials that make up the intrinsic factors define the natural aging and, its evaluation is considered an indirect estimator of the material quality. Aspects such as the chemical and mineralogical composition, petrographic features (texture, pore system), physical and mechanical properties or, even, its history (prior conservation interventions or quarry of provenance) and compatibility help to define the material alterability.

This information is essential to understand the action of decay factors under a real environment conditions, it allows identifying specific vulnerabilities to each material[15] as for instance, the behavior against acid gases or the resistance to medium. Furthermore, its characterization is also very important for restorers and conservators to design replacement strategies of reparation[16].

The factors that have a greater variability in its distribution are of extrinsic type. According to the ASTM E632-72 standard[17], this group includes different agents; environment (climate characteristics, type of atmosphere, the action of water, etc), use or structure, biology, tension and incompatibility.

Due to their variability and important influence on construction materials, the main factors are detailed in the following sections.

1.4.1.1. The environmental factor

This factor is used to evaluate the isolated or combined effects of variables such as temperature, the different states of water or the components of air and wind. In this way, it can be classified into natural and anthropogenic sources, highlighting in the later the atmospheric pollution derived from fossil fuels and the mechanical and acoustic vibrations[17].

14 A. Moropoulou, K. C. Labropoulos, E. T. Delegou, M. Karoglou, A. Bakolas. Non-destructive techniques as a tool for the protection of Built Cultural Heritage. Constr. Build. Mater.; 2013; 48: 1222-1239.

15 N. Cueto, D. Benavente, J. Martínez-Martínez, M. A. García-del-Cura. Rock fabric, pore geometry and mineralogy effects on wáter transport in fractured dolostones. Eng. Geol.; 2009; 107: 1-15.

16 C. Hammecker. The importance of the petrophysical properties and external factors in stone decay on monuments. Pure Appl. Geophys.; 1995; 145: 337-361.

17 American Society for Testing and Materials. Annual Book of ASTM STANDARDS. Conshohocken, PA; ASTM International; 1998.

One of the main stressors included in this group is **water**. It can reach the surface of the material in different ways, either by penetration or capillary action. In the first case, the entrance of water can produce a beneficial effect, washing the surface or in contrast, can cause several damages such us corrosion, loss of material and/or salt formations. In the second case, the input of water through ascendant humidity from the underground could reach different heights depending on the porosity of the material, the evaporation rate and the critical water content of the soil, producing similar damages.

Once the water, enriched in dissolved gases or salts, is inside the material, its migration through the capillary network can dissolve and transport large amounts of pollutants and salts, that can be distributed and deposited anywhere in the material.

The surface of materials is the area in contact with the atmosphere and, thus, it is where the adsorbance phenomena and desorption of matter occur and the physic-chemical properties have their maximum gradients[18]. In this way, when the humidity inside the material is not in equilibrium with the relative humidity of the environment, different surface phenomena (evaporation or condensation) occur by temperature and humidity fluctuations. As a consequence, the solution in the porous networks can reach the saturation and begin to crystallize. Then, the changes of temperature and humidity can cause the dissolution of the salt formed and the cycle can be repeated many times, producing severe damages[19] by several processes, as it will be explained in section 1.4.3.

Therefore, the water provides the medium of action to other physical and chemical processes (dissolution, hydrolysis, oxidation, freezing, biodeterioration, etc) and, in a greater or lesser extent, it is related to most indicators of stone deterioration.

Another factor related to the penetration of rain, evaporation and the formation and transport of salts is the **wind**, which is a characteristic indicator of material loss, especially in drying periods[20].

In addition to the air speed, another important point is its composition. The air naturally contains carbon dioxide (CO_2). This greenhouse gas is by far the most abundant of all atmospheric gases since it is also generated by human activities. It is

18 V. Rives, J. García-Talegon. Decay and conservation of buildings stones on cultural heritage monuments. Mater. Sci. Forum; 2006; 514: 1689-1694.

19 M. Kowacz, A. Putnis. The effect of specific background electrolytes on water structure and solute hydration: consequences for dissolution and growth. Geochim. Cosmochim. AC. ; 2008; 72: 4476-4487.

20 E. Doehne, C. Price. Stone conservation, an overview of current research. Los Angeles: The Getty conservation Institute; 2010.

considered responsible of carbonation processes and active participant in the solubilization of the stones.

Nevertheless, more reactive atmospheric pollutants of anthropic origin can be found in the atmosphere. They are mostly gases (SO_x, NO_x, NH_3), aerosols (acids, salts, metals) and particulate matter (coal) coming mainly from stationary and mobile sources of combustion. Moreover, there are secondary pollutants, generated by reactions between the primary ones, which have to be taken into account. Some examples are sulfuric and nitric acids, aldehydes, peroxides or ozone that can attack the building material by dry (direct transfer) and wet (dissolved in rain) deposition, affecting its integrity[21].

The sulfur dioxide can be considered the main gaseous pollutant species involving different degradation processes[22]. The coal particles, produced by most of the different types of combustion, can catalyze the oxidation of sulfur dioxide to sulfur trioxide, which in water becomes sulfuric acid (reactions 1.1 and 1.2). This acid erodes the original stone and cause important loss of material by dissolution of original compounds and/or by formation of new degradation compounds.

$$SO_2 + \frac{1}{2}O_2 \rightarrow SO_3 \qquad (1.1)$$

$$SO_3 + H_2O \rightarrow H_2SO_4 \qquad (1.2)$$

On the other hand, nitrogen oxides (NO_x) are typical of an urban atmosphere, characterized by an intense motorized traffic and industrial areas. In the presence of UV light, it can react with oxygen and the organic molecules present in the polluted atmosphere forming nitric acid (reactions 1.3 and 1.4). This new compound is considered a very hazardous substance since it is able to exercise, in a higher or lower measure, a corrosive action on carbonated or silicate materials[23], among many others.

$$O_2 + 2NO \rightarrow 2NO_2 \qquad (1.3)$$

$$3NO_2 + H_2O \rightarrow 2HNO_3 + NO \qquad (1.4)$$

21 G.C. Allen, K.R. Hallam, D. McLaughlin, M. Stacey. Role of NO_2 and SO_2 in degradation of limestone. Brit. Corros. J. ; 2000; 35: 35-38.

22 Siegesmund, T. S. Weiss, A. Vollbrecht. Natural Stones, Weathering Phenomena, Conservation Strategies and Case Studies. London: Geological Society of London Special Publication; 2002.

23 L. G. Johansson, O. Linqvist, R. E. Mangio. Corrosion of calcareous stones in humid air containing SO_2 and NO_2. Dur. Build. Mater.; 1988; 5: 439-449.

In addition to those, the marine aerosol is considered a natural pollutant, which can accelerate the degradation of materials. Urban settlements in proximity to a coastline can be affected by the combined effects of marine aerosols and pollutants of anthropogenic origin[24]. In fact, in the presence of sea fog, the formation of sulphuric acid is accelerated more than 10 times[25]. Besides, it can cause an accumulation of hygroscopic salts with very destructive consequence for building materials[26].

Finally, others exceptional environmental factors to be highlighted are floods, waves, volcanoes, demolition, fires and vibrations caused by construction, road and air traffic, which are generally precursors of alterations[27].

1.4.1.2. Biological factor

The plants and the microbial action of bacteria, fungi and lichens can also cause deterioration of stone, being this usually related to climatic conditions, air pollutants and physical and chemical properties of materials. Their biological actions can cause physical alteration such as pore size enlargement, cracking or changes in water circulation and, also, changes in the chemical composition of the material, leading to weakening of them[28] by, for example, segregation of acids and biominerals, penetration of hyphae, etc (Fig. 1.4).

Although the inorganic composition of the stones is not the most suitable medium for the growth of these organisms, environments with light, warm temperature and water combined with rich nutrients of organic residues deposited on stone surface can create perfect conditions for their life[29].

24 M. Pósfai, A. Molnár. Aerosol particles in the troposphere: a mineralogical introduction. Hungary: Environmental Mineralogy, EMU notes in Mineralogy; 2000.

25 I. Grgi'c, J. Tursic, B. Podkrajsek. Influence of ionic strength on aqueous oxidation of SO_2 catalyzed by manganese. Atmos. Environ.; 2003; 37: 2589-2595.

26 S. Syed. Atmospheric corrosion of materials. EJER; 2006; 11: 1-24.

27 American Society for Testing and Materials. Annual Book of ASTM STANDARDS. Conshohocken, PA; ASTM International; 1998.

28 D. Mottershead, A. Gorbushina, G. Lucas, J. Wright. The influence of marine salts, aspect and microbes in the weathering of sandstone in two historic structures. Built. Environ.; 2003; 38: 1193-1204.

29 T. H. Warscheid, J. Braams. Biodeterioration of stone: a review. Int. Biodeter. Biodegr.; 2000; 46: 343-368.

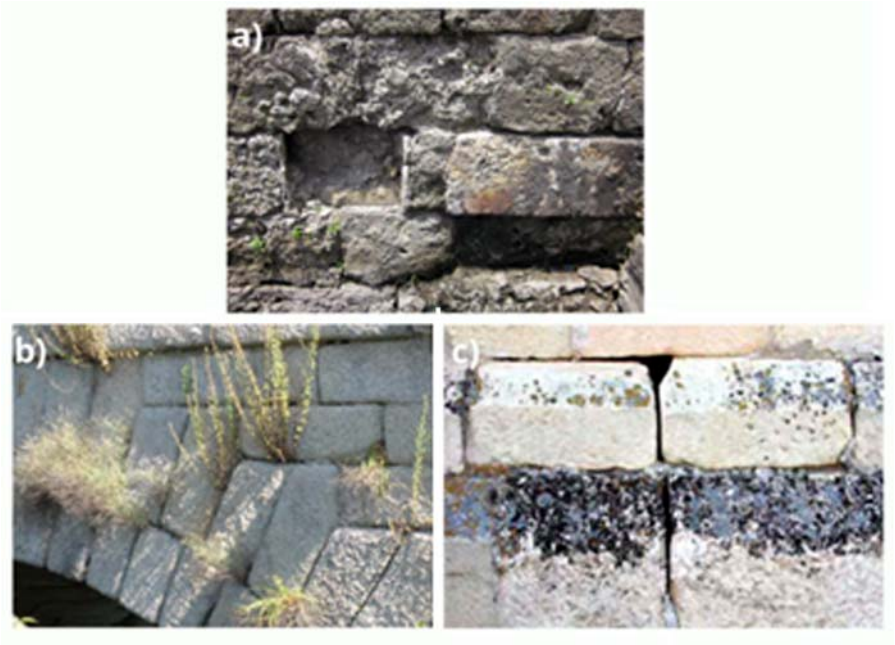

Figure 1.4. a) Blackening and material loss caused by the action of a colony of bacteria and fungi. b) Rooting higher plants in the masonry joints. c) Deterioration caused by an endolithic colonization of lichens to fill the cavities and fissures in the stone.

Therefore, only the interdisciplinary diagnosis and evaluation of the entire decay process of stone allows establishing adequate conservation strategies.

1.4.1.3. The use and structure factors

The use and structure factor encompasses the consequences derived from the executed project (Table 1.1), being some of the most highlighted ones the geographical location, design or use. However, the most determinant variable is the lack of maintenance of buildings. The abandoned buildings led to the deterioration or even the dilapidation of their structures[30].

30 American Society for Testing and Materials. Annual Book of ASTM STANDARDS. Conshohocken, PA; ASTM International; 1998.

Table 1.1. The most common structural disorders and their damage in buildings[31].

Pathological process	Damage
Settlement failure and variations of stratum support	Inclined cracks Shedding its lining and the supporting wall
Deterioration of the basement by attack of pests, plants, accidents…	Grooves and hollows in the wall Linear or radial cracks Horizontal, vertical or inclined cracks Shedding its lining and the supporting wall
Poor performance deterioration of masonry support and liners	Horizontal cracks in vertical joints Warping Release liner
Failure openings	Vertical cracks Inclined cracks Horizontal cracks Movement of parts Problem on the closing girder
Failures of execution at the top of the opening	Linear or radial cracks Horizontal cracks Bulge by compression
Insufficient penetration from the girder of the roof system	Inclinated cracks in the girders Shedding its lining and the supporting wall
Poor roof system support	Inclinated cracks Horizontal cracks Detachment of the support material
Poor evacuation of rain water on walls and ceilings	Detachment of the support material Breaks of the support parts

1.4.1.4. The incompatibility factor

This factor includes alterations derived physical or chemical contact between materials of different kind. It can cause changes of colour, salts formations and even, in the more severe cases, important ruptures. For this reason, the in situ and laboratory monitoring of restoration materials as well as the pilot applications of conservation interventions are strongly recommended in any process of decision making (Fig. 1.1).

31 M. A. Rodríguez, I. Monteagudo, B. Saroza, P. Nolasco, I. Castro. Aproximación a la patología presentada en las construcciones de tierra. Informes de Constr.; 2011; 63: 97-106.

1.4.1.5. Tension factor

The tension factor is associated with decompression effects caused by the stone extraction of the quarry or also derived from the tooled settling or structural loads. Thus, it can be a precursor of important fractures and for that reason, carry out operations such as a simply quality control can avoid important future pathologies.

1.4.2. Soluble salts in building materials

Both intrinsic and extrinsic factors are involved in the soluble salts presence, being this one of the most aggressive deterioration mechanisms that affects the built heritage[32-34] (Fig. 1.5).

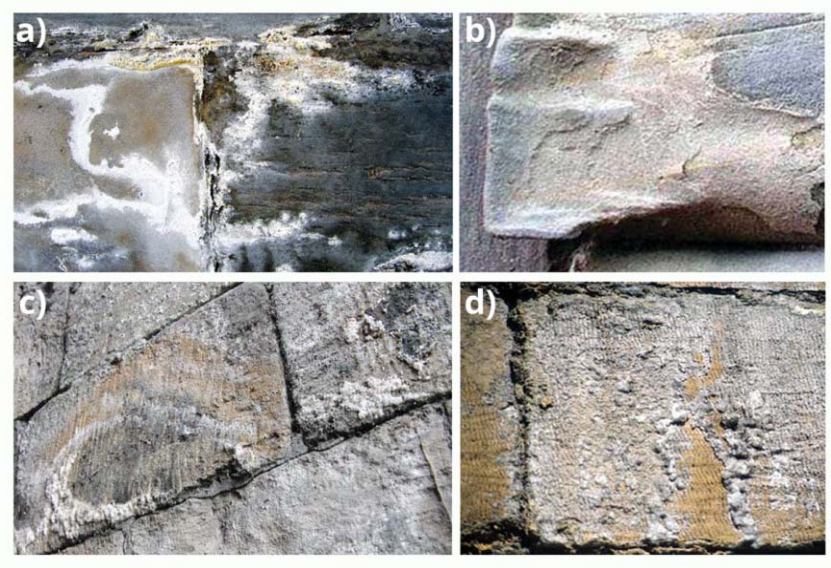

Figure 1.5. a) Efflorescence on the surface of sandstone mansory, focused at joints between masonry blocks. b) Contamined sandstone block, in which the salts crystallization induced disintegration and scaling of the stone. c) Efflorescence on dolomitic limestone related to historic air pollution. d) Salt crust of sodium chloride formed over a limestone block[35].

32 V. Matović, S. Erić, A. Kremenović, P. Colomban, D. Serćković-Batoćanin, N. Matović. The origin of syngenite in black crust on the limestone monument King´s Gate (Belgrade Fortress, Serbia) - The role of agriculture fertilizer. J. Cult. Herit.; 2012: 13: 175-186.

33 R. M. Espinosa-Marzal, G. W. Scherer. Advances in understanding damage by salt crystallization. Acc. Chem. Res.; 2010; 43: 897-905.

34 M. Steiger, S. Asmussen. Crystallization of sodium sulfate phases in porous materials: The phase diagram Na2SO4-H2O and the generation of stress. Geochim. Cosmochim.; 2008; 72: 4291-4306.

35 International Scientific Committee for Stone (ISCS). Illustrated glossary on stone deterioration patterns. France; ICOMOS; 2008.

Its formation is not only an aesthetical problem when they become visible as efflorescences, but also produces a considerable decay when salts precipitate beneath the material as subeflorescences. As a matter of fact, its formation can get to crumbling masonry of the materials and cause irreparable losses in our heritage.

In this way, the type of damage caused by these formations depends not only on the type of salt and environmental conditions, but also on the characteristics of the material itself (as it is explained in section 1.4.1). The combination of several factors such as size or voids distribution, condition the resistance of the material to the pressures generated by the salts during the crystallization processes, hydration and/or thaw. Therefore, in the followings sections their different origins and types of damage exercised are exposed in detail.

1.4.2.2. Origin of soluble salts in building materials

The origin of soluble salts in built heritage is usually associated with leaching of materials, ions from soil, atmospheric deposits or metabolite products of organisms[36-37].

In this regard, the mineral alteration of the building materials can result in the formation of soluble salts that, in turn, can also contribute to its progressive deterioration. The stones and mortars used in construction usually contain soluble salts that can act as altering agents. For example, original compounds of construction materials can react with other salts or aqueous solutions and, at the same time, can be products originated by the reaction with other salts. For instance, calcite ($CaCO_3$) can easily react with the atmospheric SO_2 and be transformed into gypsum[38] ($CaSO_4{\cdot}2H_2O$) (reaction 1.5 and 1.6).

$$SO_2 + \frac{1}{2}O_2 + H_2O \rightarrow H_2SO_4 \qquad (1.5)$$

$$CaCO_3 + H_2SO_4 + H_2O \rightarrow CaSO_4 \cdot 2H_2O + CO_2 \qquad (1.6)$$

Other similar case is the calcite dissolution of limestones, which is a constant source of Ca^{+2} and CO_3^{-2}. Although the calcium carbonate is poorly soluble in water, its dissolution as bicarbonate is higher when the water that is in contact with the stone contains certain amount of carbon dioxide, mainly coming from atmospheres of

36 E. Doehne, C. Price. Stone conservation, an overview of current research. Los Angeles: The Getty conservation Institute; 2010.

37 C. M. Grossp, R. M. Esbert. Las sales soluble en el deterioro de rocas monumentales. Revisión bibliográfica. Mater. Constr.; 1994; 235: 15-30.

38 N. Prieto-Taboada, M. Maguregui, I. Martinez-Arkarazo, M. A. Olazabal, G. Arana, J. M. Madariaga. Spectroscopic evaluation of the environmental impact on black crusted modern mortars in urban-industrial areas. Anal. Bioanal. Chem.; 2011; 399: 2949-2959.

industrial areas. The CO_2 is dissolved in water and form carbonic acid, which react with the carbonate forming bicarbonate. Then, when the wall begins to dry, the bicarbonate salts can migrate outwards and, during the evaporation phase, calcite precipitates and is deposited as efflorescence over the surface[39] (reaction 1.7), causing a loss of inside material.

$$CaCO_3 + H_2CO_3 \rightarrow Ca^{+2} + 2HCO_3^- \quad (1.7)$$

Others compounds such us potassium or sodium carbonates are usually formed from the released ions of alkaline materials such as sandstone, portland cement, or even some cleaner products[40]. Besides, alkaline carbonates can react with atmospheric sulfuric acid and form new suphated compounds (reaction 1.8).

$$K_2CO_3 + H_2SO_4 \rightarrow K_2SO_4 + CO_2 + H_2O \quad (1.8)$$

Other important source of salts is the water coming from soil. The water, that access to the building by capillary action, naturally contains carbonate, sulfate, chloride, nitrate, magnesium, calcium, sodium, potassium and/or ammonium ions. However, its amount can be highly increased by human settlements.

For example, the presence of nitrates in ground water is normally related to the natural decomposition of organic nitrogenous materials (like proteins from plants, animals, fertilizers and so on) by microorganisms actions. In the same way, sulphates and chlorides are usually used as fertilizers or road antifreeze[41-42].

Finally, the soluble salts can be originated by deposit of atmospheric products. The ions present in the atmosphere can form salts by reaction with original materials. A common case is the marine salts, which can be transported long distances, being considered as a major source of chlorides and sulfates. Besides, in polluted environments, the contaminants can be found in gas (CO_2, SO_2, N_2O_5, NO_3, NH_3, CH_4, etc), liquid (acid, saline solutions, etc) or solid state (metallic oxides, sulfides, soot, etc) facilitating the attack of building materials. One of the best known effects is the black

39 H. Morillas, M. Maguregui, J. Trebolazabala, J. M. Madariaga. Nature and origin of white efflorescence on bricks, artificial stones, and joint mortars of modern houses evaluated by portable Raman spectroscopy and laboratory analyses. Spectrochim. Acta A.; 2015; 136: 1195-1203.

40 S. Pavía. Sulfation of decrepit Portland cement mortar and its adjacent masonry. Dublín; Trinity Collage; 2008.

41 S. M. Rivera, A. L. Peña Díaz. Brick and Mortar Research. New York; Nova Science Publishers; 2012.

42 J. Pacheco Ávila, A. Cabrera Sansores. Fuentes principales de nitrógeno en aguas subterráneas. Ing.; 2003; 7: 47-54.

crusts, caused by the action of sulfur dioxide and coal particles[43]. Moreover, nitrates can also be present by combustion of fossil fuels. The nitric acid generated can attack the calcareous materials producing new degradation compounds as for example nitrocalcite (reaction 1.9).

$$CaCO_3 + 2HNO_3 + 4H_2O \rightarrow Ca(NO_3)_2 \cdot 4H_2O + CO_2 + H_2O \quad (1.9)$$

Finally, the presence of phosphate, oxalate, nitrate and sulphate salts can be also an indicator of the action of living organisms. For example, the phosphates and uric acid segregated can cause alteration in stone materials, leading to the formation of magnesium or calcium phosphates. Also, the calcium oxalates derived from the metabolic activity of some lichens species can form a protective aesthetic salts layers over the stone[44].

In summary, the salts present in the materials can have several origins and, therefore, each particular case has to be studied trying to correlate the nature of the detected salts with environmental agents and materials.

1.4.2.3. Deterioration caused by soluble salts in building materials

The damages caused by soluble salts in the building materials can be produced by several mechanisms that many times are difficult to establish. In accordance to their nature, they can be classified as crystallization, hydration and structural.

The crystallization effect is due to a combination of several factors, among which should be mentioned the type and properties of the salt (changes of solubility by fluctuations of temperature, coefficient of thermal expansion…) and, its concentration and degree of supersaturation. However, the properties of materials are also important (size, water absorption capacity, mechanical strength, distribution of empty spaces…). During the crystallization process, the thrust of the crystals to grow in pores, capillaries or fissures produces local tensions that tend to enlarge these empty spaces. The crystallization continues until the stress reaches a certain force, directly related to the degree of supersaturation and inversely with the solubility of the salt. If physical stress exceeds the tensile strength of the material deterioration occurs[45].

43 I. Martínez-Arkarazo, M. Angulo, L. Bartolomé, N. Etxebarria, M. A. Olazabal , J. M. Madariaga. An integrated analytical approach to diagnose the conservation state of building materials of a palace house in the metropolitan Bilbao (Basque Country, North of Spain). Anal. Chim. Acta.; 2007; 2: 350-359.

44 J. Garcia-Rowe, C. Saiz-Jimenez. Lichens and bryophtes as agents of deterioration of building materials in Spanish cathedrals. Int. Biodeter.; 1991; 1: 151-163.

45 A. Bernabéu, S. Ordóñez. Quantification of salt weathering in porous stones using an experimental continuos partial immersion method. Eng. Geol.; 2001; 3: 313-325.

According to the Arnold and Zehnder model, an areal distribution of salts can be observed in walls and claddings. In general, depending on the humidity of the wall, the solubility and mobility of the salts, four different levels of affection can be distinguished (Fig. 1.6); A, B, C and D[46-48].

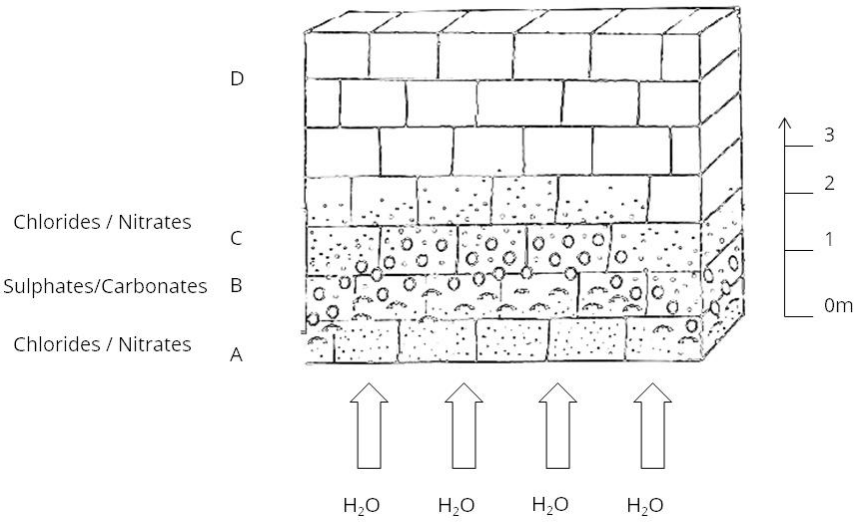

Figure 1.6. Crystallization profile modeled by Arnold and Zehnder[49].

In the nearest levels to the base (area A), the wall is usually quite wet. However, no serious damage is observed as, in this level, salts precipitate only occasionally.

Precisely, in the upper level (zone B), the strongest damages can be found as, for example, disintegration and sandification of stones and mortars or scaling of claddings. Besides, it is where the largest number of efflorescence is concentrated. The compounds present in this area are mainly calcium and magnesium sulphates or sodium and potassium carbonates, although sometimes, nitrate can also be found. All these salts have a weak or moderate solubility in water.

46 E.R. Agudo, B. Lubelli, R. V. Hees, C. Price, C.R. Navarro. An integrated methodology for salt damage assessment and remediation: the case of San Jeronimo Monastery (Granada, Spain). Environ. Earth Sci.; 2011; 63: 1475-1486.

47 M. A. Vázquez, E. Galán, P. Ortiz, R. Ortiz. Digital image analysis and EDX SEM as combined techniques to evaluate salt damp on walls. Constr. Build Mater.; 2013; 45: 95-105.

48 M. Auxiliadora Vázquez, E. Galán, M. A. Guerrero, P. Ortiz. Digital image processing of weathered stone caused by efflorescences: A tool for mapping and evaluation of stone decay. Constr. Build Mater.; 2011; 25: 1603-1611.

49 A. Arnold, K. Zehnder. Salt weathering on monuments. Bari, Italy; In F. Zezza, Proc. 1st Int. Symposium on the Conservation of Monuments in the Mediterranean; 1989.

Above this level (area C), a less intense deterioration is caused. The materials are in better state, although, are wet and darkened. The precipitated salts are essentially chlorides and nitrates as their solubility in water is moderate or high.

Finally, in zone D, the material is dry and no degradation, assignable to water infiltration, is observed.

In addition to the crystallization damage, the salts can have different hydration states. Once crystallized, salts can catch or release water of hydration due to moisture and temperature changes. In this process, the volume change produced develops a physical stress inside the pores degrading the material[50]. The case of calcium sulfate is the best known, the damage is not only caused by its precipitation since its property of crystallizing in different states of hydration such as gypsum ($CaSO_4 \cdot 2H_2O$), bassanite ($CaSO_4 \cdot 0.5H_2O$) and anhydrite ($CaSO_4$) is the most dangerous.

Finally, although not as common as the above processes, the salts can undergo structural changes[51] due to temperature and humidity changes that can lead to rupture of the material by the associated volume changes. One of the most typical cases is the transformation of calcite into its polymorph form, aragonite ($CaCO_3$).

Accordingly, the characterization of salts, in its particular environment, could be the first step to understand the chemical mechanism responsible for the material deterioration. It could provide valuable information for the selection of the appropriate restoration and conservation procedures, procuring a solution to the cause of the problem from its source rather than simply treating the symptoms.

1.5. Visual analysis: stone deterioration patterns in correlation with the damage categories

The visual analysis of the different weathering forms can help to identify the main source of deterioration as well as the need and urgency of intervention.

For that purpose, the correlation between weathering forms and cause of degradation has to consider intensity and proportion of damage (degraded parts, dimensions of the stone element, structural function, historical value, etc). Only in this way, the assessment of the damage severity contributes to classify and compare stone materials regarding their susceptibility to degradation, improving the risk estimation.

50 N. Thaulow , S. Sahu. Mechanism of concrete deterioration due to salt crystallization. Mater. Charact.; 2004; 2: 123-127.

51 A. Bernabéu, S. Ordóñez. Quantification of salt weathering in porous stones using an experimental continuos partial immersion method. Eng. Geol.; 2001; 3: 313-325.

Thanks to the investigations carried out at numerous monuments worldwide, different stones types and environments, a classification accepted by all the scientific community is nowadays provided[52-53]. According to it, the most common types of weathering forms can be divided into 4 groups (detachment, loss, formation of deposit and cracking of material) and the severity of damages can be distinguished in six categories; 0-no visible damage, I-very slight damage, II-slight damage, III-moderate damage, IV- severe damage and V- very severe damage.

Given that the use of these classifications is widely recommended for the regular reevaluation of monuments, the common deterioration patterns and their related causes are described along this section.

1.5.1. Detachment of building materials

All the weathering forms included in this group (Fig.1.7) are related to the action of chemical processes within the stone and salts crystallization.

The first one is sanding, whose presence is identified by granular or powdery particles on the stone surface.

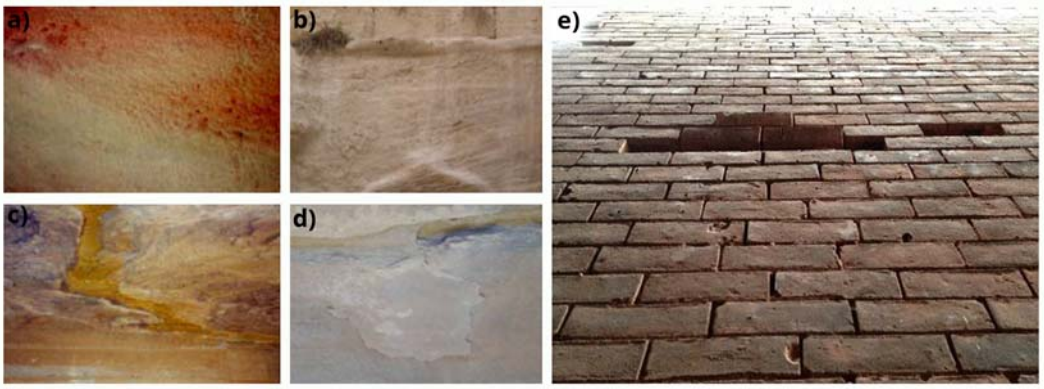

Figure 1.7. a) Sanding. b) Flaking. c) Exfoliation. d) Scaling. e) Loose of mansory[54].

On the other hand, the detachment of small, flat, thin pieces of the outer layers of the stone surface is known as flaking. However, the detachment of larges flat layers following the profile of the stone surface is called scaling. Besides, if the stone is

52 B. Fitzner. Diagnosis of weathering damage on stone monuments. Conference of weathering damage on stone monuments bacteria, Macla; 2014; 18: 21-27.

53 International Scientific Committee for Stone (ISCS). Illustrated glossary on stone deterioration patterns. France; ICOMOS; 2008.

54 B. Fitzner, K. Heinrichs (2004), Photo Atlas of Weathering forms on stone monuments: www.stone.rwth-aachen.de

degraded into thin separated layers following the bedding planes of stone surface is considered exfoliation, which is very common in sedimentary stones.

Finally, loose of masonry blocks can be presented in severe cases.

1.5.2. Loss of stone material

The first weathering form included in this group is pitting. It is identified by the presence of small cavities in the non homogenous stone surface due to the erosion. Nevertheless, if the cavities are of various sizes distributed as a honeycomb is known as alveolar weathering, commonly related to salty environments (Fig.1.8 a, b).

On the other hand outbreaks are described as missing stone pieces or compact fragments of different size and its origin is associated with mechanical stresses or vandalism. Nevertheless, if stone pieces are breaking away, spalling, is considered as natural weathering within a localized area (Fig.1.8 c, d).

Other times, eroded parts of stone surface with different colour can be presented by the washed action of the rain, also known as washout (Fig.1.8 e).

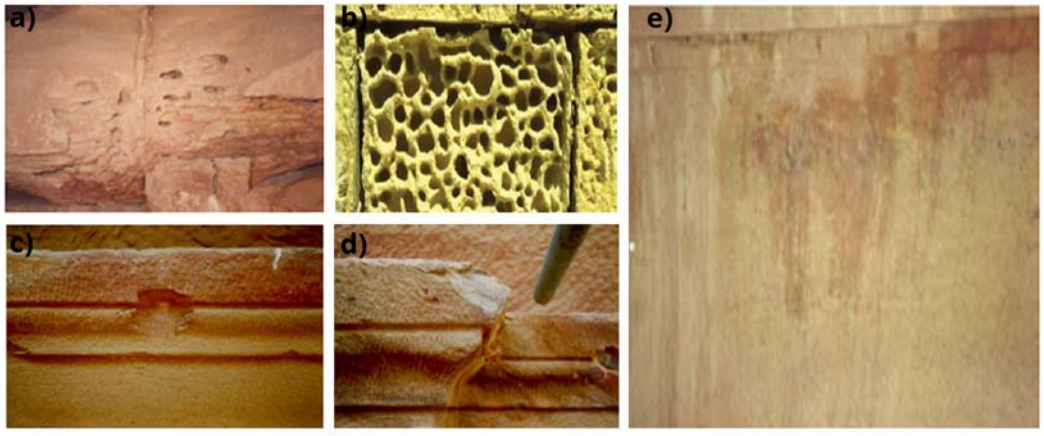

Figure 1.8. a) Pitting. b) alveolar weathering. c) Outbreaks. d) Spalling. e) Washsout[55].

1.5.3. Formation of deposit on the building materials

The existence of whitish deposits of loosely attached soluble salts on the surface as efflorescences happens when water and salt are present within the stone, as it is explained before (section 1.4). However, when a coloured thin skin is strongly

55 B. Fitzner, K. Heinrichs (2004), Photo Atlas of Weathering forms on stone monuments: www.stone.rwth-aachen.de

attached to the stone surface is considered as salt crust and, is related as leaching out of internal original compounds (Fig. 1.5).

The presence of microbiological and vegetation deterioration as well as insect colonization are easy to identify by the growth of plants and nets or by the presence of living or decayed micro-organism such as lichens, moss and fungi on the material surface (Fig 1.4).

Finally, the presence of brownish or greyish deposits not completely hiding the stone surface, resulted of dust, mud and pollutants accumulation are called soling. However, if the deposits are in form of black layers is known as black crust and its origin is associated only with the pollutants attack.

1.5.4. Cracking of the building material

Crack is defined as an identifiable fracture in the stone as a result of physical weathering and is produced by natural o constructional causes. If a plane surface of parting produced by stresses is imposed on the stone without displacement is known as joint. However, fault is a fracture displaced and it can produce more severe damage than the latter.

Other times, the numerous cracking of material produce structural instability, could cause the collapse of the wall.

1.6. The technical requirements for assess built heritage

Although, the visual analysis can be a useful tool for the early phases of study and long term monitoring, the assessment of built heritage state must include a precise damage diagnosis for the characterization, interpretation, classification, prediction of damage mechanism on building materials and response of pilot interventions as it is crucial for its sustainable preservation[56].

However, the study of this field requires special conditions. In most of the cases, sampling is restricted or not possible and for that reason, the research of non destructive methodologies to its study is booming during the last decade.

In this way, to preserve the integrity of building materials, the sampling have to be limited to a minimum, which is difficult for its measurement and interpretation. Therefore, non destructive methods that can be carried out in situ are an indispensable

56 S. Siegesmund, R. Snethlage. Stone in Architecture. Berlin; Springer;2011.

tool to perform a correct scientific diagnosis study, avoiding the necessity to make decisions only in terms of the expertise of the conservators[57-58].

However, when non destructive methods are used some special considerations are needed. The data collected are usually influenced by the fabric of the material or by other parameters like temperature, moisture and salts concentrations, which are heterogeneously distributed and even can show different gradients in space and time. The methods developed have to be suitable for fragile and complex geometric elements as columns or decorative ornaments like coats of arms or gargoyles, which have to be measured from different sides. Thus, the amount of time and labor involved for making the analysis can be considerably long. In addition to these complications, the influent of intrinsic and extrinsic factors as petrographic characteristics, pollutants and climatic conditions must be also studied[59-60].

In the last years several non destructive techniques have been tested for the maintenance and preservation of built heritage. In this way, X-ray fluorescence (XRF), energy dispersive spectroscopy (EDX), laser plasma spectroscopy (LIBS) and X-ray emission induced by particles (PIXE) are some of the elemental techniques used[61-64]. On the other hand, molecular techniques as Infrared spectroscopy (IR) and Raman

57 M. Pérez-Alonso, K. Castro, M. Álvarez, J. M. Madariaga. Scientific analysis versus restorer´s expertise fro diagnosis prior to restoration process: the case of Santa Maria Church (Hermo, Asturias, North of Spain). Anal. Chim. Acta.; 2004; 524: 379-389.

58 K. S. Andrikopoulos, Sister Daniilia, B. Roussel, K. Janssens. In vitro validation of a mobile Raman-XRF micro-analytical instrument´s capabilities on the diagnosis of Byzantine icons. J. Raman. Spectrosc.; 2006; 37: 1026-1034.

59 L. Medeghini, P. P. Lottici, C. De Vito, S. Mignardi, D. Bersani. Micro-Raman spectroscopy and ancient ceramics: applications and problems. J. Raman. Spectrosc.; 2014; 45:1244-1250.

60 J. Aramendia, L. Gómez-Nubla, K. Castro, I. Martinez-Arkarazo, D. Vega, A. Sanz López de Heredia, A. García Ibáñez Opakua, J. M. Madariaga. J. Raman. Spectrosc.; 2012; 43:1111-1117.

61 A. Nevin, G. Spoto, D. Anglos. Laser spectroscopies for elemental and molecular analysis in art and archaeology. Appl. Phys. A-Mater.; 2012; 106: 339-361.

62 S. Valadas, A. Candeias, J. Miráo, D. Tavares, J. Coroado, R. Simon, A. S. Silva, M. Gil, A. Guilherme, M. L. Carvalho. Study of mural paitings using in-situ XRF, confocal synchrotron μ-XRF, μ-XRD, optical microscopy, and SEM-EDX- the case of the frescoes from Misericordia Church of Odemira. Microsc. Microanal.; 2011; 17: 702-709.

63 A. Giakoumaki, I. Osticioli, D. Angos. Spectroscopic analysis using a hybrid LIBS-Raman system. Appl. Phys. A-Mater.;2006; 83: 537-541.

64 S. Nava, F. Becherini, A. Bernardi, A. Bonazza, M. Chiari, I. García-Orellana, F. Lucarelli, N. Ludwing, A. Migliori, C. Sabbioni, R. Udisti, G. Valli, R. Vecchi. An integrated approach to assess air pollution threats to cultural heritage in a semi-confined environment: The case study of Michelozzo's Courtyard in Florence (Italy). Sci. Total Environ.; 2010; 408: 1403-1413.

spectroscopy are ones of the most preferred by their advantages[65] (as it is detailed in chapters 4 and 5). Furthermore, there are other techniques that require a minimum sampling as X-ray diffraction (XRD) and imaging techniques such as scanning electron microscopy (SEM), which allows structural analysis[66].

Among these powerful techniques, although less known, ultrasonic pulses are mainly used to determine physico-mechanical pathologies, laser scans to obtain a digital documentation of the building, digital image analysis to quantify the surface material affected and infrared termography to register temperature and humidity fluctuations[67-70].

Although these techniques are useful and provide good quality results, sometimes a laboratory analysis is required. In this way, the destructive techniques used in this field had to be able to analyze salts, metals and organic compounds as they are the most typical substances involved in the cause of damage. Ionic chromatography (IC) is the most habitual method used to carry out soluble salts analysis. However, for metals analysis inductively coupled plasma mass spectrometry of (ICP-MS) or atomic absorption spectroscopy (AAS) are used. Finally, gas chromatography (CG) is one of the most recommended techniques for the analysis of organic compounds[71-73].

65 L. Hopkinson, K. Rutt, P. Kristova, J. Blows, C. Firth. Sourcing limestone masonry for restoration of historic buildings, a spectroscopic pilot study. J. Cult. Herit.; 2015; doi:10.1016/j.culher.2015.03.007.

66 A. Bonazza, C. Sabbioni, N. Ghedini. Quantitative data on carbon fractions in interpretation of black crusts and soiling on European built heritage. Atmos. Environ.;2005; 39: 2607-2618.

67 M. A. Vázquez, E. Galán, P. Ortiz, R. Ortiz. Digital image analysis and EDX SEM as combined techniques to evaluate salt damp on walls. Constr. Build Mater.; 2013; 45: 95-105.

68 M. Bourke, H. Viles, J. Nicoli, P. Lyew-Ayee, R. Ghent, J. Holmlund. Innovative applications of laser scanning and rapid prototype printing to rock breakdown experiments. Earth Surf. Pro. Land.; 2008; 33: 1614-1621.

69 S. De Santis, A. K. Tomor. Laboratory and field studies on the use of acoustic emission for masonry brigdes. NDT E. Int.; 2013; 55: 64-74.

70 D. J. Applications of thermography in non-destructive testing structures, NDT E. Int.; 2001; 34: 149-154.

71 N. Prieto-Taboada, O. Gómez-Laserna, I. Martinez-Arkarazo, M. A. Olazabal, J. M. Madariaga. Optimization of two methods based on ultrasound energy as alternative to European standards for soluble salts extraction from building materials. J. Ultrason. Sonochem.; 2012; 19: 1260-1265.

72 L. Bartolome, E. Cortazar, J. C. Raposo, A. Usobiaga, O. Zuloaga, N. Extxebarria, L. A. Fernández. Simultaneous microwaved-assisted extraction of polycyclic aromatic hydrocarbons, polychlorinated biphenyls, phthalate esters and nonyphenols in sediments. J. Chromatogr. A.; 2005; 1068: 229-236.

73 J. Pérez-arantegui, E. Ribechini, C. Pardos, M. colombini. Chemical investigation on black pigments in the carved decoration of sixteenth century alabaster tombs from Zaragoza (Spain). Anal. Bioanal. Chem..; 2009; 395: 2191-2197.

1.7. Steps followed in function to the pathology presented

As a brief summary, some general recommendations to preserve the monument are given in this section. In this sense, the interventions most frequently used in building conservation can be classified in 4 blocks;

A- Reconstruction/reintegration/ reinforcement.

B- Stabilization/ consolidation.

C- Protection.

D- Maintenance and preventive conservation.

Depending on the pathology present several actions are suggested by the scientific community (Table 1.2)[74]

Table 1.2. Synthesis of the relationship between indicator of alteration, deterioration triggers and recommended stages of intervention.

Level	Pathology	Agent	Phases of intervention
Superficial modifications	Crust	Water, pollutants, biotic	I. Cleaning II. Protection III. Maintenance and preventive conservation
	Dirt	Water, pollutants, wind	I. Cleaning II. Maintenance and preventive conservation
	Damp stains	Water	I. Cleaning II. Protection III. Maintenance and preventive conservation
	Efflorescences	Soluble salts	I. Cleaning II. Surface protection and drainage III. Maintenance and preventive conservation
	Discoloration	Soluble salts	I. Surface and covers protection II. Maintenance and preventive conservation
Loss of material	Erosion	Wind, water	I.Stabilization and consolidation II. Reintegration of material

74 M. A. Rodríguez, I. Monteagudo, B. Saroza, P. Nolasco, I. Castro. Aproximación a la patología presentada en las construcciones de tierra. Informes de Constr.; 2011; 63: 97-106.

Level	Pathology	Agent	Phases of intervention
			III. Protection IV. Maintenance and preventive conservation
	Disgregation	Water, temperature, sun, wing, soluble salts, biotic	I.Stabilization and consolidation II. Reintegration of material III. Protection IV. Maintenance and preventive conservation
	Material detachment	Water, climatic changes, vegetation, mechanic	I. Consolidation II. Protection II. Maintenance and preventive conservation
Ruptures	Fisures	Ambiental, movements of structure, natural disasters	I. Consolidation II. Maintenance and preventive conservation
	Cracks	Ambiental, movements of structure, natural disasters	I. Reconstruction and reinforce II. Maintenance and preventive conservation
Other forms	Antropic modifications	Humans	I. Reconstruction and reinforce II. Constructive maintenance
	Higher plants	Biotic	I. Cleaning II. Protection III. Maintenance and preventive conservation

1.8. General recommendations for the conservation of built heritage

According to the ICOMOS[75], some basic recommendations have to be followed by all the expertise involved to contribute to built heritage conservation.

The first one is catalog and document the building, detailing techniques and traditional ways to make it. Then, design and implement intervention processes that provide adequate maintenance programs to the operated buildings such as materials and treatment or disaster response capacity.

75 ICCRO, CRATerre-EAG, GCI, US/ICOMOS. Conferencia sobre la conservación de la arquitectura de Tierra. Nuevo Mexico; The Getty conservation Institute; 1990.

Moreover, the implementation of programs for training of specialists is highly recommended due to the required multidisciplinary approach.

Finally, and one of the most important, set criteria for education and sensitivity to work with cultural, environmental, technological and economic values.

CHAPTER 2: OBJETIVES

The global objective was established as follows:

"To develop analytical methodologies for the in situ diagnosis study of the urban built heritage, mainly affected by environmental factors, to contribute in its suitable preservation and maintenance".

Therefore, to achieve this goal, a series of partial aims were set:

- To study the viability of the in situ analysis based on spectroscopic techniques, specifically Raman spectroscopy, examining the advantages and disadvantages presented in this kind of matrix.

-To implement a complete in situ spectroscopic methodology, with the purpose of diagnosing the main cause of decay, and to provide valuable information for the selection of restoration and conservation procedures, studying the usefulness of multiple technique combinations to understand the chemistry behind the damage.

-To develop a multidisciplinary analytical approach to corroborate the results obtained by spectroscopic techniques and to evaluate quantitatively the results obtained.

-To study how to reduce the sampling required for obtaining quantitative results, by means of non-invasive sampling methods based on non aggressive products.

-Determinate the chemical weathering response of common stone materials after the pilot application of a new green conservation method to preserve ruins wall head, comparing the results with that occurring on bare ruined surfaces.

The thesis was performed in accordance with the research line followed by the group of Analytical Chemistry (IBeA) in the conservation of built heritage, the availability of the specific instrumentation and the framework of the R&D projects:

"Innovative analytical methodologies to diagnose the impact of combustion gases and GHC in urban buildings (IMDICOGU)".

"Deterioration of stony construction materials induced by pollutants of urban atmospheres (DEMBUMIES)".

"Innovative analytical methodologies to diagnose the impact of pollution on building materials of silicate based PRE-1930: towards new cleaning processes (DISILICA) ".

"Soft Wall Capping"

CHAPTER 3:
EXPERIMENTAL PROCEDURE

Due to the intrinsic value that built heritage represents for the society, the analytical studies attempt to minimize, or even eliminate, the sampling and treatment phases by application of in situ analytical methodologies. In this work, depending on each study case and its purpose, the sampling protocol was different and for that reason, only the common aspects are explained in this section. However, the precise specifications are detailed in each chapter.

3.1. Sampling procedure and treatment

3.1.1. Sampling

3.1.1.1. Sample collection of building materials

The sampling campaign was always performed in accordance to the visual inspection and in situ spectroscopic study taken place previously (Fig. 3.1 a, b), following the Italian guidelines (Normal 3/80)[1]. In this manner, samples were collected, just in sufficient amount for laboratory analysis (Fig. 3.1 c), using a chisel and trying to damage the building as little as possible. Besides, the environmental conditions were taking into account through a hygrothermometer (TFH 610, Ebro Electronic, Geschäftsbereich, Germany).

1 C.N.R.-I.C.R. Materiali Lapidei: Campionamento. Roma: Comas Grafica; 1980.

Furthermore, prior to the quantitative analysis, the visible efflorescences of the samples were removed in order to quantify the salt content of the building materials. All the samples were registered and stored in zip bags until the treatment.

3.1.1.2. Non destructive soluble salts collection by cellulose poultices

To determine the quantity of the soluble salts content in the materials, without taking any sample, wet paper pulps were used in the study corresponding to chapter 5.

Based on the suggestion by Arnold and Zehnder[2], which asserts that the salt content is seldom homogeneous throughout a wall, several samples were extracted to obtain indications of the salt content. In this way, cellulose pulp of approximately 12 cm^2 and 5 mm thick, soaked in de-ionized water with a pulp-to-water weight ratio of about 1/8, were applied to the sampling points for 2 hours[3] (Fig. 3.1 d). The poultices were then removed and saved to the treatment phase.

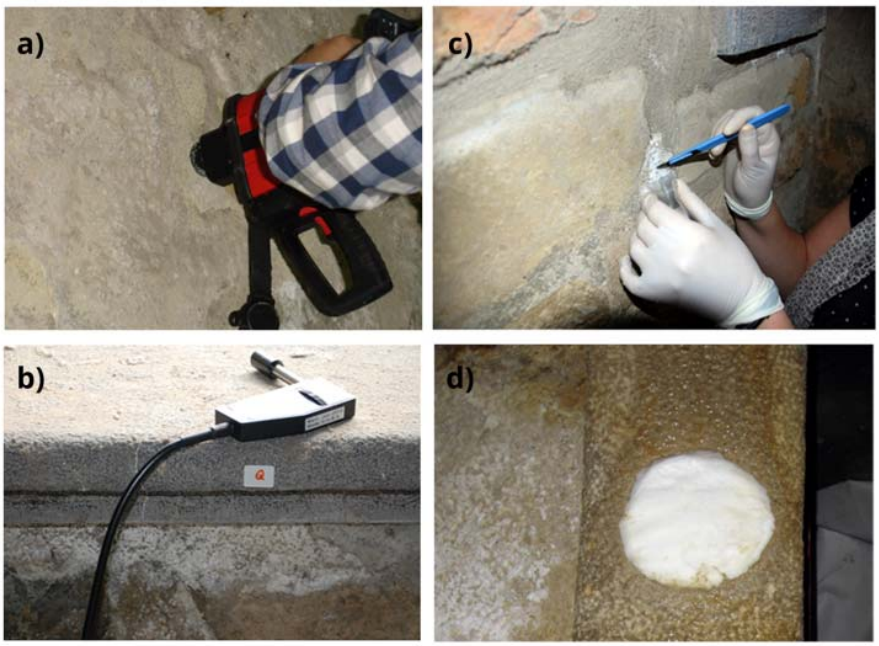

Figure 3.1. Images of the sampling procedure. a-b) Examples of in situ spectroscopic studies, assisted by Raman and DRIFT, taken place previously to the sample collection. c) Collection of an efflorescence sample .d) Extraction of soluble salt content through a cellulose poultice.

2 A. Arnold, K. Zehnder. Monitoring wall paintings affected by soluble salt. The Conservation of Wall Paintings S. Cather. Los Angeles: The Getty Conservation Institute; 1991.

3 A. Dionísio, E. Martinho, C. Grangeia, F. Almeida. Non-invasive techniques for the evaluation of stone conservation. Global Stone Congress, Trans Tech Publications; 2012:170-177.

3.1.1.3. Sample collection of soils

Soil of the areas of interest was sampled to study its influence on the material degradation. In this way, 50 g of soil were collected using a small garden shovel. Afterwards, the samples were registered and stored in zip bags until their treatment.

3.1.1.4. Sample collection of water

Retained and rain water of the areas of interest were taken to study its influence on the pathologies suffered by the materials. In this manner, approximately 250 mL of water were collected in a laboratory glass bottle, during 48 or 72 hours, depending of the case. Then, the sample was registered and preserved at 4°C.

3.1.2. Sample treatment

3.1.2.1. Preparation of samples for cross-section spectroscopic imaging analysis

Scientific studies of cultural heritage include the analysis of cross sectional samples in order to increase knowledge of the degradations suffered by building materials[4,5]. Recent works have shown the usefulness presented by this type of analysis, offering the possibility to obtain a large amount of information from the distribution and penetration grade of deteriorating agents[6].

In this manner, to obtain a focused spectroscopic image, the process of polishing was carried out smoothly by a polisher (Forcipol®1, Metkon, Turkey) to avoid the disintegration of the sample (Fig. 3.2). In addition, to avoid the dissolution of soluble salts, no water was used in the process.

4 T. Tsang, R.H. Cunningham. Some improvements in the study of cross sections. J. Am. Inst. Conservat.; 1991; 30: 163-177.

5 E. Jiménez Roca, A. Ruiz-Conde, P.J. Sánchez-Soto. Preparation of stratigraphic sections (cross-sections): some practical aspects on the analysis of strates coming from Cultural Heritage materials (pigments and supports). Bol. Soc. Esp. Ceram.; 2005; 44: 382-278.

6 N. Prieto Taboada, O. Gómez Laserna, I. Martínez Arkarazo, M.A. Olazabal, J.M. Madariaga. Relevance of cross-section analysis in correct diagnosis of the state of conservation of building materials as evidenced by spectroscopic imaging. Anal. Chem.; 2013; 85: 9501-9507.

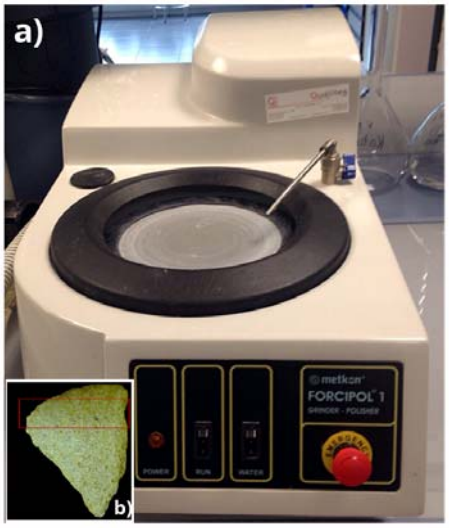

Figure 3.2. Images of cross-section samples preparation. a) Polisher Forcipol®1, Metkon. b) Polished sandstone and mortar samples.

3.1.2.2. Extraction of soluble salts for ion chromatography analysis

3.1.2.2.1. Samples of building materials

To extract the soluble salts of different materials, selected samples were treated in triplicate following an ultrasound assisted extraction method[7-8], which is an effective alternative to the standard EN 16455/2014.

The ground samples were dried at 80°C for 24 hours and then preserved in desiccators. For the analysis, 0.1 g of sample was solved in 100 mL of MilliQ water. Subsequently, the samples were introduced in an ultrasound bath for 2 hours with a frequency of 40 khz. For the extract filtration, Millipore 0.45 µm PTFE disc filters were used and then, the solutions were preserved at 4°C, in polypropylene tubes, until the analysis was carried out.

3.1.2.2.2. Soluble salts collected by cellulose poultices

To quantify the soluble salts content of building materials without sampling, cellulose poultices were used, being this method thoroughly explained in chapter 5.

7 N. Prieto Taboada, O. Gómez Laserna, I. Martínez Arkarazo, M.A. Olazabal, J.M. Madariaga. Optimizations of two methods based on ultrasound energy as alternative to European standards from soluble salts extraction from building materials. J. Ultrasound. Sonochem.; 2012; 19: 1260-1265.

8 H. Morillas, M. Maguregui, O. Gómez-Laserna, J. Trebolazabala, J.M. Madariaga. Characterisation and diagnosis of the conservation state of cementitious materials exposed to the open air in XIX century lighthouses located on the coast of the Basque Country: "The case of Igueldo lighthouse". J. Raman Spectrosc.; 2012; 43: 1630-1636.

As in the previous case, to extract the content absorbed an ultrasound assisted extraction method was used. The poultices were then removed, soaked in 100 ml MilliQ water and filtered (Millipore 0.45 µm PTFE disc filters) to remove the paper poultice. The saline solutions were preserved at 4°C, in polypropylene tubes, until the analysis was carried out.

3.1.2.2.3. Samples of soil

To extract the soluble salts of soil samples, collected samples were lyophilized and then sieved to 500 µm mesh size in order to choose the smallest particle fraction of the soil. Then, the samples were treated in triplicate following a reference method[9] similar to EPA 300.0.

In this way, MilliQ water was added in a ratio 1:10 (soil:water). Afterwards, the samples were submitted to an ultrasound bath with a constant temperature of 20°C for 10 min. The extracts were filtered using Millipore 0.45 µm PTFE disc filters and conserved in the same way as the previous solutions.

3.1.2.2.4. Samples of retained and rain water

Prior to the quantification of the ion content of the water samples, the collected samples were filtered and conserved at 4°C in glass bottles.

3.1.2.3. Acid digestion treatment for analysis of metals by Inductively Coupled Plasma-Mass Spectroscopy (ICP-MS)

The extraction of metal content was carried out following an adaptation of EPA 3051 protocol for different matrices[10-11].

In this way, 0.5 g of each sample was subjected to acid digestion in 12 ml of aqua regia (1HNO_3:3HCl). Subsequently, the samples were introduced into a microwave digestion system (Multiwave 3000, Anton Paar, Graz, Austria), provided with a microwave digestion rotor (8XF-100), in 100 mL microwave vessels of fluorocarbon polymer (PTFE) and were subject to the method.

9 M. Schreiber, M. Otto, P.S. Fedotov, R. Wennrich. Dynamic studies on the mobility of trace elements in soil and sediment samples influenced by dumping of residues of the flood in the Mulde River region in 2002. J. Chemosphere; 2005; 61: 107-115.

10 J.A. Carrero, N. Goienaga, S. Fernandez-Ortiz de Vallejuelo, G. Arana, J.M. Madariaga. Classification of archaeological pieces into their respective stratum by a chemometric model based on the soil concentration of 25 selected elements. J. Spectrochim. Acta B; 2010; 65: 279-286.

11 N.Prieto-Taboada, I. Ibarrondo, O. Gómez-Laserna, I. Martinez-Arkarazo, M.A. Olazabal, J.M. Madariaga. Buildings as repositories of hazardous pollutants of anthropogenic origin. J. Hazard. Mater.; 2013; 248: 451-460.

The protocol consists on applying an initial ramp of 175°C in less than 5 min and after, maintaining the temperature constant for 4.5 min. Once the 10 minutes lasting heating step was finished, a third cooling 15 min lasting ramp is programmed. Then, the extracts of the vessels were filtered through Millipore 0.45 µm PVDF Millex-HV filters and the acid concentration was reduced to less than 1%. Afterwards, the solutions were preserved at 4°C in the refrigerator until the time of measurement.

3.2. Instrumentation

Nowadays, the use of portable techniques is growing over traditional methods with the development of new portable devices. The need of fast analysis, which can be performed in situ with successful results, is frequently required. Moreover, the main interest is often related to carrying out the study without any sample treatment or even any sample taken. This point is of vital importance in the field of Cultural Heritage, in which the associated value of the samples is inestimable and therefore, sampling is restricted.

For these reasons, this work is focused on applying in situ methodologies that allow us to obtain the necessary information to the study. For that purpose, and given the quality of information new devices can provide, a combination of different spectroscopic techniques were used to analyse the elemental and molecular composition of the different materials. In this way, the chosen instrumentation can be classified into two groups: non destructive analytical techniques, which can be used in situ and/or in the laboratory, and quantitative destructive analytical techniques. As is shown in this thesis, the development of analysis methodologies that combine techniques from both groups, according to the needs of each case, offers many advantages, plus a significant enhancement of their abilities[12-14].

In this manner, in order to determine the elemental characterization of the original materials, the analyses were carried out by X-Ray Fluorescence Spectroscopy (XRF). This technique allows in situ analysis of a large variety of materials, without

12 T.D. Chaplin, R.J.H. Clark, M. Martinón-Torres. A combined Raman microscopy, XRF and SEM-EDX study of three valuable objects- A large painted leather screen and two illuminated title pages in 17th century books of ordinances of the Worshipful Company of Barbers, London. J. Mol. Struct.; 2010; 976: 350-359.

13 K. Castro, A. Sarmiento, M. Maguregui, I. Martinez-Arkarazo, N. Etxebarria, M. Angulo, M. Barrutia, J. Gónzalez-Cembellín, J.M. Madariaga. Multianalytical approach to the analysis of English polychromed alabaster sculptures: µRaman, µEDXRF, and FTIR spectroscopies. J. Anal. Bioanal. Chem.; 2008; 392: 755-763.

14 W. Fremout, S. Saverwyns, F. Peters, D. Deneffe. Non-destructive micro-Raman and X-ray fluorescence spectroscopy on pre-Eyckian works of art-verification with the results obtained by destructive methods. J. Raman Spectrosc.; 2006; 37: 1035-1045.

destruction or manipulation of the sample, having detection limits in the range of mg/kg.

On the other hand, Scanning Electron Microscopy coupled to the Electronic Dispersion spectroscopy (SEM-EDX) was used to analyze the structure and composition of the samples. The technique enables the morphological study of small areas, improving the analysis of light elements, very common in the type of studied matrices.

In addition, Raman spectroscopy was chosen as main technique for the molecular characterization, due to its advantages such us the possibility of carrying out non destructive in situ analysis, its high chemical specificity, the capacity to distinguish between different cations bound to the same anion or different number of hydration water and even polymorphic compounds. Although, laboratory equipment has been considered better than mobile ones, nowadays, the performance of the portable Raman systems is comparable with that of laboratory devices and they are becoming smaller, more versatile and they are able to acquire rapidly high quality spectra[15-16].

Unfortunately, in spite of the advantages, in situ Raman analyses have inconveniences when cultural heritage samples are analyzed, being fluorescence phenomenon among the most limiting ones and that can make the analysis very difficult[17]. To solve these types of problems, a novel combined analytical methodology is proposed in this work, which is based on a combination with Diffuse Reflectance Infrared Fourier Transform (DRIFT) spectroscopy. Although, in recent years Fibre Optic Reflectance Spectroscopy (FORS) has been more used, latest studies[18-19] demonstrate the powerful applicability of DRIFT portable and laboratory devices for the molecular determination of samples of cultural heritage.

As is detailed below, apart from the spectroscopic study, some physical parameters (color, hardness, material loss and so on) were measured by other

15 J. Jehlička, P. Vítek, H.G M. Edwards, M. Hargreaves, T. Ĉapoun. Rapid outdoor non-destructive detection of organic minerals using a portable Raman spectrometer. J. Raman spectrosc.; 2009; 40: 1645-1651.

16 J. Aramendia, L. Gomez-Nubla, K. Castro, I. Martinez-Arkarazo, D. Vega, A. Sanz López de Heredia, A. García Ibáñez de Opakua, J.M. Madariaga. Portable Raman study on the conservation state of four CorTen steel-based sculptures by Eduardo Chillida impacted by urban atmospheres. J. Raman Spectrosc.; 2012; 43: 1111-1117.

17 I. Arrizabalaga, O. Gómez-Laserna, J.A. Carrero, J. Bustamante, A. Rodríguez, G. Arana, J.M. Madariaga. Diffuse reflectance FTIR database for the interpretation of the spectra obtained with a handheld device on built heritage materials. J. Anal. Methods; 2015; 7: 1061-1070.

18 T. Poli, A. Elia, O. Chiantore. Surface finishes and materials: Fiber-Optic reflectance spectroscopy (FORS) problems in Cultural Heritage diagnostics. e-Preservation Scienc.; 2009; 6: 174-179.

19 I. Arrizabalaga, O. Gómez-Laserna, J. Aramendia, G. Arana, J.M. Madariaga. Applicability of a Diffuse Reflectance Infrared Fourier Transform handheld spectrometer to perform in situ analyses on Cultural Heritage materials. J. Spectrochim. Acta A; 2014; 129:259-267.

techniques that offered the option of portability[20-21]. Thus, novel instruments such as 3D laser scanning triangulation were used in chapter 7 for increasing the quantitative information obtained of stone surfaces morphology.

Finally, once completed the non destructive study and, given the needed of more quantitative studies, the most suitable techniques were selected to carry out micro destructive analysis. For that purpose, the typical composition of the samples as well as the importance of the analytes to the integrity of the materials, human health and the environment were considered. Therefore, soluble salt content was determined by ion chromatography (IC)[22-23] and the quantification of metal was carried out by Inductively Coupled Plasma Mass Spectrometry (ICP-MS)[24].

3.2.1. Non destructive analytical techniques: in situ instruments

3.2.1.1. Hardness measures: Proceq Equotip 3

When it was required, a rock surface hardness rebound device (Proceq Equotip 3, D-type, Schwerzenbach, Switzerland) was used to assess the variability in rock surface hardness (Fig. 3.3 a) The equipment operates on similar principles to the Schmidt Hammer, but has a much lower impact making it ideal for use on soft surfaces, as it produces no damage[25].

In the Equotip, a 3 mm diameter spherical tungsten carbide test tip is mounted in an impact body and impacts under spring force against the test surface from which it

20 L. Mol, H. Viles. The role of rock surface hardness and internal moisture in tafoni development in sandstone. Earth Surf. Process. Landforms; 2012; 37: 301–314.

21 M. Bourke, H. Viles, J. Nicoli, P. Lyew-Ayee, R. Ghent, J. Holmlund. Innovative applications of laser scanning and rapid prototype printing to rock breakdown experiments. Earth Surf. Process. Landforms; 2008; 33: 1614–1621.

22 Y. Matsukura, C.T. Oguchi, N. Kuchitsu. Salt damage to brick kiln walls in Japan: spatial and seasonal variation of efflorescence and moisture content. Bull Eng. Geol. Env.; 2004; 63: 167-176.

23 S.S.Seo, S.M. Son, C.H.Lee, K.K. Baek. Compositional analysis of soluble salts in bresle extraction from blocks in newbuildings shipyards. Shipbuilding Tech. ISST.; 2007: 65-70.

24 J.A. Carrero, I. Arrizabalaga, J. Bustamante, N. Goienaga, G. Arana, J.M. Madariaga. Diagnosing the traffic impact on roadside soils through a multianalytical data analysis of the concentration profiles of traffic-related elements. Scienc. Total Environ.; 2013; 458-460: 427-434.

25 H.Viles, A. Goudie, S. Grab, J. Lalley. The use of the Schmidt Hammer and Equotip for rock hardness assessment in geomorphology and heritage science: a comparative analysis. Earth Surf. Process. Landforms; 2010; 36: 320–333.

rebounds. The velocity before impact (V) and after impact (V2) are measured automatically and displayed as a ratio (V2/V), which can be denoted by the unit 'L' or Leeb Hardness (HL).

The measurements were taken, without any surface pre-treatment. The average of 10 individual measurements was taken as an indicative of the hardness of the surface and thus, by implication, the degree of weathering suffered by the material.

3.2.1.2. Colour measures: CM-700d Spectrophotometer

In some studies, a spectrophotometer (CM-700d, Konica Minolta Sensing, USA) was used to take colour measures of stone surface following the guidelines of the International Commission on Illumination (CIELAB 2000). The handheld instrument has a color LCD screen, in which spectral colour graphs are displayed at the same time that in situ measurement (Fig. 3.3 b).

In this way, to determine the change produced in the samples, hue (colour), lightness (brightness) and saturation (vividness) average measurements were performed pre and post exposure to obtain the L*a*b* colour space values, where L* indicates lightness and a*b* the chromaticity coordinates[26]. D65 standard illuminant as well as the light trap conditions required in each case (Specular component excluded, SCE, or specular component included, SCI) were used.

Besides, the SpectraMagic NX software version 2.52 (Konika Minolta, USA) is compatible so target data of the primary measurements can be associated to two or more secondary targets, allowing users to check for color difference. Moreover, it has the option of the reflectance curve study, in which it is possible to separate the light reflected from the sample with a diffraction grating, measuring the spectral reflectance at each wavelength or in each wavelength range using multiple sensors.

The calibration was performed using the White and Black references caps in accordance with the aperture used (the smallest, SAV, or the biggest, MAV) in each case according to the sample size.

3.2.1.3. Laser Scanner 3D: VI-91 3D Digitizer

The triangulation HD-laser scanner (VI-91 3D Digitizer, Konica Minolta, USA) (Fig. 3.3 c) is portable and scans from a distance of approximately 0.6 to 1m, with a resolution of 0.05mm.

26 CIE. Technical Report Colorimetry. Vienna: CIE Central; 2004.

The equipment uses series of interchangeable lenses to focus the scan area and increase (or decrease) resolution, as needed. The 3D laser scanning uses a 'triangulation light block' method that allows the acquisition of 3D measurements and the collection of approximately 300 000 points per scan.

Thanks to Polygon Editing software version 2.30 (Konica Minolta, USA), separate scans are tied together using shape-fitting algorithms and target-based registration. Once scanned and registered, triangular irregular network (TIN) models of each sample are created at the highest resolution possible. Then, the equipment offers several possibilities such as generate a computer-aided design (CAD) model for rapid prototype printing or quantification of morphologic features at a range of scales (from micrometers to meters).

Figure 3.3. Images of portable analytical equipments used to measure physic parameters. a) Rock surface hardness rebound device, Proceq Equotip 3. b) CM-700d Spectrophotometer of Konica Minolta Sensing. c) HD-laser scanner, Konica Minolta (VI-91 3D Digitizer).

3.2.1.4. X-Ray Fluorescence Spectroscopy: X-MET5100

To determine the average composition of the materials, a semiquantitative in situ analysis was carried out using a portable XRF spectrometer (X-MET5100, Oxford Instrument, UK) (Fig. 3.4 a). The equipment has an X-ray Rhodium tube that provides a 40 kV voltage.

The calibration was performed with the method of Fundamental Parameters (FP), general for different type of materials (non standard calibration). Thus, the relative percentages obtained were compared with the values calculated from the areas of each spectrum.

3.2.1.5. Raman micro-spectrometer: InnoRamanTM

The determination of the molecular composition of the materials was carried out by means of a portable (handheld) Raman spectrometer (B&WTEK inc., InnoRam, Newark, USA) (Fig. 3.4 b).

The spectrometer works with a 785 nm excitation laser of variable power to control thermal decomposition of the measured surfaces. The probe offers also the possibility to perform microscopic analysis by using optical lenses (4x, 20x and 50x), which allows measuring areas of diameters between 10 and 200 μm. For this purpose, the probe can be installed in a manually controlled mobile platform to focus on the target area or it can be put up on a motorized tripod that allows making microanalyses even in areas located higher than 2 meters from the floor.

A daily calibration was performed using the band at 520.5 cm^{-1} of a silicon chip. The spectra were collected in a fix spectral range from 3000 to 175 cm^{-1} with a resolution of 3.5 cm^{-1}, using integration times from 1 to 6 seconds and 5 to 40 accumulations to improve the signal to noise ratio.

Data acquisition was carried out with the software B&WTEK Version 3.26 (Newark, USA) and the Raman spectra were processed with the Omnic Version 7.2 software Thermo Nicolet (Madison, WI, USA). The interpretation was done using the e-VISART[27], e-VISARCH[28] and e-VISNICH[29] dispersive Raman and FT-Raman spectra databases as well as the RUFF online spectra database[30].

27 K. Castro, M. Pérez-Alonso, M.D. Rodríguez-Laso, L.A. Fernández, J.M. Madariaga. On-line FT-Raman and dispersive Raman spectra database of artists' materials (e-VISART database). J. Anal. Bioanal. Chem.; 2005 ; 382 : 248-258.

28 M. Pérez-Alonso, K. Castro, J.M. Madariaga. Investigation of degradation mechanisms by portable Raman spectroscopy and thermodynamic speciation: the wall painting of Santa María de Lemoniz (Basque Country, North of Spain). J. Anal. Chim. Acta.; 2006 ; 571: 121-128.

29 M. Maguregui, N. Prieto-Taboada, J. Trebolazabala, N. Goienaga, N. Arrieta, J. Aramendia, L. Gomez-Nubla, A. Sarmiento, M. Olivares, J. A. Carrero, I. Martinez-Arkarazo, K. Castro, G. Arana, M. A. Olazabal, L. A. Fernandez, J. M. Madariaga. Dispersive Raman spectra database of original and decayed materials belonging to the Natural, Industrial and Cultural Heritage (e-VISNICH database). Chemch Congress ; 2010: 168.

30 R. T. Downs, Program and Abstracts of the 19th General Meeting of the International Mineralogical Association in Kobe, 2006: 13.

3.2.1.6. Diffuse Reflectance Infrared Fourier Transform handheld (DRIFT) spectrometer: 4100 Exoscan

In situ diffuse reflectance spectra were acquired with a handheld FTIR spectrometer (4100 Exoscan, Agilent, Santa Clara, USA) (Fig. 3.4 c) with a diffuse reflectance sampling interface recording short acquisition times and 32 accumulations. The Michaelson interferometer has a maximum resolution of 4 cm^{-1} and a maximum spectral range of 4000–600 cm^{-1}. The system has a ZnSe beam splitter and a DTGS detector. The background is acquired with a diffuse gold reference cap.

The spectra treatment were performed using Omnic Version 7.2 software Thermo Nicolet (Madison, WI, USA) and the interpretation were done using the existing database e-VISNICH[28].

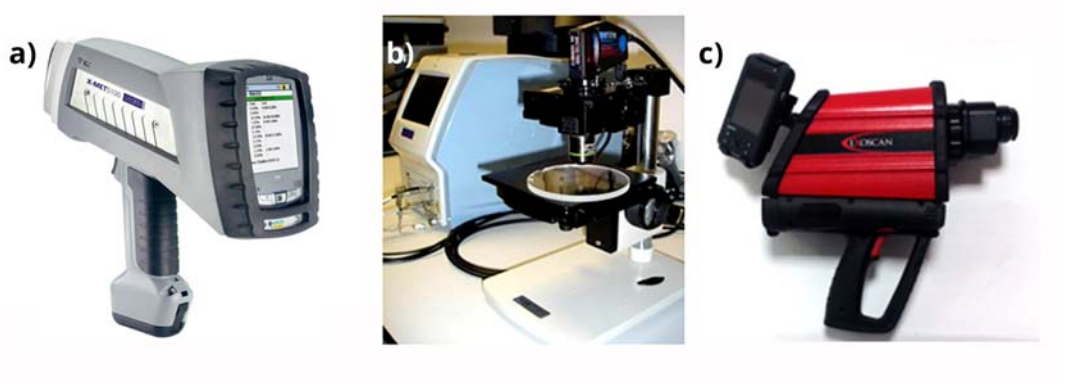

Figure 3.4. Images of portable analytical equipments used to carry out the in situ studies of building material. a) XRF spectrometer, X-MET510. b) Ultramobile Raman spectrometer, InnoRam, B&WTEK inc. c) 4100 Exoscan handheld FTIR spectrometer.

3.2.2. Non destructive analytical techniques: laboratory instruments

3.2.2.1. Microscope pictures: Leica MZ10F and Veho VMS-004

To take pictures of the surface of the samples, as well as to observe changes in porosity or material loss, a Microscope (Leica MZ10F, Germany) with a camera (DP300 DeltaPix, Maalov, Denmark) coupled was used.

The instrument offers a zoom ratio of 10:1 and a magnification from 8 to 80x with a maximum resolution of 1.33 µ. The illumination system has a TripleBeam technology with automatic adjustment to the field of view.

The treatment of the images was done using DeltaPIX InSight software version 4.1.2 (Maalov, Denmark).

Additionally, for field testing was used an USB Microscope Camera (Veho discovery VMS-004 Deluxe, UK). The instrument has a magnification of 20X, extendable by coupling lenses to 400X.

3.2.2.2. Micro-Energy Dispersive X-Ray Fluorescence Spectroscopy (μ-EDXRF): ArTax

The elemental composition of the samples was analyzed in the laboratory using a μ-XRF spectrometer (ArtTax, Rontec, nowadays Brucker AXS, Berlin, Germany) (Fig. 3.5 a).

A 50 kV voltage, 0.6 mA current, 1000 s and 0.65 mm tantalium collimator were used as measurement conditions. This equipment has a molybdenum X-ray tube, a special Xflash detector (5 mm^2) and it is provided with a measuring head implemented on a CCD camera that allows focusing on the sample by a motorised XYZ positioning unit controlled by the computer.

Previous to the analysis, the equipment was calibrated with a bronze standard. Moreover, the equipment offers the possibility of using a helium flow, necessary to identify the lightest elements.

All the spectra processing and manipulation was carried out by using ArtTAX software version 4.9.13.2 (Bruker AXS, Berlin, Germany). In addition, the program presents the possibility of perform automatic elemental maps, thanks to the monitored movement of the axes. To represent by a graph of color gradient the information obtained, Surfer[31] software version 10.7.972 (Colorado, USA) was used.

3.2.2.3. Scanning Electron Microscope-Energy Dispersive X-Ray Spectroscopy (SEM-EDS)

Prior to the analysis, the samples were covered with carbon or gold particles of <20μm, in a sputter coater vacuum chamber (K550X Emitech, quorum Technologies $_{LTD}$, Sussex, UK) (Fig. 3.5 b) to improve the signals and resolution of the samples.

31 Surfer versión 10.7.972 Surface Mapping System, Golden Software INC. E.E.U.U.; 2012.

3.2.2.3.1. EVO®40 Scanning Electron Microscope

The surface or the cross section of the samples was analyses by Energy Dispersive Spectroscopy (EDS) mapping on Scanning Electron Microscopy (SEM).

An EVO®40 Scanning Electron Microscope (Carl Zeiss NTS GmbH, Germany) coupled to an X-Max Energy-Dispersive X-Ray spectroscopy equipment (Oxford Instruments, UK) was used for electron image acquisitions and elemental composition (Fig. 3.5 c). The SEM images were acquired at high vacuum employing an acceleration voltage of 20 kV. The elemental mapping analysis (EDS) was performed using a 9 mm working distance, a 35° take-off angle and an acceleration voltage of 20 kV.

3.2.2.3.2. JEOL JSM Scanning Electron Microscope

A Jeol Scanning Electron Microscope (JSM-5910, USA) was used coupled with energy dispersive X-ray fluorescence spectrometer equipment (Oxford Instruments, UK) for electron image acquisitions and elemental composition. The SEM images were acquired at high vaccum employing an acceleration voltage of 15 kV.

For both equipments, the treatment of the data was performed with INCA Microanalysis Suite software version 4.3 (Oxford Instruments, Oxfordshire, UK).

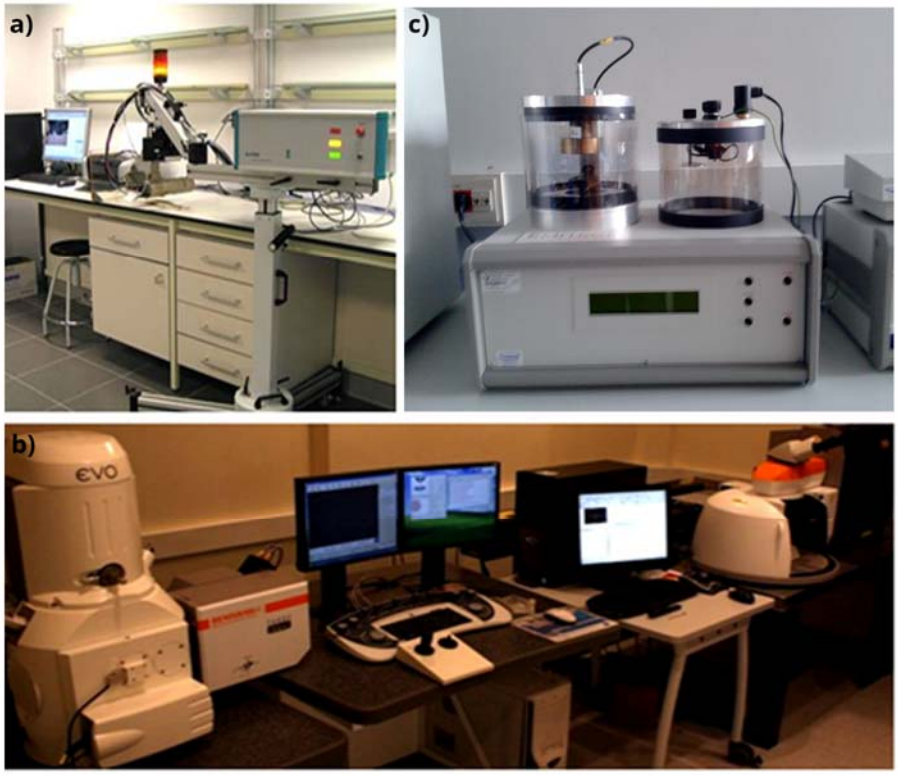

Figure 3.5. a) μ-XRF portable spectrometer ArtTax. b) Emitech K550x vacuum chamber. c) General view of the EVO®40 Scanning Electron Microscope coupled to X-Max Energy-Dispersive X-Ray spectroscopy equipment.

3.2.2.4. Raman micro-spectroscopy

3.2.2.4.1. Renishaw RA100 spectrometer

To study in depth the microsamples taken, the laboratory Raman spectrometer used was a Renishaw Raman spectrometer (RA100, Gloucestershire, UK) (Fig. 3.6 a) which has a 785 nm excitation laser. For, the microscopic analysis, 20x and 50x long-range lenses were also used mounted on a micro-video camera.

Spectra were collected from a variable range from 100 to 3500 cm-1. The exposure time for each spectrum ranged from 5 to 10 seconds and they were accumulated between 10 to 35 times in order to improve the signal-to-noise ratio. In addition, the laser power on the sample was attenuated to avoid thermal decomposition.

The instrument was calibrated daily with the 520 cm^{-1} Raman band of a crystalline silicon chip. Spectral acquisition was performed using Renishaw Wire software version 3.2 (Gloucestershire, UK).

3.2.2.4.2. Renishaw InVia confocal spectrometer

As additional laboratory equipment, for situations where resolution was critical to obtain good Raman spectra for samples with several compounds, a Renishaw InVia Raman spectrometer coupled to a Leica DMLM (UK) (Fig. 3.6 b, c) microscope with a diode lasers of 514 and 785 nm excitation wavelength and a Peltier cooled CCD detector was used for laboratory analyses.

The equipment was daily calibrated with the 520.5 cm^{-1} silicon band. In order to avoid thermal decomposition of the samples, the laser power (500 mW) was varied at 1%, 10% and 100% depending on measurements. The spectra were taken with a resolution of 1 cm^{-1} in the ranges of 2200–175 cm^{-1} or 1500-175 cm^{-1}, accumulating several scans from each spectrum to improve the signal-to-noise ratio. The microscope lenses 20x and 50x were used to focus the laser beam perfectly (approximately 10–200 μm spot) using a TV microcamera.

Data acquisition was carried out by the Wire software version 3.2 package of Renishaw (Gloucestershire, UK) and

The Raman spectra obtained, by the different equipments, were processed with the Omnic software version 7.2 (Thermo Nicolet, Madison, WI, USA) and their

interpretation was done using the e-VISART[32], e-VISARCH[33] and e-VISNICH[34] dispersive Raman and FT-Raman spectra databases as well as the RUFF online spectra database[35].

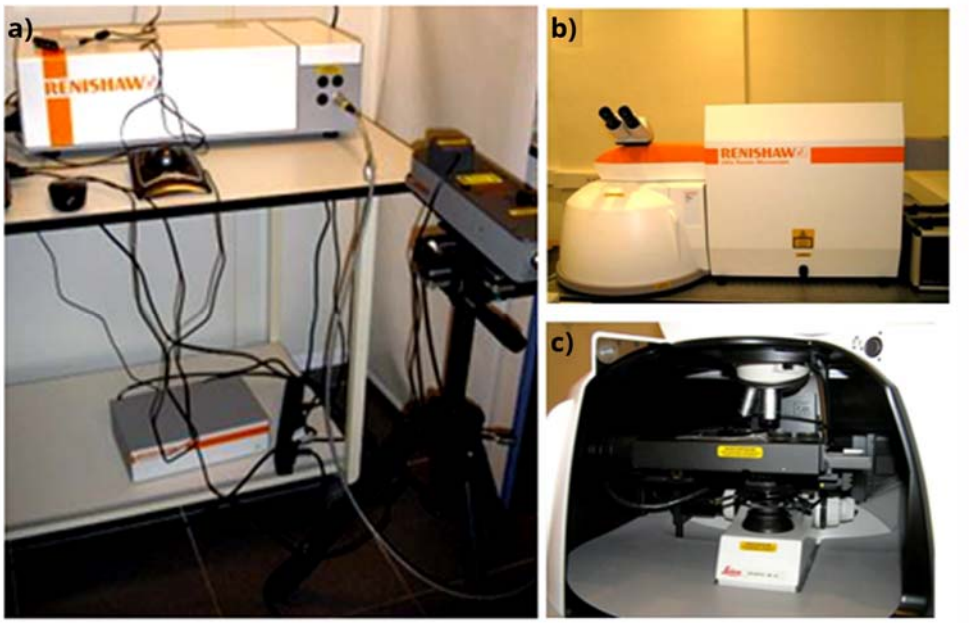

Figure 3.6. Images of Raman laboratory equipments. a) The Renishaw RA100 spectrometer. b-c) The Renishaw InVia confocal micro spectrometer

3.2.2.5. Diffuse Reflectance Infrared Fourier Transform (DRIFT) Spectroscopy: Jasco 6300

The laboratory instrument used to study more in detail the samples was a Jasco 6300 FTIR spectrophotometer, equipped with a diffuse reflection attachment

32 K. Castro, M. Pérez-Alonso, M.D. Rodríguez-Laso, L.A. Fernández, J.M. Madariaga. On-line FT-Raman and dispersive Raman spectra database of artists' materials (e-VISART database). Anal. Bioanal. Chem.; 2005; 382: 248-258.

33 M. Pérez-Alonso, K. Castro, J.M. Madariaga. Investigation of degradation mechanisms by portable Raman spectroscopy and thermodynamic speciation: the wall painting of Santa María de Lemoniz (Basque Country, North of Spain). J. Anal. Chim. Acta.; 2006; 571: 121-128.

34 M. Maguregui, N. Prieto-Taboada, J. Trebolazabala, N. Goienaga, N. Arrieta, J. Aramendia, L. Gomez-Nubla, A. Sarmiento, M. Olivares, J. A. Carrero, I. Martinez-Arkarazo, K. Castro, G. Arana, M. A. Olazabal, L. A. Fernandez, J. M. Madariaga. Dispersive Raman spectra database of original and decayed materials belonging to the Natural, Industrial and Cultural Heritage (e-VISNICH database). Chemch Congress, 2010: 168.

35 R. T. Downs, Program and Abstracts of the 19th General Meeting of the International Mineralogical Association in Kobe, 2006: 13.

(Jasco DR PR0410M, MD, USA) (Fig. 3.7), having the Michaelson interferometer a maximum resolution of 0.07 cm^{-1}.

All diffuse reflectance spectra obtained in the laboratory were collected in the middle infrared region (from 4000 to 400 cm^{-1}) recording 32 scans per spectrum at a spectral resolution of 4 cm^{-1}. The system has a Ge/KBr beam splitter and a DLATGS detector with Peltier temperature control.

KBr (99%, Sigma Aldrich, USA) powder was used as background and as diluent. All samples and standards were dispersed in KBr at proportions between 5% and 10% depending on the compound and then placed in the microsample cup to be measured[36].

Figure 3.7. Images of DRIFT laboratory equipment. a) FTIR spectrophotometer, 6300 Jasco. b) Difuse reflection module, DR PR0410M Jasco.

As in the case of in situ equipment, the spectra treatment were performed using Omnic software version 7.2 (Thermo Nicolet, Madison, WI, USA) and their interpretation was done using the existing database e-VISNICH[37].

36 I. Arrizabalaga, O. Gómez-Laserna, J. Aramendia, G. Arana, J.M. Madariaga. Applicability of a Diffuse Reflectance Infrared Fourier Transform handheld spectrometer to perform in situ analyses on Cultural Heritage materials. J. Spectrochim. Acta A; 2014; 129:259-267.

37 M. Maguregui, N. Prieto-Taboada, J. Trebolazabala, N. Goienaga, N. Arrieta, J. Aramendia, L. Gomez-Nubla, A. Sarmiento, M. Olivares, J. A. Carrero, I. Martinez-Arkarazo, K. Castro, G. Arana, M. A. Olazabal, L. A. Fernandez, J. M. Madariaga. Dispersive Raman spectra database of original and decayed materials belonging to the Natural, Industrial and Cultural Heritage (e-VISNICH database). Chemch Congress , 2010: 168.

3.2.3. Quantitative analytical techniques

3.2.3.1. X-Ray Diffraction (XRD)

The XRD analysis of the ground sample was performed with a powder diffractometer (PANalytical Xpert PRO, Ankara, Turkey), equipped with a copper tube ($\lambda Cu_{K\alpha\ mean}$= 1.5418 Å, $\lambda Cu_{K\alpha 1}$= 1.5406 Å, $\lambda Cu_{K\alpha\ 2}$= 1.54439 Å), vertical goniometer (Bragg-Brentano geometry), programmable divergence aperture, automatic interchange of samples, secondary monochromator from graphite and PixCel detector. The measurement conditions were 40 kV and 40 mA, with an angular range (2Θ) scanned between 5 and 70°.

For the data treatment of the diffractograms and the identification of the mineral phases present, the specific X'pert HighScore software (PANalytical, Ankara, Turkey) in combination with the specific powder diffraction file (PDF2) database (International Centre for Diffraction Data- ICCD, Pennsylvania, USA) was used.

3.2.3.2. Ion Chromatography (IC)

The quantification of soluble salt content was carried out by a Dionex ICS 2500 (Sunnyvaley, CA, USA) suppressed ion chromatography (IC) with a conductivity detector ED50 (Fig.3.8 a).

An external calibration from standard solutions of 1000 mg/L (Sigma Aldrich, USA) for anions (F^-, Cl^-, NO_3^-, SO_4^{-2}, ...) and 100 mg/L (Merck, Germany) for cations (Na^+, K^+, Mg^{+2}, Ca^{+2}, NH_4^+, ...) was used. The samples were treated in triplicate and blanks were used.

For the separation of anions, an IonPac AS23 (4x250 mm) column and IonPac AG23 (4x50 mm) precolumn were used. As mobile phase, solutions of 4.5 mM Na_2CO_3/0.8 mM $NaHCO_3$ were selected. The conditions of suppression current and flow applied were 25 mA and 1 mL/min, respectively. The quantification of cations was conducted by an IonPac CS12A (4x250 mm) column and IonPac CG-12A (4x50 mm) precolumn from Vertex. As mobile phase, a solution of 20 mM CH_4SO_3 was selected. The suppression current and flow applied were 50 mA and 1 mL/min, respectively.

The data processing was performed by means of the Chromaleon software version 6.60-SPla (Dionex, Sunnyvaley, CA, USA).

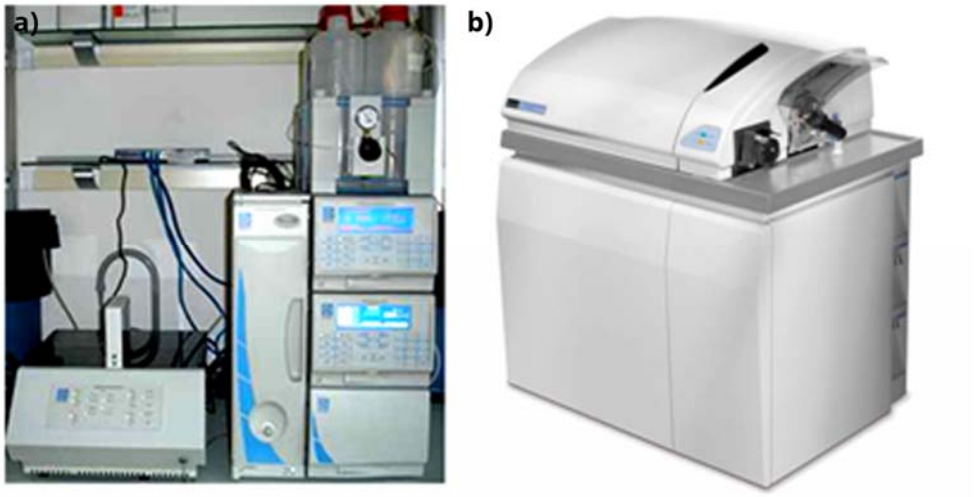

Figure 3.8. Images of micro-destructive analytical techniques used. a) The Dionex ICS 2500 Ion Chromatographic system with an ED50 conductivity detector coupled to an AS40 autosampler. b) Elan 9000 inductively coupled plasma-mass spectrometer.

3.2.3.3. Inductive Coupled Plasma Analyzer (ICP-MS)

To carry out a quantitative analysis of metals, ICP-MS standard solutions were prepared from Alfa Aesar (Specpure®, Plasma standard solution, Germany) stock solutions and argon (99,999%, Praxair, Spain) was used as gas in the ICP-MS measurements by an Elan 9000 ICP-MS (Perkin Elmer, Ontario, Canada) (Fig. 3.8 b) provided with a Ryton cross-flow nebulizer, a Scott-type double pass spray chamber and standard nickel cones.

Preparation of calibrants as well as analysis of samples was carried out in a clean room (class 100). The samples were treated in triplicate and blanks were used.

The Elan software version 3.2 (Ontario, Canada) was used to analyze the data obtained.

3.3. Programs of Chemometrics and Thermodynamic modelling

The quantitative data were analyzed through chemometric models to identify their main correlations. In this way, The Unscrambler[38] software version 9.2 s (CAMO Process AS, Oslo, Norway) was used.

38 Unscrambler ® version 9.2, Camo Process As. Norway; 2005.

For that purpose, to complete the ion chromatography results, miliequivalents (meq) of carbonate were estimated following the equation:

$$\Sigma \text{ (meq cations)} - \Sigma \text{ (meq anions)} = \text{meq (carbonate)}$$

Complementary to that estimation, the carbonate content of the samples was correctly checked by an automated system for potentiometric titrations[39] and the Unscrambler results were complemented by correlation analysis of excel software (Microsoft Office 2007).

In addition, the chemical and thermodynamic modeling of the new degradation compounds was carried out using Chemical Equilibrium Diagrams and information on stability constants, included in the free academic programs HYDRA (Hydrochemical Equilibrium Constant) and Medusa[40] (Make Equilibrium Diagrams Using Sophisticated Algorithms) software version 15 (Royal Institute of Technology, Stockholm, Sweden).

Finally, the quantitative data of soluble salt content were analyzed also by Runsalt[41] software version 1.9 (Davide Bionda, Zürich), a graphical user interface to the ECOS[42] thermodynamic model for the prediction of the behaviour of salt mixtures under changing climate conditions.

For those proposes, the atmospheric chemical conditions used for the modeling were taken in situ or obtained from the officials air-quality monitoring stations[43-45]. Besides, to improve the models, some physic-chemical parameters were measured on sample solutions using different electrodes (52-02 Crison electrode for pH measurements and 52–61 Crison for the redox potential).

39 R. Cazallas, L.A. Fernández, N. Etxebarria, J.M. Madariaga. Automated system for multiple potenciometric and spectrophotometric titrations. J. Lab. Robotics Automat.; 1993; 5: 161-169.

40 MEDUSA (Make Equilibrium Diagrams Using Sophisticated Algorithms), I. Puigdomenech., Department of Inorganic chemistry, the Royal Institute of Technology (KTH). Stockholm, Sweden:2009.

41 Runsalt website (2015): http://science.sdf-eu.org/runsalt/

42 C. A. Price. An expert chemical model for determining the environmental conditions needed to prevent salt damage in porous materials. London: European Commission Research (Protection and Conservation of European Cultural Heritage), Archetype Publications; 2000.

43 AEMET (Agencia Estatal de Meteorología, Ministerio de Medio Ambiente y Medio Rural y Marino), Gobierno de España. N.I.P.O. 784-10-001-5.

44 Euskalmet (Agencia Estatal de Meteorología), Gobierno Vasco.

45 Met Office (State Meteorological Agency), United Kingdom.

CHAPTER 4: THE VALIDATION OF THE ANALYTICAL METHODOLOGY BASED ON THE IN SITU SPECTROSCOPIC ASSESSMENT OF AN OPERATIONAL ENVIROMENT: THE CASE OF BASOZABAL PALACE

As is explained in chapter 1, the process of stone decay occurs in different ways. Sometimes it can be gradual, leaving a firm surface. Other times, it can lose its integrity and disintegrate. Even when the material appears to be in perfect conditions, it could have lost its cohesion beneath the surface. Moreover, one of the most harmful effects over construction materials that can be overlooked is caused by soluble salts[1-4].

Hence, the characterization of salts of the stone[5], in its particular environment, could be the first step to understand the chemical mechanism responsible for the

1 A.S. Goudie, H. Viles. Salt weathering hazards. Chichester, UK: Wiley; 1997.

2 C.R. Navarro, E. Doehne, E. Sebastian. How does sodium sulfate crystallize? Implications for the decay and testing materials. J. Cement Concrete Res.; 2000; 30: 1527-1534.

3 I. Martínez Arkarazo, M.A. Angulo, L. Bartolomé, N. Etxebarria, M.A. Olazabal, J.M. Madariaga. An integrated analytical approach to diagnose the conservation state of building materials of a palace house in the metropolitan Bilbao (Basque Country, North of Spain). J. Anal. Chim. Acta; 2007; 584: 350-359.

4 M. Gómez Heras, B.J. Smith, H. Viles ,J. Meneely, S. McCabe. HD Laser scanning for the evaluation of salt decay laboratory simulations of building limestone. Copenhagen: Proceedings SWBSS; 2008.

5 G.W. Scherer. Crystallization in pores. J. Cement concrete Res.; 1999; 29: 1347-1358.

material deterioration. It could provide valuable information for the selection of the appropriate restoration and conservation procedures procuring a solution to the cause of the problem from its source rather than simply treating the symptoms.

Therefore, nowadays, the development of new diagnostic methodologies has gained importance in the field of material characterization. Moreover, given the intrinsic value of the cultural heritage samples, the usefulness of non invasive methods that can be used in situ preserving the integrity of materials must be highlighted. In this sense, innovative researches are focused on developing novel study protocols[6-8] that allow performing fast scientific diagnosis, helpful for the restoration or conservation procedures and thanks to them, the need to take decisions only in terms of the expertise of the conservators could be avoided[9-10].

Taking into account these requirements, recent publications suggest the use of spectroscopic techniques as convenient tools for the analysis of this kind of matrices, pointing out the use of Raman spectroscopy and X-ray fluorescence as good combination to assess the conservation state of cultural heritage materials, since both techniques may supply complementary information in a non destructive manner[10-13].

For these reasons, this chapter examines in depth the validity of in situ Raman spectroscopic studies for the diagnosis of the decay suffered by historic stone buildings.

---

6 E.R. Agudo, B. Lubelli, A. Sawdy, R.V. Hees, C. Price, C.R. Navarro. An integrated methodology for salt damage assessment and remediation: the case of San Jerónimo Monastery (Granada, Spain). J. Environ. Earth Sci.; 2011; 63: 1475-1486.

7 A. Arizzi, C. Giuseppe. The water transfer properties and drying shrinkage of aerial lime-based mortars: an assessment of their quality as repair rendering materials. J. Environ. Earth Sci.; 2014; 71: 1699-1710.

8 M.A. Vázquez, E. Galán, P. Ortiz, R. Ortiz. Digital image analysis and EDX SEM as combined technique to evaluate salt damp on walls. J. Constr. Build. Mater.; 2013; 45: 95-105.

9 M. Pérez-Alonso, K. Castro, M. Álvarez, J.M. Madariaga. Scientific analysis versus restorer´s expertise for diagnosis prior to a restoration process: the case of Santa Maria Church (Hermo, Asturias, North of Spain). Anal. Chim. Acta; 2004; 524: 379-389.

10 K.S. Andrikopoulos, S. Daniilia, B. Roussel, K. Janssens. In vitrovalidation of mobile Raman-XRF microanalytical instruments capabilities on the diagnosis of Byzantine icons. J. Raman Spectrosc.; 2006; 37: 1026- 1034.

11 W. Fremout, S. Saverwyns, F. Peters, D. Deneffe. Non-destructive micro-Raman and X-ray fluorescence spectroscopy on pre-Eyckian works of art-verification with the results obtained by destructive methods. J. Raman Spectrosc; 2006; 37: 1035-1045.

12 G. Paternoster, R. Rinzivillo, F. Nunziata, E. M. Castellucci, C. Lofrumento, A. Zoppi, A. C. Felici, G. Fronterotta, C. Nicolais, M. Piacentini, S. Sciuti, M. Vendittelli. Study on the technique of the Romana ge mural paintings by micro-XRF with Polycapillary Conic Collimator and micro-Raman analyses. J. Cult. Herit.; 2005; 6: 21-28.

13 M. Aceto, A. Agostino, G. Fenoglioc, M. Gulmini, V. Bianco, E. Pellizzif. Non invasive analysis of miniature paintings: Proposal for an analytical protocol. J. Spectrochim Acta A; 2012; 91: 352–359.

To achieve this purpose, the present study was established in three phases; firstly, a contextualization of the main spectroscopic technique used was performed. Then, a complete in situ spectroscopic assessment of the conservation state of a historic Palace House was carried out and, finally, a quantitative study was performed to corroborate the usefulness of the spectroscopic techniques used and evaluate the origin and severity of damage caused in the Palace.

4.1. State of the Art

To contextualize the technique, the fundamental theoretical bases as well as its applicability to study pathologies of building materials induced by the main common stressors were included in this section. In addition, through various practical cases, their advantages and disadvantages of application were studied in detail and its corresponding book chapter can be consulted in the scientific publication Annex.

4.1.1. Background of Raman spectroscopy

In order to understand the benefits of Raman spectroscopy in this field it is necessary to start defining it as a technique based on the study of the molecular vibrations produced by light scattering[14]. Those vibrations can be seen in the Raman spectrum only if there is a change in polarizability; that is, merely a distortion of the electron cloud around the vibrating atoms is required. The Raman scattering occurs when radiation from a source is passed through a sample and some of the radiation is scattered by the molecules present. For simplicity, it is better to use a radiation of only one frequency that the sample should not absorb. In this way, the beam of radiation is dispersed in the space and three types of scattering occur.

Rayleigh scattering is the most common and has the same frequency as the source of radiation. It occurs as a result of elastic collisions between the photons and the molecules in the sample, although no energy is lost in the collisions. A slight interaction between the incident beam and the molecules can be observed and after that interaction, few photons (0.001%) are scattered. Raman-Stokes lines are produced by those photons scattered with less energy than the incident radiation and, on the other hand, Raman-antistokes lines belong to the photons scattered with more energy. In this manner, Raman spectrum is composed by stokes lines as Raman shift from the

14 T.D. Chaplin, R.J.H. Clark, M. Martinón-Torres. A combined Raman microscopy, XRF and SEM–EDX study of three valuable objects – A large painted leather screen and two illuminated title pages in 17th century books of ordinances of the Worshipful Company of Barbers, London. J. Mol. Struct.;2010; 976: 350-359.

Rayleigh scattering, which is placed in zero position. The Raman signals generally are represented as Raman Intensity versus wavenumber (cm^{-1})[15-16].

Raman instruments use a laser as light source mainly because a high intensity beam of radiation is needed, as the fraction of scattered photons that suffer a frequency change is scarce. Thus, it is possible to obtain Raman scattering with high signal to noise ratio[17].

Lasers are UV, Visible or NIR, being most effective (in terms of sensibility) those with shorter wavelength according to the following expression: Intensity= $1/\lambda^4$. Nonetheless, the use of short wavelength lasers favors fluorescence (which results in a curvature of the baseline, with the subsequent difficulties on band assignment) and photodecomposition of the sample[18]. If the frequency of the laser beam is close to the frequency of an electronic transition, the resonance effect is produced and scattering enhancements of up to 10^4 units have been observed. When this resonance condition occurs, new Raman bands are visible in the spectrum. For these reasons, Raman spectroscopy becomes a much more sensitive technique and, since cromophore molecules show the most efficient scattering, it will be selective for this kind of molecules of the sample.

In dispersive systems, with a visible laser as a source, the most common detectors are photomultiplier tubes. Instead, multichannel instruments use photodiode array (PDA), current injected detector (CID), or charge-coupled device (CCD) detectors (Fig.4.1). Nowadays, the selection of the suitable detector determines the speed of the measurement, the spectral range and sensitivity of the technique[19].

15 J.W. Robinson, E.M. Skelly Frame, G.M Frame II. Undergraduate instrumental analysis, New York: Marcel Dekker; 2005.

16 E. Smith, G. Dent. Modern Raman Spectroscopy - A Practical Approach,UK: Wiley; 2005.

17 E. Fouad. Coherent anti-Stokes Raman scattering: Spectroscopy and microscopy. Vibrational Spectrosc.; 2011; 55: 1-37.

18 C. Gooijer, A.J.G. Mank. Laser spectroscopy in analytical chemistry. Anal. Chim. Acta; 1999; 400: 281-295.

19 S. Jimenez-Sandoval. Micro-Raman spectroscopy: a powerful technique for materials research. J. Microelectron.; 2000; 31: 419-427.

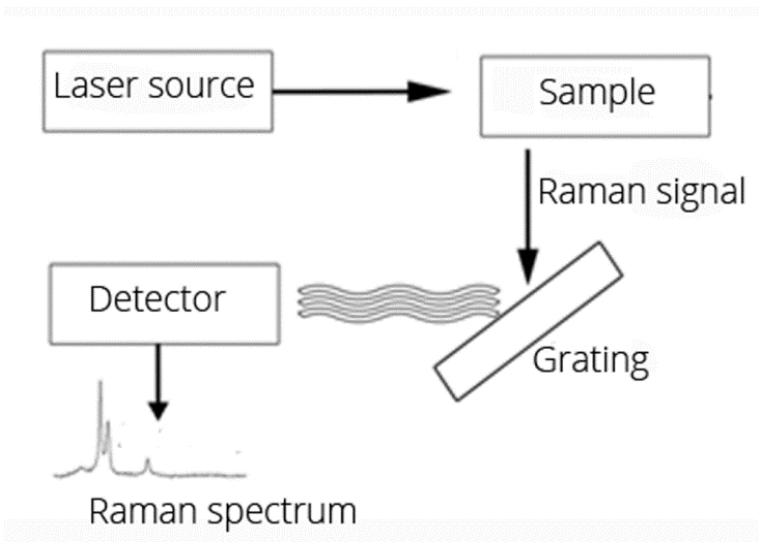

Figure 4.1. Raman spectrometer diagram.

Concerning applications of Raman spectroscopy, it presents several advantages respect to other analytical tools. It is a non destructive technique that requires little or no preparation of the sample. In the field of cultural heritage, one of the biggest advantages is the possibility of carrying out in situ analysis[20]. It is possible to measure different types of samples like compact solids (amorphous and crystalline) or even liquid, gels, films and gases by simply placing them under the laser beam. It has a wide spectral range with a high chemical specificity, therefore, the Raman peaks are easily related to the structure of compounds. It also allows the discrimination between different cations bound to the same anion and polymorphic compounds such as calcite and aragonite as can be observed in Figure 4.2. Both have the same molecular formula, $CaCO_3$, but they belong to different crystal systems (trigonal and rhombic, respectively). In addition, Raman spectroscopy can distinguish between compounds having different numbers of hydration water as in the cases of gypsum ($CaSO_4 \cdot 2H_2O$), hemihydrate ($CaSO_4 \cdot 0.5H_2O$) and anhydrite ($CaSO_4$).

20 J.W. Robinson, E.M. Skelly Frame, G.M Frame II. Undergraduate instrumental analysis, New York: Marcel Dekker; 2005.

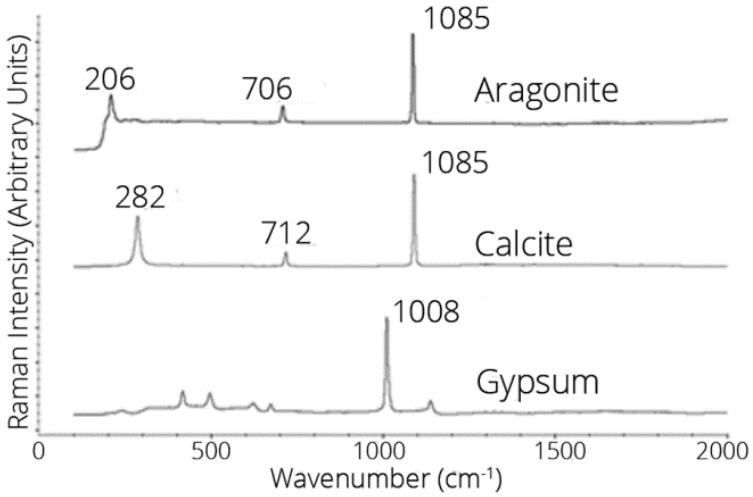

Figure 4.2. Raman spectra showing differences among polymorphous compounds (aragonite and calcite) and shift due to the presence of different functional groups, carbonates versus sulphates.

The applications of Raman spectroscopy are not only qualitative but can also be semiquantitative. Initially, it was used to examine inorganic compounds but its use is growing in organic and polymer analysis[21-23]. For example, it is used for bulk material characterization, online process analysis, remote sensing, microscopic analysis and chemical imaging[24-31]. More recently, it is spreading in pharmaceutical applications,

21 H.D. Lutz, H. Haeuseler. Infrared and Raman spectroscopy in inorganic solids research. J. Mol Struc.; 1999; 511-512: 69-75.

22 D.S Moore, S.D. McGrane. Comparative infrared and Raman spectroscopy of energetic polymers. J. Mol. Struct.; 2003; 661-662: 561-566.

23 D.S Moore, S.D. McGrane. Comparative infrared and Raman spectroscopy of energetic polymers. J. Mol. Struct.; 2003; 661-662: 561-566.

24 S. Jimenez-Sandoval. Micro-Raman spectroscopy: a powerful technique for materials research. J. Microelectron.; 2000; 31: 419-427.

25 I. Martínez-Arkarazo, M. Angulo, O. Zuloaga, A. Usobiaga, J.M. Madariaga. Spectroscopic characterisation of moonmilk deposits in Pozalagua tourist Cave (Karrantza, Basque Country, North of Spain). Spectrochim. Acta A; 2007; 68: 1058-1064.

26 I.E. Wachs, J. Jehng, G. Deo, B.M. Weckhuysen, V.V. Guliants, J.B. Benziger. In situ Raman spectroscopy studies of bulk and surface metal oxide phases during oxidation reactions. Catal. Today; 1996; 32: 47-55.

27 S. Sahu, D.L. Exline, M.P. Nelson. Identification of thaumasite in concrete by Raman chemical imaging. Cement Concrete Comp.; 2002; 24: 347-350.

28 R.H. Brody, E.A. Carter, H.G.M Edwards, A.M. Pollard. FT-Raman Spectroscopy, Applications. Encyclopedia of Spectroscopy and Spectrometry, Oxford, UK: Academic Press; 1999.

29 T. Lana-Villarreal, J.M. Pérez, R. Gómez. Surface enhanced Raman spectroscopy for adsorption studies on semiconductor nanostructured films. Surf. Sci.; 2004; 572: 329-336.

while other applications have been successfully established in characterization of pigments, semiconductors, art materials, archaeology and biotechnology[32].

In the particular case of building materials, Raman spectroscopy has demonstrated to be a powerful technique that allows characterizing both original and decaying compounds. The identification of decaying compounds formed as a consequence of the environmental impact (atmospheric pollution, infiltration waters or microorganisms) is decisive to define the conservation state and the impacts suffered by the original materials.

Generally, the alteration caused by environmental stressors (Fig. 4.3) is an irreversible process of degradation that building materials are suffered. In this process, the crystallization of soluble salts inside the building materials is considered one of the most destructive damages[33-37], as it is detailed in chapter 1. These compounds are easily detectable by Raman spectroscopy, so the characterization of salts found in the pores and surface can be approached by this technique. This identification together with the experience of the researcher is critical to diagnose the chemical process leading to the deterioration.

30 A.M. Herrero, M.I. Cambero, J.A. Ordóñez, L. De la Hoz, P. Carmona. Raman spectroscopy study of the structural effect of microbial transglutaminase on meat systems and its relationship with textural characteristics. Food Chemistry; 2008; 109: 25-32.

31 R.S. Das, Y.K. Agrawal. Raman spectroscopy: Recent advancements, techniques and applications. Vibrational Spectrosc.; 2011; 57: 163-176.

32 J.M. Madariaga. Raman spectroscopy in art and archaeology. J. Raman Spectros.; 2010; 41: 1389-1393.

33 E. Doehne, C.A. Price. Stone conservation: An overview of current research, Los Angeles; Getty Conservation Institute; 2010.

34 V. Matović, S. Erić, A. Kremenović, P. Colomban, D. Serćković-Batoćanin, N. Matović. The origin of syngenite in black crust on the limestone monument King´s Gate (Belgrade Fortress, Serbia)-the role of agriculture fertilizer. J. Cult. Herit.; 2012; 13: 175-186.

35 R.M. Espinosa-Marzal, G.W. Scherer. Advantages in understanding damage by crystallization. Acc. Chem. Res.; 2010; 43: 897-905.

36 M. Steiger , S. Asmusse Crystallization off sodium sulphate in porous materials: the phase diagram Na_2SO_4-H_2O and the generation of stress . Geochim. Cosmochim. Ac.; 2008; 72: 4291-4306.

37 M.I. Sánchez de Rojas, N. García, M. Frías. Measurement of color in different construction materials. The restoration in sandstone buildings. Mater. Construcc.; 1998; 49: 31-49.

Figure 4.3. Deteriorations in buildings materials caused by soluble salts. a) Efflorescence in an embellishing mortar. c) detachments of the rendering mortar. b-d) subefflorescence in a brick.

Apart from the environmental agents, the major biodeterioration agents associated with decaying processes in these matrices are lichens and mosses. They contribute in these processes not only mechanically and physically, but also chemically. This chemical damage has been studied by Raman Spectroscopy in last years. This technique allows determining the original compounds of the support were microorganisms are settled together with decaying compounds related with their metabolic activity.

In the last years, the spectrometers have undergone a great development and, currently, several equipments offer different possibilities depending on the characteristics of the measurements or samples. Therefore, starting from the most sophisticated laboratory non portable equipments to easy to operate handheld spectrometers are available.

To demonstrate the usefulness and efficiency of Raman spectroscopy on the characterization of building materials as well as, to extend on the mentioned accounts, some examples of materials affected by the main decaying mechanisms are presented in the following subsections.

4.1.2. Performance of commercially available Raman spectrometers

Nowadays, different Raman spectrometers offering a wide range of characteristics are commercially available. The nature of the sample and the compounds to be determined establish the requirements of the instrument to be used. However, as it is going to be demonstrated, although spectra quality can be substantially improved by using laboratory equipments, it is not always necessary to perform laboratory analysis in order to get unambiguous results. In fact, portable instruments offer a good performance and besides, to analyze materials belonging to built heritage, the use of such instruments that allow non destructive in situ analyses is essential.

Although the efficiency of portable spectrometers still shows differences in comparison with laboratory equipments, in terms of identification, the great progress in this technique is noticeable if spectra obtained with handheld or portable spectrometers and those taken in the laboratory are compared (Fig. 4.4). Nowadays, in situ measurements can be made with resolutions up to 3.5 cm^{-1}, which is good enough as to differentiate among the most common degradation compounds cited previously. The problem comes when the signal to noise ratio, which is better in non portable equipments, is not so good to distinguish low intensity Raman bands produced by poor scattering compounds or by substances at low concentration levels. This consequence aggravates when compounds producing fluorescence effect are present in the sample.

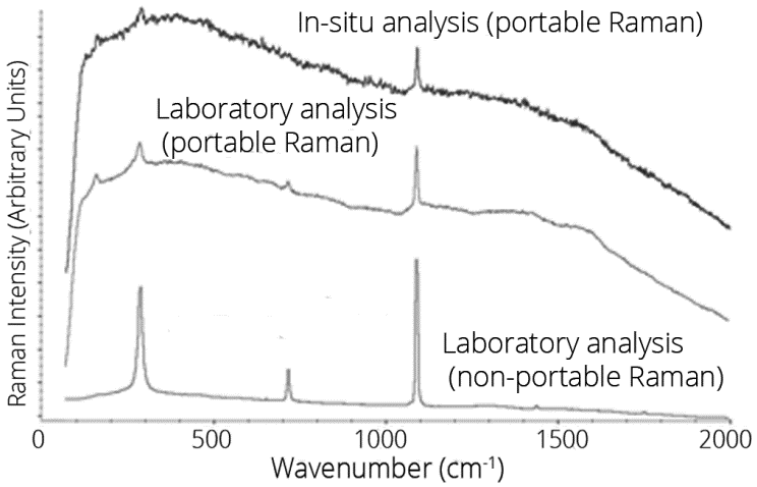

Figure 4.4. Comparison of the different spectra of calcite with portable and with a non portable spectrometer. The spectra are not treated or corrected in order to observe the differences.

On the other hand, the main disadvantages of in situ analysis are related with factors that not always can be controlled such as vibrations caused by traffic or wind, sunlight, etc. Thus, such factors can avoid correct spectral assignations or sometimes,

even disturb acquisition. For instance, the spectrum of the sunlight presents the most intense Raman bands in the spectral range where some sulphates are identified[38]. This is the case of coquimbite ($Fe_2(SO_4)_3 \cdot 9H_2O$) (Table 4.1), whose formation has been associated with polluted environments rich on particulate iron[39]. With regard to vibrations, they can render the analysis impossible if they take place at the moment of performing the measurement.

Usually, the information obtained with Raman equipments is sometimes complemented with the use of other non destructive techniques such as X-Ray fluorescence spectroscopy or infrared spectroscopy (IR). Portable equipments implementing those techniques have been developed as well. Thus, a combination of elemental and molecular information could be achieved by only carrying out in situ analysis. In this way, a complete methodology that meets the requirements for almost all fields of cultural heritage could be designed[40].

These equipments have allowed studying many types of materials and matrices, from building materials (sandstone, limestone, mortar, bricks, cement and concrete) to pigments on different supports, slags, food or geological materials such as sediments, beachrock or meteorites[41-43] . However, Raman spectroscopy is the decisive technique during diagnosis since it is the molecular spectroscopy providing specific information that allows the identification of compounds. Therefore, the results summarized in this section are focused on the Raman spectroscopic study of building materials and more specifically, on the assessment of the damage caused by the impact

38 I. Martinez-Arkarazo, U. Knuutinen, M. Maguregui, K. Castro, J.M. Madariaga. Analytica Pompeiana Universitatis Vasconicae: field multianalytical analyses in Pompeii. Book of Abstracts: 6th International Congress on the application of Raman spectroscopy in Art and Archaeology, Italy; Timeo Editore Bologna; 2011.

39 N. Prieto-Taboada, M. Maguregui, I. Martinez-Arkarazo, M. Olazabal, G. Arana, J.M. Madariaga. Spectroscopic evaluation of the environmental impact on black crusted modern mortars in urban–industrial areas. Anal. Bioanal. Chem.; 2010; 399: 2949-2959.

40 I. Martínez-Arkarazo, M. Angulo, L. Bartolomé, N. Etxebarria, M.A. Olazabal, J.M. Madariaga. An integrated analytical approach to diagnose the conservation state of building materials of a palace house in the metropolitan Bilbao (Basque Country, North of Spain). Anal. Chim. Acta; 2007; 584: 350-359.

41 M. Pérez-Alonso, K. Castro, I. Martínez-Arkarazo, M. Angulo, M.A. Olazabal, J.M. Madariaga. Analysis of bulk and inorganic degradation products of stones, mortars and wall paintings by portable Raman microprobe spectroscopy. Anal. Bioanal. Chem.; 2004; 379: 42-50.

42 M. Maguregui, A. Sarmiento, I. Martínez-Arkarazo, M. Angulo, K. Castro, G. Arana, N. Etxebarria, J.M. Madariaga. Analytical diagnosis methodology to evaluate nitrate impact on historical building materials. Anal. Bioanal. Chem.; 2008; 391, 1361-1370.

43 N. Arrieta, N. Goienaga, I. Martínez-Arkarazo, X. Murelaga, J.I. Baceta, A. Sarmiento, J.M. Madariaga. Beachrock formation in temperate coastlines: Examples in sand-gravel beaches adjacent to the Nerbioi-Ibaizabal Estuary (Bilbao, Bay of Biscay, North of Spain). Spectrochim. Acta A; 2011; 80: 55-65.

of atmospheric acid gases, water infiltration and biodeterioration in bricks and mortar of built heritage[44-46].

4.1.3. Deterioration due to atmospheric pollution

In order to explain the deterioration caused by the impact of air pollutants over these materials, it is interesting to describe briefly the deposition mechanisms of pollutants on construction materials. Dry deposition is said to occur when a contaminant is transferred from the atmosphere to the material, in the absence of rain, being more common in sheltered areas of the building[47-48]. However, wet deposition begins with the suspension of water in the atmosphere, where CO_2, SO_x and NO_x gases are converted into acid aerosols. Therefore, calcareous materials can be easily attacked and solubilized by these types of aerosols. Indeed, this problem is one of the main responsible for salts formation into construction materials. However, it should be noted that the effects from contaminants can be synergistic[49-51].

44 I. Ibarrondo, N. Prieto-Taboada, I. Martínez-Arkarazo, J.M. Madariaga. The Suitable Carotene and Xanthophyll Identification in Lecanora Lichens: Resonance Raman Spectroscopic Study. In: Lunar and Planetary Institute, editor. Conference on Micro-Raman and Luminiscence Studies in the earth and planetary sciences (CORALS II). Houston: Lunar and Planetary Institute (LPI) y Consejo Superior de Investigaciones Científicas (CSIC); 2011.

45 N. Prieto-Taboada, O. Gómez-Laserna, I. Ibarrondo, I. Martinez-Arkarazo, M.A. Olazabal, J.M. Madariaga. Cross-Section Analysis to Establish the Penetration Level of Atmospheric Pollution in Mortars. In: Lunar and Planetary Institute, editor. Conference on Micro-Raman and Luminiscence Studies in the earth and planetary sciences (CORALS II). Houston: Lunar and Planetary Institute (LPI) y Consejo Superior de Investigaciones Científicas (CSIC); 2011.

46 A. Sarmiento, M. Maguregui, I. Martínez-Arkarazo, M. Angulo, K. Castro, M.A. Olazábal, L.A. Fernández, M.D. Rodríguez-Laso, A.M. Mujika, J. Gómez, J.M. Madariaga. Raman spectroscopy as a tool to diagnose the impacts of combustion and greenhouse acid gases on properties of Built Heritage. J. Raman Spectrosc.; 2008; 39: 1042-1049.

47 M. Maguregui, A. Sarmiento, I. Martínez-Arkarazo, M. Angulo, K. Castro, G. Arana, N. Etxebarria, J.M. Madariaga. Analytical diagnosis methodology to evaluate nitrate impact on historical building materials. Anal. Bioanal. Chem.; 2008; 391, 1361-1370.

48 A.E. Charola. Review of the Literature on the Topic of Acidic Deposition on Stone. New York; The National Center for Preservation Technology and Training; 1998.

49 A. Sarmiento, M. Maguregui, I. Martínez-Arkarazo, M. Angulo, K. Castro, M.A. Olazábal, L.A. Fernández, M.D. Rodríguez-Laso, A.M. Mujika, J. Gómez, J.M. Madariaga. Raman spectroscopy as a tool to diagnose the impacts of combustion and greenhouse acid gases on properties of Built Heritage. J. Raman Spectrosc.; 2008; 39: 1042-1049.

50 E. Dotsika, D. Psomiadis, D. Poutoukis, B. Raco, P. Gamaletsos. Isotopic analysis for degradation diagnosis of calcite matrix in mortar. Anal. Bioanal. Chem.; 2009; 395: 2227-2234.

51 C.G. Allen, A. El-Turki, K.R. Hallam, D. McLaughlin, M. Stacey. Role of NO2 and SO2 in degradation of limestone. J. British Corrosion; 2000; 35: 35-38.

Nevertheless, to study the influence of pollutants on materials, the chemistry between them should be known because the effects observed are the result of their interaction. In this way, mortars are probably the most sensitive to degradation because of their calcareous nature and their porosity. Calcareous mortars are composed by quartz together with carbonates (mainly calcite, $CaCO_3$) and diverse iron oxides such as hematite (Fe_2O_3). Calcite appears in the cement when calcium oxide (CaO), belonging to the original composition, reacts exothermically with water to form calcium hydroxide ($Ca(OH)_2$), in a process called slaking. Subsequently, calcium hydroxide absorbs carbon dioxide to convert it into calcite. This process is called curing[52].

Natural calcite can be dissolved by the attack of atmospheric carbon dioxide to form hydrogencarbonate (HCO_3^-). This compound is more soluble and can migrate outward to the surface as calcite efflorescence, which can be removed by rain washing with the consequential loss of material.

Focusing on environments with high atmospheric pollution, the most common degradation products of those original compounds, were gypsum ($CaSO_4 \cdot 2H_2O$) or nitrocalcite ($Ca(NO_3)_2 \cdot 4H_2O$). Gypsum is formed by the attack of SO_x acid gases over calcite present in the mortars[53]. Analogously, nitrocalcite is formed by the reaction of NO_x atmospheric acid gases with calcite. Reactions 4.1 to 4.4 explain the formation of these types of salts, where M represents different cations of the salts, being the formation of other compounds expected, such as CO_2, H_2 or H_2O. In this sense, the presence of water in the environment can produce different hydrated forms of the salts.

Formation of the hydroxide by hydration of the oxide:

$$M_2O_m + H_2O \rightarrow 2M(OH)_m \quad (4.1)$$

Carbonation of the hydroxide:

$$2M(OH)_m + mH_2CO_3 \rightarrow M_2(CO_3)_m \cdot nH_2O \quad (4.2)$$

Reaction of the carbonates:

$$M_2(CO_3)_m + mH_2SO_4 \rightarrow M_2(SO_4)_m \cdot nH_2O \quad (4.3)$$

$$M_2(CO_3)_m + mHNO_3 \rightarrow M(NO_3)_m \cdot nH_2O \quad (4.4)$$

52 V. Johansen, W. Klemm, P. Taylor. Why Chemistry Matters in Concrete. Concrete Int.; 2002; 24: 84-89.

53 A. Charola, J. Pühringer, M. Steiger. Gypsum: a review of its role in the deterioration of building materials. Environ. Geol.; 2007; 52: 339-352.

Besides, as it is mentioned in chapter 1, other reactions that usually occur are hydration/dehydration processes of the salts, where crystallized salts change the number of hydration water molecules depending on the environmental conditions. Field analyses have demonstrated that it is possible to distinguish among such similar compounds by using the handheld spectrometer as shown in Figure 4.5. Note that not only is the main band visible but also most of the middle intensity or minor bands corresponding to anhydrite and gypsum.

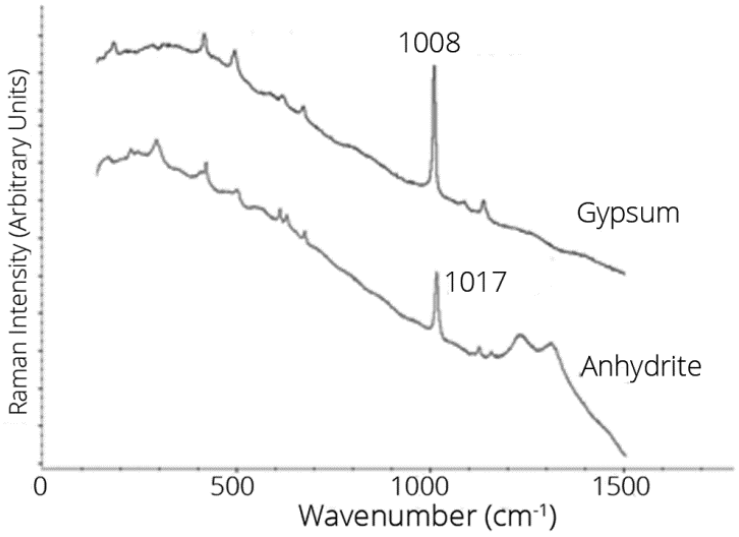

Figure 4.5. Comparison of the spectra collected by the InnoRam hand-held spectrometer (BWTEK$_{INC}$) on a brick sample. Gypsum and anhydrite are clearly identified thanks to the good quality of the measurements.

Bricks are likely the simplest construction materials to be diagnosed because it is easy to distinguish among original and degradation compounds[54]. Raw materials used for brick manufacturing are clays that are composed mainly of diverse silicates. After firing, the brick is composed mainly by oxides and silicate mixtures. So that, if other compounds such as carbonates, sulphates or nitrates are identified in bricks, they are always classified as degradation compounds.

In this way, calcite often comes from a decaying due to the hydration and subsequent carbonation (by atmospheric CO_2) of the original calcium oxide (CaO) according to reactions 4.1 and 4.2. The Raman scattering of the cited compounds is high enough as to identify them even by handheld spectrometers. Unfortunately, nitrates and chlorides have not been often detected due to their high solubility and for that reason, such soluble salts are observed in zones protected from rain washing. However, it has to be taken into account that the origin of such decaying compounds is

54 G. Cultrone, E. Sebastián, K. Elert, M.J. De la Torre, O. Cazalla, C. Rodriguez–Navarro. Influence of mineralogy and firing temperature on the porosity of bricks. J. European Ceramic Soc.; 2004; 24: 547-564.

not necessarily an atmospheric attack but they can be formed as well after infiltration of salt-rich waters.

Other original compounds can react analogously with atmospheric acid gases to form the respective carbonates, sulphates and/or nitrates. In this way, natrite (Na_2CO_3), mirabilite ($Na_2SO_4 \cdot 10H_2O$) and nitratine ($NaNO_3$) have been often referenced as soluble salts present in bricks[55]. It is remarkable that other compounds successfully identified in the brick samples were limonite ($FeO(OH) \cdot nH_2O$) and goethite (α-FeO(OH)), whose origin should be carefully studied, with special attention to when, where and how were they manufactured.

The Raman features of the compounds most usually identified by Raman spectroscopy in mortar and bricks affected by atmospheric pollution are collected in Table 4.1.

Table 4.1. Raman bands of some of the different compounds formed in mortars and bricks by the action of atmospheric pollution. Results obtained using the 785 nm laser.

Formula	Name	Raman bands ν (cm^{-1})
$CaCO_3$	Calcite	281, 712, 1085
$CaSO_4$	Anhydrite	169, 399, 417, 498, 594, 609, 628, 661, 675, 1017, 1111, 1129,
$CaSO_4 \cdot 0.5H_2O$	Bassanite	236, 322, 430, 487, 627, 668, 1015
$CaSO_4 \cdot 2H_2O$	Gypsum	414, 493, 619, 670, 1008, 1135
$Ca(NO_3)_2 \cdot 4H_2O$	Nitrocalcite	195, 719, 745, 1050
α-FeO(OH)	Goethite	302, 384, 545
$FeO(OH) \cdot nH_2O$	Limonite	240, 297, 394, 552
$Fe_2(SO_4)_3 \cdot 9H_2O$	Coquimbite	497, 598, 1025, 1092, 1198
Na_2CO_3	Natrite	193, 701, 1080
$Na_2SO_4 \cdot 10H_2O$	Mirabilite	167, 456, 617, 989, 1111
$NaNO_3$	Nitratine	190, 416, 724, 1067

55 N. Prieto-Taboada, M. Maguregui, I. Martinez-Arkarazo, M. Olazabal, G. Arana, J.M. Madariaga. Spectroscopic evaluation of the environmental impact on black crusted modern mortars in urban–industrial areas. Anal. Bioanal. Chem.; 2010; 399: 2949-2959.

4.1.4. Deterioration due to infiltration waters

As it is explained in depth in chapter 1, infiltration water is the second important impact factor affecting building materials. The water coming from the soil is rich in carbonates, sulphates, chlorides and/or nitrates and calcium, magnesium, sodium, potassium and/or ammonium. In addition, in areas with high density human settlements the soil water especially contains nitrates and chlorides. The later has been commonly related with coastal areas but, as it has been already mentioned, this mechanism is likely the principal origin for these salts. High chloride concentrations have been determined in buildings located in estuaries suffering floods or close to roads or pavements were high amount of NaCl is used during winter to avoid frost formation. However, most chlorides are not Raman active so the complementary information of other techniques is needed to characterize them.

In contrast, the presence of sulphate may be explained by the use of fertilizers in nearby fields, dedicated to agriculture, as well as water contaminated by nearby industries. Usually, the compounds are sodium or calcium sulphates with different number of hydration water as gypsum ($CaSO_4 \cdot 2H_2O$), bassanite ($CaSO_4 \cdot 0.5H_2O$) or mirabilite ($Na_2SO_4 \cdot 10H_2O$).

The formation of nitrate salts is mainly due to the impact coming from the organic matter degradation that produces ammonium nitrate (NH_4NO_3). Thanks to its acidity, this compound is very reactive and transforms the original compounds of mortars and bricks like feldspars or calcium oxide (CaO) producing frequently nitrates as for example nitratine ($NaNO_3$), nitromagnesite ($Mg(NO_3)_2 \cdot 6H_2O$) and nitrocalcite ($Ca(NO_3)_2 \cdot 4H_2O$)[56]. It is also remarkable that the composition of the salts appearing as efflorescences does not agree with the salt content of the samples. For instance, salts presence frequency order is Ca>Na>K>Mg in bricks whereas the frequency order for salts appearing as efflorescence is Na>K>Ca>Mg[57].

In this manner, the presence of one or another salt is directly related to environmental conditions such as humidity and temperature and thus, salt composition of facades affected by water infiltrations shows a clear seasonal variability[58]. Hence,

56 M. Maguregui, A. Sarmiento, I. Martínez-Arkarazo, M. Angulo, K. Castro, G. Arana, N. Etxebarria, J.M. Madariaga. Analytical diagnosis methodology to evaluate nitrate impact on historical building materials. Anal. Bioanal. Chem.; 2008; 391, 1361-1370.

57 J.M. Rincón, M. Romero. Fundamentos y clasificación de las eflorescencias en ladrillos de construcción. Mater. Construcc.; 2000; 50: 63-70.

58 Y. Matsukura, C.T. Oguchi, N. Kuchitsu. Salt damage to brick kiln walls in Japan: spatial and seasonal variation of efflorescence and moisture content. Bull. Eng. Geol. Enviro.; 2004; 63: 167-176.

Raman spectroscopy monitoring performed by portable instruments can be essential in order to determine the suitable treatment to remove the specific salts.

Apart from that, the common effects of the chemical degradation in buildings by atmospheric pollution or infiltration water are the alveoli, disaggregation, the typical disease plates and black crust formations. For instance, the latter is formed by the adhesion on the surface of wet material particles of dust, soot or smoke. Once deposited, it acts as a nucleus of reaction for chemical degradation, forming a permanent pollution patina. In the black crust common products of degradation such as toxic particulate matter, heavy metals and PAHs can be found [59].

The position of the bands of Raman spectra of the most common compounds found in mortars and bricks affected by infiltration water are in the Table 4.2.

Table 4.2. Raman bands of some of the different compounds found usually in mortars and bricks by the action of infiltration waters measured with 785 nm laser.

Formula	Name	Raman bands ν (cm^{-1})
$CaCO_3$	Calcite	281, 712, 1085
$CaSO_4$	Anhydrite	169, 399, 417, 498, 594, 609, 628, 661, 675, 1017, 1111, 1129
$CaSO_4 \cdot 0.5H_2O$	Bassanite	236, 322, 430, 487, 627, 668, 1015
$CaSO_4 \cdot 2H_2O$	Gypsum	414, 493, 619, 670, 1008, 1135
$Ca(NO_3)_2 \cdot 4H_2O$	Nitrocalcite	195, 719, 745, 1050
Na_2CO_3	Natrite	193, 701, 1080
$Na_2SO_4 \cdot 10H_2O$	Mirabilite	167, 456, 617, 989, 1111
NH_4NO_3	Nitrammite	193, 714, 1043, 1288, 1412, 1654, 1777

59 I. Martínez-Arkarazo, M. Angulo, L. Bartolomé, N. Etxebarria, M.A. Olazabal, J.M. Madariaga. An integrated analytical approach to diagnose the conservation state of building materials of a palace house in the metropolitan Bilbao (Basque Country, North of Spain). Anal. Chim. Acta; 2007; 584: 350-359.

4.1.5. Biodeterioration markers

Raman Spectroscopy is a very useful analytical technique for characterization purposes of not only inorganic compounds but also of organic compounds present in bricks and mortars. Due to the usual exposure of these materials to open atmosphere, they are colonized by a variety of microorganisms.

Crustose lichens, which are extremely attached to the stone, develop physical structures called hyphae to penetrate into stone pores. These structures cause the cracking of the materials and promote physical decaying mechanisms[60]. In this sense, mortars are more susceptible than bricks to be attacked due to their higher porosity but also because of their composition. Lichens excrete oxalic acid in high quantities which reacts with calcite present in building materials and calcium oxalates appear following reactions 4.5 and 4.6, respectively :

$$H_2C_2O_4 + CaCO_3 \leftrightarrow CaC_2O_4 \cdot H_2O + CO_2 \quad (4.5)$$

$$2H_2C_2O_4 + CaCO_3 \leftrightarrow 2(CaC_2O_4 \cdot 2H_2O) + 2CO_2 \quad (4.6)$$

Calcium oxalates can appear in the monohydrate form or mineral whewellite ($CaC_2O_4 \cdot H_2O$) or in the dihydrate form or mineral weddellite ($CaC_2O_4 \cdot 2H_2O$). Both compounds are clearly detected and differentiated by Raman Spectroscopy[61,62] as can be seen in Figure 4.6.

Lichens and mosses are photosynthetic organisms, and thus, they have different pigments that can be distinguished by Raman Spectroscopy. The most common are chlorophyll and carotenoids. Both are present in the photosynthetic reaction centre of the chloroplasts in cellular parts of these organisms. Other common pigment is phorphyrin, which appears together with chlorophyll in the photosynthetic reaction centre[63].

60 S.E. Jorge-Villar, H.G.M. Edwards. Lichen colonization of an active volcanic environment: a Raman spectroscopic study of extremophile biomolecular protective strategies. J. Raman Spectrosc.; 2010; 41: 63-67.

61 H.G.M. Edwards, M.R.D. Seaward, S.J. Attwood, S. Little, L.F.C. De Oliveira, M. Tretiach. FT-Raman spectroscopy of lichens on dolomitic rocks: an assessment of metal oxalate formation. The Analyst; 2003; 128: 1218-1121.

62 R.L. Frost. Raman spectroscopy of natural oxalates. Anal. Chim. Acta; 2004; 517: 207-214.

63 R. Withnall, B.Z. Chowdhry, J. Silver, H.G.M. Edwards, L.F.C. De Oliveira. Raman spectra of carotenoids in natural products. Spectrochim. Acta A; 2003; 59: 2207-2212.

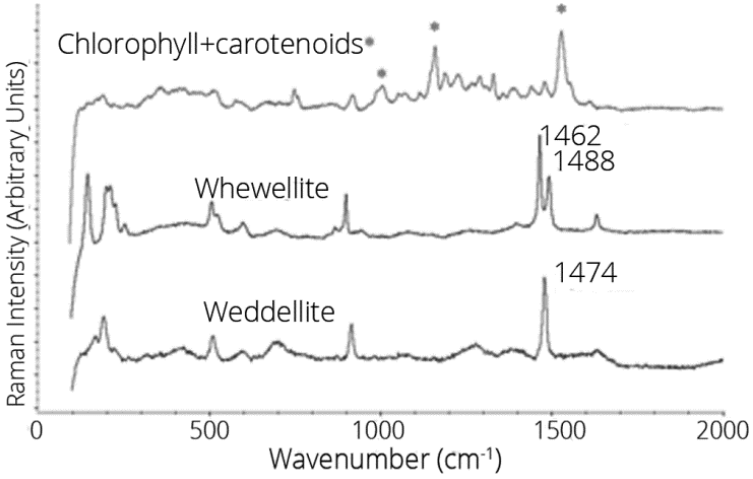

Figure 4.6. Different biodeterioration compounds found on the bricks and mortar. Spectra collected with 785 nm laser of the InnoRam (BWTEK$_{INC}$) handheld spectrometer. In the first spectrum a mixture of chlorophyll and carotenoids (peaks marked with) was identified.*

When the carotenoid type molecules are present in the target sample that is going to be analyzed by Raman Spectroscopy, another excitation laser, which allows the resonance effect of these organic compounds, can be proposed. Carotenoid molecules are chromophoric compounds which present a maximum in the blue-green region of the absorption spectra. When the excitation laser of the Raman measures coincides with a maximum of the absorption spectra, carotenoids absorb this radiation in a resonance effect. Consequently the Raman signatures of these compounds are significantly enhanced with respect to signatures of other compounds present jointly in the sample. Moreover, when the Raman spectra is extended until 3500-4000 cm^{-1} (depending on the spectral range of the equipment), new Raman signatures appear corresponding with Resonance Raman features of the carotenoid.

The global information of Raman spectra allows us to detect the presence of carotenoids as well as to distinguish among carotenes (carotenoids composed of a chain with certain quantity of polyenes) and xanthophylls (oxygen derivatives of carotenes). Figure 4.7 shows the identification and consequent differentiation between carotenoids. The spectra obtained are collected with 514 nm laser of the InVia Raman spectrometer but other research studies used the 514 nm laser with handheld instrument in order to identify carotenoids in field measurements[64].

64 P. Vítek, J. Jehlička, H. Edwards, K. Osterrothová. Identification of β-carotene in an evaporitic matrix—evaluation of Raman spectroscopic analysis for astrobiological research on Mars. Anal. Bioanal. Chem.; 2009; 393: 1967-1975.

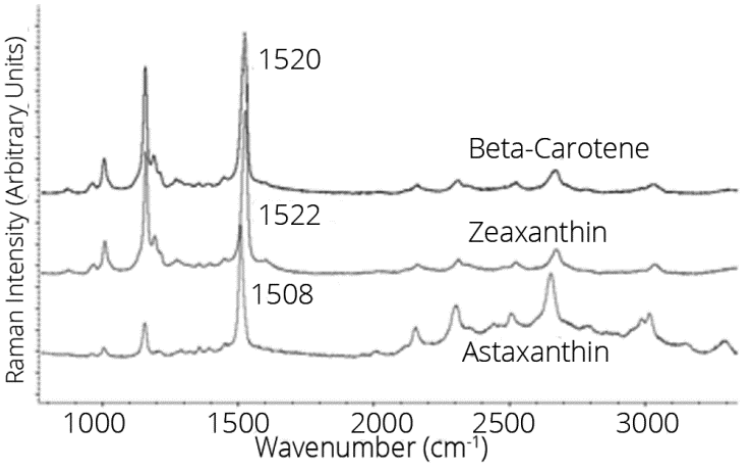

Figure 4.7. Carotenoid differentiation obtained with InVia Raman spectrometer using the laser of 514 nm which allows to achieve the Resonance effect of carotenoids.

This differentiation is based on the Raman signals appeared in the range of 1500-1550 cm^{-1} coincident with C=C stretching vibration and the Resonance Raman features appear between 2000 and 3500 cm^{-1}. On the other hand, in the case of chlorophyll and phorphyrin the use of 514 nm laser is not adequate due to the impossibility of determining them. Consequently, the Raman signals of carotenoids that appear together with these pigments are significantly improved.

Another molecule related with the metabolism of lichens is the UV screening pigment scytonemin that is unambiguously detected with Raman Spectroscopy. The position of its Raman bands does not differ essentially between two excitation lasers (785 or 514 nm), but the relative intensities of Raman bands change with the laser type. This fact makes necessary to establish a previous work to find the proper Raman signatures of each molecule with each laser or maybe in some cases it is necessary to measure pure standards of each compound[65].

The Raman features of the most common compounds are collected in Table 4.3, being its identification crucial to diagnose the biodeterioration suffered.

65 *J. De Gelder, K. De Gussem, P. Vandenabeele, L. Moens. Reference database of Raman spectra of biological molecules. J. Raman Spectros.; 2007; 38: 1133-1147.*

Table 4.3. Raman bands of some of the different compounds found usually in mortars and bricks by biodeterioration measured with 785 or 514 nm laser.

Formula	Laser(nm)	Name	Raman bands ν (cm^{-1})
$CaC_2O_4 \cdot H_2O$	785	Whewellite	140, 195, 205, 221, 503, 520, 593, 863, 895, 937, 1391, 1462, 1488, 1627
$CaC_2O_4 \cdot 2H_2O$	785	Weddellite	161, 188, 506, 589, 868, 910, 1410, 1474, 1629
$C_{55}H_{72}O_5N_4Mg$	785	Chlorophyll a	513, 744, 753, 919, 963, 986, 1048, 1068, 1110, 1185, 1221, 1286, 1326, 1385, 1438, 1550, 1606
Undetermined*	785	Carotenoids*	1003, 1156, 1524
$C_{36}H_{20}N_2O_4$	785	Scytonemin	574, 1167, 1330, 1385, 1508, 1558, 1592
$C_{36}H_{20}N_2O_4$	514	Scytonemin	439, 494, 575, 676, 1095, 1158, 1170, 1286, 1323, 1383, 1453, 1507, 1553, 1592, 1629, 1713
$C_{40}H_{52}O_4$	514	Astaxanthin	956, 1006, 1152, 1198, 1507, 2020, 2161, 2302, 2353, 2510, 2652, 2785, 2983, 3016, 3159, 3294, 3444
$C_{40}H_{56}O_2$	514	Zeaxanthin	867, 962, 1003, 1155, 1185, 1206, 1267, 1288, 1314, 1351, 1389, 1445, 1521, 2020, 2157, 2305, 2345, 2525, 2666, 2985, 3027, 3306, 3445
$C_{40}H_{56}$	514	β-carotene	959, 1003, 1155, 1186, 1207, 1520, 2156, 2309, 2521, 2672, 3030

** The carotenoid differentiation is not possible with the 785 nm laser.*

4.1.6. General remarks of the technique

Raman Spectroscopy could be a useful analytical technique to diagnose the conservation state of building materials. It has the possibility to carry out in situ analysis with a good quality results. In addition, Raman Spectroscopy can be classified as a non destructive technique, so the value, the importance and the total integrity of the samples are preserved.

Thanks to the possibility offered by this technique in distinguishing different types of molecules it could be possible to establish deterioration reactions and mechanisms based only in Raman measurements. But in the case of some compounds like calcite and gypsum, which can appear in mortars as original or decaying compounds, the criterion of the researcher is crucial to classify each one based on the shape, depth, location or even exposure suffered by the material used because Raman technique gives the same response in both cases.

In any case, the possibility that Raman spectroscopy offers for field analysis is a clear advantage that makes this technique suitable to diagnose construction materials. Even more, due to the development of new hand-held Raman spectrometers with high sensitivity and good spectral resolution, a fast diagnosis of the building materials could be performed. Hence, a restoration protocol could be more rapidly established from in situ analyses since decisions could be taken in the field.

4.2. The potential of in situ spectroscopic analysis in the diagnosis of historic buildings: operational evaluation

According to the previous study, in this section, the viability of the in situ analysis based on Raman spectroscopy as main technique will be studied in detail, examining the advantages of its combination with XRF to achieve complementary information.

For that purpose, a complete in situ spectroscopic assessment of the conservation state of building materials from a Palace house was carried out. In this way, the application of portable Raman and XRF spectrometers, to achieve complementary elemental composition in the diagnosis of the decay and to establish the chemical attack involved in the pathologies found, was studied and explained along this section and its corresponding article can be consulted in the scientific publication Annex. In addition, the impact suffered by the different materials was examined, determining the current conservation state of the building as well as the suitability of the restoring materials used in previous interventions.

4.2.1. Location of the building

The Basozabal Palace house is situated in the village of Azpeitia (Gipuzkoa, Basque Country, North of Spain), along the Urola river and, under the limestone Izarraitz massif (Fig. 4.8 a). Given its proximity to the coast, it has an Atlantic climate with an Oceanic trend (Cfb according to the Köppen-Geiger classification[66]). Although others revenues have taken over, the main economical activities of the town are linked to the primary sector, especially agriculture and livestock. Albeit reports of chemical quality and pollution of the Urola water have good levels, historically agricultural and livestock discharges were a problem, presenting moderate pollution and certain levels of eutrophy (Grade II and level 69, according to the Iberian Water BioMonitoring Procediment, IBMWP)[67,68].

66 M. Kottek, J. Grieser, C. Beck, B. Rudolf, F. Rubel. World Map of the Köppen–Geiger climate classification updated. Meteorol.; 2006; *15: 259–263.*

67 Gipuzkoa County Council. Bases para la elaboración de las directrices sobre el uso sostenible del agua en Gipuzkoa (Study of river quality), Gipuzkoa, North of Spain: Gipuzkoa County Council; 2006.

68 D. P. Moreno Franco, J. Quintero Manzano, A. Lopez Cuevas. Métodos para identificar, diagnosticar y evaluar el grado de eutrofia.ContactoS; 2010; 78: 25-33.

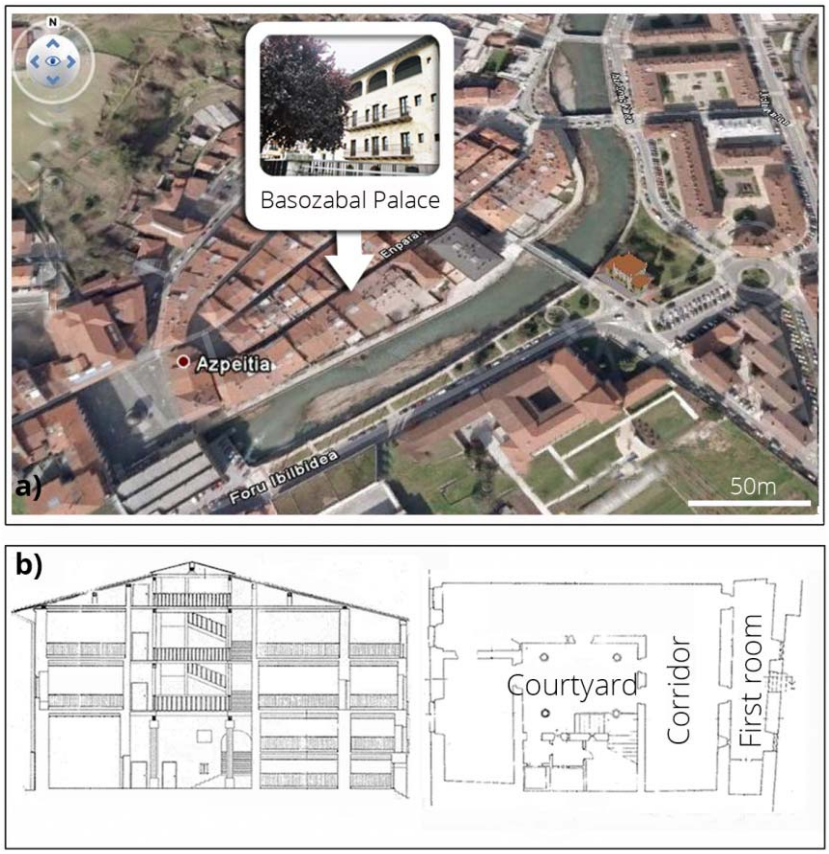

Figure 4.8. a) Geographic location of the studied historical building (Basozabal Palace House, Azpeitia, Basque Country, North of Spain). b) Architectural drawings corresponding to plan and section of the building.

4.2.2. Description of the building

The Basozabal Palace house is a historic building of the fifteenth century located close to the river, in the old quarter of the village. Throughout its history, the building has undergone several transformation actions, being in its origins an isolated tower house, which later became a building fully integrated into the urban center of the village. In 1990, the restoration project was started to use it as an exhibitions hall. However, few years later, the works were suspended and its conservation state is getting worse very rapidly. Only facades, stairway and skylight were rehabilitated.

The building is distributed into ground floor, mezzanine and two upper floors plus an undercover (Fig. 4.8 b). With an available area of 1026 m^2, the ground floor is composed of a central courtyard with a ladder attached to one side, which gives access to the upper floors. The courtyard is supported on octagonal stone columns of gothic bases and they form a perimeter corridor that allows the passage to the different rooms (Fig. 4.8 b).

The building is constructed with glauconitic subarkose sandstone and limestone slabs from Igueldo quarry (Gipuzkoa, Basque Country, North of Spain) over a concrete base. Given the existence of various studies of those stones, their petrographic features, their response to different laboratory tests as well as the behavior of mortars potentially applicable to them are already determined[69-73]. Sandstones are found throughout all the building while the limestone is only observed in the main facade and in the first room. Nevertheless, in the latter, the ashlars are very small, being sand joint mortar the predominant material. Besides, Portland cement mortar was incorporated in stairway, windows and sills of the ground floor during the restoration.

4.2.3. In situ analysis campaign

The visual inspection allowed the identification of different types of efflorescences, subefflorescences, flakings and disaggregations as the main affections of the materials in the ground floor walls (Fig. 4.9 and 4.10).

For the selection of the most appropriate points for the spectroscopic study, a first in situ sampling campaign was performed during the month of November 2011. In order to guarantee representative and reliable results, more than 80 in situ Raman measurements were carried out over deteriorated sandstones, mortars and limestones of the ground floor.

In addition, XRF measurements were carried out on the same sampling points to achieve complementary elemental information to the molecular one, thus facilitating further interpretation of the Raman spectra collected.

---

69 . García- Garmilla, I. Rodríguez-Maribona, M. Cano, M. Zalbide, J. A. Ibáñez-Gómez, K. Osa-Chans, S. Garín. An analytical comparison of two commercial consolidating products applied to eocene sandstones from 16th and 19th century monuments in San Sebastián, northern Spain. Mater. Construcc.; 2002; 52: 5-12.

70 I. Rodriguez-Maribona, M. Zalbide, F. Garmilla, F. Garcia, J.A. Ibanez, S. Garin. Chemical and mineralogical study of restoration mortars applied to the Eocene sandstones of Gipuzkoa used for building construction. Mater. Construcc.; 1999; 49: 19-30.

71 M. Cano, I. Rodriguez-Maribona, K. García-Garmilla, I. Yusta, J.A. Ibañez-Gómez, S. Garín. Caracterización y selección de morteros de restauración aplicados a areniscas del Eoceno de Gipuzkoa utilizadas en la construcción de edificios. Geogaceta; 2001; 30: 215-218.

72 J. A. Ibáñez-Gómez, I. Yusta, F. García- Garmilla, M. Cano, I. Rodriguez-Maribona, K. Beraza, S. Garín. Chemical and mineralogical study of restoration mortars applied to the Eocene sandstones of Gipuzkoa used for building construction. Geogaceta; 2001; 30: 223-226.

73 F. García- Garmilla, M. Cano, I. Yusta, J. A. Ibáñez-Gómez, K. Beraza, S. Garín. Resultados de SEM/EDXD en morteros de restauración aplicados a areniscas del Eoceno de Gipuzkoa utilizadas en la construcción de edificios. Geogaceta; 2011; 3: 219-222.

Three months later, as a result of this previous screening, a second in situ analysis campaign was developed, where over 100 in situ measurements were performed in the most affected areas of the building (Fig.4.10), the central courtyard and the first room after the back facade (adjacent to the river). In this occasion, the presence of front salts, up to 1.7 meters in height, was observed along the inner wall of the first room (Fig. 4.9 and 4.10).

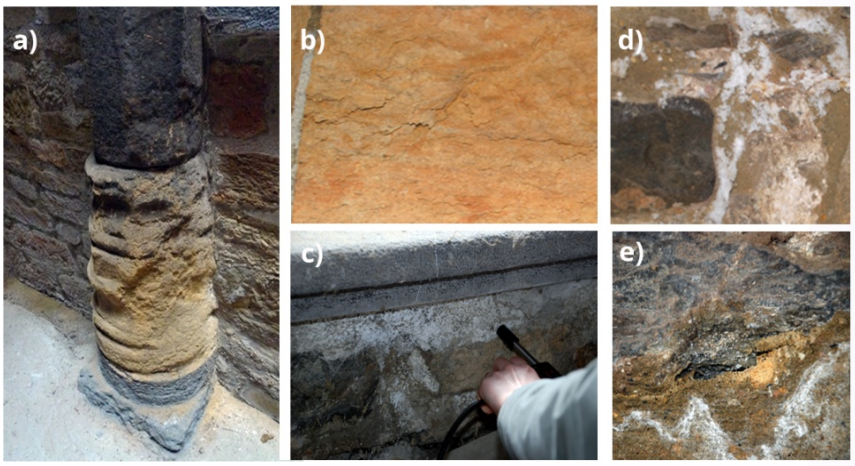

Figure 4.9. Selected photographs of the deteriorations observed in the Palace House. a) sandstone column details of the central courtyard. b) details of flaking sandstone. c) details of eflorescences over restored mortar. d) details of effflorescences observed over the limestone wall of the first room (salts front). e) details of the salts front, the image shows a severe material loss.

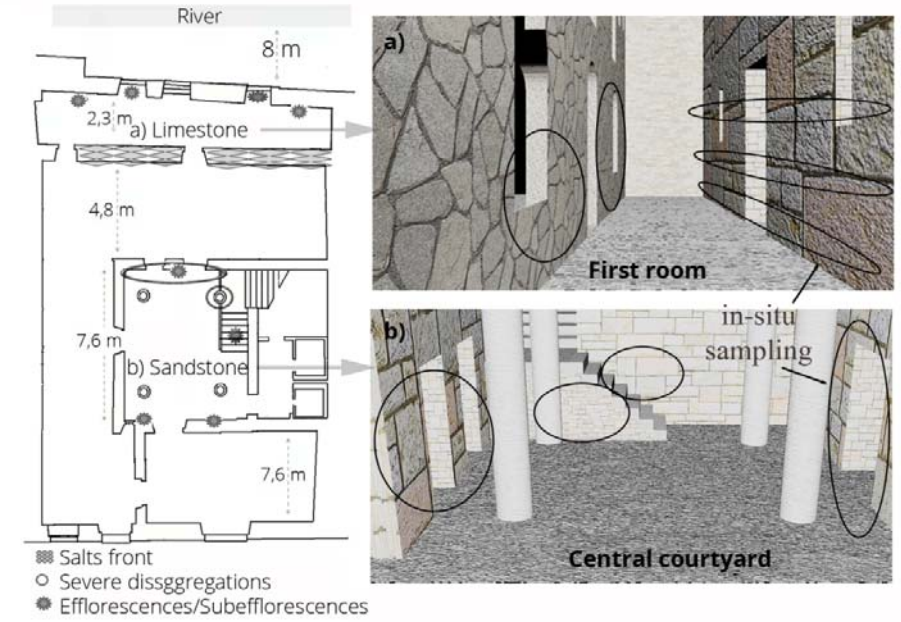

Figure 4.10. The left side shows the general view of ground floor of the Basozabal Palace where the distribution of the different building materials and the main pathologies of the sampled areas are showed. The right side shows the 3D modelling of the sampled rooms; a- first room and b- central courtyard (simulations by Autodesk®3ds Max).

Furthermore, with the purpose of knowing the elemental semiquantitative composition of original buildings materials, fresh areas of upper floors were selected to carry out XRF in situ measurements.

4.2.4. In situ results

The most relevant information obtained during the in situ analysis campaign will be discussed along this section.

4.2.4.1. X-ray fluorescence

In the analysis of sandstones Ca, Fe, Si and K were identified as major elements. Besides, Ti, Sr, Mn and Zn were identified as minor elements. The remaining composition could correspond to light elements, Na and O mainly, since their signal is too low to be detected by this portable equipment.

In mortars, Ca and Fe were identified as major elements. However, in this case Si and K were found at levels lower The remaining elements are C and O.

To end up, the main element of the limestone was Ca followed by Fe, Si, K and Al. The remaining elements are C and O

According to the results, Ca and Fe were the main elements in all of the samples showing a varying percentage, which is the typical composition for this kind of materials. On the other hand, toxic metal pollutants as Cu, Zn, Mn or Pb were not identified with a significant level either in degraded or in fresh sampling areas. Therefore, contamination cannot be considered in this situation as the results of this in-situ analysis showed the absence of pollutants related to traffic or industrial activities and avoided a later destructive analysis to detect the presence of toxic metals.

4.2.4.2. Raman spectroscopy

In relation to sandstone, natrite (Na_2CO_3, easily identified by a strong narrow peak at 1080 cm^{-1} and two weak peaks at 701 and 193 cm^{-1}), and calcite ($CaCO_3$, detected by a strong peak at 1085 cm^{-1}, a weak signal at 712 cm^{-1} and a broader band at 281 cm^{-1}) were recognized as main original compounds[74] of the samples. Besides, α-quartz (α-SiO_2, detected by a main Raman peak at 464 cm^{-1} and its secondary peak at 263 cm^{-1}) and carbon (identified by its two characteristic bands at 1600 and 1325 cm^{-1}) were found as minor original compounds.

74 F. García- Garmilla, I. Rodríguez-Maribona, M. Cano, M. Zalbide, J. A. Ibáñez-Gómez, K. Osa-Chans, S. Garín. An analytical comparison of two commercial consolidating products applied to eocene sandstones from 16th and 19th century monuments in San Sehastiány northern Spain. Mater. Construcc.; 2002; 52: 5-12.

Moreover, a mixture of sodium carbonates, natrite (identified by its Raman peaks at 1080 and 193 cm^{-1}) and trona ($Na_3(HCO_3)(CO_3)\cdot 2H_2O$, characterized by the main peak at 1061 cm^{-1} and its secondary signals at 225, 186 and 177 and 156 cm^{-1}, being the last doubtful because of the acquisition range of the equipment) were found as efflorescences and subefflorescences (Fig. 4.11 a). These compounds cannot be considered as part of the original material since, the spots taken were in areas which presented salts.

In addition, in some areas of the sandstone, efflorescences of gypsum ($CaSO_4\cdot 2H_2O$, identified by a intense peak at 1008 cm^{-1} and its two characteristic doublets at 493, 414 cm^{-1} and 670, 619 cm^{-1}, apart from other secondary signals at 1135 and 217 cm^{-1}) and calcite (identified by the main Raman band at 1085 cm^{-1}) were also observed (Fig. 4.11 b). The existence of these compounds as efflorescences suggests the presence of infiltration or/and condensation water that could cause the dissolution of the original material and the crystallization of these salts in the pores and in the surfaces of the stone.

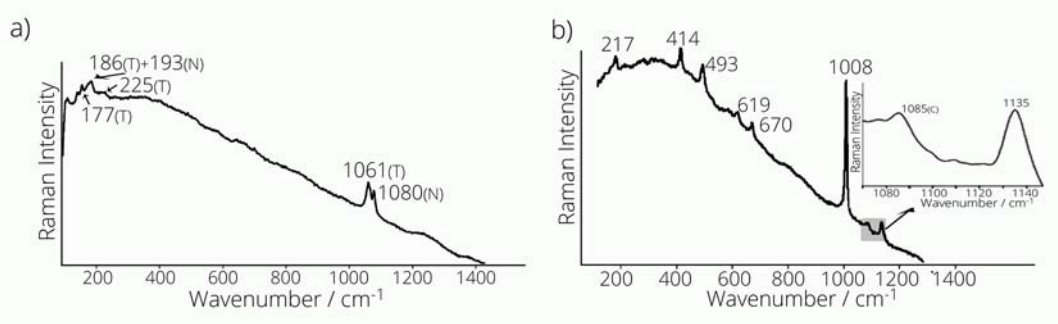

Figure 4.11. a) Raman spectrum showing a mixture of natrite (N) and Trona (T) found in situ as efflorescence and subefflorescence in sandstones of the central courtyard. b) Raman spectrum of gypsum and calcite (C) found in situ as efflorescence in sandstones of the courtyard.

Gypsum could be originated by different mechanisms: acid attack of atmospheric SO_2 gases on the carbonated cementer or dissolution of original material by the action of acid waters containing dissolved sulphate ions[75-77]. Considering the composition and placement of the original stone (Fig. 4.10) as well as the location (low areas) and distribution of the salts in the wall, the most probable cause for

75 V. Matović, S. Erić, A. Kremenović, P. Colomban, D. Serćković-Batoćanin, N. Matović. The origin of syngenite in black crusts on the limestone monument King's Gate (Belgrade Fortress, Serbia)—the role of agriculture fertiliser . J. Cult. Herit.; 2012; 13: 175-186.

76 M.I. Sánchez de Rojas, N. García, M. Frías. Influence of the environment on Weathering of limestone: study through mercury porosimetry. Mater. Construcc.; 1998; 49: 31-41.

77 N. Prieto-Taboada, M. Maguregui, I. Martinez-Arkarazo, M. A. Olazabal, G. Arana, J. M. Madariaga. Spectroscopic evaluation of the enviromental impacto n black crusted modern mortars in urban-industrial areas. Anal. Bioanal. Chem.; 2011; 399: 2949-2959.

gypsum formation could be the second one. In this way, the acidic infiltrated waters (usually below pH 5-6) react directly with the calcite surface to form gypsum following the reactions 4.7 and 4.8

$$CaCO_3 + SO_4^{-2} + H^+ \leftrightarrow CaSO_4 + HCO_3^- \quad (4.7)$$

$$CaSO_4 + 2H_2O \leftrightarrow CaSO_4 \cdot 2H_2O \quad (4.8)$$

In the case of the restored base mortars, a great affection of soluble salts was clearly observed. In this area, thenardite (Na_2SO_4, identified by the strongest Raman peak at 991cm^{-1} and the weakest pair of peaks at 466 and 451 cm^{-1} aside from other signals at 1149, 1128, 644, 632 and 621 cm^{-1}) was found as one of the decaying compounds which is one of the most harmful salts for the conservation of building materials[78-80] (Fig. 4.12).

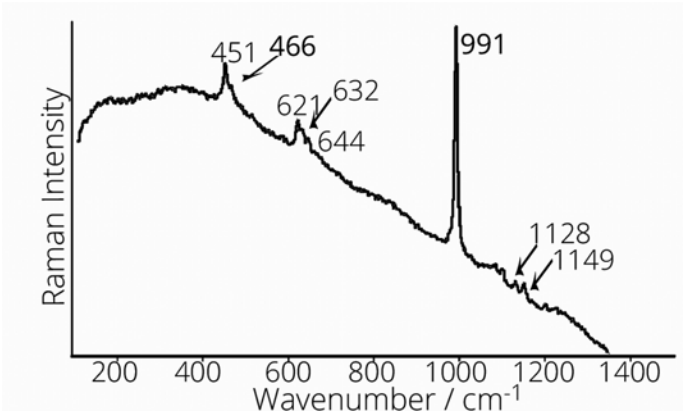

Figure 4.12. Raman spectrum of pure thenardite found in situ as efflorescence, in restored base mortars of stairs and windows sills of the first room and the central courtyard.

Thenardite presents a continuous equilibrium, through heptahidrate form, with mirabilite ($Na_2SO_4 \cdot 10H_2O$), depending on the temperature and the relative humidity[81,82] (Fig. 4.13). This transition processes between both salts promotes important cracks and

78 R. M. Espinosa-Marzal, G. W. Scherer. Advances in understanding damage by salt crystallization. Acc. Chem. Res.; 2010; 43: 897-905.

79 J. Cassar, A. Marrochi, M. L. Santarelli, M. Muscat. Controlling crystallization damage by the use of salt inhibitors on Malta's limestone. Mater. Construcc.; 2008; 58: 281-293.

80 A. Hamilton , R. I. Menzies. Raman spectra of mirabilite, $Na_2SO_4 \cdot 10H_2O$ and the rediscovered metastable heptahydrate, $Na_2SO_4 \cdot 7H_2O$ .J. Raman Spectrosc.; 201; 41: 1014-1020.

81 M. Steiger , S. Asmussen. Crystallization of sodium sulfate phases in porous materials: The phase diagram Na_2SO_4-H_2O and the generation of stress. Geochim. Cosmochim. Ac.; 2008; 72: 4291-4306.

82 N. Tsui, R. J. Flatt, G. W. Scherer. Crystallization damage by sodium sulfate. J. Cult. Herit.; 2003; 4 : 109-115.

loss of material due to the pressure caused by the salts crystallization. Due to its characteristic thermodynamic behavior, the mere transport of the sample to the laboratory may cause the change in crystallization form and therefore the identification of this salt could be incorrect[83-85].Therefore the in situ analyses become significant in these cases.

Considering the fact that thenardite was only found in restored based mortars its formation could be related with mortar composition. In this case, the new mortars were manufactured with Portland cement that presents a high content of sodium oxide (Na_2O) and gypsum as additives[86-88]. Thus, the thenardite formation could be caused by reactions between the additives of cement material and water. This result reinforces the hypothesis of water infiltration, ruling out the acid attack of atmospheric SOx as the main cause of deterioration.

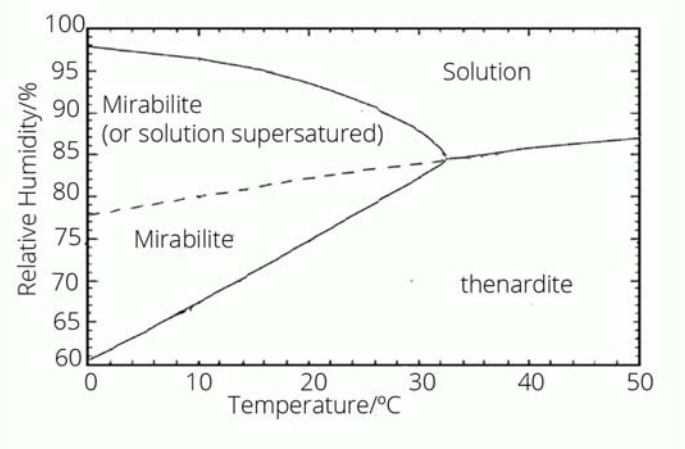

Figure 4.13. Phase diagram of sodium sulphate. The boundaries of the stable phases correspond to the continuous lines and the discontinuous line corresponds to a solution in metastable equilibrium with thenardite and supersaturated with respect to mirabilite, respectively.

83 A. Hamilton , R. I. Menzies. Raman spectra of mirabilite, $Na_2SO_4{\cdot}10H_2O$ and the rediscovered metastable heptahydrate, $Na_2SO_4{\cdot}7H_2O$ J. Raman Spectrosc.; 201; 41: 1014-1020.

84 N. Tsui, R. J. Flatt, G. W. Scherer. Crystallization damage by sodium sulfate. J. Cult. Herit.; 2003; 4 : 109-115.

85 N. Thaulow, S. Sahu. Mechanism of concrete deterioration due to salt crystallization. Mater. Charact.; 2004; 53: 123-127.

86 J. A. Ibáñez-Gómez, I. Yusta, F. García- Garmilla, M. Cano, I. Rodriguez-Maribona, K. Beraza, S. Garín. Chemical and mineralogical study of restoration mortars applied to the Eocene sandstones of Gipuzkoa used for building construction. Geogaceta; 2001; 30: 223-226.

87 R. Ylmén, U. Jälid, B. M. Steenari, I. Panas. Early hydration and setting of Portland cement monitores by IR, SEM and Vicat techniques. Cement Concrete Res.; 2009; 39: 433-439.

88 S. Pavía. SWBSS- Salt Weathering on Buildings and Stone Sculptures, Copenhagen: Technical University of Denmark; 2008.

.Concerning joint mortars, of the limestone wall, a great affection produced by nitrate salts formation was observed. Various in situ Raman measurements registered all the necessary bands for the identification of niter (KNO_3) at 1050 cm^{-1} and, more important, a conclusive peak at 715 cm^{-1} (Fig. 4.14).

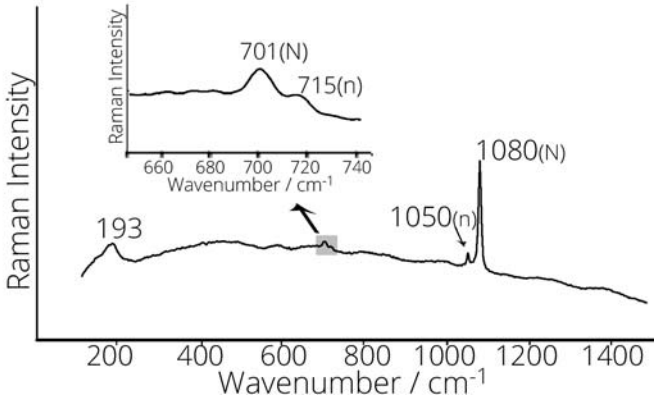

Figure 4.14. Raman spectrum of a mixture of natrite (N) and niter (n) found in situ as decaying compounds in joint mortars of the limestone wall of the first room.

Nitrates can be formed by atmospheric attack of NOx[89]or by acid water infiltration from subsoil[90]. Taking into account that the spectra were obtained inside the building and considering the location of the wall (Fig. 4.10), in front of the river, in concordance with the previous results, the atmospheric source could be ruled out, on behalf of infiltration waters. The presence of nitrates in ground water is derived from the natural decomposition of organic nitrogenous materials (like proteins from plants, animals, fertilizers and so on) by microorganisms. The ammonium ion formed during that breakdown is oxidized to nitrite and nitrate following the biological oxidation process of nitrification[91]. This fact could explain the great presence of salts in the degraded walls.

Regarding the last material analysed, the limestones presented a minor degradation in comparison to the sandstones. Nonetheless, some efflorescences in white crust form were observed. The in situ analysis revealed that the crust was

89 M. Maguregui, A. Sarmiento, I. Martinez-Arkarazo, M. Angulo, K. Castro, G. Arana, N. Etxebarria , J. M. Madariaga. Analytical diagnosis methodology to evaluate nitrate impact on historical building materials. Ana. Bioanal. Chem.; 2008; 391: 1361-1370.

90 H. Morillas, M. Maguregui, O. Gómez-Laserna, J. Trebolazabala , J. M. Madariaga. Characterisation and diagnosis of the conservation state of cementitious materials exposed to the open air in XIX century lighthouses located on the coast of the Basque Country: 'The case of Igueldo lighthouse, San Sebastian, North of Spain'. J. Raman Spectrosc;. 2012; 43: 1630-1636.

91 J. Pacheco Ávila, A. Cabrera Sansores. Fuentes principales de nitratos en aguas subterraneas. Ing.; 2003; 7-2 : 47-54.

composed of calcite, whose presence can be explained as a result of the action of acid infiltration water over the natural carbonated composition, which can be dissolved in an acid medium like the one produced by the NH_4^+ ions. The bicarbonate salts formed are very soluble and could migrate through the wall producing loss of material and the later precipitation of calcium carbonate as efflorescence and/or subefflorescence.

To conclude with the in situ investigation, it is remarkable the detection of Raman bands at 1607, 1187, 1025, 966 and 580 cm^{-1} in the first room. This spectrum is related with sunlight photons reaching the spectrometer detector that can lead to an incorrect assignment of the spectra[92], like in the case of coquimbite ($FeSO_4 \cdot 9H_2O$), whose main Raman band is also present at 1025 cm^{-1}. In consequence, Raman analyses should be performed in darkness, as long as possible. In fact, one of the most important factors to take into account in Raman studies performed in situ is to subtract the signals due to the light.

Despite some problems arising from the work in the field, as sunlight and fluorescence, numerous compounds were recognized and their Raman bands are summarized in Table 4.4.

Table 4.4. Summary of the compounds found during the field study

Compounds identified in situ		
Formula	Name	Raman bands ν (cm^{-1})
$CaCO_3$	Calcite	1435*, 1085, 712, 281
Na_2CO_3	Natrite	1080, 701, 193
$Na_3(HCO_3)(CO_3) \cdot 2H_2O$	Trona	1061, 225, 186, 177, 156
$CaSO_4 \cdot 2H_2O$	Gypsum	1135, 1008, 670, 619, 493, 414, 217
Na_2SO_4	Thenardite	1149, 1128, 991 , 644, 632, 621, 466, 451
KNO_3	Niter	1359*, 1344*, 1050, 715, 417*
SiO_2	Quartz	695*, 464, 395*, 263
	Charcoal	1600, 1325

** Raman bands identified in laboratory*

92 J. Aramendia, L. Gomez-Nubla, K. Castro, I. Martinez-Arkarazo, D. Vega, A. Sanz López de Heredia, A. García Ibáñez de Opakua, J. M. Madariaga. Portable Raman study on the conservation state of four CorTen steel-based sculptures by Eduardo Chillida impacted by urban atmospheres. J. Raman Spectrosc.; 2012; 43: 1111-1117.

4.2.5. Sampling for the laboratory analysis

During the second campaign, in order to corroborate and complete the in situ study, a little amount of non degraded sandstone, limestone and mortar samples was collected to complement the elemental information with laboratory results. Afterwards, some efflorescences and bulk samples were gathered also to continue the spectroscopic study. The selected degraded samples (sandstones, ancient mortar, new mortar and limestone) of the internal walls were taken at different heights (at ground level, 1 and 1.7 meters, approximately). Twenty seven samples were extracted using a chisel and its size ranged from 10x10 mm to 25x25 mm and 1-3 mm of thickness, approximately. Besides, ten powdery samples were scraped from different efflorescences and subefflorescences.

4.2.6. Laboratory results

4.2.6.1. μ-X ray fluorescence

All the fresh samples were analyzed at the laboratory using a helium flow in order to determine the unknown composition. The results showed the presence of Al and Na in mortars, limestone and sandstones, being Na the major component in the last one. Moreover the absence of significant concentrations of toxic metals was also verified for all the samples, through a set of more than 50 measurements per sample to ensure the representativeness of the results.

4.2.6.2. Raman spectroscopy

With respect to sandstone samples, α-quartz, α-hematite (α-Fe_2O_3, characterized by a specific intense Raman band at 605 cm^{-1} and its secondary signals at 396, 276 and 215 cm^{-1}) and presumably amorphous charcoal (assigned according to only one of its characteristic bands at 1325 cm^{-1} since the data acquisition range was registered up to 1500 cm^{-1}) were found as original compounds.

The analysis also revealed many carbonated compounds related with the nature of these sandstones[93]. In this way, efflorescences and subefflorescences were composed of calcite, natrite, termonatrite ($Na_2CO_3 \cdot H_2O$, identified by a intense peak at 956 cm^{-1} and secondary signals at 579, 428 and 306 cm^{-1}), natron ($Na_2CO_3 \cdot 10H_2O$, identified by its main peak at 1068 cm^{-1}, aside from other secondary signals at 1533 and

93 F. García- Garmilla, I. Rodríguez-Maribona, M. Cano, M. Zalbide, J. A. Ibáñez-Gómez, K. Osa-Chans, S. Garín. An analytical comparison of two commercial consolidating products applied to eocene sandstones from 16th and 19th century monuments in San Sebastián, northern Spain. Mater. Construcc.; 2002; 52: 5-12.

210 cm^{-1}), trona and gaylussite ($Na_2Ca(CO_3)_2 \cdot 5H_2O$, characterised by the peak at 1070 cm^{-1} and two more signals at 261 and 164 cm^{-1}) (Fig. 4.15).

The existence of those salts suggests again the transformation of the original compounds due to the influence of infiltrated acid waters that could dissolve at first instance the original calcium and sodium carbonates, triggering the formation of the mentioned carbonate species.

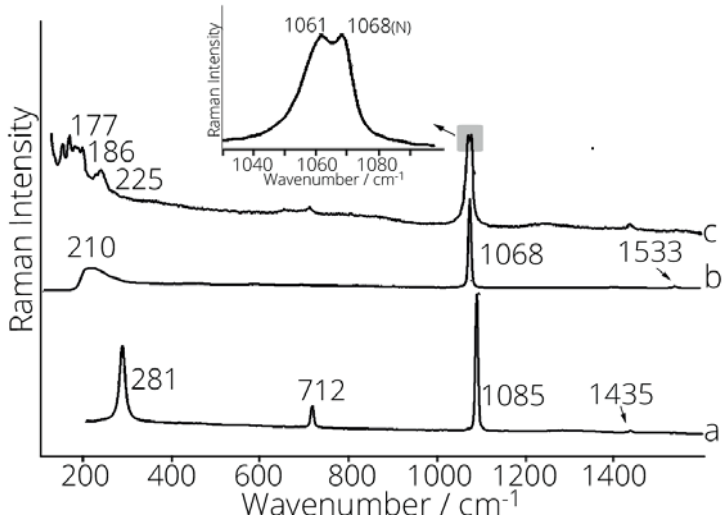

Figure 4.15. Spectra found in laboratory on sandstone of the central courtyard. a) Raman spectrum of calcite. b) Raman spectrum of natron. c) Raman spectrum of a mixture of trona and natron (N).

As in the in situ analysis, gypsum and nitratine ($NaNO_3$, with its main peak at 1067 cm^{-1}, apart from its secondary weak peaks at 1395, 724, 416 and a broad band at 190 cm^{-1}) were identified as decaying compounds in the surface of the samples analyzed in the laboratory (Fig. 4.16).

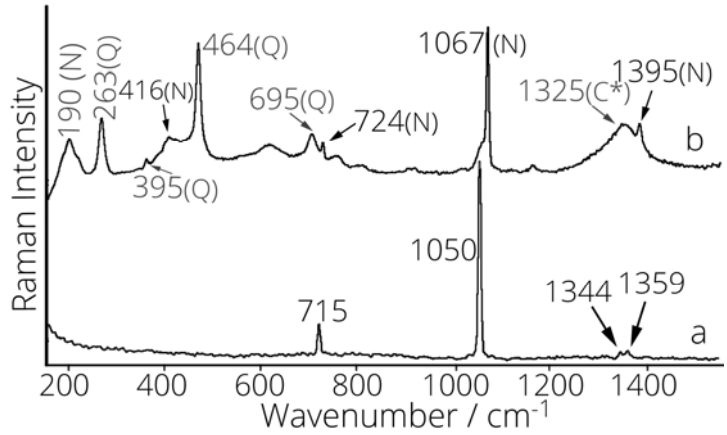

Figure 4.16. Spectra collected in the laboratory analyses. a) Raman spectrum of nearly pure niter found in joint mortar of the limestone wall. b) Raman spectrum of nitratine (N), a small amount of niter, quartz (Q) and likely charcoal (C) found in sandstone of the central courtyard.*

The source of nitratine is also related with the nitrates present in infiltration waters. The nitrates accessed by capillarity processes to the stones of the wall causing the formation of the salts by interactions between carbonate and the acid medium, giving the corresponding bicarbonate and the subsequent precipitation of the metal nitrate (see reaction 4.9). Mortars are commonly the natural way for the passage of water due to their higher porosity.

$$Na_2CO_3 + 2NO_3^- + H^+ \leftrightarrow 2NaNO_3 + HCO_3^- \quad (4.9)$$

However, in this case, the mortar presents less porosity than the sandstone as its grain size is high[94,95], allowing the stone to absorb the dampness and salinity of the infiltration water. The soluble salts are diffused through the pores causing more decaying in the sandstone carbonates than in the mortar[96], increasing the loss of the cementitious matrix, which would lead to a decrease in density, and therefore increasing the inside circulation of water and reducing the durability of the material. Therefore, the degradation of the wall could be in fact a consequence of an incorrect selection of the join mortar[95].

In all types of mortars, calcite, silicates such as orthoclase ($KAlSi_3O_8$, easily recognized by its five characteristic peaks of the feldespar-group at 1121, 513, 474, 455 and 281 cm^{-1}), rutile (TiO_2, Raman bands at 608 and 447 cm^{-1}), hematite and probably limonite ($FeO(OH)\cdot nH_2O$, Raman bands at 552, 394, 297 and 240 cm^{-1}) were identified as original compounds[96].

Moreover, the joint mortar of the sandstone wall showed carbonate based efflorescences and subefflorescences. Considering the composition of these mortars, natrite, termonatrite, natron and trona could come from the carbonate/bicarbonate ions from the sandstone, which involves, again, the entrance of water as an infiltration likely coming from the near river.

Laboratory analysis provided some other important findings regarding degradation compounds found in the in situ analysis. In this way, after the collection of several Raman spectra, mirabilite (identified by the main Raman band at 989 cm^{-1} and

94 I. Rodriguez-Maribona, M. Zalbide, F. Garmilla, F. Garcia, J.A. Ibanez, S. Garin. Chemical and mineralogical study of restoration mortars applied to the Eocene sandstones of Gipuzkoa used for building construction. Mater. Construcc.; 1999; 49: 19-30.

95 M. Cano, I. Rodriguez-Maribona, K. García-Garmilla, I. Yusta, J.A. Ibañez-Gómez, S. Garín. Caracterización y selección de morteros de restauración aplicados a areniscas del Eoceno de Gipuzkoa utilizadas en la construcción de edificios. Geogaceta; 2001; 30: 215-218.

96 F. García- Garmilla, I. Rodríguez-Maribona, M. Cano, M. Zalbide, J. A. Ibáñez-Gómez, K. Osa-Chans, S. Garín. An analytical comparison of two commercial consolidating products applied to eocene sandstones from 16th and 19th century monuments in San Sehastiány northern Spain. Mater. Construcc.; 2002; 52: 5-12.

the weakest pair of bands at 458 and 446 cm^{-1} aside from other signals at 1130, 1120, 1108, 628 and 616 cm^{-1}) was always found in restored mortars so that, the transport of the samples to the laboratory caused a change in its form of crystallization, since in the in situ analysis thenardite was identified instead of mirabilite and, thus, lack of in situ measurements would have caused an incorrect interpretation of the results.

In order to confirm that the origin of the thenardite was related mainly with the composition of the new mortar, one thin plate of Portland cement mortar was elaborated based on a commercial formulation[97] (70% siliceous sand, 12% white cement and 18% of commercial mixture of lime, calcite and porlandite). After its hardening, it was maintained in the water, with a small amount of ammonium solution (Fluka, Standard for IC) to increase the acidity thanks to the concentration of free hydrogen ions (H^+). After fifteen days, the plate was dried in the open air and one thin layer of whitish efflorescence was observed. These salts were identified as mirabilite, gypsum and calcite by Raman Spectroscopy. Although the experiment showed the possibility of forming mirabilite the amount observed was lower than expected. Hence, another source of mirabilite that could be taken into account is the ionic content of infiltration water.

With regard to the laboratory analyses on limestones, nitrocalcite ($Ca(NO_3)_2{\cdot}4H_2O$, Raman bands at 1050, 745 and 719 cm^{-1}) was identified in isolated cases, as well as niter thanks to the acquisition of the bands corresponding to its minor vibration modes at 1359, 1344 and 417 cm^{-1} (Fig. 4.16).

Niter was found from the base of the wall up to two meters height, where the presence of a salt front, uniformly distributed along the high part, can be observed. In this case, the capillarity process is different to that described for the sandstone. The infiltration water penetrated through joint mortars and found a barrier in the limestone where the soluble salts crystallized as efflorescences in the joints and the surface of the stone[98]. In fact, thanks to the high mobility of dissolved nitrates and the narrow rising path along the mortar, the presence of these nitrate compounds was observed in medium to high areas of the walls as well.

97 J. A. Ibáñez-Gómez, I. Yusta, F. García- Garmilla, M. Cano, I. Rodriguez-Maribona, K. Beraza, S. Garín. Chemical and mineralogical study of restoration mortars applied to the Eocene sandstones of Gipuzkoa used for building construction. Geogaceta; 2001; 30: 223-226.

98 M. A. Vázquez, E. Galán, M. A. Guerrero, P. Ortiz. Digital image processing of weathered Stone caused by efflorescences: A tool for mapping and evaluation of Stone decay. Constr. Build. Mater.; 2011; 25: 1603-1611.

With regard to the source of potassium, it could be explained by the acid (water is rich in ammonium) attack over original potassium feldspar[99] (orthoclase previously identified) causing its hydrolysis and the formation of the corresponding nitrate salt (see reaction 4.10).

$$KAlSi_3O_8 + 8H_2O + NO_3^- + H^+ \rightarrow Al(OH)_3 + 3Si(OH)_4 + KNO_3 + H_2O \qquad (4.10)$$

However, although the content of potassium derived from feldspar alteration is particularly high in this kind of stone[100], it is probable the existence of another source of this ion, such as water coming from the soil, which in this location contains a high amount of dissolved potassium[99].

Regarding the limestone samples, the analysis showed calcite and amorphous carbon (responsible for the characteristic black color of this stone) as original and anthropic components, respectively. Niter was also found but its presence was due to its growth as efflorescence from the adjacent mortar and not as direct degradation, as was the case in the sandstones.

All in all, the laboratory analyses provided better defined spectra in comparison to those obtained in situ as a consequence of the higher sensitivity of the equipment as well as the helpful accessories that it offers (microscopic analysis, various lasers and different ranges of spectrum acquisition), which enable the visualization of hidden signals that were not visible in the in situ spectra due to the high fluorescence. Therefore, laboratory analyses allowed the identification of some compounds that were not previously detected in the field and their corresponding Raman bands are summarized in Table 4.5.

99 V. Matović, S. Erić, A. Kremenović, P. Colomban, D. Serćković-Batoćanin, N. Matović. The origin of syngenite in black crusts on the limestone monument King's Gate (Belgrade Fortress, Serbia)—the role of agriculture fertiliser . J. Cult. Herit.; 2012; 13: 175-186.

100 I. Rodriguez-Maribona, M. Zalbide, F. Garmilla, F. Garcia, J.A. Ibanez, S. Garin. Chemical and mineralogical study of restoration mortars applied to the Eocene sandstones of Gipuzkoa used for building construction. Mater. Construcc.; 1999; 49: 19-30.

Table 4.5. Summary of the compounds found in laboratory

Compounds identified in laboratory		
Formula	Name	Raman bands ν (cm^{-1})
$Na_2CO_3·H_2O$	Termonatrite	956, 579, 428, 306
$Na_2CO_3·10H_2O$	Natron	1533, 1068, 210
$Na_2Ca(CO3)_2·5H_2O$	Gaylussite	1070, 261, 164
$Na_2SO_4·10H_2O$	Mirabilite	1130, 1120, 1108, 989, 628, 616, 458, 446
$NaNO_3$	Nitratine	1395, 1067, 724, 416, 190
$Ca(NO_3)_2·4H_2O$	Nitrocalcite	1050, 745, 719
$KAlSi_3O_8$	Orthoclase*	1121, 513, 474, 455, 281
TiO_2	Rutile*	608, 447
α-Fe_2O_3	Hematite	605, 396, 279, 215
$FeO(OH)·nH_2O$	Limonite*	552, 394, 297, 240

**Measured with 514 nm laser*

4.2.7. General remarks of spectroscopic assessment

With regards to the XRF results, this technique was profitable as it allowed discarding the presence of particulate matter of anthropogenic source, avoiding further destructive laboratory analyses. Moreover, it facilitated the interpretation of the spectra, being crucial to distinguish between some compounds, such as niter and nitrocalcite.

As for the analytical results, a variety of carbonated efflorescence salts such as calcite, natrite, termonatrite, natron, trona and gaylussite indicated a transformation of original compounds of sandstones due to the influence of water. Gypsum and nitratine were identified as the main decaying compounds of sandstones, whereas niter and thenardite were the most abundant in ancient and restored mortars, respectively. The origin of those salts lies on acidic infiltration waters and the original composition of the materials. On the other hand, the source of potassium is linked to the hydrolysis of orthoclase, whereas the input of calcium and sodium is mainly associated to acid attack over original carbonates. In both cases, the ionic content of the infiltration water increases the presence of these salts.

The combination of XRF and Raman spectroscopic techniques was a very suitable methodology for the preliminary diagnosis of the conservation state of building materials, allowing the identification of most of the degradation compounds simultaneously to the sampling campaign. The previous knowledge of the type of building materials present in the site of study, as well as the experience in measuring them assisted to a great extent in the decision making for restoration.

4.3. Analytical approach to determine the decaying mechanisms and the severity of damage caused by salt weathering

Once confirmed the affections by non destructive techniques, a multidisciplinary approach was adopted to corroborate the previous phase and to evaluate the conservation state of the Palace. In this way, the quantification of soluble salts was carried out by ion chromatography, and subsequently, a chemometric analysis of ion content data of the materials was also performed, studying the amount and mobility of the salts present. Finally, to clarify the manner in which salts can damage the building walls, thermodynamic models of the different chemical processes that take place in the building were assessed.

Thus, the purpose of this section was to corroborate the origin, mechanism and severity of the damage suffered by the different materials of the Palace, as the effectiveness of treatments of conservation, both preventive and active, will depend on them. Besides, the corresponding article can be consulted in the scientific publication Annex.

4.3.1. Sampling for the analytical study

As it was explained in the section 4.2.5, during the second in situ sampling campaign performed in February 2012, in accordance to the visual inspection and a preexisting in situ spectroscopic study, only eleven samples of sandstone and mortar were gathered, in sufficient amount for chromatographic analysis of soluble salts (Table 4.6.). Prior to the quantitative analysis, the visible efflorescences of the samples were removed in order to quantify the real content of the building materials. Moreover, the removed soluble salts were analyzed too (EM1, EM2, and EM5 samples).

Table 4.6. Building material samples collected in the Palace House studied. The kind of material, height on the wall and zone of the building is indicated.

Sample	Material	Height	Zone
SM1	Sandstone	Medium	Courtyard
EM1	Subefflorescence	Medium	Courtyard
SM2	Sandstone	Low	Courtyard
EM2	Efflorescence	Medium	Courtyard
SM3	Sandstone	Medium	Courtyard
SM4	Sandstone	Medium	First room
MM5	Mortar	High	First room
EM5	Efflorescence	High	First room
MM6	Mortar	Low	First room
MM7	Mortar	Low	First room
SM8	Mortar	Medium	First room
MM9	Mortar	Low	Corridor
MM10	Mortar	Low	Courtyard
MM11	Mortar	Low	First room

4.3.2. Analytical study results

4.3.2.1. Quantification of soluble salts by ion chromatography

Thanks to ion cromatography, soluble fluoride, sulphate, nitrite, nitrate, chloride, calcium, sodium, potassium and magnesium concentration were quantified (Table 4.7). To know if the salt removal procedure is necessary, the total soluble content of the samples was calculated (Table 4.8) in accordance with the UNI guide and

the guide of Salt Attack and Rising Damp[101-102]. Apart from that, the percentage of sulphate, chloride and nitrate of the samples were calculated separately (Table 4.8) to classify the severity of the damage presented, according to a guide issued by Fraunhofer-IRB[103].

Table 4.7. Concentration values in mg Kg^{-1} and method repeatabilities, in RSD %, obtained by ion chromatography.

Sample	Na^+	K^+	NH_4^+	Mg^{2+}	Ca^{+2}	Cl^-	NO_3^-	SO_4^{-2}
SM1	$1.1 \times 10^{+3}$	$4.1 \times 10^{+3}$	<QL	< DL	$1.3 \times 10^{+4}$	$3.4 \times 10^{+3}$	$1.6 \times 10^{+4}$	$1.8 \times 10^{+4}$
EM1	$2.2 \times 10^{+5}$	$4.3 \times 10^{+3}$	<DL	< DL	$1.7 \times 10^{+3}$	$2.8 \times 10^{+3}$	$5.9 \times 10^{+3}$	$1.6 \times 10^{+3}$
SM2	$2.1 \times 10^{+3}$	$1.1 \times 10^{+3}$	<QL	< DL	$4.4 \times 10^{+3}$	$2.4 \times 10^{+3}$	$6.6 \times 10^{+3}$	$5.7 \times 10^{+3}$
EM2	$2.8 \times 10^{+5}$	$1.0 \times 10^{+3}$	< DL	< DL	$4.3 \times 10^{+2}$	$2.4 \times 10^{+2}$	$1.5 \times 10^{+3}$	$5.9 \times 10^{+2}$
SM3	$4.4 \times 10^{+3}$	$9.6 \times 10^{+2}$	< DL	< DL	$9.7 \times 10^{+4}$	$6.4 \times 10^{+3}$	$8.0 \times 10^{+3}$	$2.4 \times 10^{+5}$
SM4	$4.9 \times 10^{+3}$	$1.1 \times 10^{+3}$	<QL	$1.80 \times 10^{+2}$	$2.8 \times 10^{+3}$	$7.1 \times 10^{+3}$	$7.9 \times 10^{+3}$	$8.2 \times 10^{+2}$
MM5	$3.2 \times 10^{+3}$	$4.7 \times 10^{+3}$	<QL	< DL	$1.1 \times 10^{+4}$	$4.3 \times 10^{+3}$	$2.2 \times 10^{+4}$	$5.1 \times 10^{+3}$
EM5	$1.5 \times 10^{+2}$	$3.8 \times 10^{+5}$	< DL	< DL	$6.3 \times 10^{+2}$	< DL	$8.1 \times 10^{+5}$	$1.2 \times 10^{+3}$
M6	$2.5 \times 10^{+5}$	$4.2 \times 10^{+3}$	< DL	< DL	$5.0 \times 10^{+2}$	$1.3 \times 10^{+3}$	$2.4 \times 10^{+3}$	$3.6 \times 10^{+3}$
MM7	$2.1 \times 10^{+5}$	$5.9 \times 10^{+2}$	< DL	< DL	$9.1 \times 10^{+2}$	$1.3 \times 10^{+3}$	$2.7 \times 10^{+3}$	$2.0 \times 10^{+3}$
SM8	$7.5 \times 10^{+3}$	$2.0 \times 10^{+3}$	<QL	< DL	$5.5 \times 10^{+3}$	$1.0 \times 10^{+4}$	$1.2 \times 10^{+4}$	$2.4 \times 10^{+3}$
MM9	$4.9 \times 10^{+2}$	$6.1 \times 10^{+2}$	<QL	$1.5 \times 10^{+2}$	$1.6 \times 10^{+3}$	$4.7 \times 10^{+2}$	$6.1 \times 10^{+2}$	$6.0 \times 10^{+3}$
MM10	$9.5 \times 10^{+3}$	$1.2 \times 10^{+4}$	<QL	$2.3 \times 10^{+2}$	$1.7 \times 10^{+4}$	$1.2 \times 10^{+4}$	$3.3 \times 10^{+4}$	$1.9 \times 10^{+4}$
MM11	$4.1 \times 10^{+3}$	$2.9 \times 10^{+3}$	<QL	$3.5 \times 10^{+2}$	$3.2 \times 10^{+4}$	$6.5 \times 10^{+3}$	$2.8 \times 10^{+4}$	$4.0 \times 10^{+4}$

101 E. Pinto. Risanamento di murate umide e degrádate. Italy: Dario Flaccovio; 2011.

102 D. Young. Salt attack and rising damp. A guide to salt damp in historic buildings and older buildings. South Australian: Heritage Council of NSW; 2008.

103 M. Auras. Leitfaden Naturstein-Monitoring. Nachkontrolle und Wartung als zukunftsweisende Erhaltungsstrategien. Fraunhofer-IRB-Verl: Stuttgart; 2011.

Sample	Na^+	K^+	NH_4^+	Mg^{2+}	Ca^{+2}	Cl^-	NO_3^-	SO_4^{-2}
RSD(%)	2	7	--	4	4	2	4	3
DL*	1.5×10^{-1}	1.5×10^{-1}	3.2×10^{-1}	2.2×10^{-1}	1.5×10^{-1}	2.3×10^{-1}	2.6×10^{-2}	1.20
QL**	4.8×10^{-1}	4.7×10^{-1}	1.70	7.4×10^{-1}	4.7×10^{-1}	5.20	1.3×10^{-1}	3.50

** DL limit of detection, ** QL limit quantification*

According to the results summarized in the Tables 4.7 and 4.8, a high soluble salt content of the materials was revealed. The samples collected in the courtyard showed as major compounds nitrates and sulphates whereas nitrates were the predominant compounds in the first room..

Table 4.8. Values of soluble salt content of the samples (referred to sample weight) obtained by ion chromatography.

Wt %	SO_4^{2-}	Cl^-	NO_3^-	Total salts*
SM1	1.8	0.34	1.6	6.9
SM2	0.57	0.24	0.6	2.5
SM3	23.9	0.64	0.0	35.7
SM4	0.08	0.71	0.9	2.8
MM5	0.51	0.43	2.2	6.3
MM6	0.36	0.13	0.24	69.7
MM7	0.20	0.13	0.27	58.2
SM8	0.24	1.0	1.2	4.7
MM9	0.60	0.05	0.06	1.0
MM10	1.9	1.20	3.3	12.2
MM11	4.0	0.65	2.8	14.0

**Taking into account bicarbonate content*

According to the classification of salts levels that are considered potentially hazardous for porous materials[104], only samples MM6 and MM7 showed low or medium levels for these compounds. The remaining samples showed severe levels, reaching Extreme Grade (IV) in most cases, which indicate high destruction and hygroscopic moisture

In samples visibly affected by salts the total content of salt shows percentages above 35%. However, values lower than 35% were found in samples that apparently did not showed efflorescences or visible damage, exceeding the limit of 10% considered as gravely polluted according to the UNI standard[105]. These high percentages, similar to values observed in Venice, could be caused by dissolution of the main component, in this case calcite. An acid pH is required for this to happen, which in this case is easily reachable by the acid infiltration water of the area, whose pH values were between 5.7 and 6.4 during the samplings carried out.

In addition, it is noteworthy to mention that, samples of mortar, MM10 and MM11, showed more than 10% of salt content. These sampling points correspond to the bases of the walls without damage. However, the top of the wall showed efflorescences, a front of salts and loss of material (Fig. 4.9 e). These samples had, as shown in the Tables 4.7 and 4.8, a high content of nitrate. This soluble salt increased in concentration with the distance to the adjacent river facade; given its distribution and high mobility, the fact that is found at such low points, suggests saline infiltration water as its main source.

According to the data registered about the water of this region, during the last years, high concentrations of ammonium are observed (Fig. 4.17), probably derived from industry and agricultural activities due to inefficient wastewater purification[106]. Ammonium nitrate can react with the original composition of mortars giving rise to the decay compounds[107,108]. The simultaneous presence of ammonium and nitrates, in the same samples, suggests that the ammonium nitrate has not reacted totally. Therefore, it seems that there is a reservoir of this compound coming from the subsoil. Over the

104 M. Auras. Leitfaden Naturstein-Monitoring. Nachkontrolle und Wartung als zukunftsweisende Erhaltungsstrategien. Fraunhofer-IRB-Verl: Stuttgart; 2011.

105 E. Pinto. Risanamento di murate umide e degrádate. Italy: Dario Flaccovio; 2011.

106 Gipuzkoa County Council. Bases para la elaboración de las directrices sobre el uso sostenible del agua en Gipuzkoa, Study of river quality. Gipuzkoa, North of Spain: Gipuzkoa County Council; 2006.

107 D. Young. Salt attack and rising damp. A guide to salt damp in historic buildings and older buildings. South Australian: Heritage Council of NSW; 2008.

108 H. Morillas, M. Maguregui, O. Gómez Laserna, J. Trebolazaba, J.M. Madariaga. Could marine aerosol contribute to deteriorate building materials from interior areas of lighthouses? An answer from the analytical chemistry point of view. J. Raman Spectrosc.; 2013; 44: 1700-1710.

years, the walls could have been feeding constantly with salt-bearing moisture, increasing the rising damp caused by capillary action.

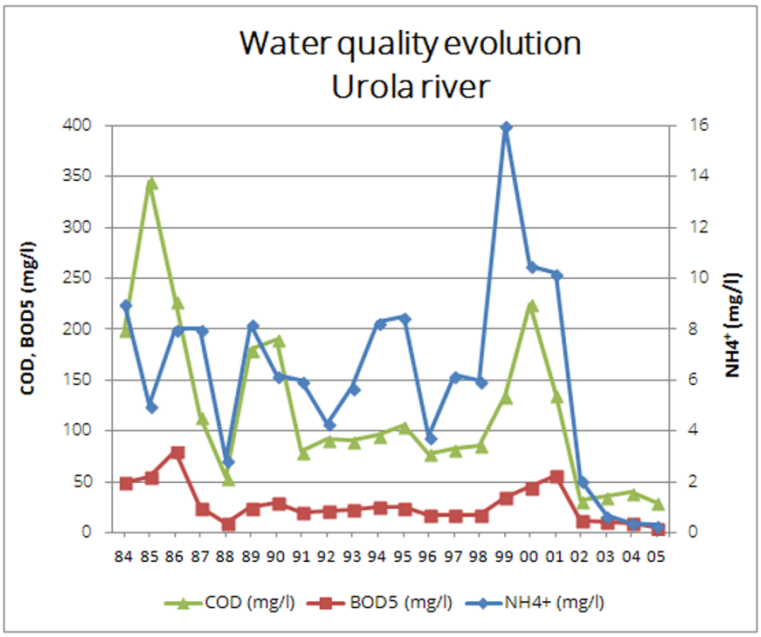

Figure 4.17. Historic values of ammonium, Chemical and Biochemical oxygen demand (COD and BOD_5, respectively) observed in the Urola River. Information extracted from the report "Bases for the elaboration of guidelines on sustainable use of water in Gipuzkoa", Gipuzkoa County Council, Department for Sustainable Development, Directorate General of Hydraulic Works.

In practice, the height to which water will rise in the wall is limited by the rate of evaporation of water from the wall surfaces (related to the masonry materials, surface coatings, climate and so on)[107]. Besides, salt zoning along the wall is the result of fractionating the solution, which depends on the nature of the salts (mobility, solubility, etc) as well as the above variables. To examine and illustrate the distribution of salt with respect to height in the case under study, the mean values for the ions quantified are shown in Figure 4.18.

A progressive distribution of salt zones was observed. From the first moment, in the rise of water through the wall, the solution starts to evaporate. However, at ground level, the evaporation rate is not enough to effectively concentrate the solution. By contrast, in low and middle areas, the evaporation rate sufficiently exceeds the supply rate of the solution, so that the concentration increases to saturate the less soluble salts, mainly calcium sulphates and sodium carbonates, as Raman spectroscopy also indicated.

Once less soluble salts precipitate, the most soluble ions are available in the solution. Then, to observe efflorescences at highest areas, high values of evaporation rates and mobility are required. In this way, chlorides are located predominantly in the middle region of the wall, and sodium and potassium nitrates at the top. Thus, in low

areas, less soluble and mobile salts could be found; in contrast, more soluble and mobile salts migrate towards higher areas.

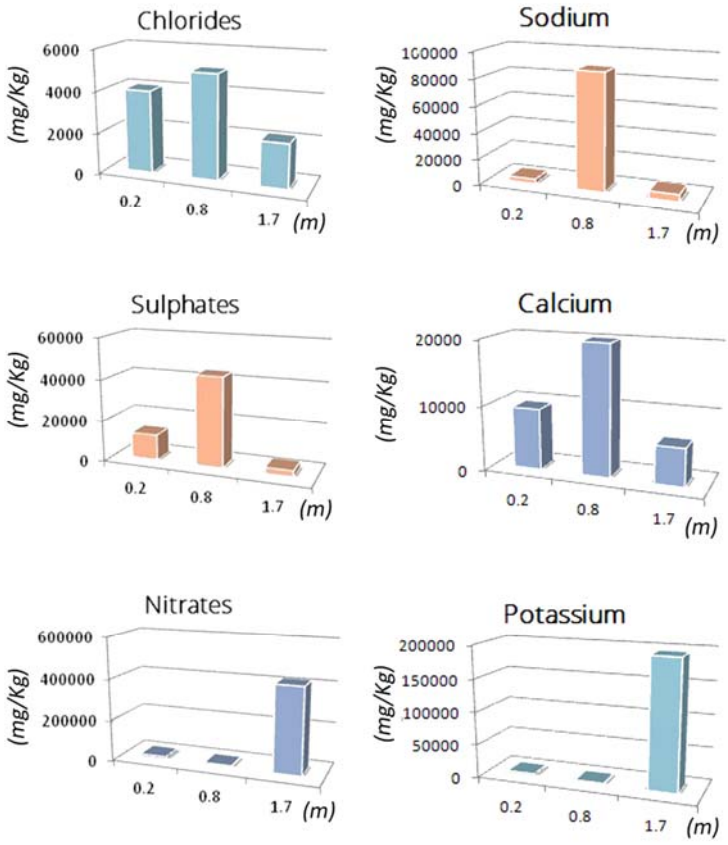

Figure 4.18. Average of ion content determined by ion chromatography at different heights in the walls at the test site.

Nevertheless, the amounts of efflorescences observed can be relatively minor, even remain unnoticed, since the precipitation of deliquescent salts depend on the absorption of water from the atmosphere and, they could be condensed, favouring or not its redissolution, as is the case of sodium carbonate. Although, the vertical distribution of salts is approximate to Arnold and Zehnder´s model[109-111], the salt

109 E.R. Agudo, B. Lubelli, A. Sawdy, R.V. Hees, C. Price, C.R. Navarro. An integrated methodology for salt damage assessment and remediation: the case of San Jerónimo Monastery (Granada, Spain). J. Environ. Earth Sci.; 2011; 63: 1475-1486.

110 M.A. Vázquez, E. Galán, P. Ortiz, R. Ortiz. Digital image analysis and EDX SEM as combined technique to evaluate salt damp on walls. J. Constr. Build Mater.; 2013; 45: 95-105.

111 M. Auxiliadora Vázquez, E. Galán, M.A. Guerrero, P. Ortiz. Digital image processing of weathered stone caused by efflorescences: A tool for mapping and evaluation of stone decay. J. Constr. Built Mater.; 2011; 25: 1603-1611.

distribution model can be slightly altered as the acid infiltrated water can increase the concentration of salts by drag from the adjacent original materials[112-113].

Besides, the presence of front salts, located in areas affected by moisture of capillary ascension, under the influence of mortars, seem to point to the idea that its origin is in the saline content of infiltration acid water, which supports the hypothesis again.

4.3.2.2. Principal component analysis of the IC results

The multivariate analysis of the data was used to obtain further information on the correlation of quantitative analysis.

The obtained Principal Component Analysis (PCA) explained 87% of the variance, using 3 PCAs to simplify the system. As can be seen in Figure 4.19, some salts formation is suggested with the grouping of three clusters; sodium and carbonate, potassium and nitrate and magnesium and chloride.

Sodium was extremely correlated with carbonated content (r = 0.999) indicating their common precedence from degradation of the original composition of sandstones. Efflorescence samples EM1 and EM2 were also close to that cluster. This fact is supported with the identification of several carbonated efflorescences in the previous spectroscopic study.

These results, together with the entry of acid waters previously shown, demonstrate the damage in the ashlars by loss of original material. In addition to its dissolution and migration, its effect is increased by the equilibrium of hydration of sodium carbonate, which is present in its mono and decahydrate form. As a result, the pressure in the network of pores is increased by the change of volume produced during hydration/dehydration cycles. In fact, natron, the decahydrated form, is ranked as the third most aggressive salt for building materials and, in this case, it is suggested as the main cause of the disintegration and flaking of sandstone[114].

112 P. Lopez Arce, E. Doehne, W. Martin, S. Pinchin. Magnesium sulfate salts and historic buildings materials: experimental simulation of limestone flaking relative humidity cycling and crystallization of salts. J. Mater. Constr.; 2008; 58: 125-142.

113 C. Hall, D.H. Willian. Rising damp: capillary rise dynamics in walls. Proc. R. Soc. A.; 2007; 463, 1871-1884.

114 J.G. Talegón, M.A. Vicente. Decay of granite monuments due to salt crystallization in a non-pollutes environment. J. Mater. Construcc.; 1998; 49: 17-27.

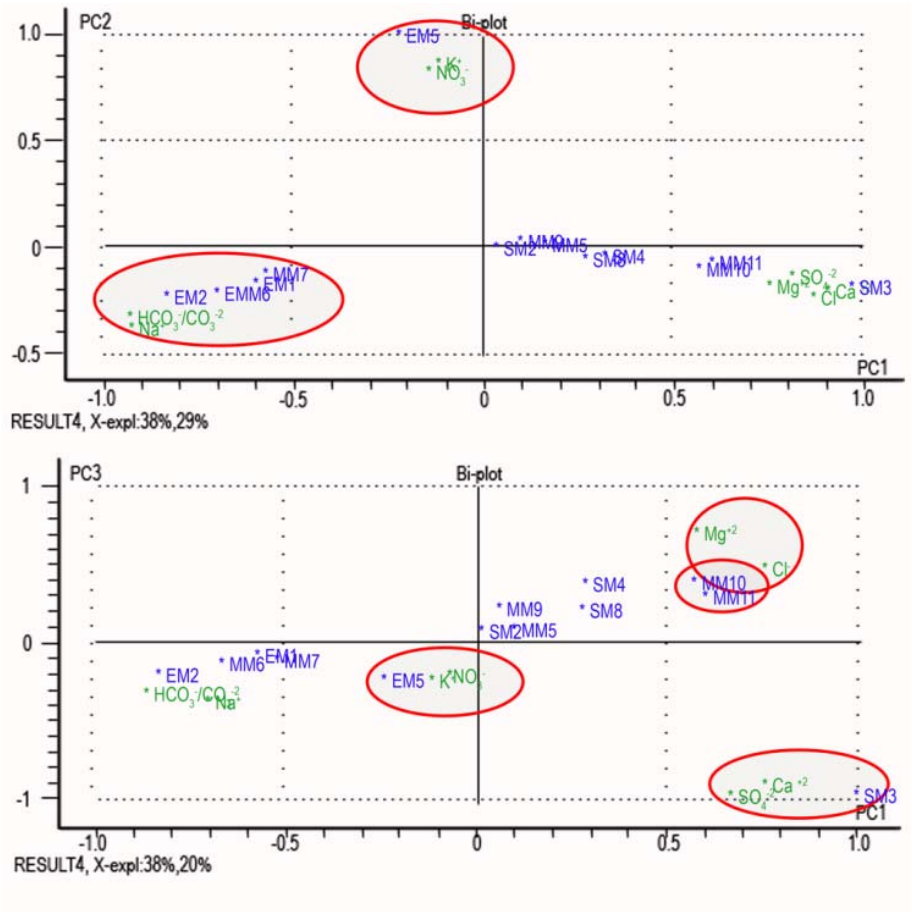

Figure 4.19. PCAs carried out by Unscrambler . a) Representation of PC1 vs PCA2 of the results obtained by ion chromatographic. b) PC1 vs PCA3. Representation of groups formed according to the main three principal components are highlighted: carbonate, nitrates, sulphates and chloride.

Moreover, sodium shows a low negative correlation with chloride (r = -0.470), which could indicate that the source of chloride is not original, confirming, as with its observed levels (Fig. 4.18), it comes with the infiltration water and its passage through the ground.

Potassium is only correlated with nitrate (r = 0.999) and, the proximity of EM5 (Fig. 4.19), efflorescence of the front salt, indicates its main composition. The origin of potassium could be related to two different sources, salt content of the infiltration water and/or it could correspond to an original compound of mortar and limestone. Therefore, this formation mechanism will be studied later in depth.

Apart from that, calcium highly correlates with sulphates (r = 0.981). The formation of calcium sulphates in carbonated materials is a known process. Its formation needs an acid medium to dissolve the original calcite and a sulphate input,

which, in this case, could be explained by the action of acid waters over original carbonate, increased by sulphate additives of new mortars and water ion content[115-117].

Finally, magnesium is correlated with chlorides, in a lesser extent. Although, in principle this salt is not considered very harmful, studies have demonstrated that the presence of chlorides in solution could encourage dissolution of calcite as well as transformation of the iron oxides[118-120].

The results are quite interesting because the formation of magnesium chloride was not previously detected by Raman spectroscopy in the previous non destructive screening as it is not Raman active. Besides, others salts such as sodium nitrate and sodium sulphate, which were detected during the screening phase, were not predicted by the chemometric study. This fact is probably due to the great amount of carbonate salts, which could make them unnoticeable, and/or the sampling was performed in a rainier season. Then, changes in weather conditions could have caused its dissolution.

4.3.2.3. Thermodynamic modelling: mechanism of potassium metasomatism and niter formation

Thermodynamic chemical modelling was focused on the better understanding of the chemical reactions involved in the formation of the salt front of nitrates. Since, the formation of calcium sulphate has been widely studied[121-122]. In this way, niter formation by action of infiltration water over the limestone wall was predicted.

115 P. Lopez Arce, E. Doehne, W. Martin, S. Pinchin. Magnesium sulfate salts and historic buildings materials: experimental simulation of limestone flaking relative humidity cycling and crystallization of salts. J. Mater. Constr.; 2008; 58: 125-142.

116 M.L. Sánchez de Rojas, N. García, M. Frías. Influence of the enviroment on weathering of limestone: study through mercury porosimetry. J. Mater. Construc.; 1998; 49: 31-41.

117 V. Matović, S. Erić, D. Srećkovic Btoćanin, P. Colobam, A. Kremenović. The influence of building materials on salt formation in rural environments. J. Environ. Earth Scie.; 2014; 72: 1939-1951.

118 J.J. McAlister, B.J. Smith, A. Török. Element partitioning and potential mobility within surface dust on building in a polluted urban environment, Budapest. J. Atmos. Environ.; 2006; 40: 6780-6790.

119 S.S. Seo, S.M. Son, C.H. Lee, K. Baek. Compositional analysis of soluble salt in Bresle Extraction from Blocks in Newbuildings Shipyards. Osaka: ISST; 2007.

120 S. Nikolaos Alexis, P. Theoulakis, C. Pilinis. Dry deposition effect of marine aerosol to the building stone of the medieval city of Rhodes, Greece. J. Built Environ.; 2009; 44: 260-270.

121 J. Aramendia, L. Gómez Nubla, K. Castro, J.M. Madariaga. Spectroscopic speciation and thermodynamic modeling to explain the degradation of weathering steel surfaces in SO2 rich urban atmospheres. J. Microchem.; 2014; 115: 138-145.

According to the discussion of the results, its origin appears to be related to the acid infiltration water action over limestone and mortar materials. Therefore, as source of potassium, the hydrolysis of the aluminum silicate was studied first (Fig 4.20 a). The mass fraction diagram of potassium shows that its hydrolysis starts at pH values lower than 8, which are easily reached by common infiltration waters. In addition, given the presence of a high concentration of ammonium in the waters of this region, the release of potassium is clear.

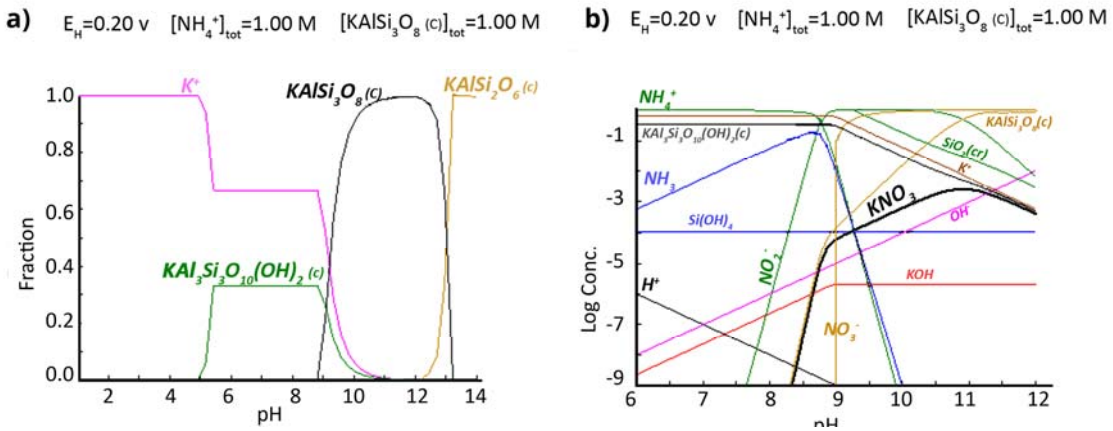

Figure 4.20. Medusa software chemical prediction of niter formation. Attack mechanism of acid waters over limestone slabs, composed by potassium feldspar and ammonium. Input concentration corresponds to the composition of each material and the historic analyses of water.

Subsequently, the action of ammonium over the feldspar was studied (Fig. 4.20 b). Potassium nitrate formation is predicted at pH values higher than 8. These facts suggest the need for its formation in two steps. Firstly, thanks to the low pH of the infiltration waters, leaching of potassium from limestone occurs. It is in the second step, as the calcareous material react (increasing pH) and the drying of materials takes place, when the saturated solution of niter precipitate. Therefore, its formation could be explained by the acid water attack over the original potassium feldspar of limestone and joint mortars. The hydrolysis and the formation of niter seem to follow the reactions 4.11, 4.12 and 4.13.

$$2KAlSi_3O_8 + 11H_2O \leftrightarrow Si_2Al_2O_5(OH)_4 + 4Si(OH)_4 + 2K^+ + 2OH^- \quad (4.11)$$

$$KAl_3Si_3O_{10}(OH)_2 + H^+ + 1.5H_2O \leftrightarrow 1.5Si_2Al_2O_5(OH)_4 + K^+ \quad (4.12)$$

$$K^+ + NO_3^- \leftrightarrow KNO_3 \quad (4.13)$$

122 M. Maguregui, U. Knuutinen, I. Martínez Arkarazo, K. Castro, J.M. Madariaga. Thermodynamic and Spectroscopic Speciation to Explain the Blackening Process of Hematite Formed by Atmospheric SO2 Impact: The case of Marcus Lucretius House (Pompeii). J. Anal. Chem.; 2010; 83: 3319-3326.

Therefore, once the acid water reaches mortar of the wall base, the water content ascends the wall by capillarity effect, hydrolyzing the original compound. The soluble salt reaches the surface and finds a barrier in the limestone, where they crystallize as efflorescences, in joints and surfaces, forming a front of salts, in which niter is the main compound by its high solubility and mobility.

However, although the content of potassium derived from feldspar alteration is particularly high in this kind of materials, and some extra amount from the subsoil is necessary, its presence is probably due to agricultural work in the area too.

4.3.3. General remarks

According to the results, the analytical methodology used allows determining the main source of degradation as acid water infiltration from the ground as well as its effect over the original materials. In addition, formation mechanisms of degradation compounds were explained applying chemometric and thermodynamics modelling software. In this manner, the applied methodology points out the importance of understanding the chemistry behind the damage caused by salt weathering over the building materials, as it not only indicates the formation of harmful salts within the materials, but rather it gives an idea of the extent of infiltration water migration in porous systems of masonry materials.

It should be noted that, areas that did not seem visibly affected by soluble salts showed high percentages of soluble salts, evidencing that, in any case, this kind of analytical study is needed not to overlook one of the most harmful pathologies of historic buildings. Likewise, quantitative analysis allowed classifying the degree of the pathology, suggesting necessary desalination process after avoiding or reducing the entrance of water. Moreover, given the loss of material suffered by the transformation of the original compounds and since, some parts such us columns have structural functions, the evaluation about residual hardness of the stones and mortars are suggested to help the conservators to identify a time limit before of a severe damage be caused in the structure. Taking into account the soluble salts values obtained, the consolidation and reinforcement works of the structures are urgent to assure the maintenance of the Palace house.

Finally, as the methodologies based on Raman cannot detect ionic bonds, they must be complemented with other analytical techniques for the detection of chlorides, as this compound plays an important role as a catalyst of degradation reactions. Apart from that, the mechanism of niter formation from pH higher than 8 evidences, one more time, the necessity of quantitative analyses to detect its presence in humid conditions, as it could be not saturated. Similarly, spectroscopy techniques are really useful to detect damage by hydration and dehydration cycles, as well as by other harmful compounds, as thenardite in this case, as their minor presences could go unnoticed by chemometric studies. Thereby, a combination of both methodologies is

really advised to perceive other important sources of degradation, like the effect of additives in materials incorporated into the building during restoration process.

4.4. Conclusions

Overall, the work performed in Basozabal Palace House shows how useful is use the Raman spectroscopy as a main technique in the diagnosis of historic buildings. Besides, the advantages presented by its combination with elemental spectroscopic techniques such as XRF have to be highlighted in the development of non destructive in situ studies, since it allows finding out the origin of the different pathologies in a fast, economical way.

Moreover, the combination of spectroscopic techniques with analytical methodologies proves to be a good tool to be used as a routine protocol, thus avoiding to overlook the presence of harmful compounds for stony materials, such as chlorides. In addition, thanks to this protocol, the severity of the pathologies suffered by building materials can be quantified, ensuring compliance with existing regulations in restoration.

CHAPTER 5: ANALYTICAL METHODOLOGY BASED ON THE IN SITU SPECTROSCOPIC ASSESSMENT INCLUDING DRIFT IN AN OPERATIONAL CASE: THE GUEVARA PALACE

After demonstrating the usefulness of in situ spectroscopic assessment as well as the added benefits of its combination with analytical methodologies, a novel approach is addressed in this work with the goal of minimizing the drawbacks observed in the diagnosis protocol proposed to study historical buildings.

Unfortunately, as it was explained in Chapter 4, the materials of built heritage often contain cromophore compounds which can produce a great fluorescence in the Raman signal, hampering the in situ analysis. Some of them are inherent in the composition such as clays[1-2]. However, others are incorporated to the material by infiltration or deposition of external agents as organic matter[3] or dust[4].

1 M. Julleh, J. Alalur, R. Ahman, S. Higeyuki, S. Uzuki. Geochemistry of sandstones from the Miocene Surma Group, Bengal Basin, Bangladesh: Implications from Provenance, tectonic setting and weathering. Geochem. J.; 2007; 41: 415-428.

Although, some techniques like photobleaching (overexposure to laser) can help to reduce this effect, the reality is that the options that could be taken in field analyses are complex to accomplish. Adding to this issue, the interferences arising from the environmental conditions[5-6], as the effect of strong sunlight, make sometimes the analysis more complicate, could result in the overlapping of peaks or even, in the worst cases, in the absence of a valid signal. For this reason, in order to minimize these problems, the diagnosis protocol proposed in chapter 4 could be complemented by other technique of molecular characterization.

In this sense, Fourier Transform Infrared spectroscopy (FTIR) is a powerful technique to study compounds with different nature and, it is one of the most appreciated tools for having a lot of flexibility, as it can be used in various modes such as pellets[7], diamond anvil[8], diffuse reflectance[9] (DRIFT), specular reflectance[10] and Attenuated Total Reflection[11] (ATR). Besides, according to the literature, different kinds

2 J. Arostegui, M.J. Irabien, F. Nieto, J. Sangüesa, M.C. Zuluaga. Microtextures and the origin of muscovite-kaolinite intergrowths in sandstones of the Utrillas Formation, Basque Cantabrian basin, Spain. Caly Caly Miner. ; 2001; 49: 529-539.

3 E. Plaster. Soil Science and Management. Albany: Delmar Publishers; 1996.

4 N. Prieto-Taboada, I. Ibarrondo, O.Gómez-Laserna, I. Martínez-Arkarazo, M.A. Olazabal, J.M. Madariaga. Buildings as repositories of hazardaous pollutants of anthropogenic origin. J. Hazard Mater.; 2013; 248-249: 451-460.

5 J. Jehlička, P. Vítek, H.G.M. Edwards, M. Hargreaves, T. Ĉapoun. Rapid aoutdoor non-destructive detection of organic minerals using a portable Raman spectrometer. J. Raman Spectrosc.; 2009; 40: 1645-1651.

6 J. Aramendia, L. Gomez-Nubla, K. Castro, I. Martinez-Arkarazo, D. Vega, A. Sanz López de Heredia, A. García Ibáñez de Opakua, J.M. Madariaga. Portable Raman study on the conservation state of four Corten steel-based sculptures by Eduardo Chillida impacted by urban atmospheres. J. Raman Spectrosc.; 2012; 43: 1111.

7 K. Castro, A. Sarmiento, E. Princi, M. Perez-Alonso, M.D. Rodriguez-Laso, S. Vicini, J.M. Madariaga, E. Pedemonte. Vibrational spectroscopy at the service of industrial archaeology: Nineteenth-century wallpaper.TRAC-Trends Anal. Chem.; 2007; 26: 347-359.

8 K. Kavkler, N. Gunde-Cimerman, P. Zalar, A. Demsar. FTIR spectroscopy of biodegraded historical textiles. Polym. Degrad. and Stabil.; 2011; 96: 574-580.

9 N. Navas, J. Romero-Pastor, E. Manzano, C. Cardell. Benefits of applying combined diffuse reflectance FTIR spectroscopy and principal component analysis for the study of blue tempera historical painting .Anal. Chim. Acta; 2008; 630: 141–149.

10 W. Vetter, M. Schreiner. Characterization of pigment-binding media systems: comparison of Non-Invasive in-situ reflection FTIR with transmission FTIR Microscopy. e-Preservation Science; 2011; 8:10-22.

11 R. Chércoles Asensio, M. San Andrés Moya, J.M. De la Roja, M. Gómez. Analytical characterization of polymers used in conservation and restoration by ATR-FTIR spectroscopy. Anal. Bioanal. Chem.; 2009; 395: 2081-2096.

of analyses have been carried out in several materials such as pigments[12], binders[13], parchment documents[14], cross sections of paintings[15] as well as coatings for marbles[16] and limestones[17].

If we focus in the in situ measurements performed in reflectance mode, we can find two types of reflectance equipments. The first one is Fibre Optic Reflectance Spectroscopy (FORS) equipment and the second one, FTIR handheld device. FORS[18-20] technique has been applied to a variety of samples achieving very good results. Nevertheless, in recent works[21-22], benefits and limitations of non FORS equipments in cultural heritage have been discussed, opening a new path in the in situ analyses by reflectance spectroscopy.

In this way, diffuse and specular reflectance can allow us to perform analyses in solid materials without sampling or sample preparation. However, the spectra obtained

12 C. Genestar, C. Pons. Earth pigments in painting: characterisation and differentiation by means of FTIR spectroscopy and SEM-EDS microanalysis. Anal. Bioanal. Chem.; 2005; 382: 269-274.

13 A. Sarmiento, M. Pérez-Alonso, M. Olivares, K. Castro, I. Martínez-Arkarazo, L.A. Fernández, J.M. Madariaga. Classification and Identification of Organic Binding Media in Artworks by means of Fourier Transform Infrared Spectroscopy and Principal Component Analysis. Anal. Bioanal. Chem.; 2011; 399: 3601-3611.

14 *M. Bicchieri, M. Monti, G. Piantanida, F. Pinzari, A. Sodo. Non-destructive spectroscopic characterization of parchmnet documents. Vib. Spectrosc.; 2011; 55: 267-272.*

15 S. Prati, F. Rosi, G. Sciutto, R. Mazzeo, D. Magrini, S. Sotiropoulou, M. Van Bos. Evaluation of the effect of six different paint cross section preparation methods on the performances of Fourier transformed infrared microscopy in attenuated total reflection mode. Microchem. J.; 2012; 103: 79–89.

16 C. Anselmi, F. Presciutti, B. Doherty, B.G. Brunetti, A. Sgamellotti, C. Miliani. The study of cyclododecane as a temporary coating for marble by NMR profilometry and FTIR reflectance spectroscopies.. Appl. Phys.; 2011; 104: 401-406.

17 T. Poli, A. Elia, O. Chiantore. Surface Finishes and Materials: Fibre-Optic Reflectance Spectroscopy (FORS) Problems in Cultural Heritage Diagnostics. e-Preservation Science; 2009; 6: 174-179.

18 C. Ricci, C. Miliani, B.G. Brunetti, A. Sgamellotti. Non-invasive identification of surface materials on marble artifacts with fiber optic mid-FTIR reflectance spectroscopy. Talanta; 2006; 69: 1221-1226.

19 L. Appolonia, D. Vaudan, V. Chatel, M. Aceto, P. Mirti. Combined Use of FORS, XRF and Raman Spectroscopy in the Study of Mural Paintings in the Aosta Valley (Italy). Anal. Bioanal. Chem.; 2009; 395: 2005-2013.

20 T. Poli, A. Elia and O. Chiantore. Surface Finishes and Materials: Fibre-Optic Reflectance Spectroscopy (FORS) Problems in Cultural Heritage Diagnostics. e-Preservation Science; 2009; 6: 174-179.

21 C. Miliani, F. Rosi, F. Daveri, B.G. Brunetti. Reflection infrared spectroscopy for the non-invasive in situ study of artists´pigments. Appl. Phys. A; 2012; 106: 295-307.

22 I. Arrizabalaga, O. Gomez-Laserna, J. Aramendia, G. Arana, J.M. Madariaga. Diffuse reflectance FTIR database for the interpretation of the spectra obtained with a handheld device on built heritage material . Spectrochim. Acta Part A; 2014; 129: 259-267.

by diffuse, specular or total reflectance, may result difficult to interpret, as their quality heavily depends on the characteristics of the sample surface. Besides, in the measurements performed in situ by reflectance spectroscopy, the biggest drawback is that the diffuse component cannot be optically separated from the specular one and this interaction is the main source of distortions. For that reason, in the in situ spectra obtained with the handheld device there are usually inverted bands created by the Resthralen[23] effect and thus, the interpretation of these spectra can result complicate.

However, recently published works of our research group[22-25] have tested the possible application of DRIFT to perform in situ analysis of building materials, studying successfully how to reduce the spectral distortions by applying mathematical algorithms as well as indicating a few guidelines to acquire good in situ spectra.

Taking all this information into account, and trying to reduce the handicaps of the field analysis, the in situ spectroscopic assessment based on XRF and Raman was complemented by the use of DRIFT, studying along this Chapter its usefulness as diagnostic tool in the diagnosis of historic buildings (the corresponding article can be consulted in the scientific publication Annex).

Finally, it is noteworthy, that one of the main problems in the study of monumental stone decay is related to the impossibility of taking samples. In this sense and taking into account the importance of the quantification of soluble salts affection, one of the most dangerous pathologies[26], a non invasive sampling method of its extraction is required to corroborate and complete the spectroscopic assessment.

In this way, works of our research group have demonstrated[27] that agar-based gels are an interesting application to sample black crusts and other patinas and a useful tool in the risk assessment analysis of built heritage affected by atmospheric pollution. Nonetheless, its penetration capacity is not the most suitable for monitoring the soluble

23 G. Kortum. Reflection spectroscopy. Berlin: Springer; 1969.

24 I. Arrizabalaga, O. Gomez-Laserna, J. Aramendia, G. Arana, J.M. Madariaga. Detremination of the pigments present in a wallpaper of the middle nineteenth century: The combination of mid-diffuse reflectance and far infrared spectroscopies. Spectrochim. Acta Part A; 2014; 124: 308-314.

25 J. Aramendia, L. Gómez-Nubla, I. Arrizabalaga, N. Prieto-Taboada, K. Castro, J. M. Madariaga. Multianalytical approach to study the dissolution process of weathering steel: The role of urban pollution. Corros. Sci.; 2013; 76: 154-162.

26 K. Agyekum, J.Ayarkwa, C. Koranteng. Holistic Diagnosis of Rising Damp and Salt Attack in Two Residential Buildings in Kumasi, Ghana. J. Constr. Eng.; 2014; 2014: 1-13.

27 N. Prieto-Taboada, C. Isca, I. Martínez-Arkarazo, A. Casoli, M.A. Olazabal, G. Arana, J.M. Madariaga. The problem of sampling on built heritage: a preliminary study of a new non-invasive method. Environ. Sci. Pollut. Res.; 2014; 21: 12518-12529.

salt content. This is why the utility of other non invasive methods, based on paper pulp poultices, were tested for the extraction of the soluble salts samples. In this manner, spatial patterns models of the salt distribution can be obtained using ion chromatography as quantitative technique.

Moreover, chemometric analysis and thermodynamic models of the chemical deterioration processes identified were carried out to complete the study.

5.1. Features of the operational case under study

5.1.1. Location of the building

The Guevara Palace house is located in the village of Segura (Gipuzkoa, Basque Country, North of Spain) (Fig. 5.1 a), along the Oria river, on a ground mostly composed of limonites and sandstones. According to the lithology[28-29] of the area, soils are rich in organic matter, have a high content of silt and clay, which increases the cation-exchange capacity (CEC) (Ca^{+2}>Mg^{+2}>K^{+}) of the soil. Furthermore, given its composition and the oceanic climate (Cfb, Köppen-Geiger classification[30]) of the area, the high rainfall could increase the percolation of alkalizing elements, thereby tending to acid saturation of the soil.

On the other hand, the main economical activities of the village are related to the livestock and meat processing industry, although, non ferrous metal and paper industries are located in nearby areas. Nevertheless, the reports of chemical quality of air and water show admissible levels[31].

28 E.V.E. Mapa geológico del País Vasco. Beasain: E.V.E; 2010.

29 J.A. Vera. Geología de España. Barcelona, IGME; 2004.

30 M. Kottek, J. Grieser, C. Beck, B. Rudolf, F. Rubel. World Map of the Köppen–Geiger climate classification updated. Meteorol.; 2006; *15: 259–263.*

31 Gobierno Vasco: Agencia Vasca del agua, Seguimiento de ríos y Medioambiente.

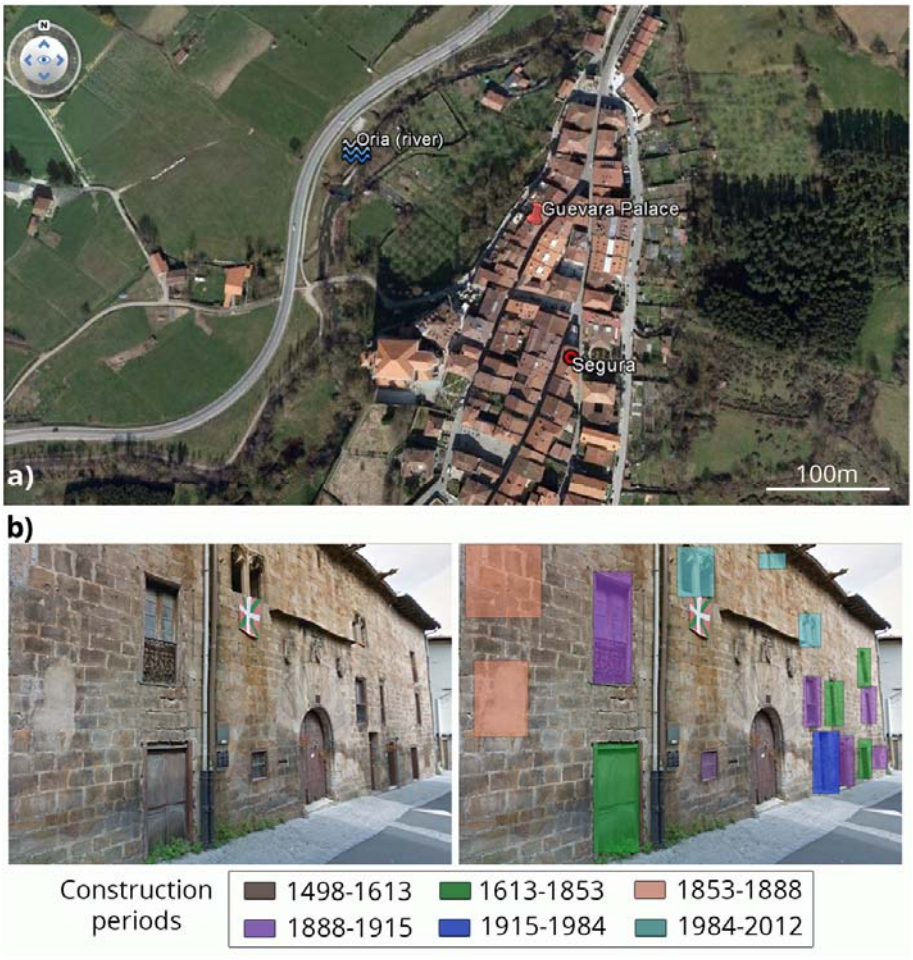

Figure 5.1. a) Geographic location of the studied historical building (Guevara Palace House, Segura, Basque Country, North of Spain). b) Architectural study of corresponding construction periods of the building facade.

5.1.2. Description of the building

The Guevara House is one of the best examples of gothic pre-renaissance urban palace present in the Basque Country. The historic building of the fifteenth century is classified as a Cultural Asset (7/90, Basque Cultural Heritage Law), having been declared as a National Historic Monument (Decree Number 265/1984). Regrettably, the characteristic components of this construction system are in danger of disappearing[32], as most of the interventions carried out are limited to maintain the facade, losing a large part of building elements of great historical value.

32 D. Luegas Carreño, S. Sánchez Beitia. Las residencias señoriales bajomedievales en el País Vasco: Análisis de la evolución del sistema constructivo y sus elementos singulares. Latin American Congress Rehabend. Santander, Spain, 2014.

In this case, the building has undergone several transformation actions (Fig. 5.1 b) and the adjacent areas to the central body are used as housing. The rehabilitation works, which are currently in process, are focused on refurbishing the central building, preserving unchanged the facade and central inner wall, known as the fire wall typical of the time.

The front elevation of the building has two floors, in which the disposition of the bays has certain order, prioritizing the main body over the lateral ones. In this way, architectural forms of great interest such us the balls cornice and the gargoyles, are highlighted (Fig. 5.1 b). The main and back entrances are composed by archs of ample vaulting, that gives direct access to the stables (ground floor under restoration) and to the hall, where the access ladders to the upper floor (fully restored) are found. Besides, to communicate both instances of the ground floor, one more arch, which has an important structural function and historical value, can be found in the middle of the central inner wall.

Regarding the materials used, the building is constructed with sandstone ashlars over a concrete base. However, in the interior of building, the blocks are only visible in the central wall since the rest of them has been leveled and plastered. Moreover, the joint mortar of the facade is practically absent (Fig. 5.3) and the interior one is apparently composed of cement and sand.

5.1.3. In situ analysis campaign

The visual inspection allowed us to identify the different types of pathologies (Fig. 5.2). In this way, several black crusts could be observed in the main facade, being especially notable in the coat of arms and in the basal voussoirs of the entrance arch. Moreover, the latter suffers material loss, observing intense disaggregation in decorative ornaments and in the lower ashlars. Besides, areas of reddish, whitish and yellowish colors, flakings, efflorescences and subefflorescences were heterogeneously distributed along the surface of the facade. Finally, ferns, mosses and lichens were growing on the gargoyles and in the nearby areas of the drainpipe of the roof gutter.

In addition, inside the building, given the cultural value and its structural function, the arch of the central wall was studied. Several salt crusts (approximate thickness of 3 mm) were observed on the joint mortars and sandstone materials. Moreover, the base of the arch was wet to the touch and showed a severe degradation (Fig. 5.3).

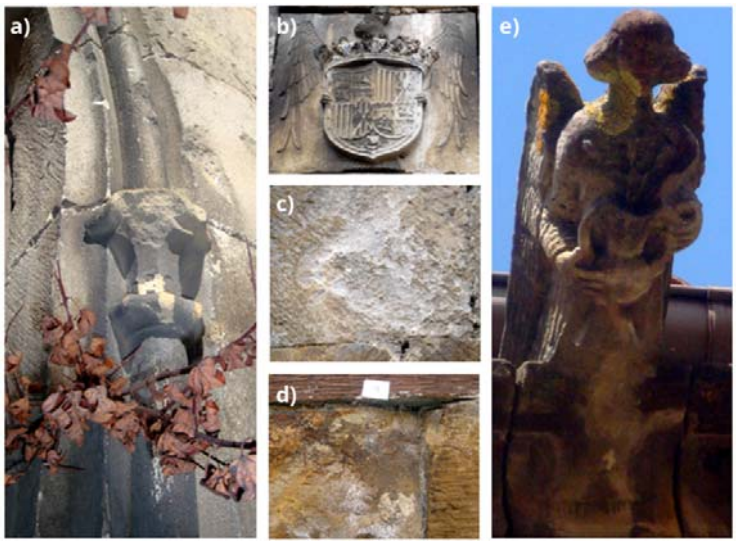

Figure 5.2. Selected photographs of the deteriorations observed in the facade of the Guevara Palace House. a) different colorations and material loss found in the basal voussoir of the entrance arch. b) black crusts over the coat of arms. c-d) flaking, efflorescences and subefflorescences details. e) biodeterioration suffered by gargoyles.

After indentifying the points of interest, a first in situ study campaign was developed during the month of May, after ten days without rain. In this manner, more than 100 in situ spectroscopic measurements were collected in order to characterize the composition of the original materials so as to identify the decaying compounds present. Besides, measurements of temperature and relative humidity were taken outside as well as inside the building (21°C-65% and 19°C-71% respectively) to help establishing the chemical degradation mechanisms that were taking place.

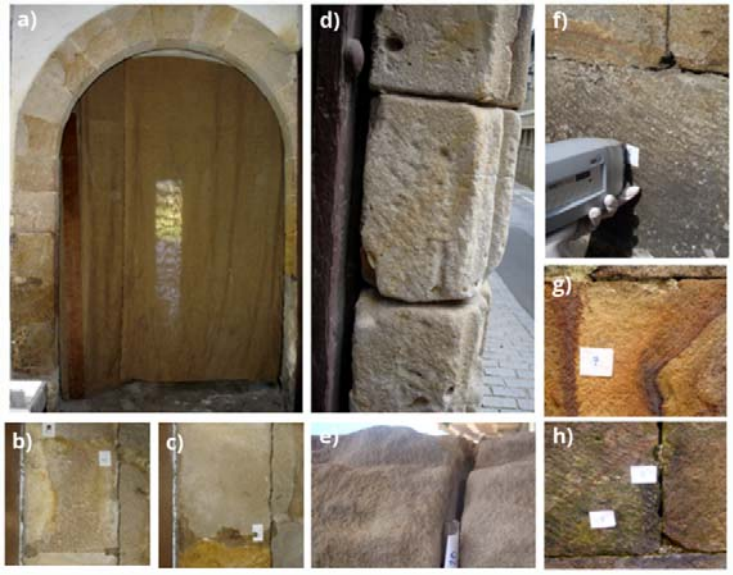

Figure 5.3. Selected photographs of the affections observed in the Palace. a) general view of the central wall arch. b-c) details of efflorescences found in the arch. d-e) material loss observed in the ashlars of the main entrance. f) example of in situ analysis of blackened areas. g) areas with change of coloration. h) biodeterioration and efflorescences found close to the drainpipe.

Six months later, as a result of this previous screening, a second campaign was carried out, in which over 120 in situ spectroscopic measurements were performed in the non restored areas of the building (ext: 9°C-73%, int: 10°C-77%). In this occasion, although some efflorescences were observed in the arch of the central inner wall, the salt crust measured during the first campaign had almost disappeared, probably as a consequence of the change of climatic conditions.

5.1.4. In situ results

The most relevant information obtained during the in situ analysis campaigns will be discussed along this section.

5.1.4.1. X-ray fluorescence

Regarding the original materials characterization, the analysis of sandstones showed Si as the main major element, followed by Ca, K and Al but in a lower proportion. Furthermore, Cl, S and Fe were identified as minor elements. The remaining composition could correspond to light elements such us Na and O, since their signals were too low to be detected.

Therefore, given its appearance and the percentage of Si, Ca and Fe detected, it could be classified as subarcose or sublitoarenite[33-35]. In this way, the main cement could be of micaceous nature. However, the sandstones that are more yellowish could also present small percentages of ferruginous cement. This hypothesis appears consistent with the kind of stone from nearby quarries as Aizpea or Bergara.

In the case of mortars, Ca was identified as major element, followed by light elements as Na and O, whose assigned percentage was 30% approximately. Besides, as minor elements, Si and Al were also detected. Thus, it could be classified as cement mortar, corroborating the visual inspection.

Additionally, XRF analyses were carried out, in the same points of Raman and DRIFT measurements, to obtain complementary information, thus contributing to facilitate the interpretation of the spectra collected.

33 R.G.C Bathurst. Glossary of Sedimentological terms. En: Carbonate Sediments and their diagenesis. Developments in sedimentology. Amsterdam, Kingdom of the Netherlands: Elservier; 1975.

34 M. Fregenal, J. López Gómez, J. Martín Chivelet. Ciencias de la Tierra. Diccionarios Oxford-Complutense. Madrid, Spain: Complutense; 2000.

35 P.A. Scholle. A color guide to the petrography of carbonate rocks: grain, textures, porosity, diagenesis. Tulsa, E.E.U.U; A.A.P.G Memoir77; 2006.

Finally, It should be noted that, despite the appearance of the facade, no signal of toxic metal pollutants such as Cu, Zn, Mn or Pb were identified with a significant level either in degraded or in fresh areas. In this sense, destructive analysis to detect pollutants related to traffic or industrial activities was not considered necessary in this situation.

5.1.4.2. DRIFT and Raman spectroscopy

Before starting to analyze the in situ spectra obtained by DRIFT and Raman spectroscopy, it is necessary take into account several concepts related with the distortions observed in the reflectance measurements, which are the key to understand what is happening and therefore, to achieve a correct interpretation of the signals collected, complementing in this way the molecular characterization study.

As it was mentioned in the introduction of this Chapter, the biggest drawback of the DRIFT in situ analysis is the appearance of inverted bands in the spectra, as can be seen in the Figures 5.4 a and 5.6. The cause is that the diffuse component of the reflectance cannot be optically separated from the specular one by the current handheld devices, being its interaction the main source of distortions.

In this sense, all specular reflectance measurements are ruled by the Fresnel equation[36-39] and thereupon, the obtained spectra depend on the refractive index (n) and absorption index (k) of the material. According to this equation, two types of spectral distortion could happen. The first, when the compound has a k<1, is observed in the majority of organic molecules, being their spectra characterized by derivative-like features. The second one can appear when the sample contains a compound with a k >>1. In these cases, Reststrahlen bands appear, being very common in most inorganic salts. As it will see along this section, the oxyanions content of the samples such as carbonates, sulphates and silicates cause an increase of the reflectance up to 80% and, as consequence, the inverted bands appears in the corresponding area[40].

36 E.H. Korte, A. Roseler. Infrared reststrahlen revisited: commonly disregarded optical details related to n<1. Anal. Bioanal. Chem.; 2005; 382: 1987-1992.

37 A. Roseler, E.H. Korte. Reflection anomalies related to n=1. Vib. Spectrosc.; 2007; 43: 111-115.

38 L. Monico, F. Rosi, C. Miliani, A. Daveri, B.G. Brunetti. Non-invasive identification of metal-oxalate complexes on polychrome artwork surfaces by reflection mid-infrared spectroscopy. Spectrochim. Acta Part A; 2013; 116: 270-280.

39 C. Miliani, F. Rosi, F. Daveri, B.G. Brunetti. Reflection infrared spectroscopy for the non-invasive in situ study of artists´pigments. Appl. Phys. A; 2012; 106: 295-307.

40 G. Kortum. Reflection spectroscopy. Berlin: Springer; 1969.

In addition, the diffuse reflectance, which is ruled by the Kubelka– Munk model (KM), depends on the diffuse reflectance coefficient of an infinitely thick sample (R∞), the scattering coefficient of the sample (s), the absorption coefficient (K), the molar absorptivity (a) and the analyte concentration (c)[41]. In this way, if the spectra obtained in transmittance and in diffuse reflectance mode are compared, differences in the relative intensities of IR bands can be observed. In the Diffuse reflectance measurements the width of the sample appear larger since, many reflections take place in the sample and, thanks to that, overtones and combination bands increase their signals, which helps to perform a correct assignation of the obtained spectra.

Moreover, correction algorithms can be used to attempt to minimize these distortions, although the successful results depend on the characteristics of the sample surface. In this way, when the analyzed sample has a large specular component, the relation of the refractive index and the absorption coefficient are corrected using the Kramers–Kronig (K–K) algorithm[42-45]. However, if both, the specular and diffuse components, are present in the measurement, the K–K transform cannot be applied and the obtained spectrum is more difficult to interpret[46].

Therefore, knowing that the in situ measurements are determined by the properties of the sample and given that, in this case, their surface is not the most suitable for using the K-K correction algorithm[47], the spectral assignment was performed based on the secondary bands as well as in the intensification of the overtones, according to the requirements of each case.

41 G. Dupuis, M. Menu. Quantitative characterization of pigment mixtures used in art by fibre-optics diffuse-reflectance spectrsocopy. Appl. Phys. A; 2006; 83: 469-474.

42 S. Bruni, F. Cariati, F. Casadio, L. Toniolo. Spectrochemical characterization by micro-FTIR spectroscopy of blue pigments in different polychrome works of art. Vib. Spectrosc.; 1999; 20: 15-25.

43 N. Salvado, S. Butı, M.J. Tobin, E. Pantos, A.J.N.W. Prag, T. Pradell. Advantages of the use of SR-FT-IR microspectroscopy: Applications to Cultural Heritage. Anal. Chem.; 2005; 77: 3444-3451.

44 F. Rosi, A. Federici, B.G. Brunetti, A. Sgamellotti, S. Clementi, C. Miliani. Multivariate chemical mapping of pigments and binders in easel painting cross-sections by micro IR reflection spectroscopy. Anal. Bioanal. Chem.; 2011; 399: 3133-3145.

45 T. Poli, O. Chiantore, M. Nervo, A. Piccirillo. Mid-Ir fiber-optic reflectance spectroscopy for identifying the finish on wooden furniture.Anal. Bioanal. Chem.; 2011; 400: 1161-7.1

46 D. Buti, F. Rosi, B.G. Brunetti, C. Miliani. In-situ identification of copper-based green pigments on paintings and manuscripts by reflection FTIR . Anal. Bioanal. Chem.; 2013; 405: 2699-2711.

47 I. Arrizabalaga, O. Gómez-Laserna, J. Aramendia, G. Arana, J.M. Madariaga. Applicability of a diffuse reflectance infrared Fourier transform handheld spectrometer to perform in situ analyses on Cultural Heritage materials. Spectrochim. Acta A; 2014; 129: 256-267.

In this way, in relation to the original composition of the sandstone, the spectra of several compounds were collected by DRIFT. However, as it can be seen in Fig.5.4 a, the obtained spectra were distorted by the Reststrahlen effect. In this way, the regions around 1000 cm^{-1} (Si-O asymmetric stretching of silicates) and 1400-1500 cm^{-1} (the CO_3^{-2} asymmetric stretching) were inverted and, for that reason it was not possible to perform the assignation using the main bands. Therefore, to carry out the correct assignation of the compounds detected, the secondary bands and overtones were used. In this way, the potassium carbonate was detected by its bands at 2482, 2422 and 1748 cm^{-1}, calcite by its bands at 2869, 2513 and 1794 cm^{-1} and a great amount of silicates by its characteristic bands at around 1000 and 3500-3600 cm^{-1}.

In addition, Raman analysis determined α-quartz (α-SiO_2, detected by its main peak at 464 cm^{-1} and secondary at 263 cm^{-1}) as majority compound. Moreover, as minor compounds, calcite ($CaCO_3$, detected by its principal peak at 1085 cm^{-1}), hematite (α-Fe_2O_3, identified by its bands at 404, and 289 cm^{-1}), rutile (TiO_2, by its bands at 446 and 612cm^{-1}) and phyllosilicates as kaolinite ($Al_2Si_2O_5(OH)_4$, by its characteristics broad bands at 915, 794 and 745 cm^{-1}) and probably some kind of muscovite ($KAl_2(Si_3Al)O_{10}(OH)_2$, identified by its peaks at 749, 408 and 261) were found (Fig. 5.4 b). Apart from the clay content, the presence of carbon (identified by its two characteristic bands at 1600 and 1325 cm^{-1}) caused a great fluorescence in the spectra collected. Hence, the previous XRF and DRIFT analyses performed in the same points were crucial to achieve the spectral assignation.

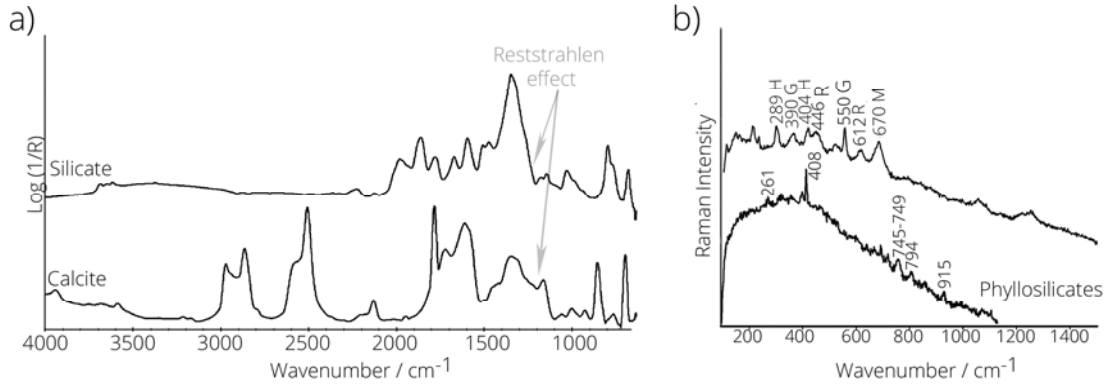

Figure 5.4. a) DRIFT spectra of calcite and silicates identified in situ as original materials of sandstone. b) Raman spectra of phyllosilicates (kaolinite and probably muscovite), hematite (H), rutile (R), goethite (G) and magnetite (M) found in the matrix of sandstone.

In the case of mortars, calcite (identified by its characteristic Raman bands at 1085 and 712 and 280 cm^{-1}) and α-quartz (α-SiO_2, detected by its main Raman peak at 464 cm^{-1}) were found as major original compounds. The DRIFT analysis corroborated the main composition detecting calcite and several silicates also.

Once the original nature of each material is classified, the decaying compounds found are exposed regarding the area studied.

Firstly, in the analysis of the facade, magnetite (Fe_3O_4, detected by its Raman band at 670 cm^{-1}) and goethite (α-FeO(OH), detected by its Raman bands at 550 and 390 cm^{-1}) (Fig. 5.4 b) were determined as main degraded compounds of the reddish areas (Fig.5.3 g). Then, according to the bibliography[48-50] and given its location on the facade, they could be transformation products of the original hematite by the action of atmospheric pollutants. The process could start with the formation of crystalline lepidocrocite (γ- FeOOH) and magnetite, which could crystallize and precipitate during the drying stage. In turn, lepidocrocite could be transformed into maghemite (γ- Fe_2O_3) by deshydroxilation and/or into the amorphous ferric oxyhydroxide ($FeO_x(OH)_{3-2x}$) by a dissolution-precipitation processes. All these iron forms are poorly crystallized and quite unstable. Therefore, they tend to transform into goethite, the most thermodynamically stable mineral phase[51-52]. Taking into account the nature of iron compounds and their locations, always in yellowish sandstone, it was classified as a direct degradation of the ferruginous cement caused by atmospheric attack. Besides, the dissolution of the main cement and the volume changes suffered during the mentioned transformations could produce severe pathologies as disaggregation, fractures and, when the ashlars have structural function, even important loss of stability. Although, in this case, the ashlars of this kind of stone are a minority, the mechanism of damage will be studied in detail further on.

Moreover, in the degraded areas of the facade, calcite (Raman peaks at 1085, 712 and 280 cm^{-1}), gypsum ($CaSO_4 \cdot 2H_2O$, detected by its main Raman signal at 1008 cm^{-1}) and anhydrite ($CaSO_4$, Raman band at 1017 cm^{-1}) were found as main degradation compounds of efflorescences and subefflorescences. Thus, the existence of these compounds, in this form and heterogeneously distributed, suggests the attack of atmospheric pollutants over the original calcite. In this way, carbonic and sulphuric acid aerosols[53] can cause the dissolution of the original material and its crystallization into

48 W. Chesworth. Encyclopedia of Soil Science. Netherlands: Springer; 2008.

49 R.M. Cornell , U. Schwertmann. The iron oxides: structure, properties, reactions, occurrences and uses. Weinheim: Wiley; 2003.

50 J. Aramendia. PhD Thesis: Analytical diagnosis of the conservation state of weathering steel exposed to urban atmospheres.

51 Y. Qian , C. Ma, D. Niu, J. Xu, M. Li. Influence of alloyed chromium on the atmospheric corrosion resistance of weathering steels. Corros. Sci.; 2013; 74: 424-429.

52 U. Scwhertmann, R.M. Taylor. The transformation of lepidocrocite to goethite. Clay.Clay. Miner.; 197; 20: 151-158.

53 M. Manning. Air pollution, acid rain and the enviroment: Corrosion of building materials due to atmospheric pollution the United Kingdom. Netherlands: Springer; 1988.

the pores. As a consequence of these dissolution-precipitation and hydratation-deshydratation processes, severe damage in decorative door elements, flaking and loss of material could be observed (Fig.5.2 and Fig.5.3).

On the other hand, in the areas affected by black crusts, carbon (identified by two broad Raman bands at 1600 and 1325 cm^{-1}), calcite (Raman band at 1085 cm^{-1}), gypsum (identified by a intense peak at 1008 cm^{-1}) and nitromagnesite ($Mg(NO_3)_2 \cdot 6H_2O$, detected by the presence of its main peak at 1059 cm^{-1}) were observed as decaying compounds by Raman spectroscopy (Fig. 5.5). Moreover, thanks to the DRIFT analysis, the presence of these compounds was corroborated in situ (Fig. 5.6 a). According to the literature[54-57], these degradations compounds are usually related to this affection as the crust could act as catalytic support to promote the oxidation of atmospheric SO_x and NO_x gases.

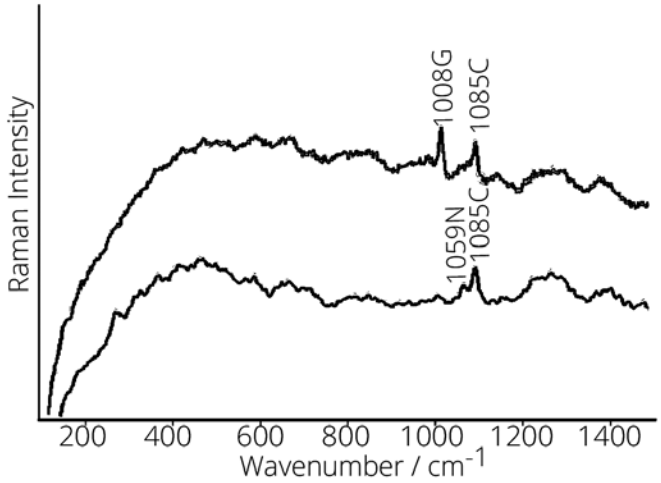

Figure 5.5. The upper in situ spectrum shows the presence of gypsum (G) and calcite (C) as main compounds of efflorescences and subefflorescences found in the facade. Besides, in the lower spectrum, nitromagnesite (N) and calcite were identified in the surface of black crusts.

Finally, in areas unprotected by the cornice located next to the drainpipe, where different vegetation was growing, calcite (determined by its Raman bands at 1085

54 A. Bonazza, C. Sabbioni, N. Ghedini. Quantitative data on carbon fractions in interpretation of black crust and soiling on Europen built heritage. Atmos. Environ.; 2005; 39: 2067-2618.

55 N. Prieto-Taboada, M. Maguregui, I. Martinez-Arkarazo, M. Olazabal, G. Arana, J.M. Madariaga. Spectroscopic evaluation of the enviromental impacto n black crusted modern mortars in urban-industrial areas. Anal. Bioanal. Chem.; 2010; 399: 2949-2959.

56 G. C. Galletti, P. Bocchini, D. Cam, G. Chiavari, R. Mazzeo. Chemical charazterization of the black crust present on the stone central portal of St. Denis Abbey Fresenius. J. Anal. Chem.; 1997; 357: 1211-1214.

57 Y. Bai, G. E. Thompson, S. Martinez-Ramirez, S. Brüeggerhoff. Mineralogical study of salt crusts formed on historic buildings stones. Sci. Total. Environ.; 2003; 302: 247-251.

and 712 cm^{-1}), gypsum and nitrate were identified by their Raman bands at 1008 and 1050 cm^{-1}, respectively. However, due to the high fluorescence it was not possible to discern which nitrate was present since, as it was explained in Chapter 4, the band at 1050 cm^{-1} is common to some of them. Nevertheless, the DRIFT analysis of the same area complemented the results founding gypsum (assigned by the DRIFT bands at 1683 and 1620 cm^{-1}), niter (KNO_3, identified by its bands at 2736, 2396, 2066, 1760, 1490 and 825 cm^{-1}) and nitratine ($NaNO_3$, determined by its bands at 2756, 2435, 2095, 1786, 1534 and 837 cm^{-1}) (Fig. 5.6 b). These compounds could be originated by different mechanism, although considering the original material composition, placement and location, the most probable cause for their formation could be the acid attack of the atmospheric NO_x gases over the feldspar cement of the stone, being aggravated by the penetration of water from the drainpipe. In fact, the growth of vegetation, only observed in this area, could be caused as a consequence of the water, while also the roots could be promoting the infiltration of water into the material.

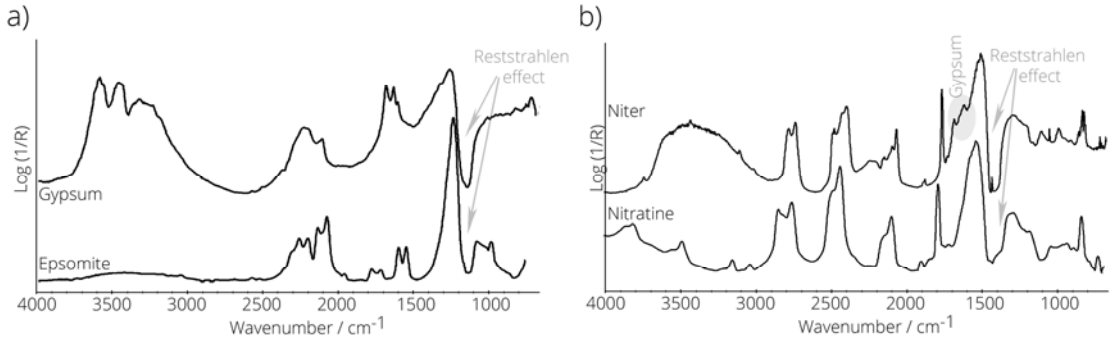

Figure 5.6. DRIFT spectra of a) gypsum identified in situ as decaying compound of a black crust area. b) nitratine and niter collected in the sandstone ashlars in low-lying areas of the facade, next to a drainpipe.

Given its structural and historical value, the arch of the inner wall was studied in depth. According to the visual inspection, a great amount of salt crusts were observed at different heights. Only one side of the arch shows this pathology, being its base wet to the touch. Thus, the origin of the affection could be related to a problem of water infiltration and therefore, the spectroscopic study was carried out at different heights. In this manner, depending on the efflorescences found, the right side of the arch was divided into 8 zones (Table 5.1) to determine the salt distribution model, by spectroscopic techniques.

Table 5.1. Classification of the zones analyzed spectroscopically in the inner arch.

Sample	P1	P2	P3	P4	P5	P6	P7	P8
Height (m)	0	0.2	0.4	0.6	0.8	1.2	1.6	2

In this way, niter (identified by the presence of the totality of its Raman bands at 1358, 1344, 1050 and 715 cm^{-1}) was found from the base (P1and P2) of the arch up to 1.6 meters height (P7). Besides, gypsum (Raman band at 1008 cm^{-1}) and calcite (identified by its main Raman peak at 1085 cm^{-1}) were determined mainly in the middle zone (P2 and P3). Above the middle level, thenardite (Na_2SO_4, identified by the strongest Raman peak at 991 cm^{-1} and the weakest pair of peaks at 466 and 451 cm^{-1} aside from other signals at 1149, 1128, 644, 632 and 621 cm^{-1}) and epsomite ($MgSO_4 \cdot 7H_2O$, Raman band at 985 cm^{-1}) were identified, only over the joint mortars (P4 and P5) (Fig. 5.7). It should be noted that in the zones P5 and P6, no salt crust was observed.

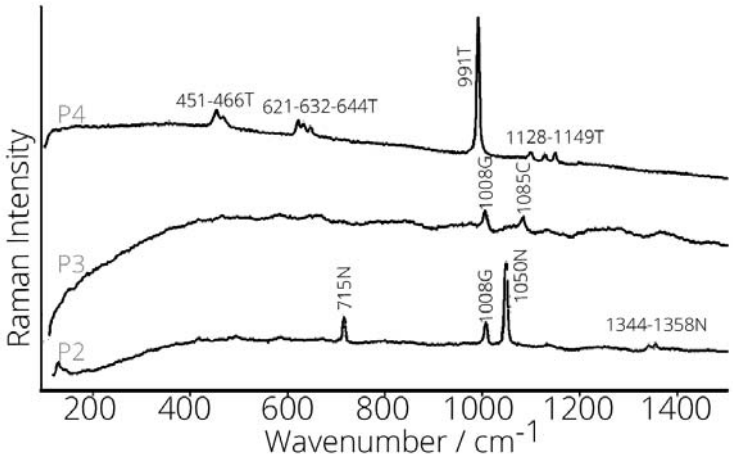

Figure 5.7. Raman spectra collected in the arch of the inner wall. Niter (N), gypsum (G), calcite (C) and thenardite (T) were found as main decaying compounds of the efflorescence crusts.

Afterwards, semiquantitative DRIFT analysis of the same areas corroborated the existence of a special zoning salt distribution, which is approximate to Arnold and Zehnder´s model[58-60]. In this way, the DRIFT spectra collected in the P1 zone showed mixture of two compounds. As it can be seen in the P1 spectrum (Fig. 5.8 a), the signal obtained was distorted in two regions, suggesting the presence of nitrate and sulphate containing compounds. Niter was identified as a majority compound by its characteristics bands at 3746, 3426, 3103, 2778, 2737, 2477, 2397, 2095, 2068, 1761, 1503 and 826 cm^{-1}), although the correct assignation of the sulphate was not possible due to the Reststrahlen effect. In the P2 zone, gypsum (DRIFT bands at 1684 and 1624

58 E.R. Agudo, B. Lubelli, A. Sawdy, R.V. Hees, C. Price, C.R. Navarro. An integrated methodology for salt damage assessment and remediation: the case of San Jerónimo Monastery (Granada, Spain). J. Environ. Earth Sci.; 2011; 63: 1475-1486.

59 M.A. Vázquez, E. Galán, P. Ortiz, R. Ortiz. Digital image analysis and EDX SEM as combined technique to evaluate salt damp on walls. J. Constr. Build Mater.; 2013; 45: 95-105.

60 *M. Auxiliadora Vázquez, E. Galán, M.A. Guerrero, P. Ortiz. Digital image processing of weathered stone caused by efflorescences: A tool for mapping and evaluation of stone decay. J. Constr. Built Mater.; 2011; 25: 1603-1611.*

cm^{-1}) and niter (bands at 2779, 2738, 2390, 1760 and 826 cm^{-1}) were found but this time, the majority compound was sulphate. Continuing with the analysis by heights, a great amount of gypsum (detected by its DRIFT bands at 2232, 2132, 1684 and 1620 cm^{-1}) and some calcite (DRIFT bands at 2972, 2870, 2519, 1795 and 876 cm^{-1}) were detected in the P3 area. However, only thenardite (identified by DRIFT bands at 2180 and 2104 cm^{-1}) was identified as decaying compound in the P4 zone, not detecting almost any sulphates in the next zones (P5 and P6). Finally, in the upper level (P7), only niter was identified as main compound of the salt crust, disappearing in the highest level P8 (Fig.5.8).

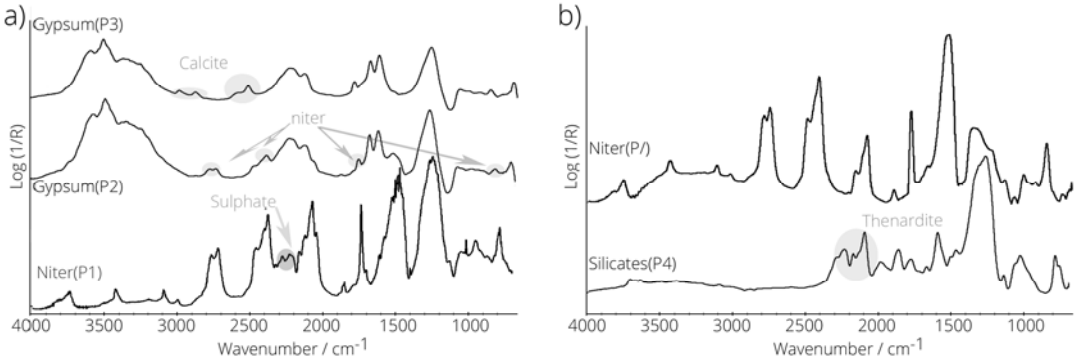

Figure 5.8. DRIFT spectra collected in the arch of the inner wall. a) niter, gypsum and calcite found in the P1, P2 and P3 Zones. b) silicates, thenardite and niter detected in the P4 and P7 zones.

According to the spectroscopic results, a progressive distribution of salts was observed, whose origin seems to be the ingress of water from the subsoil[61]. In fact, the point of entry could be the base of the arch, since a large amount of sulphates and nitrates was detected at ground level (P1). As it was explained in the Chapter 4, the infiltration of groundwater and its capillary ascension through the wall could cause a severe damage in building materials. In this case, the loss of material observed could be a direct consequence of the physical stress suffered by hydration-dehydration processes as well as by transformation of original materials due to dissolution-precipitation and crystallization processes. Clear examples of water effect are the hydrolysis of feldspars cements and the equilibrium of thenardite with its decahidrated form, one of the most dangerous salts to the building materials[62].

For all of this and taking into account also the structural function of the wall, dangerous cracks could appear if no restoration action is performed.

61 *H. Morillas, M. Maguregui, O. Gómez-Laserna, J. Trebolazabala , J. M. Madariaga. Characterisation and diagnosis of the conservation state of cementitious materials exposed to the open air in XIX century lighthouses located on the coast of the Basque Country: 'The case of Igueldo lighthouse, San Sebastian, North of Spain. J. Raman Spectrosc;. 2012; 43: 1630-1636.*

62 W. Heilen. Silicone resins and their combinations. UK: European coatings industry; 2014.

5.1.5. Sampling for the laboratory analysis

During the second campaign, a very little amount (approx 0.10 g) of non degraded sandstone was collected to complement the information about its original composition in the laboratory.

Afterwards, some interesting samples of the facade were gathered using a chisel (between 0.10 and 0.15 g of each one) to continue the spectroscopic study.

Moreover, according to the salts distribution detected in the historical arch, samples of each zone (from P1 to P7) were extracted for quantitative analysis. For that purpose, a method based on cellulose pulp was chosen to complement the semiquantitative spectroscopic analysis since sampling was restricted inside the Palace and, besides, the salt crust had almost disappeared in the second campaign.

The extraction method is based on the suggestion of Arnold and Zehnder[63], who state that salt content is seldom homogeneous throughout a wall. In this way, 8 samples were taken by cellulose pulp of approximately 12 cm^2 and 5 mm thick soaked in de-ionized water with a pulp-to-water weight ratio of about 1/8. The poultices were applied to the sampling points for 2 hours[64] and then they were removed and stored until the analysis (more information can be consulted in the section 3.1.1.2 of Chapter 3).

5.1.6. Laboratory results

The most relevant information obtained during the laboratory analysis will be discussed along this section.

5.1.6.1. X-Ray Diffraction (XRD)

To increase the knowledge about the original materials, two samples of non degraded sandstones were analyzed by “Rocks and Minerals Unit” of the University of The Basque Country (EHU / UPV). Regarding the results (Fig. 5.9), quartz was the major compound with an estimated percentage of 88%. Besides, the remaining argillaceous content was identified as phyllosilicates of kaolinite and illite group. Therefore, the kind of sandstone, classified in situ as subarkose with micaceus cement was confirmed (Fig.

63 A. Arnold A, K. Zehnder. Monitoring wall paintings affected by soluble salt. The Conservation of Wall Paintings S. Cather. Los Angeles: The Getty Conservation Institute; 1991.

64 A. Dionísio , E. Martinho, C. Grangeia, F. Almeida. Non-invasive techniques for the evaluation of stone conservation. Switzerland: Global Stone Congress, Trans Tech Publications; 2012:170-177.

5.9) In addition, in only one of the samples gypsum was found as degraded compound in an estimated percentage of 1% (Fig. 5.9 b).

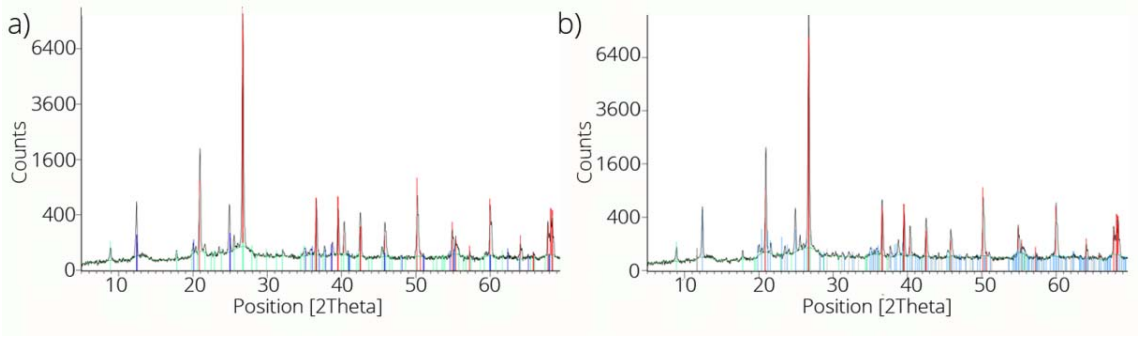

Figure 5.9. X-Ray diffraction results. Quartz signals are red colored, also phyllosilicates signals of kaolinite and illite group are marked in blue and green, respectively. Besides, in b) gypsum presence marked in grey colour can be observed. The peak located approximately 25.5°2 theta is due to an instrumental effect caused by the tungsten cathode of RX, usually observed in quartz-rich samples.

5.1.6.2. DRIFT and Raman spectroscopy

According to the original composition of the sandstone, the presence of calcite (detected by its characteristics bands at 2976, 2869, 2513, 2139, 1794, 1439, 874 and 710 cm^{-1}) (Fig 5.10), hematite (501 and 453 cm^{-1}) and silicates (bands at 3500-3600 and 1000 cm^{-1}) were corroborated using the DRIFT mode of the laboratory equipment.

However, this time, no distortions were observed in the spectra obtained, since in the configuration of the laboratory equipment, the interference of specular reflection is almost eliminated. In addition, to reduce de specular component, the samples were ground (particles <10 μm), favoring the diffuse component of the sample surface. However, when the analyzed sample is highly absorbent, it can be diluted in a non absorbent matrix like KBr (section 3.2.2.5 of Chapter 3) to generate even less specular component in the surface, increasing the contribution of the diffuse reflectance component. With these two simple operations the specular component is reduced achieving almost pure diffuse reflection spectra. In this way, an example is displayed in Figure 5.10, where the DRIFT spectrum of calcite taken in situ with the handheld device and the spectra obtained in the laboratory can be compared, observing that the contribution of the specular reflection is nearly negligible. Therefore, the less intense bands have increased their intensity and, what is even more important, the spectra obtained in the laboratory are not distorted by the Reststrahlen effect.

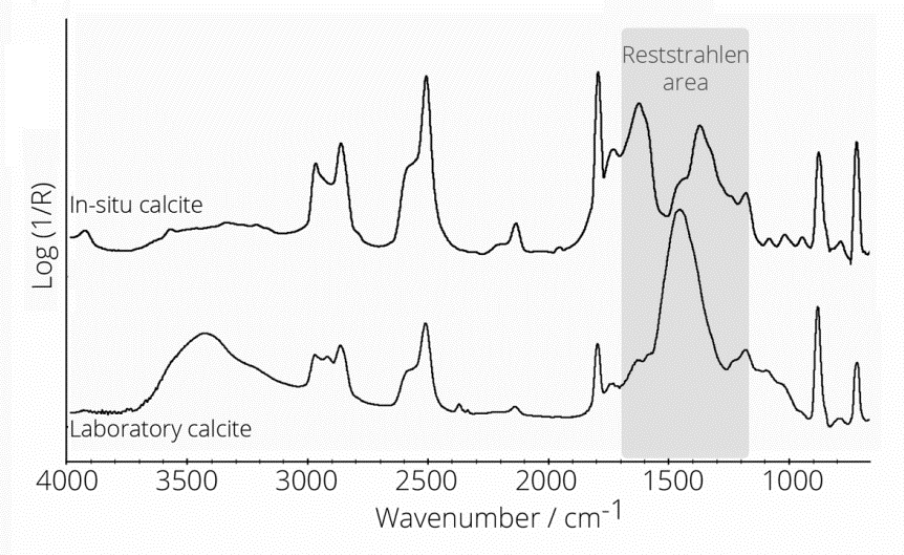

Figure 5.10. Comparison between DRIFT spectra of calcite collected in situ with the handheld device and the spectrum obtained in the laboratory.

On the other hand, Raman analysis completed the in situ study detecting the full spectra of calcite (Raman bands at 1435, 1085, 712 and 281 cm^{-1}), quartz (Raman bands at 695, 464, 395 and 263 cm^{-1}), hematite (Raman bands at 404, 289 and 223 cm^{-1}), rutile (identified by its characteristic Raman bands at 612 and 446 cm^{-1}) and kaolinite (Raman bands at 915, 795, 745, 460, 431, 333, 264 and 240 cm^{-1}). In addition, limonite (FeO(OH)·nH2O, identified by its bands at 552, 394, 297and 240 cm^{-1}), calcium silicate (Ca_3SiO_5, detected by its main bands at 1075, 578 and 370 cm^{-1}) and albite ($NaAlSi_3O_8$, identified by its main bands at 507 and 478 cm^{-1}) were found also (Fig. 5.11).

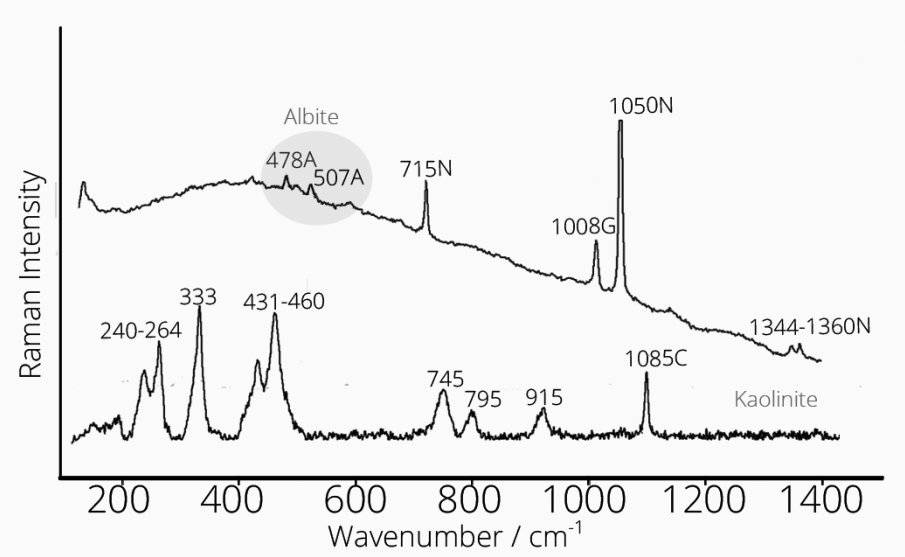

Figure 5.11. Raman spectra collected in the laboratory. Kaolinite, calcite (C) gypsum (G), niter (N) and albite (A) were found in a facade sample of sandstone.

Regarding the original mortar composition, calcite (Raman bands at 1085, 712 and 280 cm^{-1}), quartz (Raman bands at 464, 395 and 263 cm^{-1}) and hematite (Raman bands at 405, 289 and 224 cm^{-1}) were corroborated as major original compounds by Raman and DRIFT also.

Following with the **analysis of the facade,** the laboratory results of the reddish areas confirmed the results obtained in situ. In this way, thanks to Raman spectroscopy, the presence of magnetite (detected by its Raman band at 670 cm^{-1}) and goethite (identified by its Raman bands at 549 and 390 cm^{-1}) were confirmed. Besides, DRIFT analysis corroborated these results detecting goethite also (by its characteristic infrared absorption bands at 3129, 910, 798 and 623 cm^{-1}) (Fig. 5.12). Moreover, lepidocrocite (detected by its main Raman band at 250 cm^{-1}) was found. The presence of this intermediate transformation product evidenced that the degradation mechanism of ferruginous cement was taking place. Adding to this, the physical stress produced by the dissolution and crystallization processes of iron oxides, which leads to the bad state of conservation observed in these ashlars was explained.

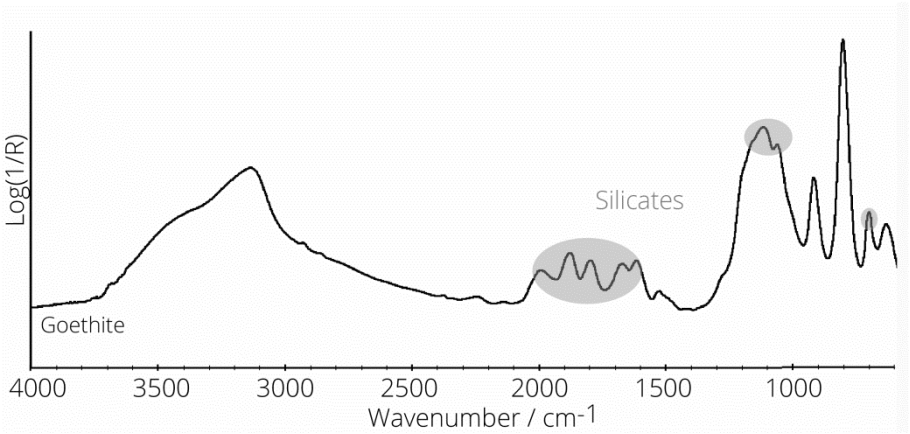

Figure 5.12. DRIFT spectrum collected in the laboratory from a sandstone sample of the facade. The corresponding bands of goethite and signals of silicates were identified.

The analysis of the efflorescences collected in areas close to bars and locks revealed the presence of coquimbite ($Fe_2(SO_4)_3 \cdot 9H_2O$), identified by its main Raman band at 1025 cm^{-1}), gypsum (Raman signal at 1008 cm^{-1}) and siderite ($FeCO_3$, Raman bands at 1090 and 302 cm^{-1}). Once again, these compounds suggest the atmospheric attack suffered by Segura Palace, since CO_2 and SO_2 gases are deteriorating the iron elements of the facade, and their respective salts could be filtered to the stone, causing material loss by crystallization processes. Due to its decaying influence, their formation processes will be studied in detail further on.

Finally, the in situ analyses of the areas with vegetation, closed to the general drainpipe, were confirmed by both techniques and, in addition, carotenoids (identified by Raman bands at 1154, 1512, 1003 cm^{-1}) were found (Fig. 5.13).

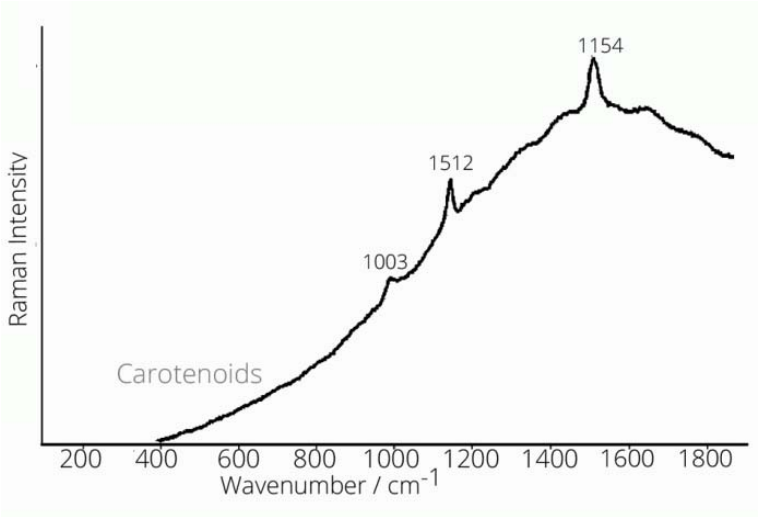

Figure 5.13. Raman spectrum of caratenoids found in a sandstone sample of the facade.

These signals are related to Salinibater[65], which produces an unusual carotenoid, salinixanthin. According to the literature[66], it cannot grow below 20% salt concentration so its presence could be successfully used as biomarker of stone salt weathering. Besides, these bacteria use KCl and NaCl for osmotic adjustment of their cytoplasm, and mainly possess salt-requiring enzymes with a large excess of acidic amino acids. In this way, the formation of niter and nitratine, only observed in this area of the facade, could be promoted by the action of these organisms over de feldspar matrix, facilitating its hydrolysis and, therefore, its decay.

5.1.6.3. Quantification of soluble salts by ion chromatography

To assess the salts distribution of the historical arch, the samples taken by cellulose pulp method at different heights (Table 5.1) were analyzed by ion chromatography. In this manner, soluble sulphate, nitrate, chloride, ammonium, sodium, potassium, calcium and magnesium concentration were quantified (Table 5.2).

65 J. Jehlička, K.Osterrothová, L. Nedbalová, N. Gunde-Cimerman, A.Oren. Discrimination of pigments of microalgae, bacteria and yeasts using lightweight handheld Raman spectrometers: Propects for astrobiology. 11th International GeoRaman Congress. St. Louis, Missourri, USA, 2014.

66 A. Oren. Salinibacter: an extremely halophilic bacterium with archaeal properties. FEMS Microbiol. Lett.; 2013; 342: 1-9.

Table 5.2. Concentration values in mg cm^{-2} and method repeatabilities, in RSD %, obtained by ion chromatography.

Sample	Na^{+}	K^{+}	NH^{4+}	Mg^{2+}	Ca^{+2}	Cl^{-}	NO^{3-}	SO_4^{-2}
P1	0.02	2.19	<QL	0.02	0.26	0.01	5.89	0.51
P2	0.16	0.32	<QL	0.03	0.37	0.19	2.38	0.23
P3	0.14	0.15	<QL	0.02	0.32	0.27	1.65	0.37
P4	0.09	0.04	< DL	0.01	0.10	0.08	0.35	0.41
P5	0.05	0.05	< DL	0.01	0.00	0.13	0.46	0.08
P6	0.00	0.03	<DL	0.01	0.05	0.00	0.05	0.09
P7	0.01	2.70	<DL	0.01	0.00	0.01	3.80	0.04
P8	0.00	0.05	--	0.01	0.00	0.00	0.06	0.11
RSD (%)	2	6	--	2	4	3	4	4

DL limit of detection, QL limit of quantification

The distribution of salts of the inner arch appear to be accumulated not only in the lower levels but also at higher levels as spectroscopic techniques indicated during the in situ analyses. Moreover, as is expected in cases of rising damp[67-68], distinct salt content zones were observed depending of the height, suggesting the presence of infiltrated water from the ground level. Hence, the water was transporting and dissolving the salts from the inner part of the stone to the surface until reached a height in the wall of 1.6 m.

The average values of IC analyses (Fig. 5.14 and Fig. 5.15) showed the presence of large quantities of sulphates up to the P4 zone (0.6 m) with a decrease of concentration in P2 (0.2 m). Nitrates were also found from the lowest level to P7 (1.6 m) without showing high concentrations at the intermediate points. However, chlorides seem to be more homogeneously distributed suggesting its natural presence in the stone, as original compounds. In this way, the vertical distribution of salts was approximated to Arnold and Zehnder´s model[69] since, the less soluble sulphates such us gypsum, thenardite or epsomite were accumulated in low and middle zones whereas nitrates, mainly niter, is only concentrated in the lowest zone and at the top.

67 E. Ruiz-Agudo, B. Lubelli, A. Sawdy, R. Van Hees, C. Price, C. Rodriguez-Navarro. An integrated methodology for salt damage assessment and remediation: the case of San Jeronimo Monastery (Granada, Spain). ***Environ. Earth. Sci.;*** *2011; 63:1475-1486.*

68 S. Siegesmund, R. Snethlage. Stone in Architecture: Properties, durability. Germany: Spinger; 2011.

69 M.A. Vázquez, E. Galán, P. Ortiz, R. Ortiz. Digital image analysis and EDX SEM as combined technique to evaluate salt damp on walls. J. Constr. Build Mater.; 2013; 45: 95-105.

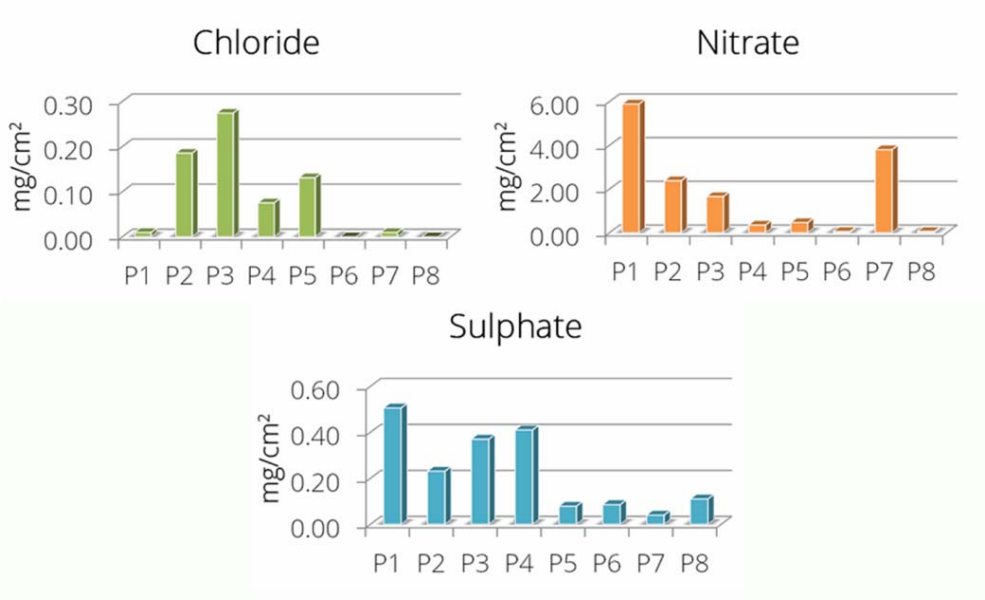

Figure 5.14. Average anion content determined by ion chromatography at different heights (0, 0.2, 0.4, 0.6, 0.8, 1.2, 1.6 and 2 m) in the historical arch of the Guevara Palace.

Given the salt distribution and the interruption of concentration zones observed, the origin of the damage suffered by the historical arch is clearly caused by the capillary rise and evaporation of water infiltration. In this way, the leached content of the soil passed through the ashlars causing several pathologies as a consequence of dissolution, hydration and crystallization processes.

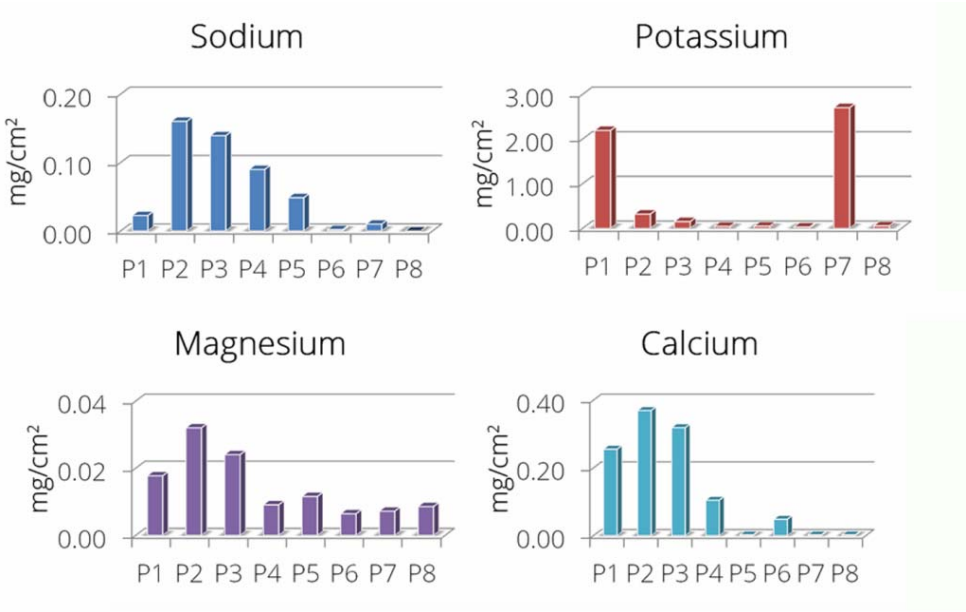

Figure 5.15. Average cation content determined by ion chromatography at different heights (0, 0.2, 0.4, 0.6, 0.8, 1.2, 1.6 and 2 m) in the historical arch of the Guevara Palace.

Besides, it should be mentioned that no high concentrations of sulphates at high points were determined and, therefore, dragging salts from plaster layers applied to the restoration was ruled out as the source of the pathologies. However, if the water ingress is not stopped, it is a matter of time it will begin to produce new problems by salts drag, which may deteriorate even more rapidly its state of preservation.

5.1.6.4. Principal component analysis of the IC results

In order to corroborate the DRIFT potential as a tool for in situ analysis and if the vertical distribution of salts within the materials is approximated to what spectroscopic results seem to indicate, a multivariate analysis of the data was used to obtain further information on the correlation of IC analysis.

The obtained Principal Component Analysis (PCA) explained 89% of the variance, using 3 PCAs to simplify the system. As can be seen in Figure 5.16, the grouping of three clusters is suggested; potassium and nitrate, calcium and magnesium sulphates and sodium and chloride.

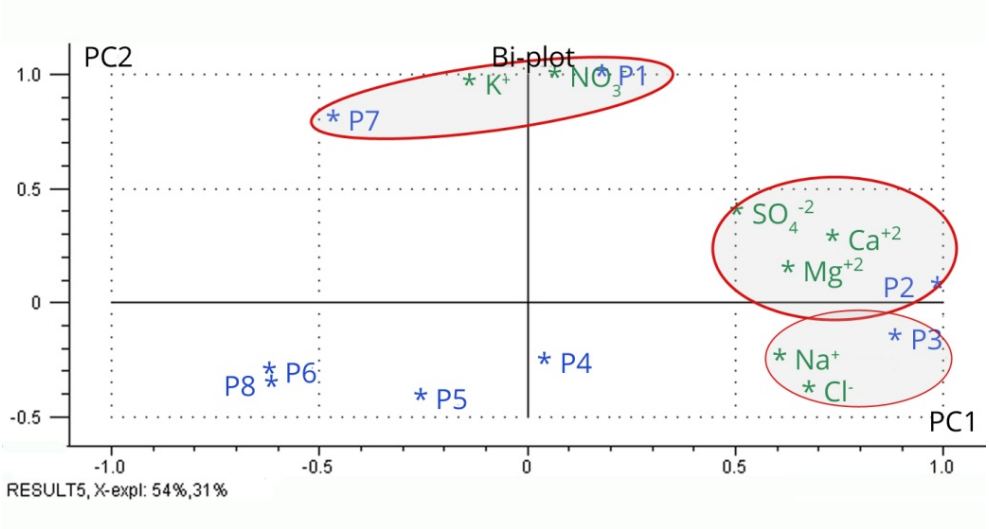

Figure 5.16. Representation of PCAs carried out by Unscrambler. The image shows the soluble content results obtained by ion chromatography. The groups formed according to the PC1 vs PC2 are highlighted: nitrates, sulphates and chlorides.

In this way, sodium was the most correlated with chloride content (r= 0.910), indicating their abundance in P3 zone. However, as the quantitative results obtained by IC suggested, its origin is natural in this kind of stone. However, it could be slightly more concentrated in this zone as a consequence of the water ingress.

In the middle zone of the arch, sulphates of magnesium and calcium were correlated (r < 0.5). The fact is supported with the identification of gypsum efflorescences by both spectroscopic techniques. Nevertheless, the in situ results of the surface showed the presence of thenardite and calcite also. Probably, the differences

are caused by seasonal changes and/or the extraction method used, since these results correspond to a certain depth, and may have differences of concentration between the exterior and interior zones. Moreover, the penetration and extraction capacity of the patches is affected by the solubility of each salt in water, the saturation effect and the application time. Therefore, for next studies, an optimization of the method (solvent, size and time) is recommended in order to find the most suitable option for each case.

Finally, potassium and nitrate were highly correlated (r= 0.873), as spectroscopic techniques pointed out identifying niter as main degradation compound in the P1 and P7 zones. In this way, one more time, the capillary rise through the wall is suggested.

In this manner, the quantitative result and the chemometric study shown demonstrate the damage suffered by the ashlars is produced by the hydration/dehydration/dissolution/crystallization cycles. Moreover, the study complemented the spectroscopic in situ analysis revealing the chlorides presence as original compound.

5.1.6.5. Thermodynamic modelling: degradation mechanisms of the cementitious matrix and iron salt formation

Given that the sandstone of ferruginous cement is a typical construction material of the Basque built heritage[70,71], this thermodynamic study is aimed to predict the formation of the identified decay compounds to understand the mechanisms involved in its degradation, since the dissolution of the stone cement could cause severe disaggregations and material losses.

The ferruginous cement, mainly composed by hematite (α-Fe_2O_3) can be transformed to goethite (α-feOOH) by intermediate mechanisms that take place in aqueous medium as the Pourbaix diagram[72] indicates (Fig. 5.17 b) Depending on the potential of the medium and pH, hematite can release Fe^{+2} cations (Fig. 5.17 b), which are hydrated first to generate the thermodynamically less stable species, lepidocrocite (γ- FeOOH)[73,74]. The latter is transformed quickly into the more stable goethite.

70 C. Martínez Gorriarán, I. Aguirre Arriaga. Estética de la diferencia: el arte vasco y el problema de la identidad, 1882-1966. Irun, North of Spain: Alberdania; 1995.

71 L. Rodríguez-Maribona, M. Zalbide, F. García Garmilla, J. A. Ibáñez, S. Garín. Conservation study of the stone material used in the Culture House of Almirante Oquendo, in San Sebastian. Mater. Construcc.; 1999; 49: 19-30.

72 M. Pourbaix. Atlas of electrochemical equilibria in aqueous solutions. Houston, Texas: National Association of Corrosion Engineers; 1974.

73 R.M. Cornell, U. Schwertmann. The iron oxides: structure, properties, reactions, occurrences and uses. Weinheim: wiley; 2003.

According to the spectroscopic results, these transformations were taking place as the presence of lepidocrocite and goethite was detected.

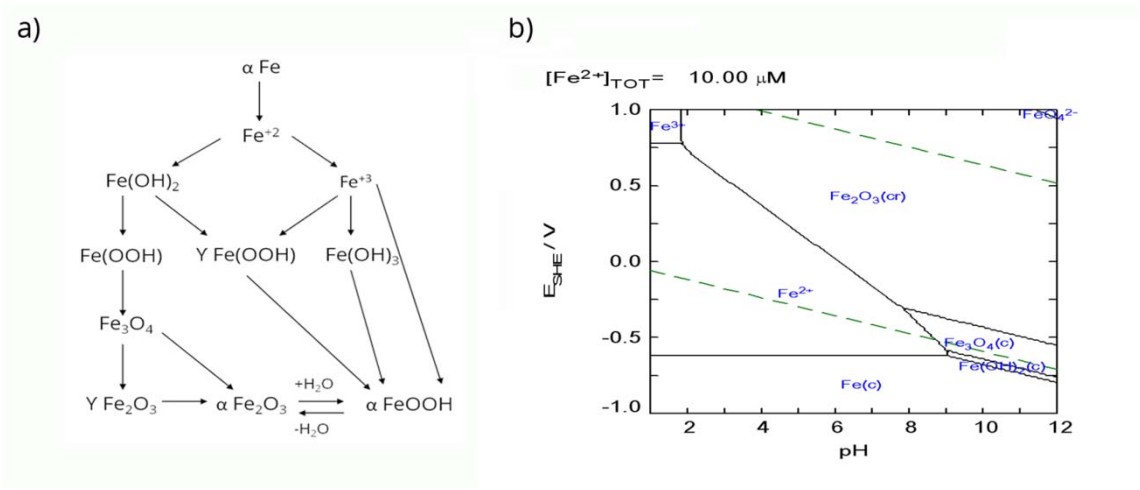

Figure 5.17. Transformation suffered by hematite. a) Outline of Fe/H2O system b) Pourbaix diagram with phase changes experienced by the different iron compounds in function of pH and redox potential of the medium.

Knowing that the measured redox potential was about 0.29 V, the pH necessary for the release of Fe^{+2} cations had to be lower than 4.5 (Fig. 5.18). This value can be easily achieved in the pores of the stone by the action of environmental pollutants and their deposition on materials.

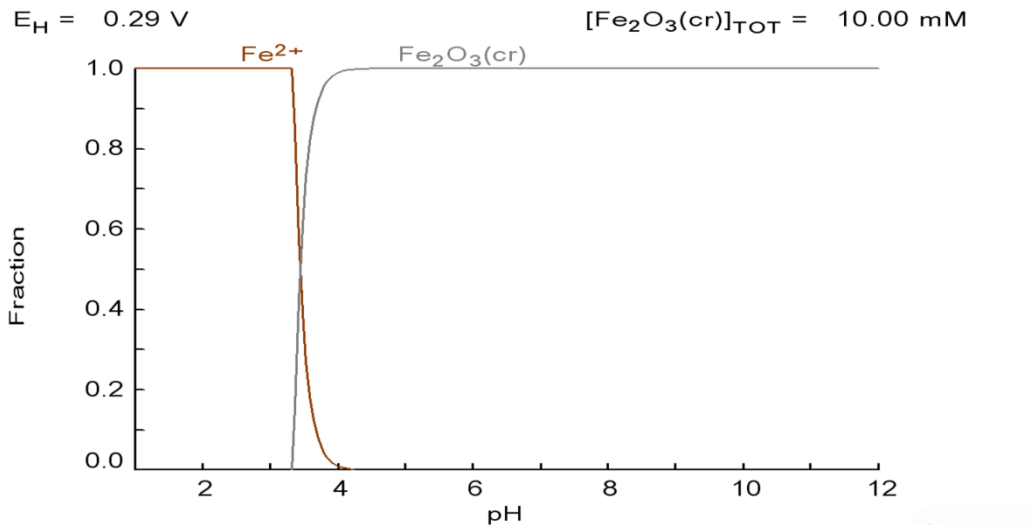

Figure 5.18. Molar fraction diagram of hematite depending on pH of the medium.

The collected Raman spectra of coquimbite ($Fe_2(SO_4)_3 \cdot 9H_2O$) and siderite ($FeCO_3$) prove again that the degradation suffered by the ferruginous cement is due to the action of CO_2 and SO_x gases. In this manner, in conditions that may occur in the porous network, the formation of iron sulphate (Fig. 5.19 a) is predicted at pH values lower than 4.5, after the coquimbite formation is produced by a hydration processes. At this point, its amount will depend on the pollutants concentration of the environment (Fig. 5.19 b).

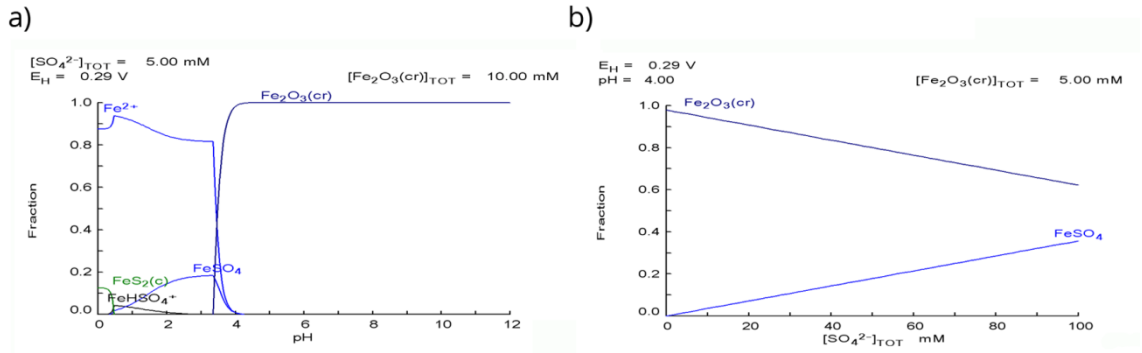

Figure 5.19. Molar fraction diagram of iron sulphate formation depending on a) the pH and b) sulphated pollutants concentration.

On the other hand, siderite formation requires pH values comprised between 7.5 and 11 (Fig. 5.20) demonstrating the variety of physicochemical conditions that can occur inside the pore system.

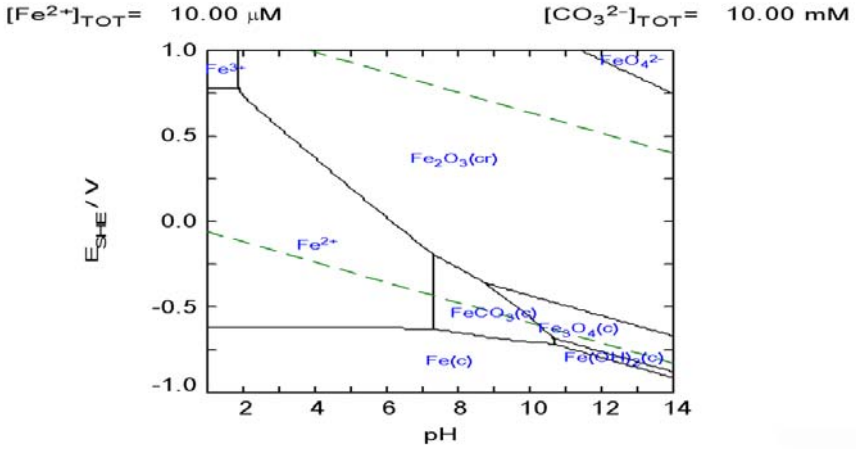

Figure 5.20. Phase changes experienced by the iron compounds as a function of pH and redox potential of the medium, under the influence of carbonate.

All of these mechanisms have harmful consequences for materials since the behavior of stone against the stresses or strains can cause deformation and fractures, depending on the petrologic and petrographic properties (degree of cementation, porosity type, etc) and external conditions in which the rock suffers tensions (temperature, presence of water, etc). Therefore, the mechanical strength that determines its durability could be seriously affected resulting in serious pathologies.

To prevent and stop these phenomena of deterioration, consolidant products can be used. In the absence of cementitious matrix, they can fix the grains of the material, providing strength and more durability to ashlars[75]. To ensure the reliability of the interventions, it is necessary to carry out this type of studies to determine the suitability of the consolidant used and in this way, select the most appropriate for each case.

5.1.7. Conclusions

The multianalytical methodology carried out allows us to demonstrate that the main source of the decaying process observed in the facade was the effect of the atmospheric pollutants, also detecting pathologies caused by biodeterioration in areas close to the main drainpipe. However, the poor state of preservation observed in the historical arc was related to the water infiltration and its capillary rise through the fire wall. In addition, the Raman identification of the carotenoids related to the Salinibacter make possible its use as biomarker, thereby obtaining a valuable indicator for salt content when sampling is restricted, facilitating in this way the establishment of degradation mechanisms.

Moreover, the advantages of the DRIFT as semiquantitative tool in the identification of compounds and salt zoning distribution were highlighted, as this technique significantly minimizes the problems presented in Raman spectroscopy by fluorescence effect in this kind of samples, making the identification of a higher number of compounds possible and helping to interpret the Raman spectra obtained (e.g. it was indispensable for the identification of various silicates). Therefore, this work shows the complementation of these non destructive techniques in the field of built heritage.

Although in situ DRIFT analyses are conditioned by external factors which are difficult to control, if the procedures are followed correctly, their minimization is possible and good in situ spectra can be obtained, making sure that the sample interface makes stable contact with the sample surface. However, the diffuse reflectance interface fits better with not too hard samples allowing better contact and achieving a good spectrum in a single measurement, instead of on hard samples in which the contact is not complete and several measures are needed to achieve a good spectrum. It should be noted that by DRIFT iron oxides cannot be observed by means of in situ analysis as the main vibration signals appear around 900 cm^{-1}, which is the same area that is distorted by the Resthralen effect. However, to achieve good laboratory results, simple operations such as grinding and mixing our sample with a non

75 L. Rodríguez-Maribona, M. Zalbide, F. García Garmilla, J. A. Ibáñez, S. Garín. Conservation study of the stone material used in the Culture House of Almirante Oquendo, in San Sebastian. Mater. Construcc.; 1999; 49: 19-30.

absorbent compound can minimize the contribution of the specular component successfully to determine them.

In addition, the DRIFT usefulness in the field analysis could be improved much better if the existing databases included a bigger number of standards, thus allowing the identification of the silicates collected in the in situ analysis.

Finally, given the differences observed of the results caused by seasonal changes, a monitoring of the salts present is advised in order to select the most suitable resin or inhibitor to prevent the progress of existing pathologies of the arch. Moreover, given the usefulness shown by cellulose patches for the salt extraction, its optimization is recommended in order to adapt the method to each situation.

CHAPTER 6: MULTIANALYTICAL APPROACH TO DIAGNOSE THE ENVIRONMENTAL IMPACT AND PROPOSAL OF INTERVENTION. THE OPERATIONAL CASE: FISHERMEN´S ASSOCIATION BUILDING

This chapter is focused on the application and improvement of the methodology developed along this thesis in order to diagnose the impact suffered by our built heritage in marine environments. In this manner, its practical utility is evaluated during a real intervention process, actively participating in the decision making of the restoration process.

Therefore, the scientific study carried out in the Association of Fishermen, consists of different phases in accordance with the requirements of the practical case.

Firstly, in situ analyses based on X-ray Fluorescence (XRF), Raman and diffuse reflectance infrared spectroscopies (DRIFT) were performed to study the pathologies most urgent to intervene. Once the origins of the damages were proposed through spectroscopic techniques, the provenance of the most influential weathering agents and the severity of the pathologies were quantitatively assessed by ion chromatography (IC) and inductively coupled plasma mass spectrometry (ICP-MS) analysis to check out the possible presence of dangerous compounds to the preservation of the building that could have been overlooked by spectroscopic techniques.

Given the environment in which the historical building is located, an improvement of the multianalytical methodology was proposed by the implementation of micro invasive mapping techniques such as μ-X Ray Fluorescence (μ-XRF) and scanning electron microscopy with energy-dispersive X-ray spectroscopy (SEM-EDX) to determine the distribution and penetration capacity of the contaminants in the building materials[1-2]. In this way, the cleaning needs and the consolidation requirements could be recommended.

Moreover, according to the variability of the salt content observed in the previous chapters, its monitoring was performed with the aim to advise the most appropriate intervention actions, taking into account the seasonal influence.

Finally, to study the behavior of aqueous salt solution in building materials, under changing climatic conditions, the application of a chemical predictive model[3-5] developed by the research at the University of East Anglia, University College London and the University of Hamburg was proposed. This model improves the Pitzer[6] thermodynamic model with experimental data, resolving the limitations related with non equilibrium conditions. In this way, the spectroscopic results of different campaigns could be corroborated by the prediction of the crystallization form of the quantitative soluble content data.

1 S. Valadas, A. Candeias, J. Mirao, D. Tavares, J. Coroado, R. Simon, A. S. Silva, M. Gil, A. Guilherme, M. L. Carvalho. Study of mural paintings using in situ XRF, confocal synchrotron-μ-XRF, μ-XRD, Optical Microscopy, and SEM-EDS-The case of the frescoes from Misericordia Chursch of Odemira. Microsc. Microanal.; 2011; 17: 702-709.

2I. Reiche, K. Müller, E. Itié, M. Eveno, M. Menu. Depth-profiling reveals multiple paint layers of Louvre Renaissance paintings using non-invasive compact confocal micro-X-ray fluorescence. J. Anal. Atom. Spectrom.; 2012; 27: 1715-1724.

3 C. A. Price. An expert chemical model for determining the environmental conditions needed to prevent salt damage in porous materials. London: European Commission Research (Protection and Conservation of European Cultural Heritage), Archetype Publications; 2000.

4 A. Sawdy, C. Price. Salt damage at Cleeve Abbey, England. Part I: a comparison of theorical predictions and practical observations. J. Cult. Herit.; 2004; 6: 125-135.

5 A. Sawdy, C. Price. Salt damage at Cleeve Abbey, England. Part II: seasonal variability of salt distribution and implications for sampling strategies.

6 P. Marliacy, N. Hubert, L. Schuffenecker, R. Solimando. Use of Pitzer´s model to calculate thermodynamic properties of aqueous electrolyte solutions of Na2SO4 + NaCl between 273.15 and 373.15 K. Fluid Phase Equilibr.; 1998; 148: 95-106.

6.1. Features of the operational case under study

6.1.1. Location of the building

The building of Fishermen´s Association is located in the emblematic dock promenade of Donostia (Gipuzkoa) (Fig. 6.1) at approximately 5 m over the sea level, with its back facade directly attached to the Urgulls´s hill, which is an area of great landscape and heritage value as it is considered a privileged defensive enclave from the middle ages.

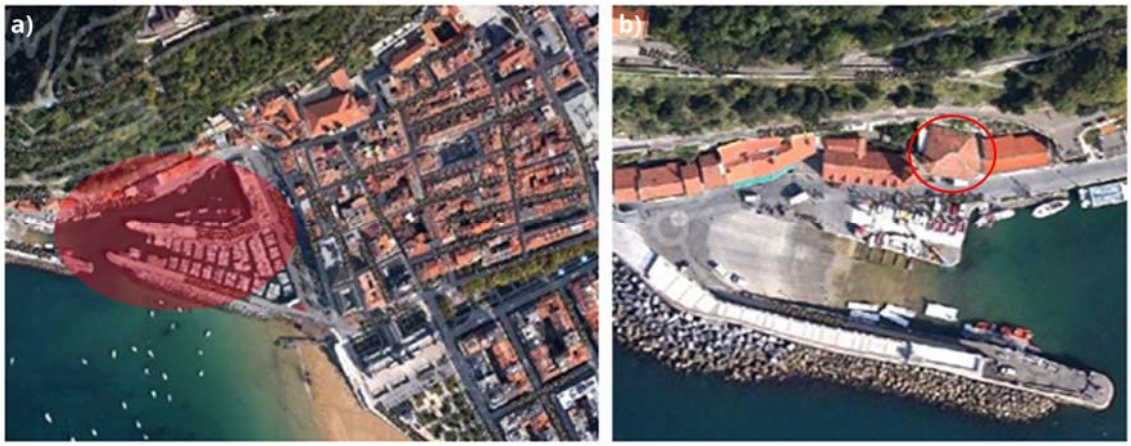

Figure 6.1. a) Location plan of the studied area (Port of Donostia). b) Site plan of the historical building under study (Association of Fishermen, Donostia).

The climate in the city is classified as Atlantic (Cfb, Köppen-Geiger[7]), with an average[8] annual temperature of around 13 ºC and rainfall of 1400 mm. The atmospheric humidity is high during all the year with an average of 77.8 %. Moreover, due to the marine influence, days of fog and wind are very common with a velocity of 4.5 m/s, as it is reflected in the rose of winds[9] (Fig. 6.2).

7 M. Kottek, J. Grieser, C. Beck, B. Rudolf, F. Rubel. World Map of the Köppen–Geiger climate classification updated. Meteorol.; 2006; 15: 259-263.

8 Basque Meteorology Agency (2014). Euskalmet: www.euskalmet.euskadi.net

9 J. Gómez Piñero, J. A. Sáez García. Geografía e Historia de Donostia- S. Sebastián. Donostia: Ingeba; 2010.

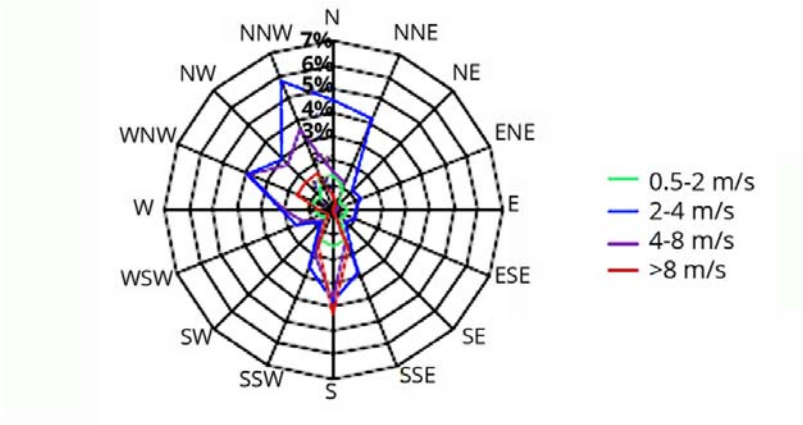

Figure 6.2. Rose of the winds of Donostia, which shows the predominant wind direction (representation of the data collected during 1971-2000 in the Igueldo station[10]).

In accordance with the latest reports from the Basque Government[11], Donostia´s atmosphere shows medium pollution levels, placing it as one of the least polluted cities in Spain. However, the port traffic next to the building could have increased the concentration of anthropogenic pollutants of the area.

6.1.2. Description of the building

The building was constructed in 1929 and its structure remained unchanged until 1991, when some detachments of Urgull's hill occurred. Due to this fact, the building and the surroundings suffered several damages. Given that, and in accordance with the Artistic Elements catalog of historical interest of the city, the building was classified as secondary protection grade and it was completely renovated, keeping the facades and the interior structure unchanged.

In addition, from 1995, it is also included in the Special Plan for the Rehabilitation of the old quarter and port of the city. Therefore, nowadays, the possible interventions that can be performed on the building must be only aimed to rehabilitation, avoiding any modification of its current aesthetic (Fig. 6.3).

10 IDAE, Institute of Energy of Spain. Ahorro y eficiencia energética en climatización de edificios: Guía Técnica. Madrid: IDAE ;2010.

11 Department of Environment and Territorial Policy (2014). Basque Government: www.ingurumena.ejgv.euskadi.eus

Figure 6.3. Photo-replacement of Blogspot 3D Gipuzkoa, in which the main facade of the building and aesthetic composition is observed.

The construction consists of a main volume with a rectangular floor of 228 m^2, attached to the side of Urgull hill (north-west). The front facade, oriented to south-east is facing the dock promenade and the port. In the east wall, the stairs that give access to the second floor are placed, adjacent to an abandoned terrain full of undergrowth (Fig. 6.4).

It has three levels above ground plus the roof, with a symmetrical composition altered with a transverse wink, where the main entrance is located on the ground floor.

The ground floor is used as garage and is composed by masonry sandstone ashlars on a bed of limestone. The interior wall, adjacent to the hill, is coated by white plaster, in the same manner as the first and second floor (Fig. 6.3).

The composition of the facade emphasizes its centrality by providing on the first floor of a balcony with some institutional character and 20th century regionalist style. In this way, the cover was composed by wood and concrete corbels carved, and the structure is made of pillars and slabs of reinforced concrete, using the facade walls and gutters as support elements.

Lastly, the roof is in a bad condition, as some concrete blocks have fallen into the third floor. The exterior walls were painted in the past for a certain period, but the paint was removed to leave the stone exposed and preserve the architectural ensemble of the houses surrounding the building.

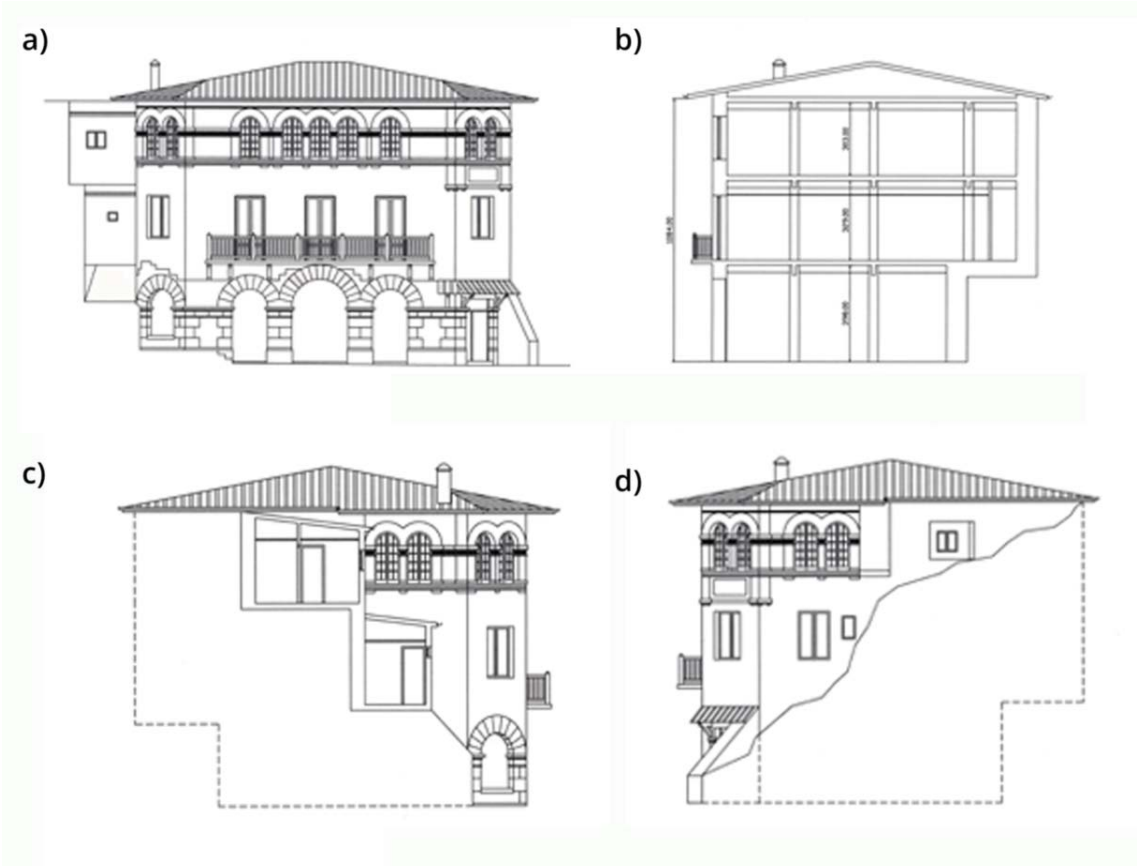

Figure 6.4. Elevation and cross-section planes. a) South facade. b) cross-section. c) West facade. d) East facade.

According to the last project of rehabilitation, the original sandstone belongs to Igueldo quarry (Gipuzkoa). Thus, it could be composed by a high percentage of quartz and other unstable compounds such us feldspar, plagioclases and glauconite grains[12].

6.1.3. In situ analysis campaign

Given that the building rehabilitation project was active during this study, the visual inspection was focused on identifying the main pathologies, trying to assess the degree of severity and, thus, its necessity of intervention.

For that purpose, several visits were carried out, as it will be detailed below, which were documented photographically and advised by a technical architect, studying with particular emphasis the more urgent affections.

12 I. Rodríguez-Maribona, M. Zabalbide, F. García Garmilla, J. A. Ibáñez and S. Garín. Conservation study of the Stone material used in the Culture House of Almirante Oquendo, in San Sebastian. Mater. Construcc.; 1999; 49: 19-30.

It should be noted that the accessible areas for the study were outdoor, ground floor and third floor. However, according to risk prevention plan, the state of the supporting floor structure of the undercover made the access to that area with the necessary equipment to perform in situ analysis not allowed.

In this way, during the visual inspection the different types of pathologies were identified and are set out below.

In the facade, the joint mortar was almost nonexistent and sandstone ashlars showed severe loss of material, especially in the west and south facade, the most exposed to wind and rain. This material loss was manifested as different affections as flaking, disintegrations and alveolizations. Besides, several efflorescences and subefflorescences were heterogeneously distributed along the facade, displaying it more sharply at the main entrance and on the south west side, in which the wet areas were also affected by biodeterioration (Fig. 6.5).

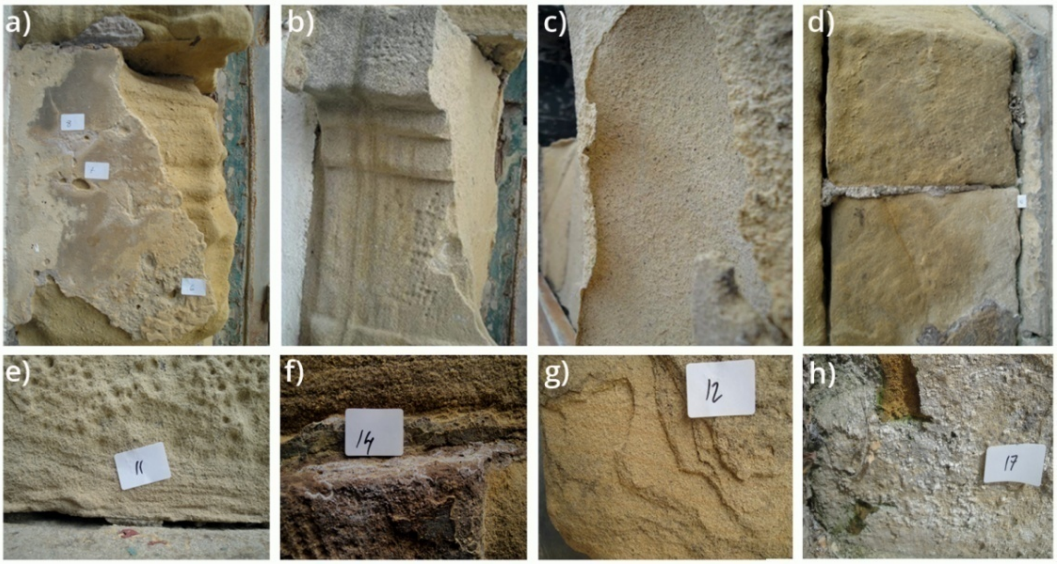

Figure 6.5. Selected photographs of the affections observed in the facade of Fishermen´s Association. a-b-c) sanding, detachment and disintegration of ashlars. d) details of lack of joint mortar, in which gaps are observed with insect nests. e-f-g-h) details of alveolization, efflorescences, flaking and biodeterioration found close to the south west side.

In addition, in balconies and areas exposed to water seepage from the roof, several detachments and cracks of the concrete structure were observed. The pathology was accentuated in the low flying of balcony and roof structure, in which the affection could cause the release of large shards. In this way, they could cross the false ceiling of the office area causing damage to the workers. Several attempts to remedy it are observed in an interior pillar, in which the protective layer of steel was broken off exposing the concrete structure as well as the later reinforcement. However, despite these attempts, the pathology continued corroding the steel until it exploded again (Fig. 6.6).

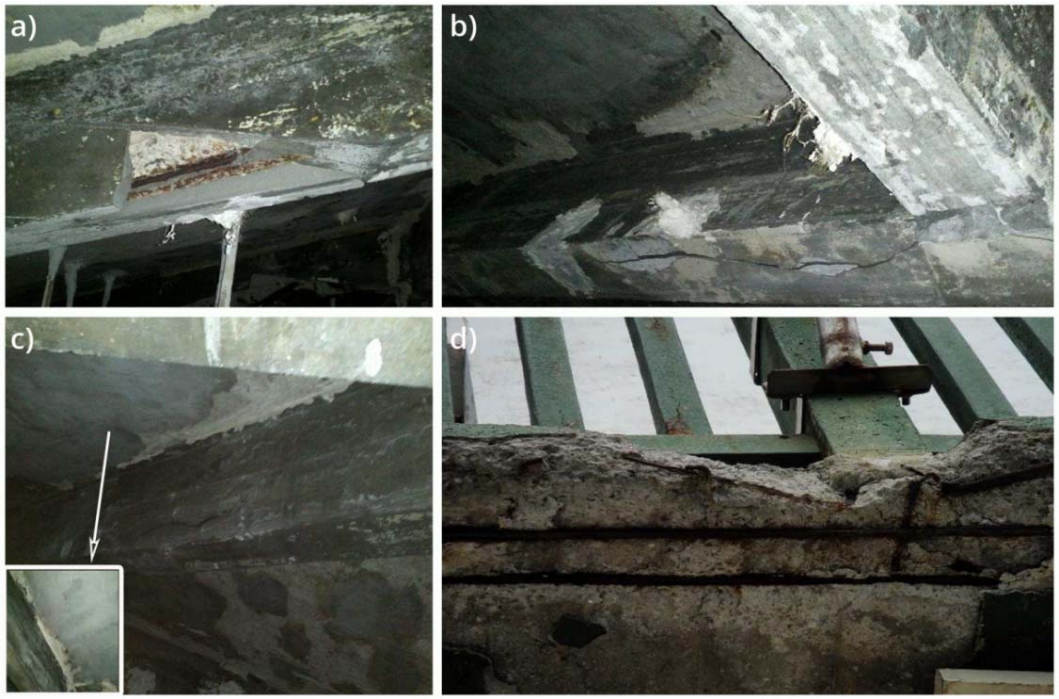

Figure 6.6. Selected photographs of the affections observed in the structures of Fishermen´s Association. a) Detachment of the roof structure, where the primitive concrete and the new concrete reinforcement can be observed. b) Cracking in the direction of the reinforced. c) The enlarged detail shows a reconstructed area based on layers of Portland cement mortar. d) The balcony structure completely exposed to the atmosphere.

On the other hand, the masonry wall on the ground floor was wet and completely covered of efflorescences (Fig. 6.7). According to the restoration project of 1991, the wall has a thickness of 1.5 m and it is in direct contact with the hillside of Urgull hill. Therefore, it is the building shell and, in turn, the retaining wall of the hillside. However, an intermediate space is not included and no effective water drainage system is observed, although several putlog holes for drainage of water from the mountain were constructed, thereby eliminating part of the overpressure.

Finally, in the areas of stairs that give access to the upper floors, whose walls are adjacent to the garage of the ground floor, several detachment of gypsum plaster layer were observed, leaving uncovered some structures and numerous subefflorescences (Fig. 6.7).

Figure 6.7. Selected photographs of the affection observed in the masonry wall of the groundfloor. a) Salt efflorescence and detachment of the plaster of the wall. b) Accentuated precipitation of salts around putlog holes. c) Enlargement of one of the most affected areas in which the efflorescences, the layer of Portland cement plaster and the original sandstone masonry can be observed.

Taking into account the visual inspection, a first in situ campaign was performed during the month of October. More than 100 measurements were collected by Raman, DRIFT and XRF on the affecting areas to corroborate the original composition of the building materials so as to identify the decaying compounds present. Besides, measurements of temperature and relative humidity were taken during the study (17-20 ºC and 73-71%, respectively) as complementary information.

Figure 6.8. Selected photographs of the affection observed in the stairs area. a) Salt efflorescences and detachment of the plaster of the wall. b-c) Wet structures covered by efflorescences.

Seven months later, after several rainy days, a second campaign was carried out. In this way, more than 150 spectroscopic measurements were collected in order to study in detail some affections and to observe possible variations caused by the change of climatic conditions (22-25 ºC of temperature and 80- 72% of relative humidity).

6.1.4. In situ results

The most relevant information obtained during the in situ analysis campaigns will be discussed along this section.

6.1.4.1. X-ray fluorescence

The characterization analysis of sandstone showed Si as the main major element, followed by Ca, Al, K and Cl but in a lower proportion. Moreover, S, Fe, Ni and Cu were identified as minor elements. The remaining composition could correspond to light elements, Na and O mainly, since their signal is too low to be detected by this portable equipment.

Given its visual appearance and the elemental percentages detected, the results seemed to be in accordance with the data indicated in the rehabilitation project. Therefore, it could be classified as glauconitic subarkose sandstone with a high percentage of fragmentary quartz, as main constituent of the cement[13] . Besides, a little amount of calcium carbonate could take part as minority cement as well as other chemically unstable compounds such us feldspar, plagioclases and glauconite grains that could be included in its composition, explaining the percentages obtained of Al or Na[14-15].

The analysis of the joint mortars of the facade showed, Si and Ca as major elements, followed by K, Al, S and Cl in lower proportion. In addition to these, a little amount of Ni was detected. In the same way at the previous case, the remaining composition could correspond to other light elements such us Na and O whose

13 M. Fregenal, J. López Gómez, J. Martín Chivelet. Ciencias de la Tierra. Diccionarios Oxford-Complutense. Madrid, Spain: Complutense; 2000.

14 I. Rodríguez-Maribona, M. Zabalbide, F. García Garmilla, J. A. Ibáñez and S. Garín. Conservation study of the Stone material used in the Culture House of Almirante Oquendo, in San Sebastian. Mater. Construcc.; 1999; 49: 19-30.

15 García- Garmilla, I. Rodríguez-Maribona, M. Cano, M. Zalbide, J. A. Ibáñez-Gómez, K. Osa-Chans, S. Garín. An analytical comparison of two commercial consolidating products applied to eocene sandstones from 16th and 19th century monuments in San Sebastián, northern Spain. Mater. Construcc.; 2002; 52: 5-12.

assigned percentage was lower than 8 %. Thus, it could be classified as a cement mortar, as its visual appearance seemed to indicate.

The lining mortar characterization of the masonry wall located in the garage could not provide conclusive data since the wall was completely covered of efflorescences and, therefore, its elemental analysis could not represent the original composition. However, its visual appearance and the information contained in the rehabilitation project indicated that the mortar used was based in Portland cement.

In addition, taking into account the area in which the building is located and the detection of Ni and Cu, destructive analysis were recommended with the purpose of determining quantitatively the level of toxic metals.

Finally, XRF analyses were performed, in the same points as Raman and DRIFT in situ measurements to obtain complementary information in order to facilitate the interpretation of the spectra collected.

6.1.4.2. DRIFT and Raman spectroscopy

According to the in situ Raman analysis of the sandstones, α-quartz (α-SiO_2, detected by its main peak at 465 cm^{-1} and secondary at 263 cm^{-1}), calcite ($CaCO_3$, detected by its characteristic peak at 1085 cm^{-1}), and microcline ($KalSi_3O_8$, by its characteristics bands at 512, 475, 456 and 288 cm^{-1}) were identified as original compounds (Fig. 6.10). The DRIFT analysis corroborated the main original composition by means of the secondary bands and overtones as the Reststrahlen effect distorted the spectra in the regions around 1000 cm^{-1} (Si-O asymmetric stretching of silicates) and 1400-1500 cm^{-1} (the CO_3^{-2} asymmetric stretching). In this way, calcite (identified by its secondary bands at 2869, 2513 and 1795 cm^{-1}) and silicates (detected by their characteristic bands at around 1000 and 3500-3600 cm^{-1}) were found (Fig. 6.9). These results were in accordance with the sandstone classification as subarkose and, given the existence of various studies, their petrographic features and their response to different laboratory tests are known[16].

According to the literature, their absorption and suction index are high, which could facilitate the dissolution of the cement. This fact is caused by its porous distribution, thus enhancing the water penetration through the material. The microstructure of this type of stone and its weatherability are reflected on its poor durability against salt crystallization, as this property is closely related to the flow of water through the material.

16 I. Rodríguez-Maribona, M. Zabalbide, F. García Garmilla, J. A. Ibáñez and S. Garín. Conservation study of the Stone material used in the Culture House of Almirante Oquendo, in San Sebastian. Mater. Construcc.; 1999; 49: 19-30.

On the other hand, the spectroscopic analysis of the mortars revealed the presence of calcite (detected by its principal peak at 1085 cm^{-1} and secondary at 712 cm^{-1}), α-quartz (detected by its main peak at 464 cm^{-1}) and hematite (α-Fe_2O_3, identified by its bands at 403, and 289 cm^{-1}) as main original compounds. In the same manner as the previous case, the DRIFT analysis corroborated the main composition detecting calcite and silicates also.

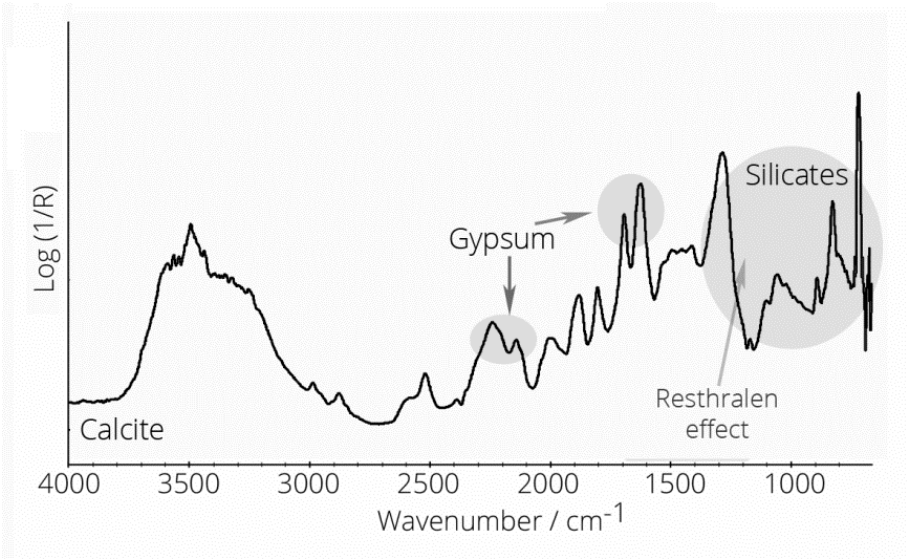

Figure 6.9. DRIFT spectra of calcite and silicates identified in situ as original materials of sandstone. Moreover, the secondary signal of gypsum can be observed also.

Once the original nature of each material is determined, the degradation compounds found are exposed regarding the area studied.

Firstly, in the analysis of the facade, gypsum ($CaSO_4 \cdot 2H_2O$, detected by its main Raman signal at 1008 cm^{-1}) (Fig. 6.10) and mirabilite ($Na_2SO_4 \cdot 10H_2O$, detected by its main peak at 989 cm^{-1}), one of the most dangerous sulphates for building materials[17-18], were identified as main degraded compounds of efflorescences and subefflorescences of the detached and disintegrated ashlars. Moreover, calcite (detected by its main band at 1085 cm^{-1}) and trona ($Na_3(HCO_3)(CO_3) \cdot 2H_2O$, detected by its principal peak at 1061 cm^{-1}) were found also but in a lower proportion, being mainly found in the joint mortars (Fig. 6.10). The DRIFT analysis of the same points corroborated the salts presence by the spectra collection of calcite (by its bands at 2869, 2514 and 1795 cm^{-1}) and suphated mixtures, in which only gypsum (assigned by the bands at 1682 and 1620 cm^{-1}) could be identified due to the distortions caused by the Resthralen effect.

17 S. F. Pop, R. M. Ion. Thermal analysis of the chemical weathering of chalk stone materials. J. Optoelectron. Adv. M.; 2013; 15: 888-892.

18 N. Tsui, R. J. Flatt, G. W. Scherer. Crystallization damage by sodium sulfate. J. Cult. Herit.; 2003; 4 : 109-115.

These compounds were classified as direct degradation of the original calcite and silicates caused by atmospheric acid attack[19-20] as well as the wet deposition of marine aerosol, which could encourage the transformation processes occurred[21-22]. In addition to the loss of material by dissolution, given the vulnerability against the salt crystallization of this stone, the volume changes suffered during these dissolution-precipitation and hydratation-dehydratation processes could clearly explain the pathologies presented and the severe loss of material observed (Fig. 6.5).

In addition to this, nitratine ($NaNO_3$, detected by its characteristic Raman band at 1067 cm^{-1}) and niter (KNO_3, detected by its bands at 1050 and 715 cm^{-1}) were also indentified in the efflorescences and subefflorescences of the west side of the facade, in which the wet areas were also affected by biodeterioration. Thanks to DRIFT analysis the presence of both degradation compounds were corroborated by the identification of niter (DRIFT bands at 2735, 2396, 2066, 1760, 1491 and 826 cm^{-1}) and nitratine (determined by its bands at 2757, 2435, 2096, 1786, 1535 and 836 cm^{-1}).

However, it should be noted that nitrates were only found in situ during the first campaign, being this fact attributed to the washing materials by the action of rain.

Taking into account that this side of the facade is totally exposed to the rain, wet to the touch, and that the growth of vegetation is only observed in this area, the nitrate presence could be explained as a consequence of the attack of the atmospheric gases over the silicate compounds, being also aggravated by the roots action which could promote the infiltration of water, contributing to its disaggregation.

Finally, it is noteworthy that some green particles were found heterogeneously distributed in the lower ashlars, although at first sight it seemed biodeterioration, all this part was painted in a similar color in the past. In this way, the remains of that coloration were identified as Windsor & Newton green pigment (by its Raman bands at 1535, 1143, 1417, 1336, 1281, 1210, 1129, 1081, 817, 776, 740, 684 cm^{-1}) (Fig 6.10). Given the colour and the similarity of bands found with those of the porphyrin family, which are biomarkers of photosynthetic species and produce resonance effect by its excitation,

19 N. Prieto-Taboada, M. Maguregui, I. Martinez-Arkarazo, M. Olazabal, G. Arana, J. M. Madariaga. Spectroscopic evaluation of the environmental impacto n black crusted modern moratars in urban-industrial areas. Anal. Bioanal. Chem.; 2010; 399: 2949-2959.

20 Y. Bai, G. E. Thompson, S. Martinez-Ramirez, S. Brüeggerhoff. Mineralogical study of salt crusts formed on historical building stones. Sci. Total Environ.; 2003; 302: 247-251.

21 S.S. Seo, S.M. Son, C.H. Lee, K. Bask. Compositional analysis of soluble salt in Bresle extraction from blocks in Newbuildings Shipyards. ISST, Osaka, 2007.

22 S.A. Nikolaus, P. Theoulakis. C. Pitinis. Dry deposition effect of marine aerosol to the building stone of the medieval city of Rhodes, Greece. Built. Environ.; 2009; 44; 260-270.

the spectrum could be correctly assigned thanks to the information provided by the restoration project.

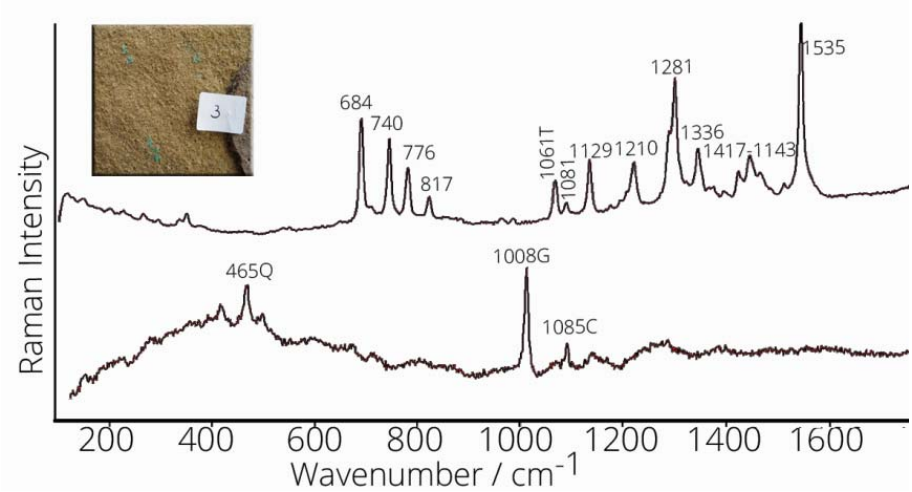

Figure 6.10. The lower in situ spectrum shows the presence of calcite (C) and α-quartz (Q) as main original compounds of the sandstone, besides, gypsum (G) could be observed as its direct degradation product. In the upper spectrum, trona (T) and the Windsor & Newton green pigment can be observed.

In the interior wall of the ground floor (Fig. 6.3), gypsum (identified by its main Raman band at 1008 cm^{-1}), mirabilite (main Raman band at 989 cm^{-1} and the weakest bands at 458 and 446 cm^{-1} aside from 1130, 1120, 1108, 628 and 616 cm^{-1}), thenardite (Na_2SO_4, identified by the strongest peak at 993cm^{-1} and the weakest pair of peaks at 466 and 451 cm^{-1} aside from the signals at 1149, 1128, 644, 632 and 621 cm^{-1}) (Fig. 6.11), nitrocalcite (identified by its Raman at 1050 and 719 cm^{-1}), niter (detected by its main peak at 1050 and its secondary at 1359, 1344 and 715 cm^{-1}) and nitratine (identified by its Raman bands at 1067 and 724 cm^{-1}) were identified as the main compounds of the efflorescences. These results were in situ corroborated thanks to the DRIFT identification of several mixtures of sulphates and nitrates.

The origin of this high amount of salts is related to the water infiltration from the hill, which is in direct contact with this wall (1.5 m of thickness). The water totally charged of leachate passed through the wall thanks to the porous network, causing the dissolution of the original materials that are dragged to the surface.

Besides, this pathology is aggravated by the plaster layer that covers the entire wall. This layer is dissolved by action of the infiltrated water, increasing the amount of sulphate in solution and, thus, the amount of sulphated efflorescences. Furthermore, the pressure exerted by the different crystallization processes produces the detachment of the layer, revealing the presence of subefflorescences.

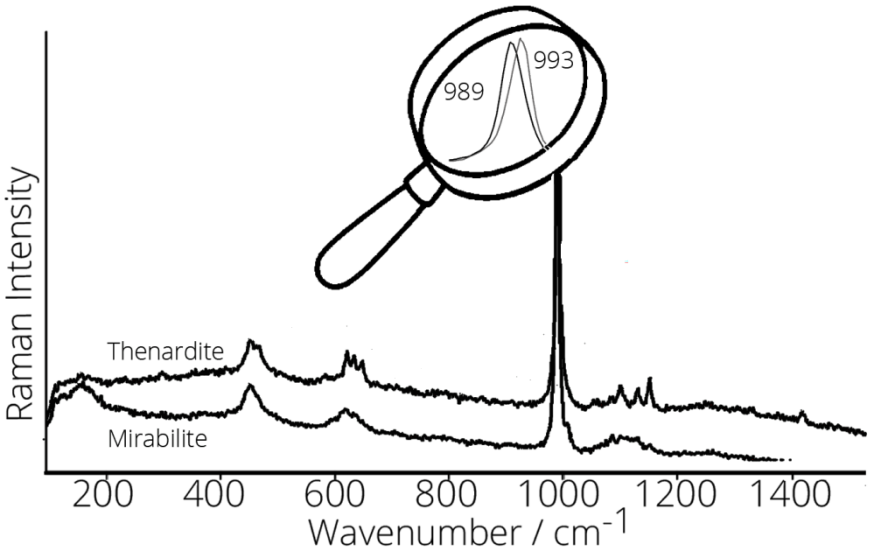

Figure 6.11. The spectra collected in situ in the interior wall of the ground floor, in which the thenardite and mirabilite can be observed. Besides, their main Raman peaks are enlarged to facilitate the differentiation.

Given the amount of nitrates found and the location of the wall, the atmospheric attack of NO_x gases could be ruled out, as the most likely source is coming from the infiltrated water and its content of organic matter in degradation[23,24]. In fact, the Raman analysis of the pathologies found (Fig. 6.7) in the stairs area, whose walls are adjacent, showed the same results. Thus, the infiltrated water could reach the adjacent wall thanks to its transport through the pores network.

The last area of interest was the internal structures, which due to the decaying processes were totally exposed to the open air (Fig. 6.6). The Raman analysis revealed the severity of this pathology since, several iron oxides such us hematite (assigned by its bands at 404, 289 and 223 cm^{-1}), akaganeite (β-FeO(OH), assigned by its Raman bands at 311 and 393 cm^{-1}) (Fig. 6.12) and lepidocrocite (γ- FeOOH, detected by its main Raman band at 250 cm^{-1}) were identified evidencing the severe affection suffered by this material.

23 M. Maguregui, A. Sarmiento, I. Martínez-Arkarazo, M. Angulo, K. Castro, G. Arana, N. Etxebarria, J.M. Madariaga. Analytical diagnosis methodology to evaluate nitrate impact on historical building materials. Anal. Bioanal. Chem.; 2008; 391, 1361-1370.

24 V. Matović, S. Erić, A. Kremenović, P. Colomban, D. Serćković-Batoćanin, N. Matović. The origin of syngenite in black crusts on the limestone monument King's Gate (Belgrade Fortress, Serbia)—the role of agriculture fertiliser . J. Cult. Herit.; 2012; 13: 175-186.

Moreover, coquimbite ($Fe_2(SO_4)_3 \cdot 9H_2O$), identified by its Raman peaks at 1025 and 496 cm^{-1}) (Fig. 6.12), gypsum (identified by its bands at 1008, 670, 493 and 414 cm^{-1}) and calcite (assigned by its main band at 1085 cm^{-1}) were also found as degradation compounds of the efflorescences located over the structures.

The layer of concrete that covers the internal structures has a certain durability, which is strongly influenced by the environmental factors. In fact, in marine atmospheres, it can be severely degraded due to the chlorides that could accelerate the corrosion process[25]. Therefore, to avoid these problems, the EHE-08 (Structural Concrete Instruction 1247/2008) established a minimum cover requirement to ensure the durability of the structures.

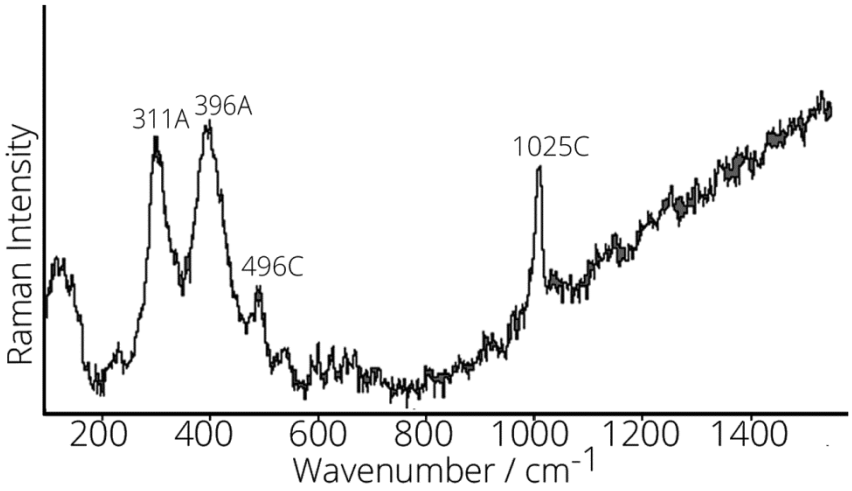

Figure 6.12. The spectrum collected in situ over the interior structures, in which the signals of akaganeite (A) and coquimbite (C) can be observed.

However, at the time of construction, these requirements were not taken into account and, the works performed during the rehabilitation project were limited to cover the damage with new layers of concrete, regardless of the carbonation process occurred.

This chemical process is caused by a decrease of pH value inside the material, which occurs due to the penetration of water and atmospheric CO_2. The dissolved gas attacks the porous matrix, transforming the original calcium hydroxide, $Ca(OH)_2$, in calcium carbonate, $CaCO_3$. This causes vulnerability of the reinforced concrete. The protective oxide layer of reinforcement steel is achieved by the passivation of its surface, only stable in highly alkaline environments. If the carbonation process progresses and it reaches the steel, the protective layer loses stability. In this manner, at

25 L. G. Johansson, O. Linqvist, R. E. Mangio. Corrosion of calcareous stones in humid air containing SO_2 and NO_2. Dur. Build. Mater.; 1988; 5: 439-449.

pH levels lower than 11, the corrosion starts and could cause cracking and spalling of the material[26-27].

In this manner, the entrance of water and atmospheric pollutants is facilitated and, then, the pathology increases until the concrete layer explodes, leaving the internal structures totally exposed to the aggressive atmosphere.

The presence of calcite efflorescences evidences the severe grade of carbonation suffered by the structures and, besides, the identification of akaganeite is especially highlighted as, for its formation, a high concentration of chlorides in the surrounding of the iron piece is necessary, evidencing the loss of the passivation layer suffered by the internal structures[28].

According to the in situ study, this pathology is one of the most dangerous as it could affect the stability of the building. Furthermore, the detachment of the roof structure could cause workers getting injured by falling debris in the office area. Moreover, the flights of the balconies are also affected by the carbonation process and given that these elements are declared historical heritage and that they are in danger of collapse, they require an urgent intervention.

6.1.5. Sampling for the laboratory analysis

As result of the first in situ study, during the second campaign, a very little amount (approx. 0.13 g) of non degraded sandstone was collected to complement the information of original composition in the laboratory.

Moreover, the selected degraded samples (efflorescences, sandstones, mortars and structures) from the facade, balcony, garage and stairs were gathered using a chisel (from 0.1 to 0.4 g of each one) to continue the diagnosis study in the laboratory.

In addition, in order to know the composition of the run offs that come from the mountain and could be affecting the building, some soil samples, rain and standing water of the part adjacent to the hill were collected to be analyzed (more information can be consulted in chapter 3, section 3.1.1).

26 E. Chávez-Ulloa, R. Camacho-Chab, M. Sosa-Baz, P. Castro-Borges, T. Pérez-López. Corrosión Process of Reinforced Concrete by Carbonation in a Natural Environment and an Accelerated Test Chamber. Int. J. Electrochem. Sci.; 2013; 8: 9015-9029.

27 A. V. Saetta, R. V. Vitaliani. Experimental investigaction and numerical modeling of carbonation process in reinforced concrete structures: PartI: Theoretical formulation. Cement Concrete Res.; 2004; 34: 571-579.

28 L. Selwyn. Overview of archaeological iron: the corrosion problem, key factors affecting treatment, and gaps in current knowledge. Australia: Metal National Museum of Canberra; 2004.

Apart from that, due to the differences observed in the results, a second sampling campaign was perform during the month of July, in which 8 more samples of sandstone were collected to be analyzed in the laboratory and compare with the latest (collected during the first sampling campaign).

6.1.6. Laboratory analyses

The most relevant information obtained during the laboratory analyses will be discussed along this section.

6.1.6.1. X-Ray Diffraction (XRD)

To corroborate the classification of the sandstone carried out in the in situ analysis, two samples of apparently non degraded sandstones were analyzed by "Rocks and Minerals Unit" of the University of The Basque Country (EHU / UPV).

According to the results (Fig. 6.13), quartz was the major compound with an estimated percentage of 90-92%. Besides, the remaining content was identified as calcite and argillaceous compounds of illite group, although low levels of halite (NaCl) and were also found. Therefore, the kind of sandstone, classified in situ as subarkose was confirmed.

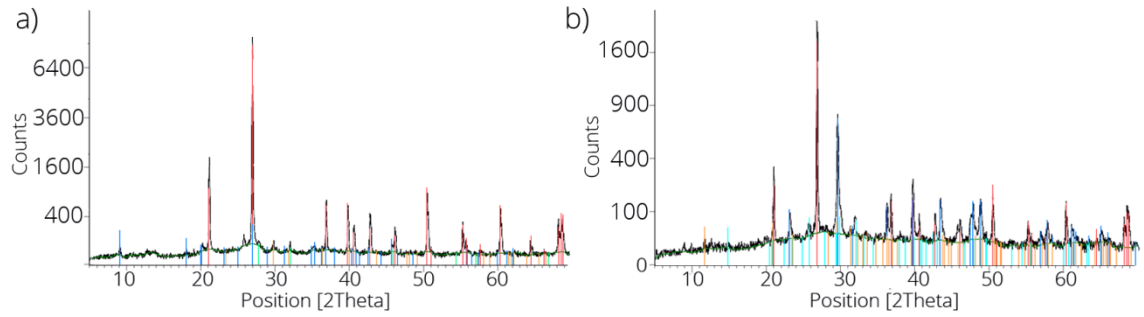

Figure 6.13. X-Ray diffraction results. a) non degraded sandstone sample, in which quartz signals are red colored, phyllosilicates of illite group are marked in blue and halite and calcite are marked in green and orange, respectively. b) degraded sandstone sample, in which quartz signals are red colored, calcite and gypsum are marked in dark blue and orange, respectively. Besides, reflection signals of halite, caolinite and illite are observed at 12,4ª 2 and 9ª 2 theta.

Additionally, a highly degraded sample of the facade was also analyzed in order to compare their compositions. In this way, quartz and calcite were identified with an estimated percentage of 60% and 40%, respectively. Besides, little amounts of gypsum, bassanite ($CaSO_4 \cdot 0.5H_2O$), halite, caolinite and illite were found (Fig. 6.13).

The amount of quartz obtained is much lower than expected, thus, the disaggregation pathology suffered by the cementitious matrix could be severe. However, the proportion of calcite found is much higher than expected, denoting the

aggressive action of the CO_2 gases as well as its deposition. Finally, the presence of gypsum, bassanite and halite demonstrate once again the transformation processes caused by the SO_x gases and the deposition of marine aerosol.

6.1.6.2. Mapping analysis by μ-XRF and SEM-EDX

According to the in situ results, the sandstone sample selected from the facade was prepared for cross-section analysis (more information can be consulted in chapter 3, section 3.1.2), avoiding the loss of soluble and weakly anchored compounds.

In this way, thanks a combination of μ-XRF and SEM-EDX, the elemental distribution and the penetration capacity of the pollutants was evaluated in order to establish the thickness affected and, thus, to define the requirements of restoration such us cleaning procedures or penetration capacity of the consolidants.

The elemental distribution of the sample (Fig. 6.14) evidences silicon as main component of the cementitious matrix, which is homogeneously distributed. The areas with lowest concentration of this element correspond to the highest levels of potassium and calcium. This fact is attributed to the natural percentage of calcium carbonate and feldspars inherent to the material, as was indicated by the previous analysis. However, in the deepest areas, which correspond to a natural fracture, no element related to the cementer is observed, explaining the release of the sandstone piece.

In the same manner, the iron distribution is homogenous as it was expected by the glauconitic grains of its natural composition.

On the other hand, lead shows higher values in areas close to the surface, evidencing its penetration by anthropogenic sources, although, the most external areas could be washed by rain. For this reason, a quantitative analysis of heavy metals is recommended to determinate the level of affection.

The observed distribution of zinc was not expected, since no compound of this nature was identified. However, given its distribution, its origin is probably natural and attributed to the feldspar content, which was not identified due to fluorescence effect in the Raman measurements and the lack of its standards in the DRIFT database.

Besides, chloride levels clearly demonstrate the marine aerosol deposition, evidencing its ability to penetrate inside the material, even in the most non degraded samples as it was also indicated by the XRD analysis.

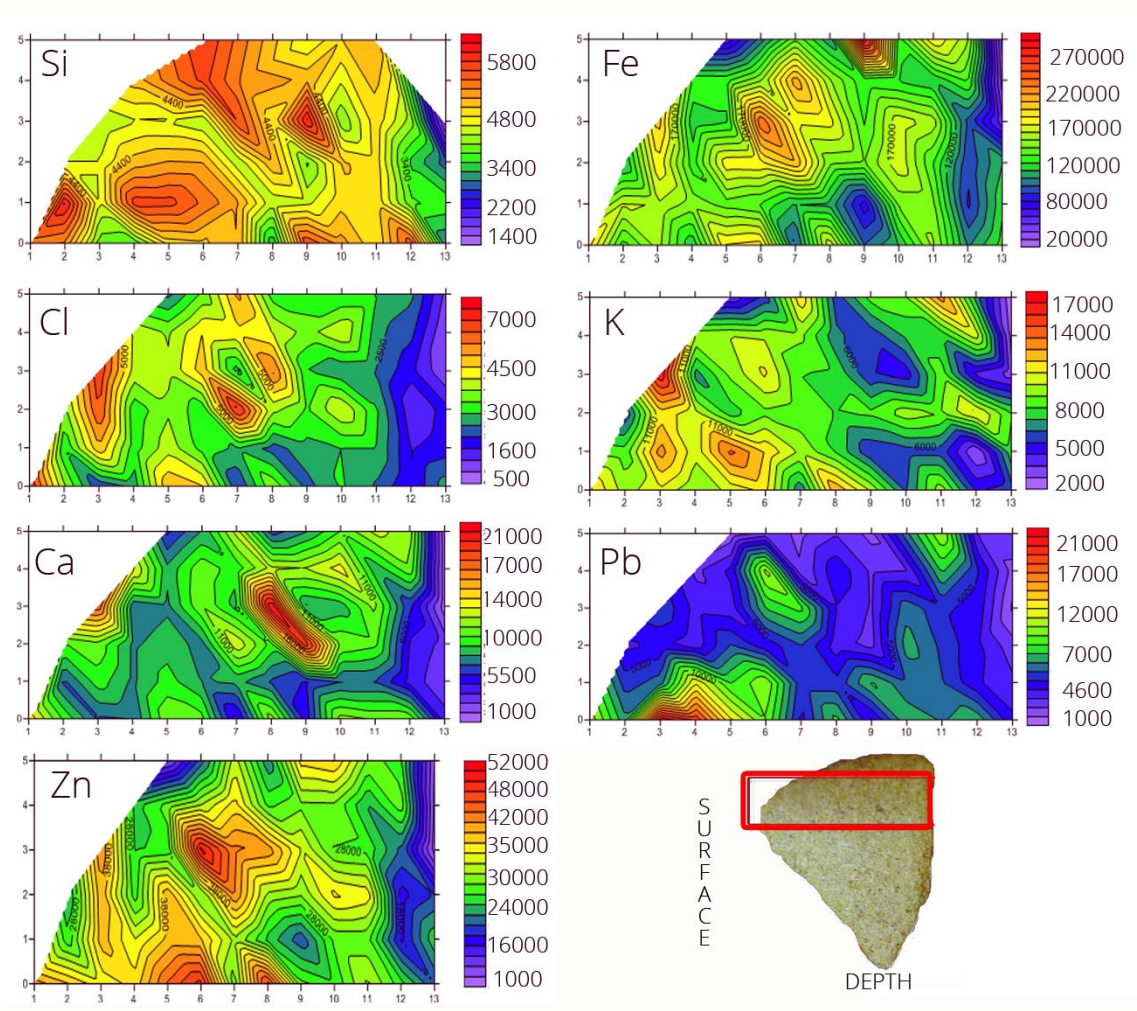

Figure 6.14. Cross section analysis of the sandstone sample using Surfer 10 software. In this way, the elemental distribution and abundance are showed.

Thanks to this analysis, the elemental distribution of the material could be studied, suggesting an impact of external sources such as marine aerosol. Moreover, it was possible to detect a common pattern to all the original compounds, the low concentration presented in the break area, explaining the detachment of the piece by the lack of cementer particles.

Finally, the break area was examined in depth by SEM-EDX to detect new correlations between the lightest elements. The surface was not flat and only the points at 2 mm of the crack (Fig. 6.15) could be correctly focused. In this way, several potassium and magnesium feldspar were identified as original compounds, homogenously distributed. However, other degradation compounds such us halite and gypsum were also found.

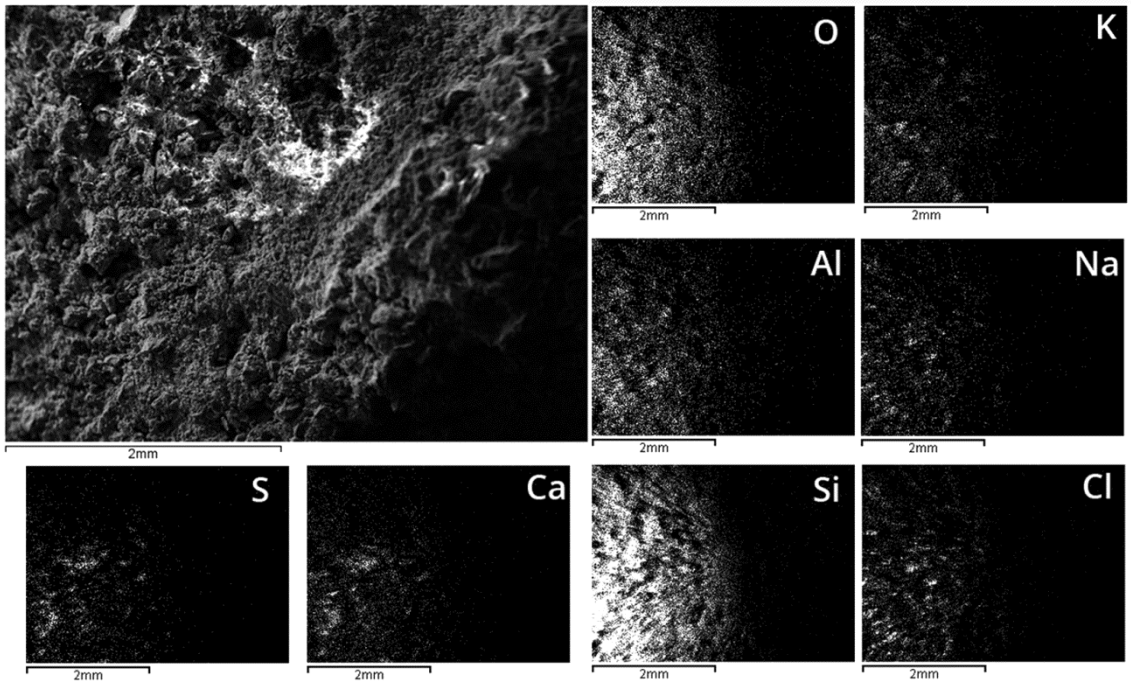

Figure 6.15. Images of EDS element mappings, in which the elemental distribution of the break areas is showed.

In addition, along the entire area of fissure, the same soluble salts could be observed in detail (Fig. 6.16), demonstrating the penetration capacity of the marine aerosol and SO_x gases inside the material, as well as is harmful effect.

Considering these results, the cross-section analysis allowed us to corroborate that the superficial data obtained in situ were representative of the internal damage as well as to determinate its penetration capacity.

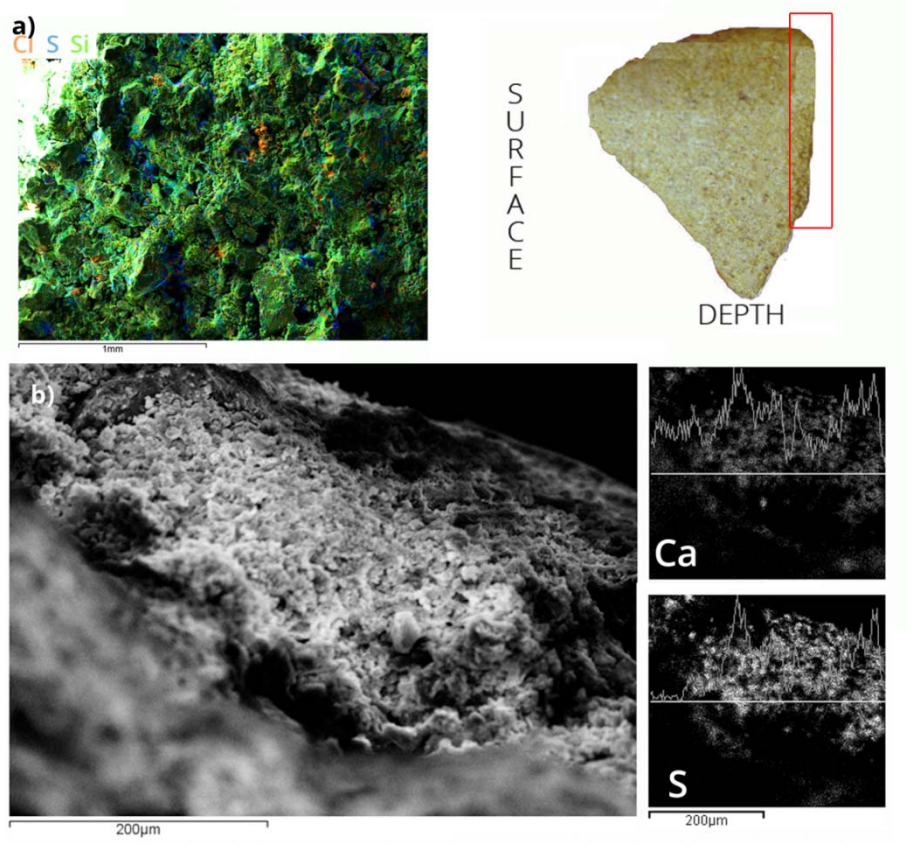

Figure 6.16. a) False colour image performed over the break areas, in which the energies of Cl are presented in red, of S in blue and of Si in green. b) EDS element mappings in which the distribution profile of the degradation products found is shown.

6.1.6.3. Raman spectroscopy

Thanks to the laboratory Raman analysis of the sandstones samples, the full spectra of α-quartz, calcite, and microcline were obtained, corroborating the original composition (Fig. 6.17). Addition to this, glauconite ($(K, Na)(Fe^{+3}, Al, Mg)_2(Si, Al)_4O_{10}(OH)_2$, assigned by the Raman bands at 1121, 1064, 680, 550, 463, 378, 350, 255 and 201 cm^{-1}) was found as original compound also, corroborating again the type of stone.

In the same manner, calcite, gypsum and mirabilite were identified as main degraded compounds of efflorescences and subefflorescences, demonstrating the atmospheric acid attack and the deposition of the marine aerosol.

Moreover, in the samples taken from the west side of the facade, mainly affected by biodeterioration, no nitrate salt was identified probably due to the sampling being carried out during the rainy season. However, in this area, glauberite ($Na_2Ca(SO_4)_2$ assigned by its Raman band at 1002 cm^{-1}) was found, complementing in this way the spectroscopic analysis, even if only its main signal was detected due to the fluorescence effect.

In the same manner, calcite, gypsum and mirabilite were identified as main degraded compounds of efflorescences and subefflorescences, demonstrating the atmospheric acid attack and the deposition of the marine aerosol.

Moreover, in the samples taken from the west side of the facade, mainly affected by biodeterioration, no nitrate salt was identified probably due to the sampling being carried out during the rainy season. However, in this area, glauberite ($Na_2Ca(SO_4)_2$ assigned by its Raman band at 1002 cm^{-1}) was found, complementing in this way the spectroscopic analysis, even if only its main signal was detected due to the fluorescence effect.

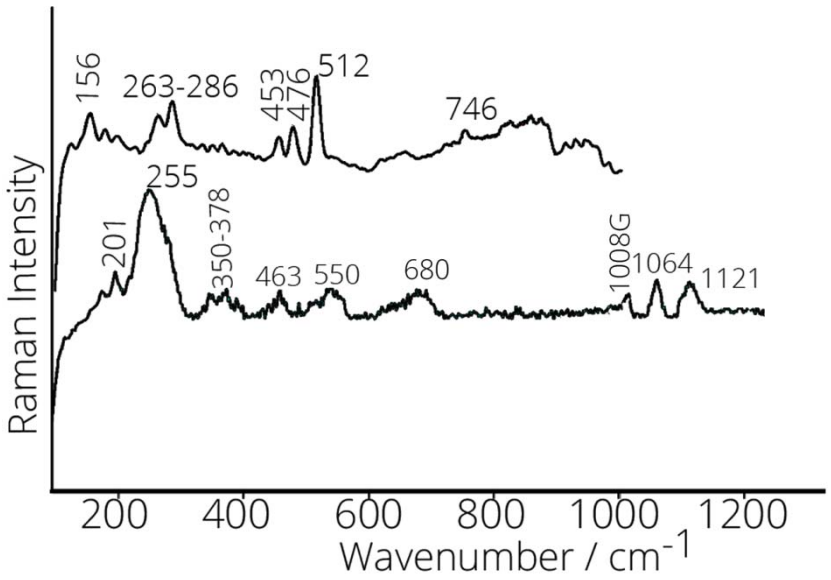

Figure 6.17. The lower in situ spectrum shows the presence of glauconite and gypsum (G) in the sandstone samples. In the upper spectrum, microcline signals can be observed.

The formation of this mixed sulphate is very common in rich medium in sulphate and chlorides. In fact, glauberite usually crystallize together with mirabilite and halite. Given the great amount of sulphates identified and the marine environment, its presence is quite likely.

According to the analysis of the samples collected in the interior wall of the ground floor (Fig. 6.3), gypsum, mirabilite, nitrocalcite and nitratine were identified as the main compounds of the salt crust layer. Furthermore, this time, the full spectra of glauberite (Raman bands at 1140, 1106, 1002, 644 and 471 cm^{-1}) was found.

On the other hand, the analysis of the samples collected in the internal structures corroborated the in situ results thanks to the identification of hematite, akaganeite, lepidocrocite and besides, goethite (α-FeOOH, assigned by its Raman bands

at 529, 475, 384, 300 and 248 cm^{-1}), evidencing again the loss of the passivation layer by the attack of the marine environment.

Finally, the efflorescence samples found over the structures allow us establishing that the carbonation process was taken place, thanks to the identification of calcite and kalicinite ($KHCO_3$, detected by its Raman bands at 1027, 637 and 188 cm^{-1}). Moreover, coquimbite, basanite ($CaSO_4 \cdot 0.5\ H_2O$, Raman bands at 1015, 668, 627, 487 and 429 cm^{-1}) and bianchite ($ZnSO_4 \cdot 6H_2O$, Raman bands at 1025, 624, 423 and 284 cm^{-1}) were also found as minor compounds, demonstrating the severity of this pathology.

6.1.6.4. Soluble content quantification by ion chromatography: Soil and water samples

Thanks to the ion chromatography, the soluble ionic composition of soil, rain and standing water samples of the part adjacent to the hill were analyzed (more treatment information can be consulted in chapter 3, sections 3.1.2).

According to the rain water results (Table 6.1), sulphates and sodium were the most concentrated ions that could penetrate in the sandstone materials and to the internal structures by the rain action. Once again, these data point out as main cause of degradation, the attack of SO_x atmospheric gases (by wet or dry deposition) over the original materials, explaining its transformation into gypsum, mirabilite, coquimbite and even trona.

Moreover, the common fogs and the marine aerosol could increase the concentration of ions in the atmosphere such us chlorides, promoting further the corrosion, dissolution and salt damage processes[29-30].

29 S.S. Seo, S.M. Son, C.H. Lee, K. Bask. Compositional analysis of soluble salt in Bresle extraction from blocks in Newbuildings Shipyards. ISST, Osaka, 2007.

30 S.A. Nikolaus, P. Theoulakis. C. Pitinis. Dry deposition effect of marine aerosol to the building stone of the medieval city of Rhodes, Greece. Built. Environ.; 2009; 44; 260-270.

Table 6.1. Concentration values in mg·Kg^{-1} and method repeatabilities, in RSD %, obtained by ion chromatography.

Sample	Na^+	K^+	NH_4^+	Ca^{2+}	Cl^-	NO_3^-	SO_4^{2-}
Rain water	$2.8 \times 10^{+3}$	<QL	<QL	<QL	<QL	<QL	$1.44 \times 10^{+3}$
Standing water	$3.1 \times 10^{+4}$	$1.1 \times 10^{+4}$	$1.2 \times 10^{+4}$	$5.4 \times 10^{+4}$	$5.6 \times 10^{+4}$	$7.6 \times 10^{+3}$	$2.1 \times 10^{+4}$
*Soil	$1.61 \times 10^{+3}$	$3.1 \times 10^{+3}$	$1.0 \times 10^{+3}$	$4.4 \times 10^{+3}$	$1.8 \times 10^{+3}$	$2.5 \times 10^{+3}$	$1.4 \times 10^{+3}$
*RSD (%)	3	4	2	5	3	4	2

The soluble content of the soil and standing water support the proposal of runoff water infiltration being the main cause of degradation of the inner wall. As the quantitative data show, the rainwater can leach large amounts of nitrates, chlorides and sulfates of the soil content and drag them through the wall, causing the severe saline pathology studied.

6.1.6.5. Soluble content quantification by ion chromatography:

Stony samples

To determinate the salts content, the efflorescences, sandstones and mortar samples taken during the second campaign were analyzed by ion chromatography. In this manner, soluble sulphate, nitrate, chloride, sodium, potassium, calcium and magnesium concentration were quantified (Tables 6.2 and 6.3) (more information can be consulted in chapter 3, section 3.1.2).

Moreover, the percentage of sulphate, chloride and nitrate of the samples were calculated also (Tables 6.2 and 6.3) in order to classify the severity of the damage shown, according to a guide issued by Fraunhofer-IRB[31].

According to the results, a high soluble salt content of the materials was revealed. The sandstone samples collected in the facade showed as major compounds sulphates, although important amounts of nitrates were also found.

[31] *M. Auras. Leitfaden Naturstein-Monitoring. Nachkontrolle und Wartung als zukunftsweisende Erhaltungsstrategien. Fraunhofer-IRB-Verl: Stuttgart; 2011.*

Table 6.2. Concentration values of sandstone samples in mg·Kg-1 and method repeatabilities, in RSD %, obtained by ion chromatography. Besides, the percentages of sulphate, chloride and nitrate are shown.

Sample	Na^+	K^+	Ca^{2+}	Cl^-	NO_3^-	SO_4^{2-}	Wt% (SO_4^{2-})	Wt% (NO_3^-)
1A	--	--	$1.7 \times 10^{+4}$	<QL	<QL	$3.7 \times 10^{+4}$	3.7	--
3A	$6.7 \times 10^{+3}$	<QL	$2.2 \times 10^{+3}$	<QL	<QL	$8.6 \times 10^{+3}$	0.8	--
4A	$4.1 \times 10^{+3}$	<QL	$1.1 \times 10^{+3}$	<QL	<QL	<QL	--	--
5A	$2.7 \times 10^{+3}$	<QL	$5.1 \times 10^{+3}$	<QL	$5.6 \times 10^{+3}$	<QL	--	0.6
6A	$5.3 \times 10^{+3}$	<QL	$1.6 \times 10^{+4}$	<QL	$9.3 \times 10^{+3}$	$1.2 \times 10^{+4}$	1.2	0.9
12A	$5.0 \times 10^{+3}$	<QL	$7.6 \times 10^{+3}$	<QL	$8.1 \times 10^{+2}$	$1.0 \times 10^{+4}$	1	8.1×10^{-2}
19A	$2.7 \times 10^{+3}$	<QL	<QL	<QL	$6.2 \times 10^{+3}$	$8.2 \times 10^{+3}$	0.8	1.0×10^{-2}
20B	<QL	<QL	$7.8 \times 10^{+3}$	<QL	<QL	$2.3 \times 10^{+4}$	2.3	--
*RSD (%)	4	--	3	--	3	5	--	--

Table 6.3. Concentration values of mortar and efflorescence samples in mg·Kg^{-1} and method repeatabilities, in RSD %, obtained by ion chromatography. Besides, the percentages of sulphat, and chloride are shown.

Sample	Na^+	K^+	Ca^{+2}	Cl^-	NO_3^-	SO_4^{-2}	Wt% (SO_4^{-2})	Wt% (Cl^-)
6A	$5.7 \times 10^{+4}$	$2.4 \times 10^{+3}$	$1.6 \times 10^{+4}$	$8.8 \times 10^{+4}$	--	$1.0 \times 10^{+4}$	1	8.8
8A*	$3.3 \times 10^{+5}$	--	$1.2 \times 10^{+4}$	$5.2 \times 10^{+5}$	--	--	--	51.9
13A	$1.0 \times 10^{+4}$	--	$9.4 \times 10^{+3}$	$9.5 \times 10^{+3}$	--	$6.2 \times 10^{+3}$	0.6	0.9
1B	$8.5 \times 10^{+3}$	$2.5 \times 10^{+3}$	$2.2 \times 10^{+4}$	$1.9 \times 10^{+4}$	--	$2.4 \times 10^{+4}$	2.4	1.9
2B	$1.5 \times 10^{+4}$	$2.2 \times 10^{+3}$	$3.0 \times 10^{+4}$	$2.2 \times 10^{+4}$	--	$5.6 \times 10^{+4}$	5.6	2.2
3B	$2.3 \times 10^{+4}$	--	$1.8 \times 10^{+4}$	$4.2 \times 10^{+4}$	--	$7.3 \times 10^{+3}$	0.7	4.2
4B*	$4.1 \times 10^{+5}$	$1.9 \times 10^{+3}$	$3.2 \times 10^{+3}$	$7.1 \times 10^{+5}$	--	--	--	70.7
5PB**	$1.6 \times 10^{+5}$	--	$1.0 \times 10^{+4}$	$2.5 \times 10^{+5}$	<QL	--	--	24.7
6PB**	$1.2 \times 10^{+5}$	--	$2.6 \times 10^{+4}$	--	<QL	$4.0 \times 10^{+5}$	40.3	--
21**	$6.6 \times 10^{+3}$	--	$1.8 \times 10^{+4}$	$2.0 \times 10^{+4}$	--	$7.0 \times 10^{+3}$	0.7	2
22**	$5.3 \times 10^{+3}$	--	$1.6 \times 10^{+4}$	--	--	$1.9 \times 10^{+4}$	1.9	--
27**	$1.8 \times 10^{+5}$	--	$3.8 \times 10^{+4}$	$1.8 \times 10^{+4}$	--	$5.8 \times 10^{+5}$	58.6	1.8
*RSD (%)	5	3	4	6	--	5	--	--

* efflorescence sample of mortars/** efflorescence sample of internal structures

In accordance with the classification of salts levels that are considered potentially hazardous for porous materials[32], only samples 4A, 5A and 6A showed medium levels. The remaining samples showed severe levels, reaching Extreme Grade (IV) in most cases, which evidences the high damage found in the sandstone ashlars.

On the other hand, according to the mortar and efflorescence results (Table 6.3), high amounts of chlorides and sulphates were observed. Although some amount of chlorides is expected in sand mortars, these high values could be only explained by the sea spray deposition, which can easily penetrate by the holes of the joint mortars as well as by the cracks of the lining of structures. Besides, the concentration found was classified as Extreme Grade (IV) for all the samples, explaining the salt damage found and the poor conservation state of the joint mortars.

Finally, the ion content of the efflorescences collected on the surrounding of the internal structures evidence the massive attack of sulphates and chlorides to which the structures are exposed, implying the danger of this pathology.

6.1.6.6. Thermodynamic modelling to study the behaviour of the soluble salt content: Runsalt

According to the variability of the salt formations observed during both in situ spectroscopic studies, the sandstones samples of the second sampling were analyzed by ion chromatography to study the seasonal influence.

For that purpose, soluble sulphate, nitrate, chloride, sodium, potassium, calcium and magnesium concentrations were quantified (Tables 6.4).

[32] *M. Auras. Leitfaden Naturstein-Monitoring. Nachkontrolle und Wartung als zukunftsweisende Erhaltungsstrategien. Fraunhofer-IRB-Verl: Stuttgart; 2011.*

Table 6.4. Concentration values of the sandstones samples in mg·Kg^{-1} and method repeatabilities, in RSD %, obtained by ion chromatography.

Sample	Na^+	K^+	Ca^{+2}	Cl^-	NO_3^-	SO_4^{-2}	Mg
14B	$2.2 \times 10^{+4}$	$8.2 \times 10^{+3}$	$1.6 \times 10^{+4}$	$3.7 \times 10^{+4}$	$1.8 \times 10^{+4}$	$2.7 \times 10^{+4}$	--
S2	$4.3 \times 10^{+3}$	$6.5 \times 10^{+2}$	$4.9 \times 10^{+3}$	$6.2 \times 10^{+3}$	$3.2 \times 10^{+3}$	$2.2 \times 10^{+4}$	--
S5	$1.9 \times 10^{+3}$	$4.6 \times 10^{+2}$	$1.1 \times 10^{+4}$	$4.6 \times 10^{+3}$	$1.2 \times 10^{+3}$	$5.5 \times 10^{+3}$	<QL
S6	$1.7 \times 10^{+3}$	$3.9 \times 10^{+2}$	$5.7 \times 10^{+3}$	$3.7 \times 10^{+3}$	$1.1 \times 10^{+3}$	$8.0 \times 10^{+3}$	--
S7	$1.6 \times 10^{+3}$	$5.1 \times 10^{+2}$	$3.8 \times 10^{+3}$	$3.2 \times 10^{+3}$	$1.8 \times 10^{+3}$	$6.2 \times 10^{+3}$	<QL
M9	$1.2 \times 10^{+3}$	$3.8 \times 10^{+2}$	$1.9 \times 10^{+3}$	$2.8 \times 10^{+3}$	$8.4 \times 10^{+2}$	$2.7 \times 10^{+3}$	--
M10	$1.2 \times 10^{+3}$	$1.2 \times 10^{+3}$	$1.7 \times 10^{+3}$	$1.9 \times 10^{+3}$	$2.2 \times 10^{+3}$	<QL	--
M11	$1.0 \times 10^{+3}$	$2.6 \times 10^{+3}$	$2.8 \times 10^{+3}$	$1.8 \times 10^{+3}$	$1.9 \times 10^{+3}$	$7.0 \times 10^{+3}$	$4.2 \times 10^{+2}$
*RSD (%)	4	4	3	5	3	5	2

In accordance with the spectroscopic study, the soluble content of the sandstones ashlars was strongly influenced by the rainy season. Thanks to the data comparison of both samplings (Fig. 6.18), a high increase of chloride and nitrates was observed, although sulphates showed the opposite behavior.

As XRD and spectroscopic techniques indicated, nitrates and chlorides were mainly correlated with potassium and sodium, being these salts highly soluble. Therefore, its washing by the rain action is more likely. On the contrary, the sulphates are correlated with calcium mostly, which is more insoluble and, then, its concentration remains more stable. Furthermore, the concentration changes of the salt mixtures affect the balance of their formations, promoting the sulphates formation during the rainy season.

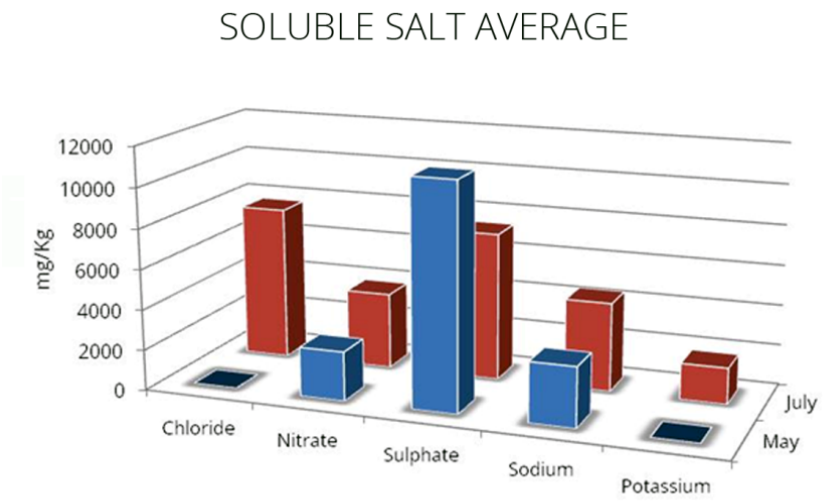

Figure 6.18. Average ion content determined by ion chromatography of sandstones samples of the facade at different months.

Nevertheless, in order to find out the influence of relative humidity and temperature changes[33] in the activation of salt damage, the quantitative results of the samples taken during the driest month were treated by means of a chemical predictive thermodynamic model[34].

The complex mathematical calculations [35-36] involved the demand that the ionic balance of the samples were close to unity and for that reason, the data of calcium were adjusted according to equivalents of carbonate (more information can be consulted in chapter 3, section 3.3).

In this manner, during the cold months, the formation of gypsum and halite is predicted to an average temperature of 10 ºC. On the other hand, if the temperature increase up to 15 ºC, the amount of gypsum and halite decrease, allowing the formation of new sulphated compounds such us mirabilite, glauberite and gorgeyite ($K_2SO_4 \cdot 5CaSO_4 \cdot H_2O$). Finally, during the summer, the nitrate presence is predicted in form of nitratine (Fig 6.19).

33 Basque Meteorology Agency (2014). Euskalmet: www.euskalmet.euskadi.net.

34 C. A. Price. An expert chemical model for determining the environmental conditions needed to prevent salt damage in porous materials. London: European Commission Research (Protection and Conservation of European Cultural Heritage), Archetype Publications; 2000.

35 A. Sawdy, C. Price. Salt damage at Cleeve Abbey, England. Part I: a comparison of theorical predictions and practical observations. J. Cult. Herit.; 2004; 6: 125-135.

36 A. Sawdy, C. Price. Salt damage at Cleeve Abbey, England. Part II: seasonal variability of salt distribution and implications for sampling strategies.

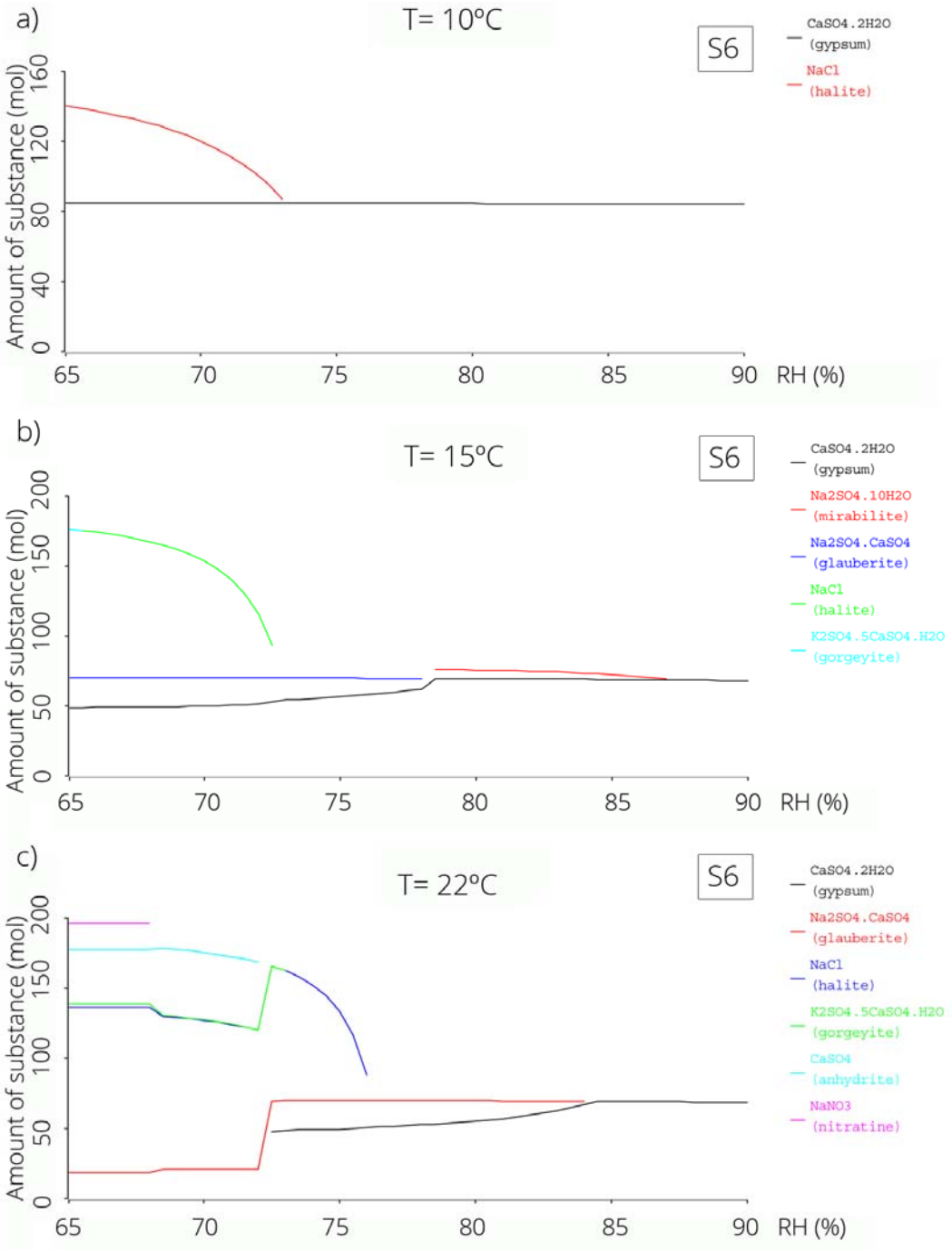

Figure 6.19. Thermodynamic analysis using Runsalt. Crystallization sequence of soluble salts extracted from the sample S6 at a) 10ºC, b) 15ºC and c) 22ºC in accordance with variable values of relative humidity.

The behavior of the aqueous solution is similar to the 14B, S2, S5 and S6 samples. However, the soluble content of the sample M11 predicts the formation of new degradation compounds (Fig. 6.20) such us niter, sylvite (KCl), aphthitalite ($Na_2SO_4 \cdot 3K_2SO_4$), hexahydrite ($MgSO_4 \cdot 6H_2O$) and picromerite ($K_2SO_4.MgSO_4 \cdot 6H_2O$).

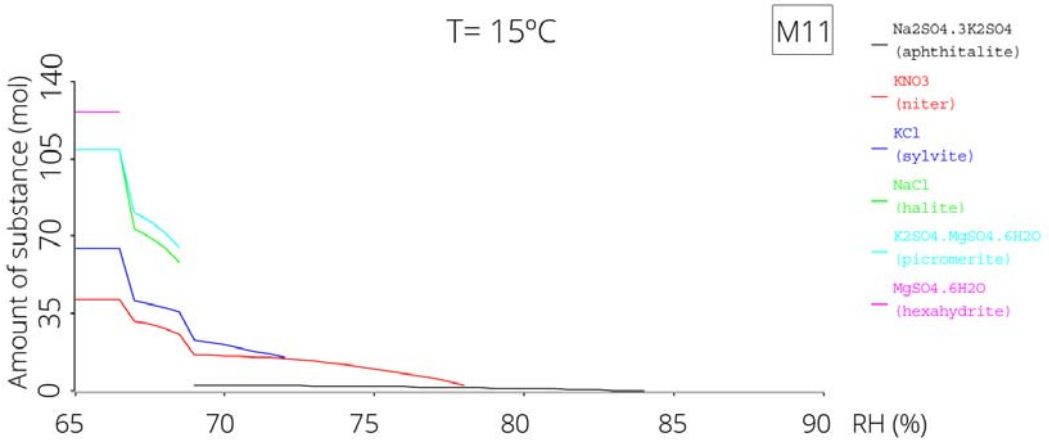

Figure 6.20. Thermodynamic analysis using Runsalt. Crystallization sequence of soluble salts extracted from the sample M11 at 15ºC in function of the relative humidity.

Some of the formations predicted were also detected by spectroscopic techniques along the annual study performed, demonstrating the usefulness of this software to correlate phenomenological, analytical and environment information. The application of this kind of study enables us to determine the damage of building material associated with the crystallization and deliquescence of soluble salts, demonstrating that little environmental changes are enough to activate salt damages cycles.

However, it is impossible for the thermodynamic model used to take into account variations in concentration caused by external factors such as surface washing, industrial activity, fog, etc). Therefore, for a correct prediction, the collection of representative samples, paying attention to the seasonal conditions, is crucial.

In addition, this tool could provide valuable information to indicate the best dates to perform in situ analysis and sampling campaigns. Thanks to its use, the diagnosis study could be performed much faster, reducing the number of campaigns and the progress of the pathologies. Moreover, it could avoid the erroneous decision taking in its preservation such as the selection of consolidating products not suitable for salts, which could be overlooked (in this case chlorides and nitrates) or the introduction of harmful additives by the use of new restoration materials (as for example mortars based in Portland cement).

Finally, its greatest usefulness is shown for the conservation of masterpieces (paintings, ceramics, etc) located indoor, in which the environmental conditions can be adequately controlled.

6.1.6.7. Heavy metal quantification by ICP-MS: stony samples

To assess quantitatively the concentration of heavy metal, the sandstones and mortar samples taken during the second campaign, in sufficient quantity, were analyzed by inductively coupled plasma mass spectrometry. In this manner, lead, cadmium, manganese, nickel, iron, copper, aluminum and cobalt were quantified (Tables 6.5 and 6.6).

Table 6.5. Concentration values of heavy metals found in the sandstone samples. The results are shown in μg·Kg^{-1} and their combined uncertainty.

Sample	Pb	Cd	Mn	Ni	Fe	Cu	Al	Co
1A	<QL	<QL	21 ± 1	1.9 ± 0.1	<QL	3.3 ± 0.2	7 ± 1	<QL
5A	<QL	<QL	<QL	1.4 ± 0.1	24 ± 6	<QL	18 ± 5	<QL
6A	<QL	<QL	<QL	1.5 ± 0.3	<QL	<QL	303 ± 18	<QL
10A	<QL	<QL	<QL	1.2 ± 0.3	<QL	2.3 ± 0.2	26 ± 4	<QL
12A	<QL	<QL	21 ± 2	1.6 ± 0.3	41 ± 7	2.7 ± 0.1	48 ± 15	<QL
19A	<QL	<QL	7.6 ± 0.4	1.4 ± 0.1	37 ± 13	2.6 ± 0.3	30 ± 13	<QL
20B	<QL	<QL	<QL	1.2 ± 0.1	<QL	3 ±1	34 ± 10	<QL

Although the building is placed in front of the port, no influence of the boats´ fuel emission was detected. The results shown in Table 6.5 demonstrate that there are not alarming levels of these toxic metals. However, it was not possible to compare this values with the legislation levels as nowadays, there are not legal limits established to building materials.

Moreover, the values obtained to Fe, Ni, Cu and Al seem to corroborate the in situ elemental analysis, in which, Al was the predominant metal attributed to the feldspar matrix and Fe to the glauconite grains. Besides, Ni and Cu were identified as minor elements attributed to anthropogenic deposition.

Table 6.6. Concentration values of heavy metals found in the mortar samples. The results are shown in μg·Kg^{-1} and their combined uncertainty.

Sample	Pb	Cd	Mn	Ni	Fe	Cu	Al	Co
21A	<QL	<QL	<QL	1.28 ± 0.04	<QL	<QL	367 ± 13	<QL
22A	<QL	<QL	<QL	1.3 ± 0.1	<QL	<QL	1008 ± 98	<QL
27A	<QL	<QL	<QL	1.17 ± 0.03	23 ± 5	<QL	189 ± 6	<QL

In the same manner, the results of the joint mortar samples indicate the same conclusion, explaining the iron content observed as original composition of the material, being attributed its results to iron oxide grains (e.g. hematite) heterogeneously distributed in the matrix.

6.1.7. Intervention proposal based on the chemical study

Thanks to the scientific chemical study carried out, as well as to the assistance provided by the technical architect, in this section, some examples of intervention actions on the most severe pathologies found are suggested.

6.1.7.1. Carbonation of the concrete structure

Nowadays, there are few effective repair options to treat the severe corrosion, cracking and chipping caused by the carbonation process and, thus, the existing solutions are presented in this section.

In this sense, the cathodic protection (CP) could be useful in cases of severe corrosion[37]. However, this is an expensive option and requires the electrical continuity of the reinforcement, as well as high costs for its maintenance.

On the other hand, the realkalization and electrochemical extraction of chlorides are repair techniques recommended to the reinforced concrete, in cases of damages by corrosion. In this way, they can be applied to structures contaminated with carbonate and chloride, restoring the pH of the concrete and re-passivating the steel[38]. However, the method is expensive and it has a limited history.

In this way, the most feasible option is to repair and protect the concrete. This choice is the fastest for the owner. However, to repair the visible damage does not guarantee the correction of severe cases, as it was demonstrated along this chapter. If only the visible damage is resolved, without worrying about the underlying causes, the pathology could reappear even more aggravated.

Today, to effectively stop the spread of "carbonation front", anti-carbonation coatings are usually recommended. Contrary to masonry paintings or elastomeric coatings, anti-carbonation coatings are specifically designed to stop the penetration of carbon dioxide. Thanks to it, new standardized methods are being tested in order to

37 R. J. Kessler, R. G. Powers, I. R. Lasa. Zinc metalizing for galvanic cathodic protection of steel reinforced concrete in marine environment. Nace Corrosion/90; 1990; 324.

38 L. Bertolini, F. Bolzoni, B. Elsener, P. Pedeferri, C. Andrade. La realcalización y la extracción electroquímica de los cloruros en las construcciones de hormigón armado. Mater Constr.; 1996: 46: 45-55.

evaluate the resistance against CO_2 attack, and the results seem to indicate the success of the anticarbonation coating[39], which can add several centimeters of protection.

Unfortunately, the pathology is so advanced that the application of these methods is not feasible. Therefore, the only interventions that could solve the problem are very aggressive and more expensive than the methods mentioned above.

Thus, the best option to solve the pathology would be the demolition of the existing structure and the construction of a new one, which must take into account the new legislation requirements and the building environment. The work would have an approximately cost of 85,000 EUR[40].

Given its setting, the high presence of sulphate salts (bassanite, gypsum, mirabilite and thenardite) and the attack of chlorides observed (akaganeite) and, in accordance with the instructions of the EHE-08 (Structural Concrete Instruction 1247/2008), the cement recommended for its reconstruction is HA 30 / P / 20 / IIIa / Qb, with a minimum coating of 40 mm and a water ratio of 0.5 (HA: Reinforced concrete, 30: N/mm^2 of resistance, P: Plastic consistency, 20: máx size of aggregate, IIIa: type of exposure and Qb: specific type of exposure).

6.1.7.2. Disintegration of the sandstone ashlars

Firstly, since the deterioration is very advanced, the most urgent action is to stop its progress by means of a cleaning and desalination process as well as by biocide application and, then, the consolidation could be carry out.

In this way, the main objective of the consolidant surface application is its penetration inside the material. Thus, the product polymerizes to recover the inter-granular cohesion, adhering the unaltered matrix to the affected one. Thanks to it, the mechanical cohesion could be restored, protecting the material against future attacks.

39 Faircoat. Protecction of concrete structures with anticarbonation coating. International conference on construction chemicals, "Global trends in Construction Chemicals", 2012.

40 A. Hormaetxe. Proyecto de Restauración de la Cofradía de Pescadores, Nuestra Señora del Carmen. Medidas de actuación basadas en los análisis químicos de las patologías. Master's Thesis of Rehabilitation, Restoration and Comprehensive Management of Built Heritage and Existing Buildings EHU/UPV. Bilbao, 2014.

However the product selected must meet certain requirements[41], which are listed below.

Consolidant should be impermeable to rainwater but in turn, it should guarantee total water vapor permeability.

The products used must not alter the aesthetic or chromatic materials characteristics such us appearance, brightness or color.

The consolidation must be performed without altering the physicochemical properties of materials and without leaving residues that could cause new damages by the formation of harmful products.

In order to perform a good quality control of the materials used, the selection of readu to use manufacturing products is recommended to avoid undesirable changes during its preparation.

Finally, for the choice of most suitable product and application system, several chemical tests (permeability, penetration, durability, etc) should be performed.

Taking into account these requirements as well as the chemical study carried out along this chapter, the consolidants[42] proposed are listed below:

Durcipierre (Ciments Lafarge) based on hydrofugous ethyl silicate.

Tegovakom (Goldschmidt) based on siliceous ester and methylsiloxane.

Wacker OH (Wacker Silicone) based on ethylic ester of salicylic acid.

6.1.7.3. Humidity filtration from the adjacent hill

The origin of the pathology is the lack of an effective isolation of the buried wall. Therefore, the most immediate solution is to avoid contact with the ground wall. To achieve this purpose, there are two techniques[43]:

41 E. Doehne, C. Price. Stone conservation, an overview of current research. Los Angeles: The Getty conservation Institute; 2010.

42 I. Rodríguez-Maribona, M. Zabalbide, F. García Garmilla, J. A. Ibáñez and S. Garín. Conservation study of the Stone material used in the Culture House of Almirante Oquendo, in San Sebastian. Mater. Construcc.; 1999; 49: 19-30.

43 A. Hormaetxe. Proyecto de Restauración de la Cofradía de Pescadores, Nuestra Señora del Carmen. Medidas de actuación basadas en los análisis químicos de las patologías. Master's Thesis of Rehabilitation, Restoration and Comprehensive Management of Built Heritage and Existing Buildings EHU/UPV. Bilbao, 2014.

The screen wall is the most effective alternative, since it avoids physical contact between the ground and the wall. Thus, the new wall could contain the lands, leaving a gap between the wall and the hill. Nevertheless, this intervention involves the excavation of the hill, which is a very expensive and almost unworkable solution, given the orography of the land.

The second option is a buried drainage system, in which waterproofing and water channeling of the wall could be easily implemented. The system consists of installing a water collection tube on the outside base of the wall, which together with the impermeabilización, ensures the water evacuation, avoiding accumulations and pressures (Fig. 6.21).

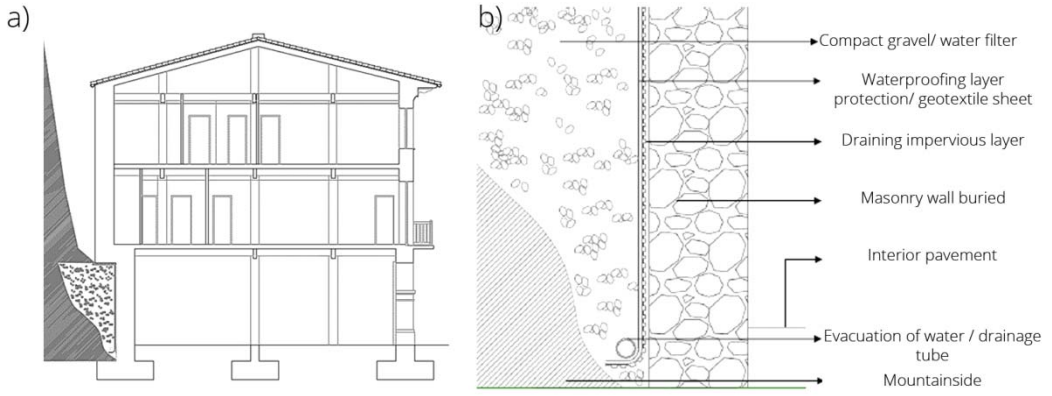

Figure 6.21. Intervention proposal. a) Section of the building and drainage system. b) Drainage system proposal to the buried wall.

In this manner, the horizontal barrier could prevent the ascent of ground water, sealing the wall to its full extent. Furthermore, to prevent the ingress of water from the ground other barrier based on silanes resin could be applied (Fig. 6.22 a).

Finally, the construction of a ventilation chamber, artificially ventilated, can prevent the formation of efflorescences (Fig. 6.22 b).

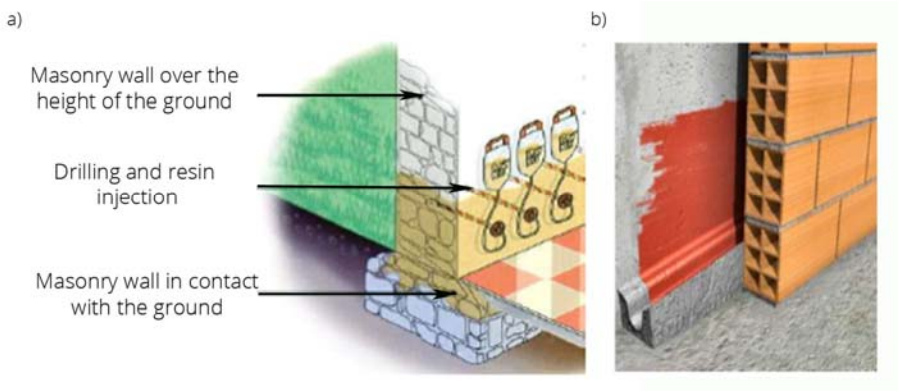

Figure 6.22. Intervention proposal. a) Detail of the execution of the court capillary barrier. b) Drainage system proposal to the wall buried.

6.1.8. Conclusions

The multianalytical approach performed demonstrated that the main source of the decaying process observed in the facade was the effect of the atmospheric pollutants and marine aerosol, also detecting pathologies caused by biodeterioration. On the other hand, the interior wall of the ground floor was severely affected by salt damage, whose provenance was the infiltration water from the adjacent hill. However, the most dangerous pathology observed in the building is the damage suffered by the interior structures as a consequence of the carbonation process, which seriously affected the stability of the building and the safety of the workers. Moreover, as direct consequence, elements declared historical heritage could be in danger of disappearance as is the case of the balconies.

Overall, the work performed in the Fishermen´s Association shows how useful the use the Raman spectroscopy is as a main technique in the diagnosis of historic buildings as well as the advantages presented by its combination with other spectroscopic techniques such as XRF or DRIFT. In fact, the origin of the pathologies could be proposed only based on in situ campaign results, corroborating the Raman information obtained in situ by means of DRIFT. Although it is noteworthy, that in this case, the collection and assignation of DRIFT spectra was complicated due to a layer of plaster that completely covered the interior walls. Its composition as well as its flat surface did not allowed the completely assignment of salt mixtures and the collection of useful spectral signals.

In addition to this, the laboratory mapping analysis allowed us to determinate the penetration capacity of the pollutants inside the porous matrix and their distribution, even for undetectable compounds to Raman spectroscopy as chlorides, helping to find out the washing occurred by the rain action. Furthermore, the cause of the internal cracks due to the physical stresses could be also identified. Thanks to the mapping images of the cross section samples, the material thickness affected was determined. Finally, guidelines to select the most suitable cleaning process and consolidant product were given.

Moreover, the combination of spectroscopic techniques with quantitative analytical methodologies proves to be a good tool, to avoid overlooking the presence of harmful compounds for its preservation, quantifying is severity in accordance with the existing regulations in restoration.

On the other hand, thanks to the Runsalt program, the spectroscopic results of different campaigns could be corroborated and completed. Its use could achieve a faster diagnosis study for future works, providing valuable information to indicate the best time to perform in situ campaigns, avoiding the progression of the pathologies. Moreover, it could help to select the best restoration materials, inhibitors and consolidant products, avoiding to overlook the presence of harmful compounds. Finally,

this thermodynamic chemical model could be really useful to the preservation of other type of masterpieces affected by soluble salts, increasing the knowledge of the environmental influence in the damage.

The work performed along this chapter shows the utility of scientific studies to rehabilitate our built heritage, promoting the inter-disciplinarity between the different professions. The information provided by this methodology could avoid the selection of erroneous actions and therefore, higher costs.

In fact, it is noteworthy, the little economic impact that the application of this methodology involves in a real restoration project. If the cost is calculated in function of the information obtained only in situ and the interventions proposed in this work, the percentage corresponding to this type of study does not exceed 0.4% of the total cost.

By contrast, the absence of a chemical study could cause tens of thousands of euros.For example, in this case, if the concrete selected would be again unsuitable for the environment in which the building is located.

Unfortunately, these work protocols are not requested by the ignorance of its utility among the architects community. Thanks to the awareness and development work carried out by ICOMOS, the current vision and the way of working is changing today.

CHAPTER 7:
SOFT WALL CAPPING, A BETTER WAY OF CONSERVING RUINS? INVESTIGATING THE USE OF SOIL AND OTHER PLANTS TO PROTECT RUINED WALL HEADS

Along this chapter, an innovative and sustainable method to preserve ruins wall heads is addressed. The collaboration in the Soft capping project has been possible thanks to the international doctoral stay in the *Oxford Rock Breakdown Laboratory (OxRBL)* in the *School of Geography and the Environment* of Oxford University (UK), under the direction of the Prof. Heather Viles.

Firstly, given the different fields of study that are involved in this project and its novelty, it is necessary introduce the research project as well as the progresses achieved so far since the work presented in this chapter is focused on studying some of the proposed goals for testing the effectiveness of the Soft capping method and determine the best practice for its implementation.

7.1. State of the Art

As was demonstrated previously, our built heritage is prone to decay, being the characteristics of the stone and the environmental agents the most determinants factors of its degradation. In this regard, in many sites of UK, ruins of historical monuments such as monasteries, towers and castles are regrettably preserved without their protective roofs (Fig.7.1) thereby, they are totally exposed to rainwater, one of the most aggressive environmental stressors. In addition of its direct effect, the water action

also promotes indirectly biological growth such us algae, fungi and bacteria[1-2]. This biological growth leads to biodegradation, damaging the stone surface by bioweathering (physical breakdown and chemical deterioration) and biofouling (negative aesthetic impact)[3]. For all these reasons, conservation methods have as main aim to establish protective measures to minimize the negative effects of rainwater as well as temperature fluctuations suffered by ruins wall heads[4].

Figure 7.1. Images of ruins of monuments of UK. a) Cistercian abbey of Hailes (founded in 1246), Gloucestershire, England. b) Whitby abbey (founded in 657), Yorkshire, England. c) Balveniere castle (founded in 1280), Dufftown, Scotland. d) Rievaulx abbey (founded in 1132), Yorkshire, England.

Particularly, in ruined wall heads of UK, two main types of conservation strategies exist: Hard capping and Soft capping[5] methods.

1 A.A. Gorbushina. Life on the rocks. Environ. Microbiol.; 2007; 9: 1613-1631.

2 A.M. Bellinzoni, G. Caneva, S. Ricci. Ecological trends in travertine colonisation by pioneer algae and plant communities. Int. Biodeterior. Biodegrad.; 2003; 51: 203-210.

3 N. Cutler, H. Viles. Eukaryotic microorganisms and stone biodeterioration. Geomicrobiol. J.; 2010; 27: 630-646.

4 V. Steef, H. Viles. Can plants keep ruins dry? A quantitative assessment of the effect of soft capping on rainwater flows over ruined walls. Ecol. Eng.; 2014; 71: 173-179.

5 H.A. Viles, C. Wood. Green walls? Integrated laboratory and field testing of the effectiveness of soft wall capping in conservating ruins. Building stone Decay: From diagnosis to conservation. London: Geological Society of London Special Publication; 2007.

The Hard capping (Fig.7.2) was widely implemented during much of the 20th century since it was considered as the best practice for inhibiting the ingress of moisture to ruinous masonry, while at the same time it imitates the original fabric of the wall[6]. The treatment starts removing the natural vegetation growing of the top of the ruin and then, the head of the wall is reset in cement or hydraulic lime mortars to form an impermeable cap, which helps to minimize the water ingress into the wall. The goal of this method is to renew the adhesion of the mortar and for that purpose, the surface joints are raked out and pointed with fresh mortar, either directly into the cavities or over cement that is used for tamping at the back joint. If the mortar presents loss of cohesion in the wall, liquid cement is usually pumped inside to set as a solid mass[7].

Figure 7.2. Images of a ruin historical monument of England, in which the Hard capping method was applied.

Although this method is successful and appropriate in some cases, it also has some disadvantages[8-9]. Hard caps protect the wall head and core, however, wall surface are unprotected against rainwater action. Besides, the hard caps based on impermeable hard cements can produce fissures and cracks due to the thermal expansion, between the cement and the original materials. As direct consequence of this mechanism of degradation, moisture can ingress easier into the wall head producing severe freeze/thaw damage (Fig.7.3). Moreover, the hard cement applied also

6 T. Morton, J. Anderson, H. Lindsay, R. Little, J. Mackintosh, E. Parker. Soft capping in Scotland. The context and potential of using plants to protect masonry. Edinburgh: Historic Scotland; 2011.

7 M.W. Thompson. Ruins: their preservation and display. London: British Museum Publications Limited; 1981

8 Z. Lee, H. Viles, C. Woods. Soft capping historic walls: A better way of conserving ruins? English Heritage Research Project Report. 2009.

9 C. Wood. Soft capping: justifying a return to the picturesque. Context 90; 2005; July: 22-24.

prevents moisture escaping from the wall, promoting the colonization of algae and microflora, which can produce new pathologies, as it was detected in many english heritage sites. Furthermore, apart from these inconveniences, Hard capping treatment is relatively expensive to install and requires extensive long term maintenance.

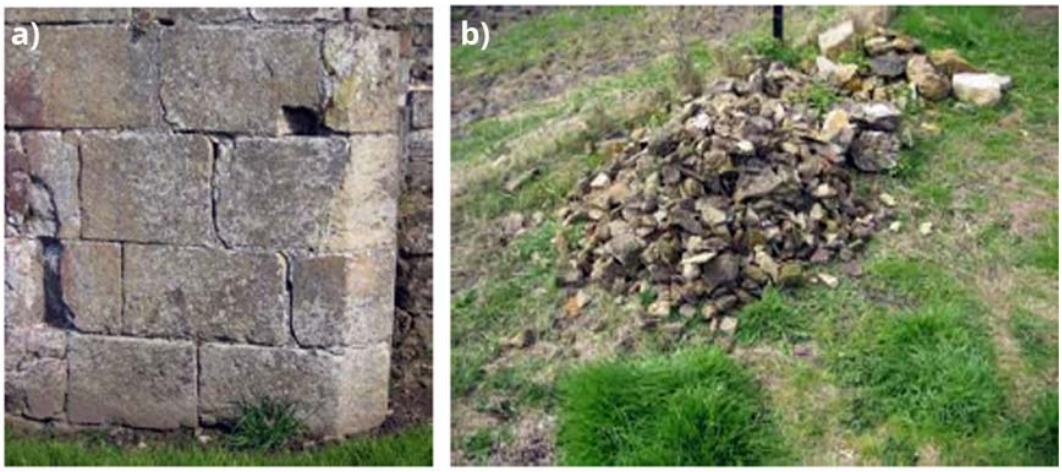

Figure 7.3. Images of Byland abbey (1135), Yorkshire, England. a) Vertical cracking on one of the walls. b) Half a tone masonry which fall from the monument in only three months during the winter[10].

Given the drawbacks observed, other new alternative strategies to protect ruined wall heads were investigated. In this way, the natural growth of vegetation on ruined masonry sites, alongside the popular idea of romantic ruin associated to it, through literary movements of the time (18th and 19th centuries), was taken into account to appreciate the natural appearance of the ruins and value their current state was highlighted. Firstly, the attention was focused on aesthetic, spiritual and philosophical issues. However, in 1980, the English Heritage (Official body of the Member State) began to study the real advantages presented by new green methods, recognizing the importance of the connection between the built and natural heritages, changing the cultural attitudes towards its preservation (Fig.7.4). In this manner, preservation methodologies that involved to integrate the visual presence of the monument with its landscape setting were deeply studied, finding out the benefits of treatments based on the use of soft caps.

10 Z. Lee, H. Viles, C. Woods. Soft capping historic walls: A better way of conserving ruins? English Heritage Research Project Report. 2009.

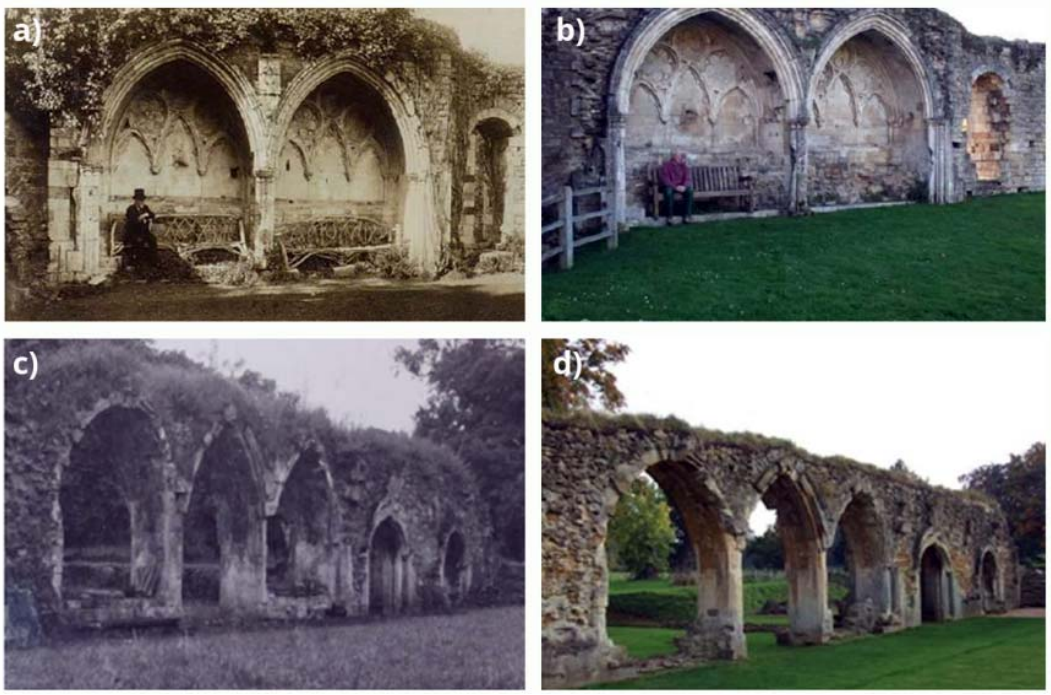

Figure 7.4. Images of ruins historical monuments of England, in which their past and present state can be compared. a-b) Kirkham Priory (19th image vs 2007) where past conservation methods led to removal of the protective vegetation cover. c-d) Hailes abbey (1937 vs 2007), where an alternative green method was applied[10].

Focusing on Soft capping treatment, it can be defined as the use of grass and other plants plus soil to cover largely horizontal surface to lay down a protective layer to masonry structures (Fig.7.5), trying to inhibit the decay caused by the mechanism of surface erosion, leaching of soluble binding materials and freeze/thaw cycles. The technique gained recognition due to its varied benefits[11]. Apart from being a non destructive and reversible method, is also sustainable and environmentally sensitive, as the materials used are non polluting and low in waste energy. Moreover, living plants have potential to make a positive contribution to a local eco-system and are often a cost effective means of protective masonry[12]. If the methodology is correctly designed and applied, the soft caps can be self-healing and require little maintenance, achieving landscape preservation and reflecting its age at the same time.

11 T. Morton, J. Anderson, H. Lindsay, R. Little, J. Mackintosh, E. Parker. Soft capping in Scotland. The context and potential of using plants to protect masonry. Edinburgh: Historic Scotland; 2011.

12 A. Palla, I. Genecco, L.G. Lanza. Hydrologic restoration in the urban environment using green roofs. Water; 2010; 2: 140-154.

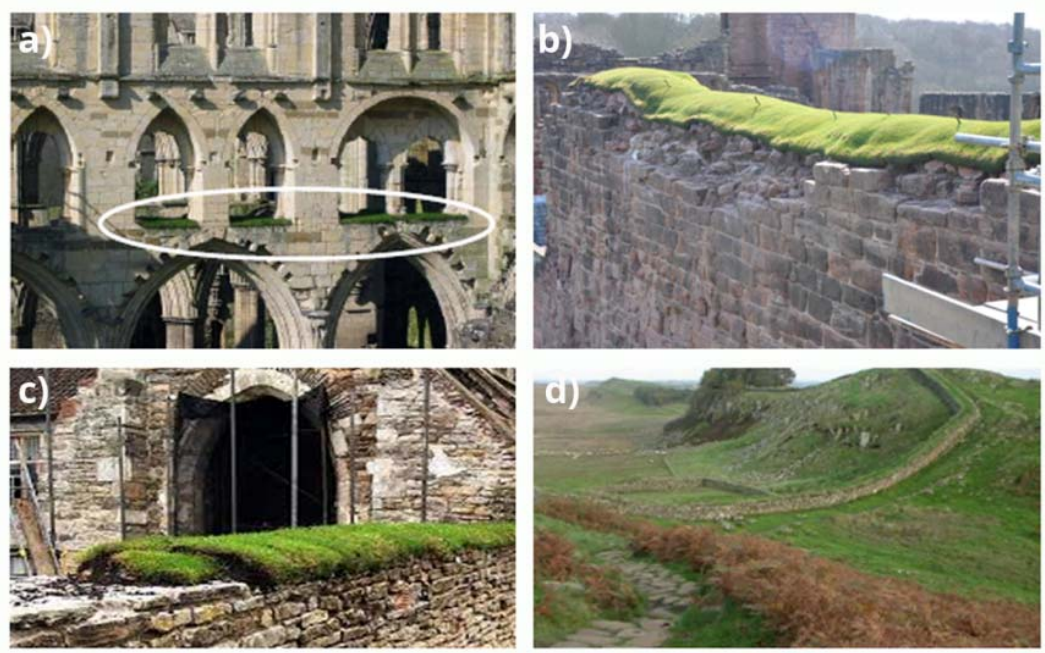

Figure 7.5. Images of monuments in ruins, where Soft capping method have been applied[13]. a-b-c) Rievaulx abbey, Yorkshire, England. d) Hadrians wall a defensive fortification in the Roman province of Britannia.

During the last four years, the research project was focused on selecting carefully the plants and soils materials appropriate to each local environment and climate, considering the seasonal growth patterns of the plants. Furthermore, the performance of Soft capping was compared with Hard capping under a wide range of conditions[14-16]. The work combined field and laboratory studies, and Soft and Hard capping trials in different locations of England were established. Thanks to it, it was demonstrated that Soft capping method provides a better thermal blanket than Hard capping. Daily temperature variations were successfully reduced using soft caps, minimizing the damage arising from thermal expansion and contraction, especially in walls that were consolidated using hard mortars. Moreover, temperature drops below 0ºC were avoided, decreasing the risk of frost damage. Its influence on moisture regimes within the wall heads was studied also, showing some support for the hypothesis that Soft capping method can reduce the frequency of short term wetting

13 Z. Lee, H. Viles, C. Woods. Soft capping historic walls: A better way of conserving ruins? English Heritage Research Project Report. 2009.

14 V. Steef, H. Viles. Can plants keep ruins dry? A quantitative assessment of the effect of soft capping on rainwater flows over ruined walls. Ecol. Eng.; 2014; 71: 173-179.

15 H. Viles. Greening Stone conservation: Exploring the protective role of plants and microbes. Book of Abstract: 12th International Congress on the Deterioration and Conservation of Stone, New York; Columbia University; 2012.

16 C. Wood. Soft capping: justifying a return to the picturesque. Context 90; 2005; July: 22-24.

and drying of wall heads[17-18]. Moreover, the field trials performed showed that this green method is relatively cheap and easy to install and maintain, in comparison with Hard capping.

Nevertheless, Soft capping, as any conservation technique, should be used carefully and can only contribute to avoid some deterioration problems which affect ruined monuments[19].

To decide whether or not to use Soft capping method, some points have to be considered[16-20]. Firstly, it is important to address the philosophical issues and agree what is the purpose of the conservation action. Principles of reversibility, minimum intervention and the use of original materials as well as taking into account conservation theories of "conserve as found, must be considered before starting any action. Nowadays, the Soft capping studies present this method often less invasive and more easily reversible than the other conservation strategies. However, it could not always be the most appropriate due to the perceived value of a monument and how it should look. Furthermore, it is important also to understand the fabric that were employed and the mechanism of damage that are taking place. Thus, it can be very beneficial where there is a risk of surface erosion from run-off and if there is the threat of frost damage or differential thermal expansion. Under other circumstances of deterioration or climatic conditions, Soft capping can result less effective. For example, drought-prone areas could not be suitable for turf capping, although, other plants as sedums could thrive successfully even under dry conditions[21-22]. In fact, its use in other similar green methods as Green roofing is widely recognized[23-25]. Finally, it is important

17 A.B. Lim. Soft capping of archaeological masonry walls: Far View House, Mesa Verde National Park. Thesis (Historic Preservation). University of Pennsylvania; 2010.

18 E.L. Villareal, L. Bengtsson. Response of a Sedum green-roof to individual rain events.Ecol. eng.; 2005; 25: 1-7.

19 Z. Lee, H. Viles, C. Woods. Soft capping historic walls: A better way of conserving ruins? English Heritage Research Project Report. 2009.

20 T. Morton, J. Anderson, H. Lindsay, R. Little, J. Mackintosh, E. Parker. Soft capping in Scotland. The context and potential of using plants to protect masonry. Edinburgh: Historic Scotland; 2011.

21 J.M. Bousselot, J.E. Klett, R.D. Koski. Moisture content of extensive green roof substrate and growth respose of 15 temperate plant species during dry down. Hotsicience; 2011; 46: 518-522.

22 A. Nagase, N. Dunnett. Drought tolerance in different vegetation types for extensive green roofs: Effects of watering and diversity. Landscape and Urban Planning; 2010; 97: 318-327.

23 A. Palla, I. Gnecco, L.G. Lanza. Hydrologic restoration in the urban environment using green roofs. Water; 2010; 2: 140-154.

24 E. Eumorfopoulou, D. araventinos. The contribution of a planted roof to the thermal protection of buildings in Greece. Energ. Buildings; 1998; 27: 29-36.

to consider a monitoring and maintenance regime since taking simple pictures or carrying out visual inspections can provide good evidence of the action of soft caps during seasonal changes.

Currently, this conservation method is successfully applied at over 50 sites in the world such as England, Scotland, Ireland, Sweden, Germany, Denmark, Faroe Islands, Iceland, Poland and so on.

7.2. Aims of the study

To continue advancing in the research and cover different cases, more tests about whether Soft capping works effectively as well as to determine the best practice for its implementation in each situation are required. In particular, this study evaluates whether soft capping enhances or reduces chemical weathering of vulnerable common stone materials in comparison with that occurring on bare ruined surfaces and, in this way, it helps to determine what Soft capping general requirements for different materials types are.

For that purpose, a field trial was carried out, in which some samples of different materials were exposed to open air and others covered with diverse kinds of caps. The samples were analyzed pre and post exposure in order to find out the main degradation suffered by the materials in each case, applying a portable and non destructive methodology, which resulted useful to monitor real conservation cases.

7.3. Field trials: establishment, monitoring and sampling

7.3.1. Location

The Castle Acre Priory was chosen for this trial study. It is located in Castle Acre village, near the north Norfolk coast (England, UK). Although the village has changed dramatically since the Middle ages, it is one of the best examples of a fortified Norman town, which was protected by its own bank, ditch and gateways to guard the entrance.

The Priory (Fig.7.6) was founded in 1090 by the first Cluniac order of monks of England and nowadays, it is one of the largest and best preserved monastic sites. Since its construction, the Priory gained land and buildings from different benefactors (Warenne family, Henry I and Henry II) and even was a visit home to prominent figures such as Edward I and Queen Eleanor. It passes through many owners, falling into ruin until it was obtained in 1615 by Sir Edwards Coke, the famous chief Justice. Under the

25 M.A. Monterusso, D.B. Rowe, C.L. Rugh. Establishment and persintence of Sedum spp. And native taxa fro green roof applications. Hortscience; 2005; 40: 391-396.

instructions of King James, he spent £60 repairing the ruins of the Castle, one of the earliest records of conservation work by a private individual. The castle remains was property of his descendants and since 1984, it has been looked after by English Heritage[26].

Figure 7.6. Images of ruins Castle Acre Priory[27] (Norfolk, England, UK). a) The front view of the entrance to the Priory. b)The Nave of the Priory Church.

Regarding to the climatology of the area, it can be classified as oceanic climate, temperate and warm (Köppen-Geiger Cfb)[28], in which the average annual temperature is 9.4 ºC and the rainfall is about 615 mm throughout the year[29].

26 Castle acre Priory (2015) tourist information: www.tourist-information-uk.com/castle-acre-priory.htm.

27 Castle acre Priory (2015). English Heritage: www.english-heritage.org.uk/daysout/properties/castle-acre-castle-acre-priory.

28 M. Kottek, J. Grieser, C. Beck, B. Rudolf, F. Rubel. World Map of the Köppen–Geiger climate classification updated. Meteorol.; 2006; *15: 259–263.*

29 Government Weather Office: www.metoffice.gov.uk/climate/uk/.

7.3.2. Preparation and analysis of the test samples

Four samples of each kind of material (calcite, gypsum and limestone) were prepared to be exposed to different soft caps as well as to the open air.

In this way, 48 samples were cut (approximately 3.5 cm x 3.5 cm) and marked at 3 different points along their diagonal line in order to carry out the control measures in the same points every time, previously and after the exposition. Moreover, 4 blank samples (LC) of each material were stored in the laboratory.

The analyses of the samples were performed by a combination of non destructive techniques with the purpose of designing an analytical methodology useful for monitoring real conservation treatments. In this way, digital pictures, microscope and 3D images, weight, colour and hardness measures were taken to test the physical changes. Besides, to study them in depth and find out the chemical weathering suffered in each case, XRD, SEM and Raman spectroscopy analysis were performed in all samples (more experimental information can be consulted in chapter 3, section 3.2.1). Finally, when it was required, IC analysis, chemometric and thermodynamic tools were used, helping to establish and contrast the degradation mechanism produced.

In this manner, depending on the material characteristics, different techniques were used and only the more conclusive results are showed along this chapter.

7.3.3. Establishment of the soft caps

In February 2012, a low wall (1 m of height approximately) located a few meters from the Priory was selected to start the test. It is constructed of mixed flint, brick, chalk and limestone. During the visual inspection, a previous treatment based on Hard capping method was observed. Although its application looked recent, the lime mortar used as hard cap was shrinking away from the stones. In fact, from the East side of the wall, the whole hard cap was detaching from the underlying stonework. Besides, lots of moss and some sedums were growing on it close to fissure areas.

The wall was divided in three adjacent strips of about 1 m (strip1, strip 2 and strip 3) in order to test the chemical weathering caused by different types of soft caps. Then, 4 blocks of gypsum, limestone and calcite per strip were numbered (Table 7.1), placed on the wall head and covered with soil (approximately 10 cm of thickness). Besides, to study the effectiveness of Soft capping treatment, 4 control blocks of each material were exposed to open air on different higher walls out of sight (Fig.7.7).

Figure 7.7. a) Wall selected for the soft caps (Castle Acre Priory, Norfolk, England). b-c-g) blocks displayed on top of the ruined walls to test the method effectiveness . Insertion of the samples before covering, d-e-f) strip 1, 2 and 3, respectively.

Lastly, after the soil, a turf layer and the selected vegetation were placed for the study. Taking into account previous investigations, sedum species can facilitate the growth of grasses during dry periods, preventing evaporation from the soil surface. This effect could be particularly useful in the preservation of ruined wall as large fluctuations in moisture and temperature conditions can accelerate weathering processes[30]. In this way, strip 1 was composed by a mixture of grass and sedum plugs, being Supurium tricolour the species native to the UK selected by its suitable characteristics (very common, resistant to winds and high temperatures, low fertility and limited water necessity)[31]. Strip 2 was composed by grass and strip 3 only by the same sedum mat (Table 7.1), in which a fine membrane was applied between the soil and the turf layer in order to avoid the root damage (Fig.7.8).

30 H. A. viles. Weathering systems. In: D.S.G. Thomas. Arid Zone Geomorphology. Chichester: Wiley-Blackwell; 2011.

31 N.D. Van Woert. Watering regime and green roof substrate desing affect. Sedum plant growth. Hortscience. 2005; 40: 659-664.

Figure 7.8. Establishment of soft caps. a) Placing the turf layer .b)Securing the sedum mat. c) Management the blocks. d) Adding the sedum plugs. e) The Soft capping test areas finished. f) Top of the test areas (viewed from East).

Table 7.1. Summary of the field trials carried out, in which strips composition and samples exposed are showed.

	Laboratory control											
Material	Calcite				Limestone				Gypsum			
Sample	LC1	LC2	LC3	LC4	LC1	LC2	LC3	LC4	LC1	LC2	LC3	LC4
	STRIP1: Grass & Sedum plugs											
Material	Calcite				Limestone				Gypsum			
Sample	GS1	GS2	GS3	GS4	GS1	GS2	GS3	GS4	GS1	GS2	GS3	GS4
	STRIP2: Grass											
Material	Calcite				Limestone				Gypsum			
Sample	GSS1	GSS2	GSS3	GSS4	GSS1	GSS2	GSS3	GSS4	GSS1	GSS2	GSS3	GSS4
	STRIP3: Sedum mat											
Material	Calcite				Limestone				Gypsum			
Sample	SS1	SS2	SS3	SS4	SS1	SS2	SS3	SS4	SS1	SS2	SS3	SS4
	Exposed open air											
Material	Calcite				Limestone				Gypsum			
Sample	Exp1	Exp2	Exp3	Exp4	Exp1	Exp2	Exp3	Exp4	Exp1	Exp2	Exp3	Exp4

7.3.4. Monitoring and sampling

In March 2013, one year after the application of the method, the different field trials were checked (Fig.7.9 a). The strips looked in good state, although, some erosion was observed on the South side. The sedum plugs of the strip 1 seemed to be healthier than the strip 3 (sedum mat). Besides, some bits of sedum had become detached and established on underlying ledges. However, the mortar repairs of adjacent walls showed considerable winter erosion.

Regarding to the open air test, some of the samples had disappeared. The gypsum samples were totally dissolved and the others were probably dragged by the wind or birds. For this reason, the lost samples were replaced by new ones with the same characteristics.

In addition, soils samples were collected at different depths for a parallel study. In this way, temperature, pH, conductivity, volumetric water content, organic matter and ions concentrations data of each strip were used to help to explain the degradation mechanisms that took place in each experiment.

In March 2014, the wall was checked again (Fig.7.9 a) and the samples were removed carefully and transferred to the laboratory (Fig.7.9 b, c). The soil layers were quite dry and after collecting the samples, no obvious damage to stone underneath was observed. Although, it should be mentioned that one calcite crystal of the strip 2 could not be located and a few gypsum samples of strip 1 were broken. To study whether root growth caused some fissure in the exposed samples, the state of the turf layer was examined. According to the visual inspection, roots of grass from strip 1 and 2 penetrated all the way through the soil, however, roots from sedum of strip 3 only penetrated slightly under mat.

Figure 7.9. a) The wall after one year of soft caps application, where the state of each strip can be observed. b-c) extraction of the samples.

After collecting the samples, they were smoothly brushed to remove the soil attached and then they were stored until the analysis. It should be highlighted that before carrying out colour and weight measurements, the samples were washed with miliQ water and dried at 25ºC during 24h.

7.4. Results and discussion

To facilitate the comparison of the effects suffered by the exposition to different types of soft caps, the results are divided by materials.

7.4.1. Calcite

7.4.1.1. Visual inspection

According to the digital pictures taken pre and post exposition, the strip 2 (grass) and 3 (sedum mat) seemed to be the worst preserved. Moreover, the samples with a non flat surface looked more affected, probably due to the imperfections facilitating the action of the degradation agents (Fig. 7.10).

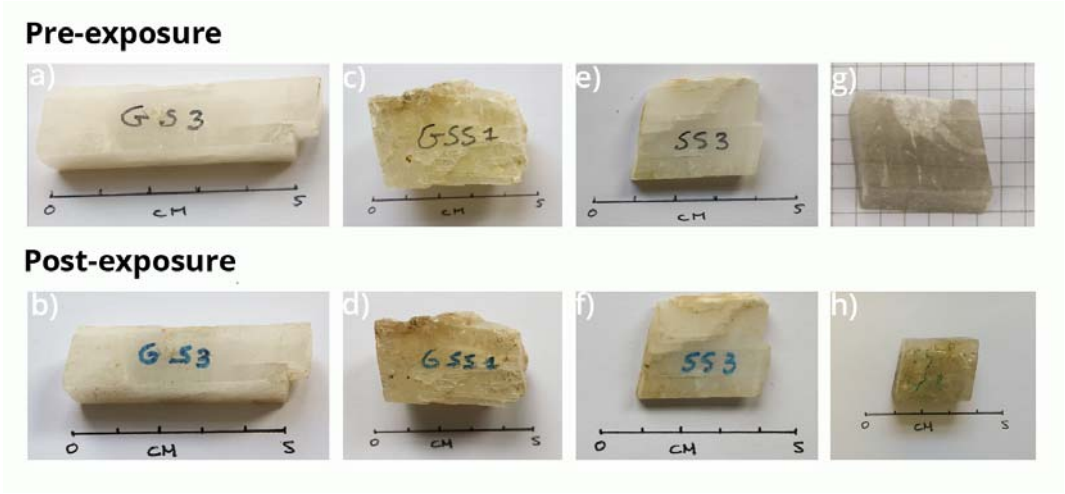

Figure 7.10. Comparison of sample pictures taken pre and post-exposure to each experiment. a-b) strip 1 (grass). c-d) strip 2 (grass & sedum plugs). e-f) strip 3 (sedum mat). g-h) open air.

Regarding the samples exposed to the open air and given their disappearance, the comparison had to be performed with the replacements, which were only exposed during 9 months.

7.4.1.2. Weight analysis

All the samples showed little loss of material from 0.10 to 0.27 % of their weights. According to the results of Soft capping samples, the strip 1 (grass & sedum plugs) seemed to be the best option to preserve this material since its weight loss percentage was substantially lower than the rest of strips (Fig.7.11).

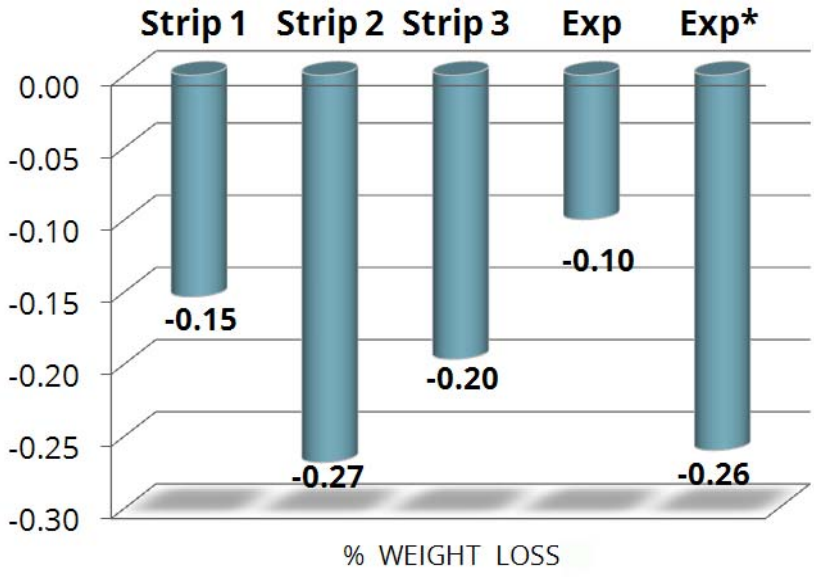

Figure 7.11. Comparison of weight loss average produced in 2 years by each kind of exposition, in which the data of degradation by open air (Exp) correspond to only 9 months of experiment and (Exp) to its extrapolation.*

Moreover, in only 9 months, the samples exposed to the open air (Exp) showed weight loss very similar to the strip 1 value. If the percentage is extrapolated to compare the effectiveness of the Soft capping method, the value of the lost material obtained was one of the highest (Fig.7.11).

7.4.1.3. Colour analysis

To determine the change of colour produced in the samples, hue (colour), lightness (brightness) and saturation (vividness) average measurements were performed in SCE mode (specular reflectance excluded to measure the colour in the same way that it is perceived by the observer). Therefore, L*a*b* colour space values were taken pre and post exposure according to the International Commission on Illumination (CIELAB 2000) and compared, where L* indicates lightness and a*b* the chromaticity coordinates[32] (more detailed information about the colour measurements can be consulted in chapter 3, section 3.2.1). Moreover, in order to classify the severity of the changes produced, the CIELAB norm was applied following the criteria (ΔE*ab), in which 1.8, 3.8 and 9.8 values correspond to just noticeable, distinctively perceptible and disturbing limits, respectively[33].

32 CIE. Technical Report Colorimetry. Vienna: CIE Central; 2004.

33 K. Bieske, I.D. Cornelia. A study about Colour-Difference Thresholds. Lux et color vespremiensis; 2007: 1-11.

According to the results, in only nine months, the samples exposed to the open air (Exp) exceeded all the values presenting, the highest change of colour. In this way, strip 1 (grass and sedum plugs) and strip 3 (sedum mat) were the less degraded, on the limit of just noticeable (Fig.7.12), as the analysis of loss of material previously indicated.

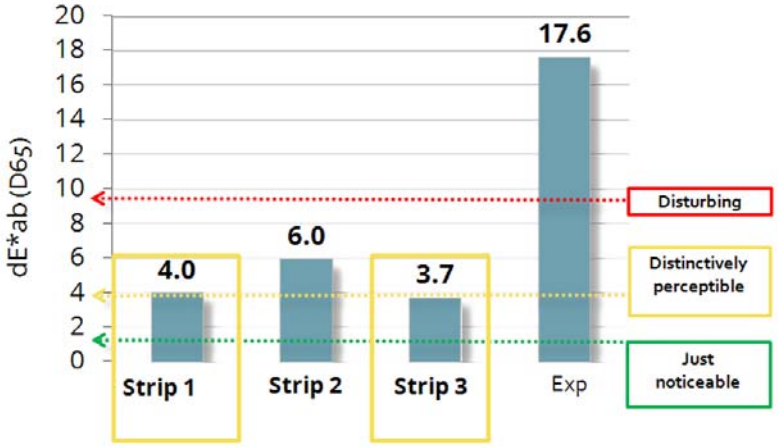

Figure 7.12. Comparison of colour changes produced in 2 years by each kind of exposition, in which the data of degradation by open air (Exp) correspond to only 9 months of experiment. The CIELAB norm was applied to determinate the severity of the degradation.

In addition, the spectral reflectance curve of each sample pre and post exposure were compared as its shape and the presence or absence of absorption features represents changes in material composition[34]. For that purpose, the measurements were performed in SCI mode (Specular component included to obtain the values regardless of surface conditions).

According to the changes of values observed, the results agree with previous analysis, being the samples of strip1 the best preserved (Fig.7.13).

34 L.S. Galvao, A.R. Formaggio, E. G. Couto, D.A. Roberts. Relationships between the mineralogical and chemical composition of tropical soils and topography from hyperspectral remote sensing data. Photogramm. Rem. S.; 2008; 63: 259-271.

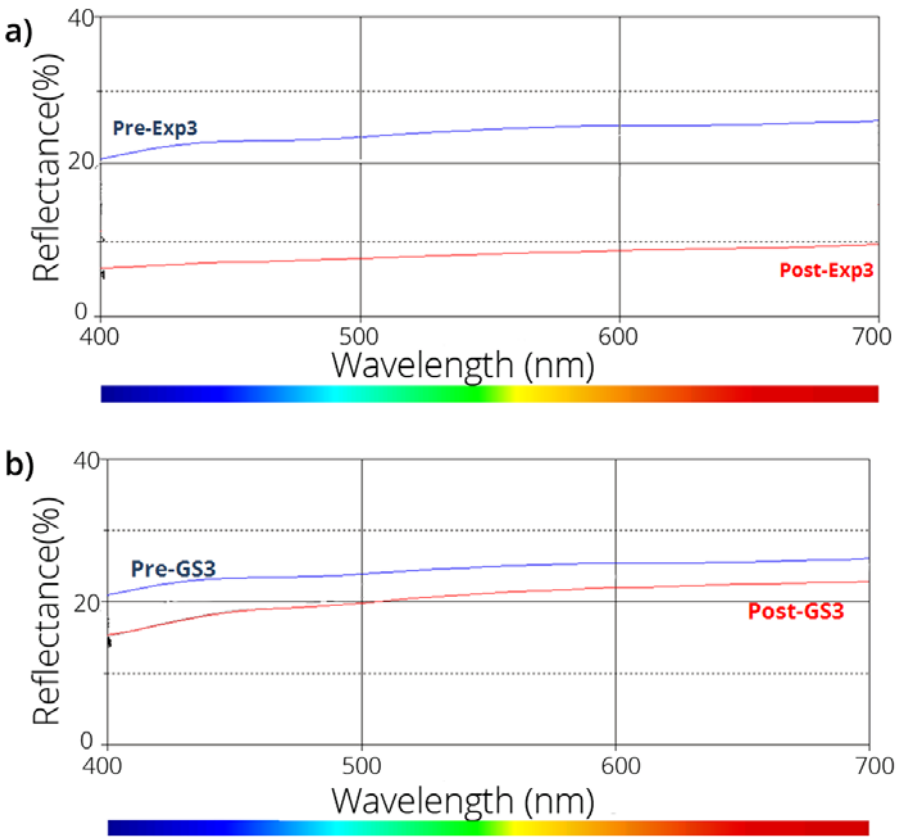

Figure 7.13. Reflectance curves of the samples, where the changes produced pre and post-exposure can be compared. a) changes suffered by samples of open air in 9 months and b) by samples of strip 1 (grass and sedum plugs) in 24 months.

7.4.1.4. SEM analysis

Focusing on the Soft capping samples, one sample per strip was selected based on which was closer to its average (loss weight, % reflectance and size). In this way, GS1, GSS1, SS3 and LC4 were chosen for the analysis (Table 7.1).

The electron microscope images of their surfaces were compared in order to corroborate the previous results as well as to characterize the new degradation compounds formed. In this way, the strip 1 seemed to be the best preserved, once again. Besides, a great amount of gypsum crystals were observed in the fissures of the strip 2 samples (Fig.7.14), evidencing the sulphate attack more severe than in the rest of them.

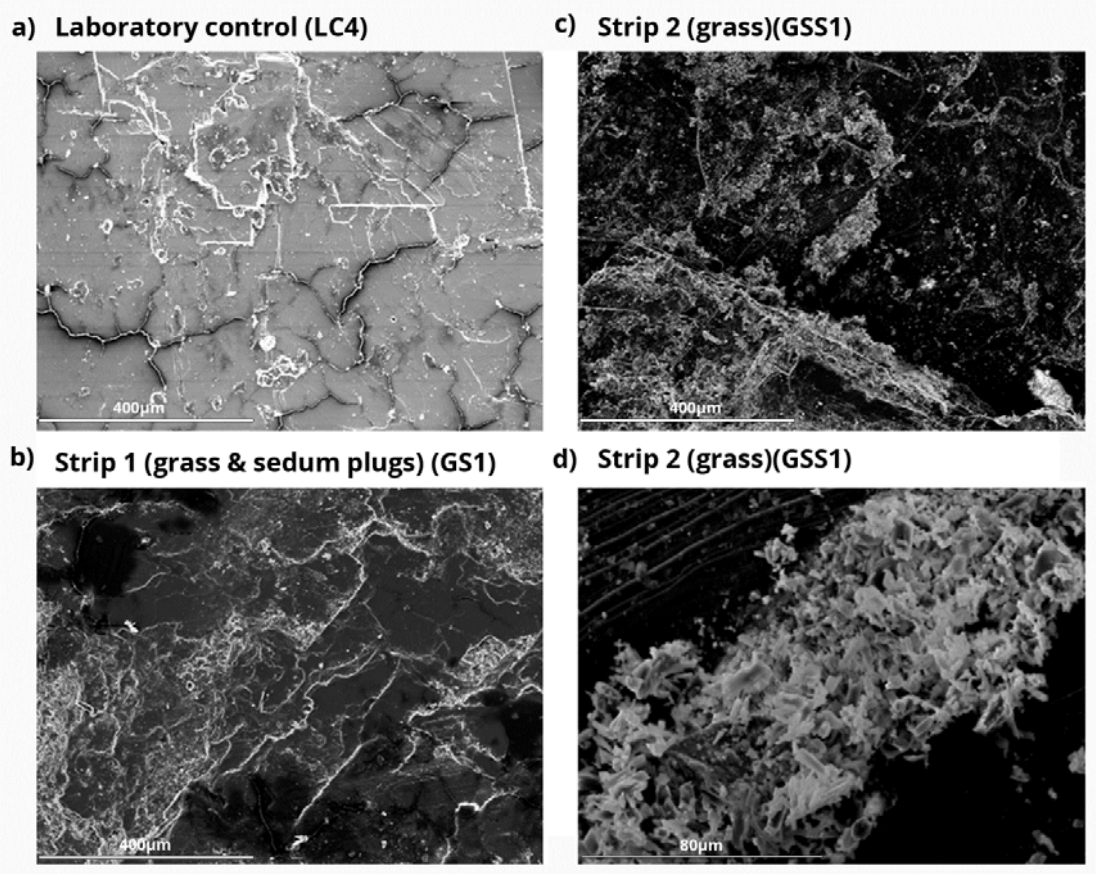

Figure 7.14. Electron microscope images taken of the Soft capping sample surface. a) Laboratory control sample, b) sample of strip 1 (composed by grass and sedum plugs) and c) sample of strip 2 (composed by only grass). d) fissure area enlargement of sample corresponding to strip2.

7.4.1.5. Raman analysis

The spectroscopic analysis (Fig.7.15) of the samples revealed as original compounds calcite ($CaCO_3$, identified by its characteristic bands at 1085 and 712 cm^{-1}) and high magnesium calcite ($Ca_{1-x}Mg_xCO_3$, assigned according to its main band at 1087 cm^{-1}). Moreover, gypsum ($CaSO_4 \cdot 2H_2O$, Raman bands at 1132, 1008, 672, 416 and 162 cm^{-1}) was identified as main degradation compound in the samples exposed to the open air as well as in the Soft capping samples. However, nitrocalcite ($Ca(NO_3)_2 \cdot 4H_2O$, identified by its peak at 1049 cm^{-1}) was only identified as decaying compounds in the open air samples (Exp), evidencing the nitrated attack suffered under the action of atmospheric pollutants.

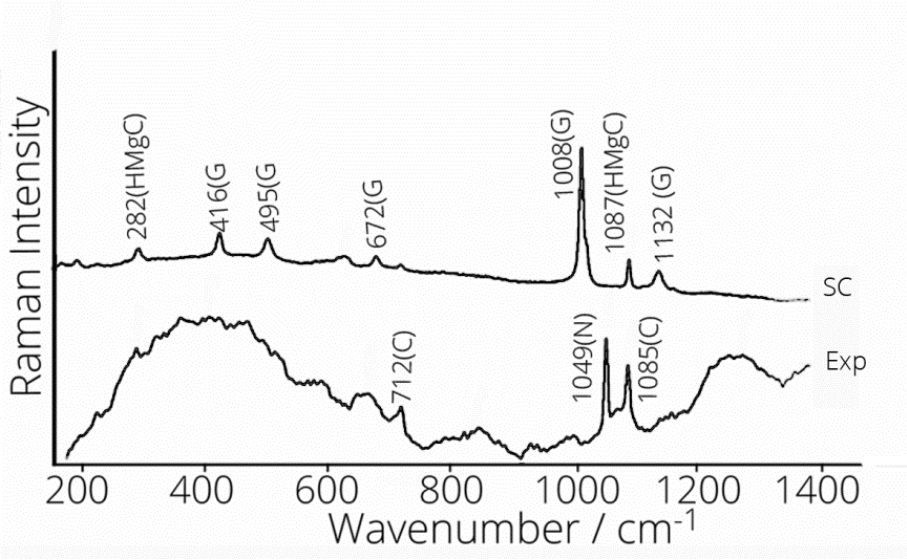

Figure 7.15.Raman spectra obtained of open air samples (Exp) and soft capping samples (SC), where calcite (C), High magnesium calcite (HMgC), gypsum (G) and nitrocalcite (N) were found.

7.4.1.6. Thermodynamic modelling: degradation mechanisms observed in calcite samples by sulphate and nitrate attack

To establish the mechanism of degradation, data contamination of the area and soils were used. In this way, the thermodynamic of the models (Fig.7.16) found coincided with previous results, predicting the formation of nitrocalcite to pH lower than 5.5. This value is very similar to that of rainfall in the area. For this reason, this hazardous salt appears only in the open air samples (Exp), since the pH of the soils is higher (around 7.7). Therefore, it explains why this transformation (reactions 7.1 and 7.2) of the original compounds is produced only under atmospheric exposition, increasing the suffered loss of original material.

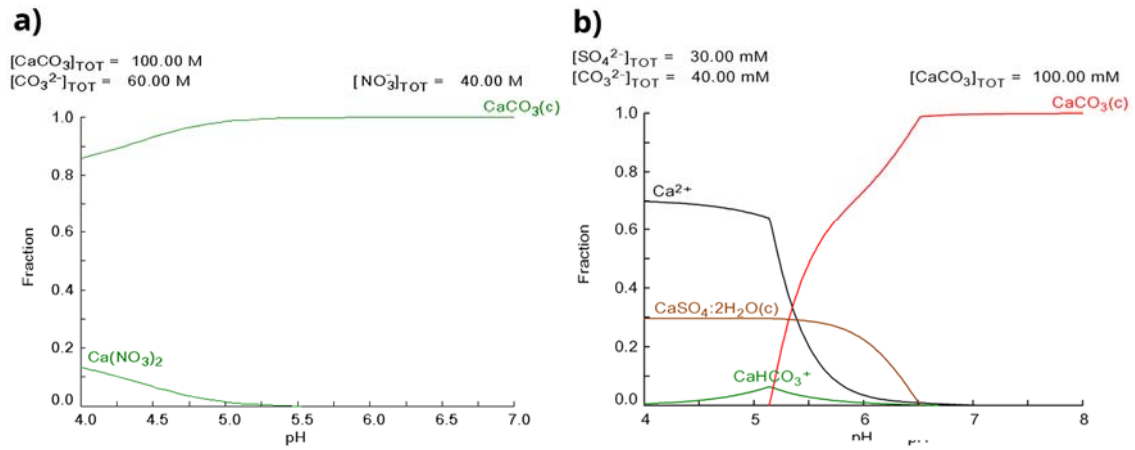

Figure 7.16. Medusa Software chemical prediction of a) nitrocalcite and b) gypsum formation. Attack mechanisms of atmospheric pollutans and soil content over the calcite samples.

$$CaCO_3 + 2NO_3^- + H^+ \rightarrow Ca(NO_3)_2 + HCO_3^- \quad (7.1)$$

$$Ca(NO_3)_2 + 4H_2O \rightarrow Ca(NO_3)_2 \cdot 4H_2O \quad (7.2)$$

Regarding the Soft capping samples, the gypsum formation occurs at pH lower than 7. The pH of the soil is a little higher than this value, thus the formation of gypsum (reactions 7.3 and 7.4) took place but in lower proportion.

$$CaCO_3 + SO_4^{-2} + H^+ \rightarrow CaSO_4 + HCO_3^- \quad (7.3)$$

$$CaSO_4 + 2H_2O \rightarrow CaSO_4 \cdot 2H_2O \quad (7.4)$$

7.4.1.7. Discussion

Rainwater dissolves CO_2 from the atmosphere and, when the water is absorbed by the ground, it dissolves even more CO_2 of the soil pores. Immediately several reactions (7.5, 7.6 and 7.7) occur[35-37]

$$CO_2(g) + H_2O \leftrightarrow H_2CO_3 \qquad K_{CO2} = 10^{-1.47} = [H_2CO_3]/P_{CO2} \quad (7.5)$$

$$H_2CO_3 \leftrightarrow HCO_3^- + H^+ \quad K_{H2CO3} = 10^{-6.35} = [H^+][HCO_3^-]/[H_2CO_3] \quad (7.6)$$

$$HCO_3^- \leftrightarrow CO_3^- + H^+ \quad K_{HCO3-} = 10^{-10.33} = [H^+][CO_3^{-2}]/[HCO_3^-] \quad (7.7)$$

According to their equilibrium constants, and in the experimental conditions, the reaction 7.6 reaches the equilibrium at higher concentration of HCO_3^- than H_2CO_3 and, in the same way, the reaction 7.7 reaches the equilibrium at concentration of CO_3^{-2} much lower than HCO_3^- .

The fraction of carbonate species calculated by Medusa software shows that, in acid water, the H_2CO_3 is predominant and in very basic water, CO_3^- is the most abundant. Taking into account the previous chemical equilibrium, the dissolution of calcite in pores full of water occurs according to the reaction 7.8. However, most of the carbonate is hydrolysed and converted into bicarbonate (reaction 7.7). Therefore, while the carbonate disappears, the equilibrium is never reached and the calcite continues dissolving. Similarly, part of the bicarbonate is transformed into H_2CO_3 (reaction 7.6) and then, it is transformed into CO_2 and water (7.5).

$$CaCO_3 \leftrightarrow CO_3^- + Ca^{+2} \qquad K_{CaCO3} = 10^{-8.40} = (CO_3^-)(Ca^{+2}) \quad (7.8)$$

35 S.K. Lower. Carbonate equilibria in natural waters. Chem.1 Environ. Chem.; 1999; 1: 1-26.

36 V.L. Snoeyink, D. Jenkins. UK; Wiley: 1980.

37 R.Chang. Chemistry. Colombia; Mc Graw Hill: 2002.

Therefore, the dissolution of calcite consumes acidity. If the process of dissolution occurs in an environment with CO_2 available (open system), the more calcite will dissolve. However, if the system is closed, the reaction will reach the equilibrium before and calcite will not dissolve so much.

The equilibrium pH is around 7.3[35] thereby, a pH more acidic tends to dissolve it and a pH more basic causes its precipitation. The pH of the soils layers was around 7.7 and the pH of groundwater was between 7 and 9. Then, bicarbonate is the dominant species in solution and calcite precipitates. On the other hand, the pH of the rain was around 5.6, therefore, carbonic acid is dominant causing it dissolution. Furthermore, the temperature is an influencing variable since in this case, less temperature favours the dissolution. Given that the soft caps act as a thermal blanket and the temperature of the soils were higher than the average of the atmosphere during the exposed period, the effectiveness of the Soft capping with respect to the preservation of bare ruins method could be explained.

Moreover, to understand the reasons of the best performance of the strip 1 (grass and sedum plugs), in addition to pH and temperature, other variables such as pressure, biological activity and organic matter had to be taken into account[38] since these have a great influence in dissolution of calcareous materials. In this manner, the biological activity affects to the pressure because the vegetation consumes CO_2 in the process of photosynthesis. Then, if the concentration of CO_2 decreases, the concentration of H_2CO_3 is reduced and this fact minimizes the dissolution of calcite. Besides, the organic matter also affects this equilibrium as in the process of putrefaction, high amounts of H_2S and CO_2 are produced, which increase the calcite dissolution also. However, anaerobes organisms associated to this process generate ammonium salts, favouring the calcite precipitation.

According to the values of temperature, pH, organic matter and ammonium taken from the soils layers for a parallel study, the strip 1 presented the most suitable conditions to preserve the calcite samples, which agrees with the result of the trial field carried out. Besides, as research focused on green roofing methods indicated[39-41], the mixture of grass and sedum plugs managed to maintain a better blanket effect.

38 S.K. Lower. Carbonate equilibria in natural waters. Chem.1 Environ. Chem.; 1999; 1: 1-26.

39 A. Palla, I. Gnecco, L.G. Lanza. Hydrologic restoration in the urban environment using green roofs. Water; 2010; 2: 140-154.

40 E. Eumorfopoulou, D.Araventinos. The contribution of a planted roof to the thermal protection of buildings in Greece. Energ. Buildings; 1998; 27: 29-36.

41 M.A. Monterusso, D.B. Rowe, C.L. Rugh. Establishment and persintence of Sedum spp. And native taxa fro green roof applications. Hortscience; 2005; 40: 391-396.

7.4.2. Gypsum

7.4.2.1. Visual inspection

All the samples exposed to the open air were missing. According to gypsum solubility constant and the environmental conditions of the experiment, all the open air samples were totally dissolved. However, Soft capping samples were preserved, although, strip 1 (grass & sedum plugs) and 2 (grass) seemed to be the more degraded than strip 1 (sedum mat) (Fig.7.17).

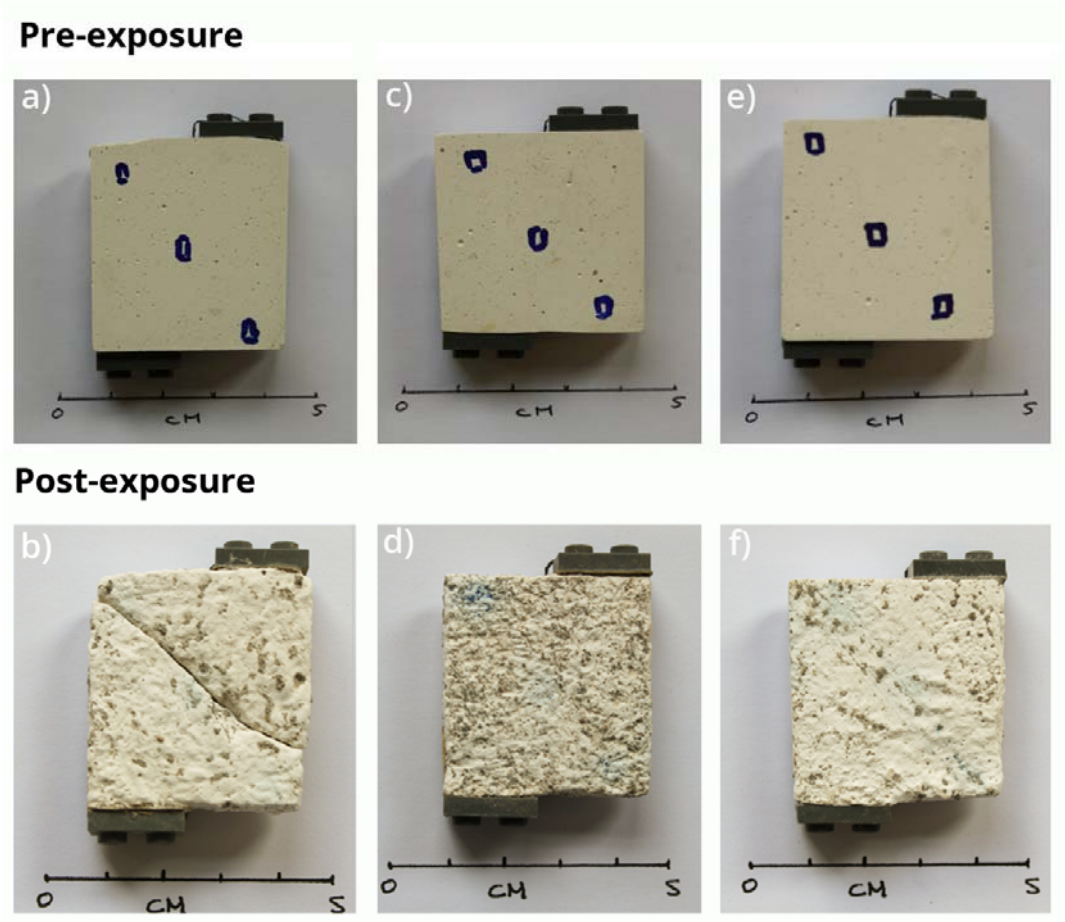

Figure 7.17. Comparison of sample pictures taken pre and post-exposure to each experiment. a-b) strip 1 (grass). c-d) strip 2 (grass & sedum plugs). e-f) strip 3 (sedum mat).

7.4.2.2. Microscope image analysis

The results seemed consistent with the visual analysis. In this way, Strip 1(grass & sedum plugs) presents the most severe dissolution effect, however the strip 3 (sedum mat) seemed to be the best preserved (Fig.7.18).

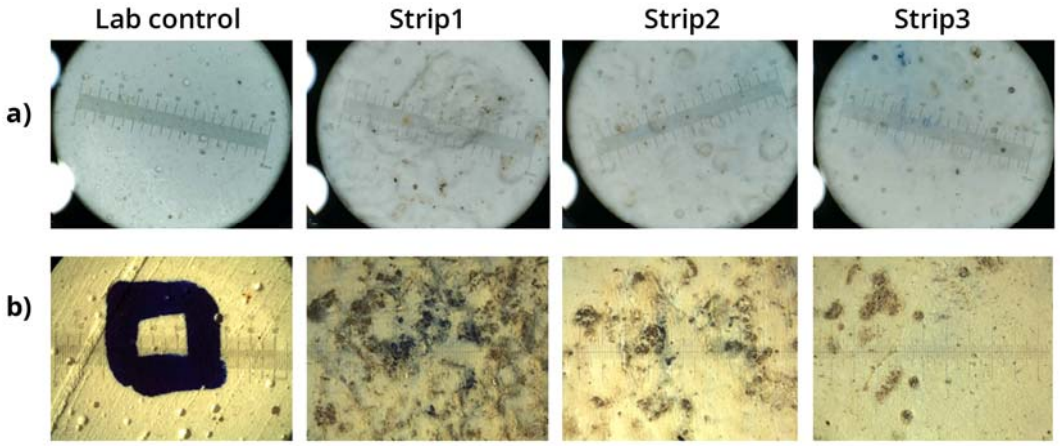

Figure 7.18. Comparison of sample microscope images (20 X) of each experiment taken by a) portable USB microscope camera and b) Leica microscope.

7.4.2.3. Weight analysis

According to the calculations, the open air samples were totally dissolved. Soft capping samples were better preserved, being the strip 3 the best option to preserve them (Fig.7.19).

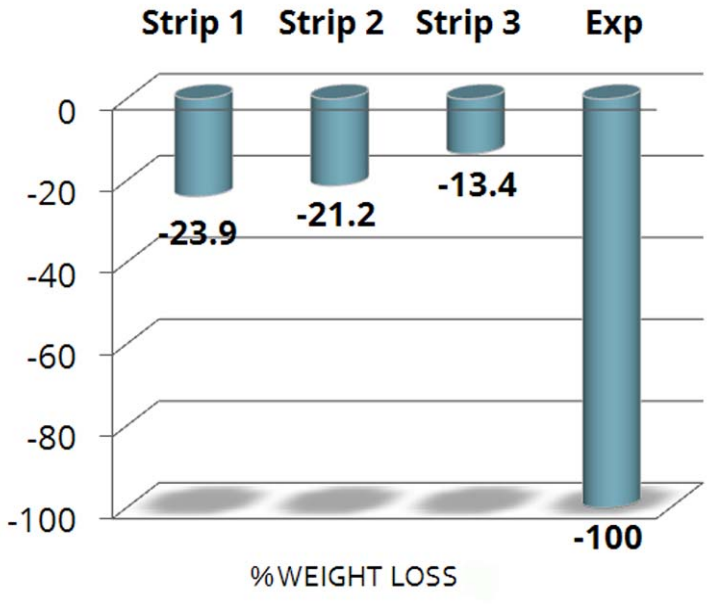

Figure 7.19. Percentage comparison of weight loss average produced in 2 years under each kind of experiment.

7.4.2.4. Colour analysis

According to the CIELAB norm[42] and the criteria (ΔE*ab), strip 3 (sedum mat) was the less deteriorated once again, being its differences of color in the range of just noticeable (Fig.7.20). Moreover, the spectral reflectance curve of each sample pre and post exposure was compared, indicating the same result.

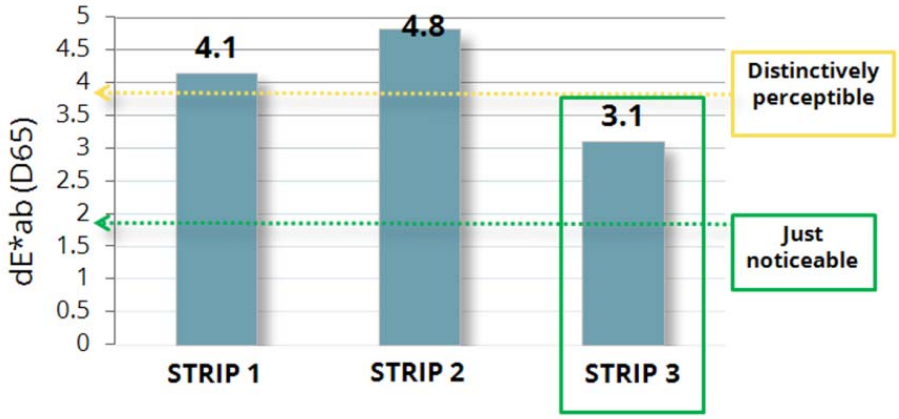

Figure 7.20. Comparison of colour changes produced in 2 years by each kind of exposition, in which the CIELAB norm was applied to determinate the severity of the degradation.

7.4.2.5. SEM analysis

One sample per strip was selected taking into account which was closer to its degradation average (loss weight, % reflectance and size). In this way, the representative samples (GS2, GSS2, SS2 and LC2) were chosen for the spectroscopic analysis (Table 7.1).

The electron microscope images of their surfaces seem to indicate that strip 1 (grass and sedum plugs) and strip 2 (grass) were the worst preserved, in comparison with the strip 3 (sedum mat). Furthermore, the composition mapping of the cross section analysis revealed the presence of chloride and magnesium ions, (Fig.7.21 and 22), evidencing the homogeneous distribution in the samples.

42 K. Bieske, I.D. Cornelia. A study about Colour-Difference Thresholds. Lux et color vespremiensis; 2007: 1-11.

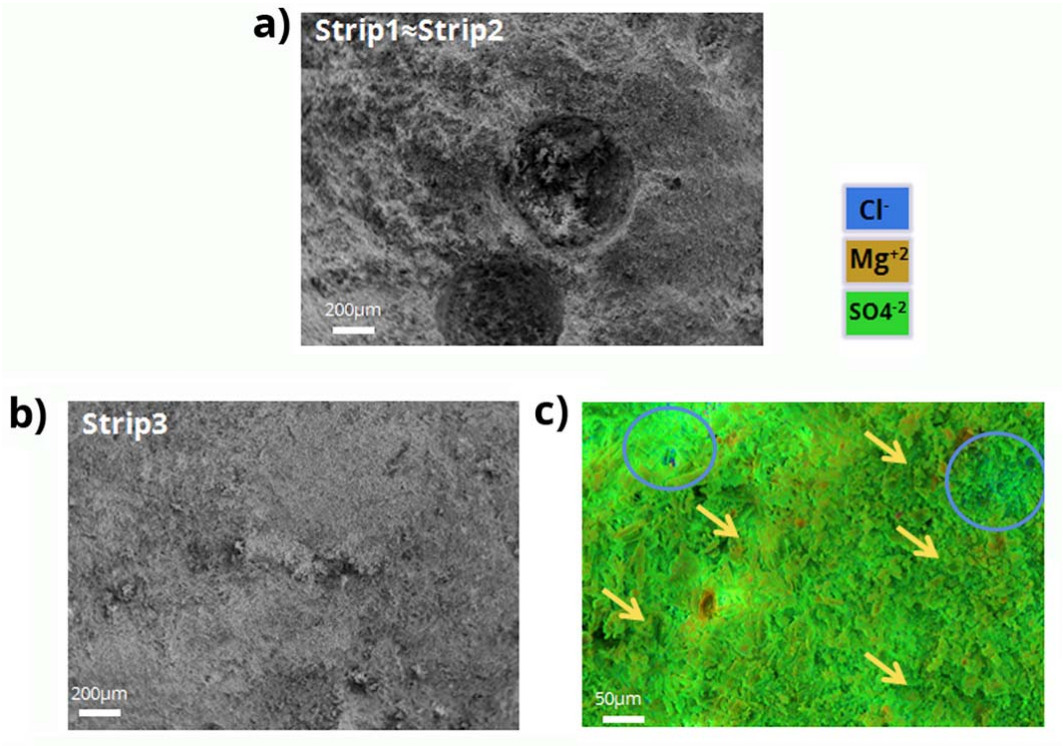

Figure 7.21. Electron microscope images taken of the Soft capping samples. a) sample surfaces of strip 1 and 2, which showed similar degradation process. b) sample surface of strip 3. c) cross section composition mapping of a sample corresponding to strip3.

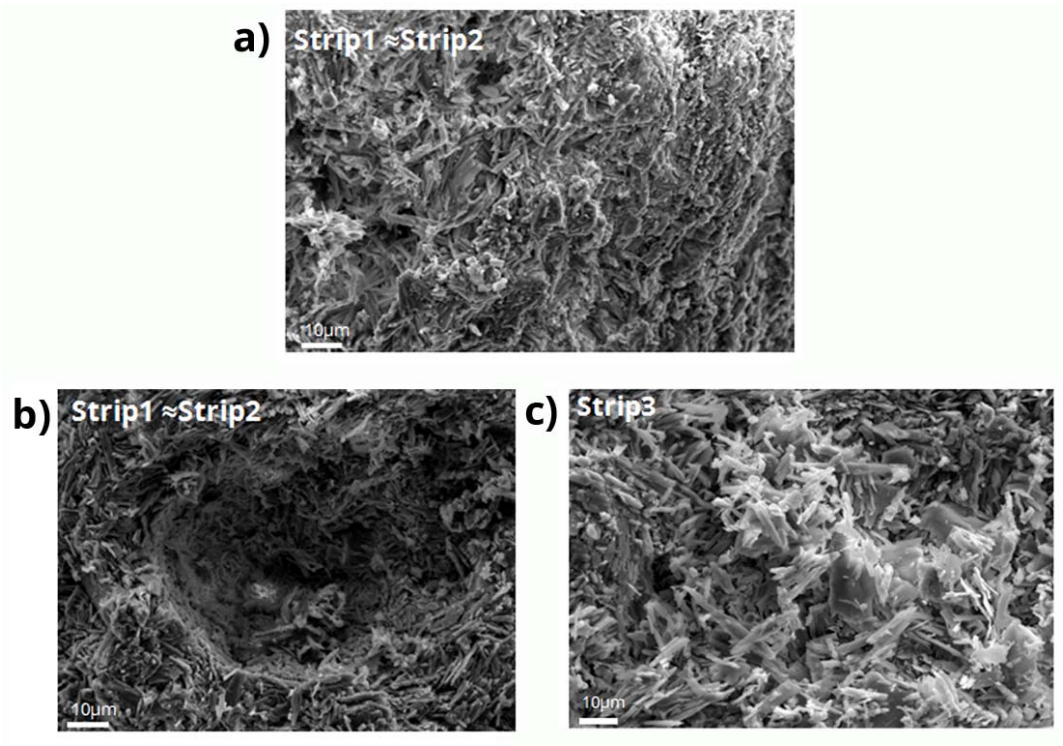

Figure 7.22. Electron microscope images taken of the Soft capping samples. a-b) sample surfaces of strip 1 and 2, which showed severe dissolution. c) sample surface of strip 3 presented good state of gypsum crystals.

7.4.2.6. Raman analysis

The cross section Raman study corroborated the presence of magnesium, identifying epsomite ($MgSO_4 \cdot 7H_2O$, by its characteristic band at 986 cm^{-1}) as main degradation compound. As this salt can present changes in its number of hydration waters by hydratation/deshidratation processes, it could produce inner cracks caused by temperature fluctuations.

7.4.2.7. Discussion

In accordance with the results, the success of any of the soft caps used is clear. Although, for the purpose of determining the most suitable conditions to preserve materials based on gypsum using the Soft capping method, the monitoring of some parameters can be suggested.

In this way, the strip 3 (sedum mat) seemed to be the best option to preserve the gypsum samples due to its temperature as well as its lowest magnesium concentration. Magnesium sulfate is more soluble and mobile than gypsum so epsomite is easily washed by rain, but in sheltered areas it remains in contact with the stone so it can penetrate further and could play a prominent part in causing decay. In this way, its presence could explain the broken samples collected.

Moreover, the soft caps composed by sedum mat achievement minimize also the water ingress into the soil in comparison with the soft caps of grass. Therefore, these variables should be taken into account before selecting the vegetation and soil composition of soft caps.

7.4.3. Limestone

7.4.3.1. X-Ray Diffraction (XRD) analysis

To determine the original composition of the stone, one laboratory control sample was analyzed by the X-Ray Service “Rocks and Minerals Unit” of the University of The Basque Country (UPV/EHU). According to the results (Fig. 7.23), calcite was the main compound with a percentage of 98-99% and the remaining content of 1-2% was identified as quartz (SiO_2).

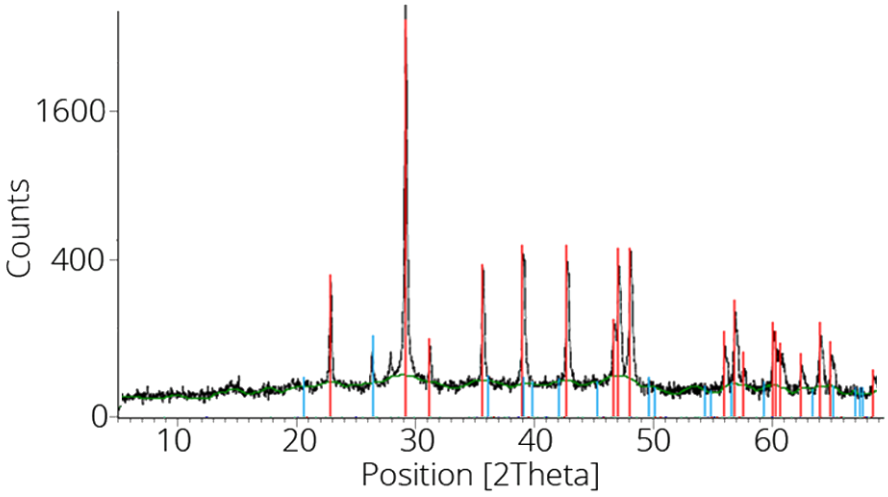

Figure 7.23. X-Ray diffraction results. Quartz signals are blue colored and calcite signals are marked in red.

7.4.3.2. Visual inspection

All the samples seemed to be in good state. Although visually it was difficult to discern, in only 9 months the samples exposed to the open air (Exp) appeared to be the worst preserved since its brightness was reduced and the surface was rough to the touch.

Focusing on the soft capping samples, strip 1 (grass and sedum plugs) was without any doubt the worst option to preserve this kind of material because some samples were broken at the corners.

7.4.3.3. Microscope image analysis

With regard to soft capping samples, although there were traces of soil trapped in the pores, strip 3 appeared to be the best option. As can be seen in the marked areas of the Figure 7.24, several loss of material was observed in the rest of strips, increasing thus the size of pores. Hence, the water absorption capacity was affected, probably increasing the vulnerability of the stone.

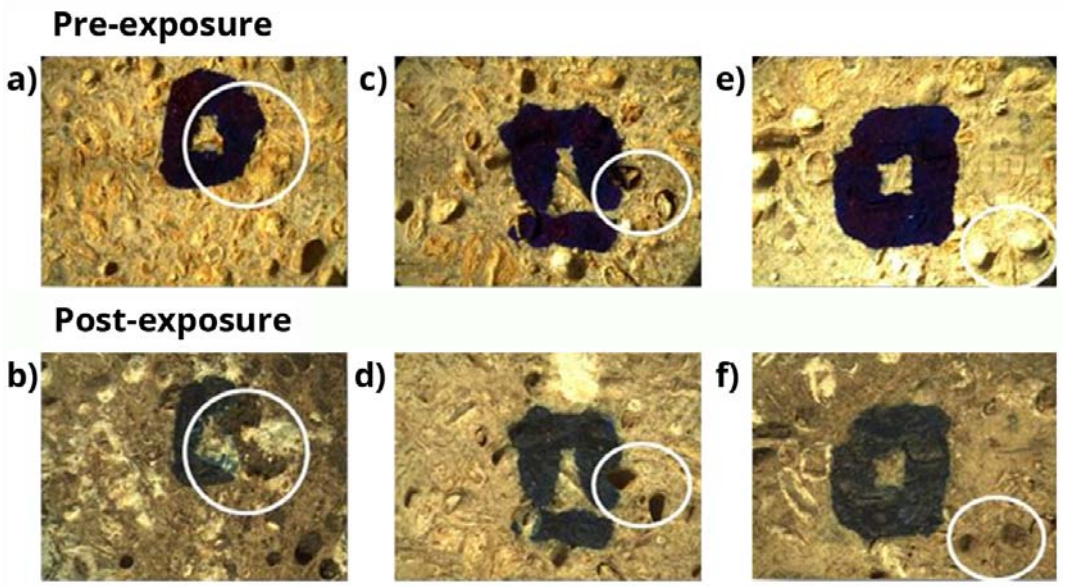

Figure 7.24. Comparison of sample microscope images of each experiment taken by Leica microscope (20 X), in which the interesting areas are highlighted. a-b) strip 1 (grass and sedum plugs), c-d) strip 2 (grass) and e-f) strip 3 (sedum mat).

7.4.3.4. Weight analysis

According to the data, the samples exposed to the open air (Exp), in only 9 months without any extrapolation applied, presented the highest loss of material. Nevertheless, soft capping samples were better preserved, seeming the strip 3 (sedum mat) again the best option to protect limestone material (Fig.7.19). The weight gain presented was probably caused by soil particles trapped, although the samples were washed, brushed although not too hard to avoid surface damage.

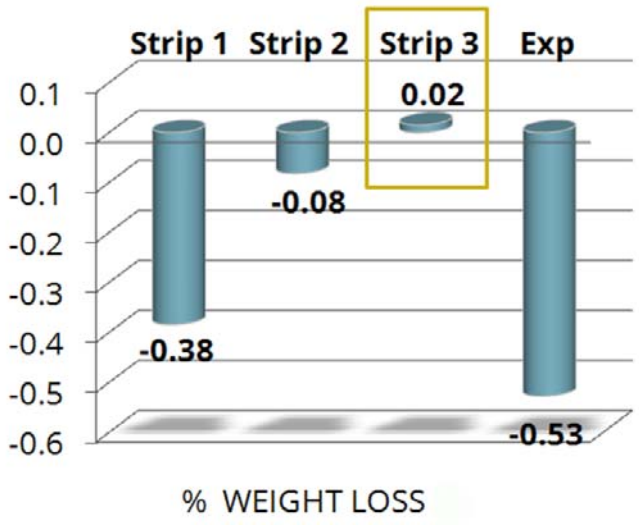

Figure 7.25. Percentage comparison of weight loss average produced under each kind of experiment, in which the values of the open air samples (Exp) correspond to 9 months of exposition and the rest of them to 24 months.

7.4.3.5. Colour analysis

As was observed visually, the color difference suffered by this material was severe in any of the exposure conditions. All the samples presented values around the limit of disturbing, in accordance to the CIELAB norm[43]. In spite of this, strip 3 (sedum mat) was the less deteriorated once again, being minor its differences of colour.

7.4.3.6. Hardness analysis

The characteristic of limestone material allowed performing a hardness study to determine to what extent the strength of the stone was altered. Therefore, average value of each sample was taken following the measurement protocol[44], though due to the small sample sizes, the repeatability of the method was affected. The results (Fig.7.26) showed that the samples exposed to the open air were the most deteriorated, although, they were exposed only half the time, evidencing once again the preservation provided by the soft caps, seeming the strip 3 (sedum mat) composition the best option to preserve this material.

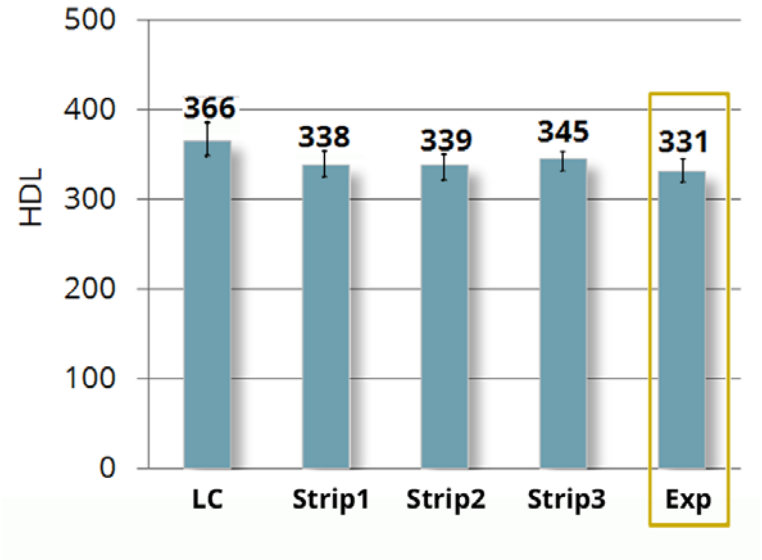

Figure 7.26. HDL values of hardness average presented by the different samples after each kind of experiment, in which the values of the open air samples (Exp) correspond to 9 months of exposition and the rest of them to 24 months.

43 K. Bieske, I.D. Cornelia. A study about Colour-Difference Thresholds. Lux et color vespremiensis; 2007: 1-11.

44 H.Viles, A. Goudie, S. Grab, J. Lalley. The use of the Schmidt Hammer and Equotip for rock hardness assessment in geomorphology and heritage science: a comparative analysis. Earth Surf. Process. Landforms; 2010; 36: 320–333.

7.4.3.7. 3D Laser Scanner analysis

To quantify and compare the changes in the surface topography of limestone samples, a 3D triangulation scanning study was carried out to investigate any important scaling relationships suffered[45]. However, the results were not conclusive since the changes after exposure were, mostly, lower than the resolution of equipment (more information can be consulted in chapter 3, section 3.2.1). In addition, the marks made on the samples as a reference system caused interferences in the measurements. Therefore, only the average changes of maximum and minimum height could be quantified (Fig.7.27), showing, one more time, the soft caps composed by sedum mat (strip 3) as the best option.

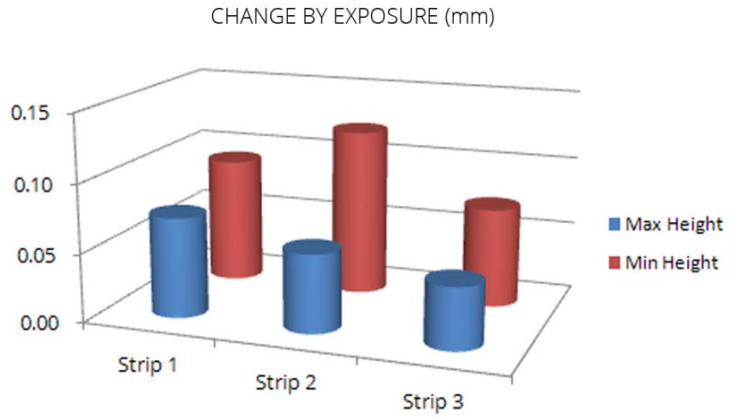

Figure 7.27. Values of differences in the average of maximum (blue colour) and minimum (red colour) height of the soft capping samples.

7.4.3.8. SEM analysis

As in the previous analysis, one sample per strip was selected. In this way, LC1, GS3, GSS2 and SS1 samples were analysed by spectroscopic techniques (Table 7.1).

The study of their surfaces indicated that strip 3 (sedum mat) was the least degraded. Focusing on the most degraded strips and to find out the main cause of degradation, the areas corresponding to the pores, which increased their size, were amplified (Fig.7.28) and several particles of NaCl were indentified. Although this salt is not considered very harmful, last studies have demonstrated that it can increase the

45 M. Bourke, H. Viles, J. Nicoli, P. Lyew-Ayee, R. Ghent, J. Holmlund. Innovative applications of laser scanning and rapid prototype printing to rock breakdown experiments. Earth Surf. Pro. Land.; 2008; 33: 1614-1621.

calcite dissolution apart from other pathologies[46-48]. Therefore, the chloride content of the soil used by the soft caps as well as the effect of the vegetation in this value should be taken into account since it could be related to the observed loss of material.

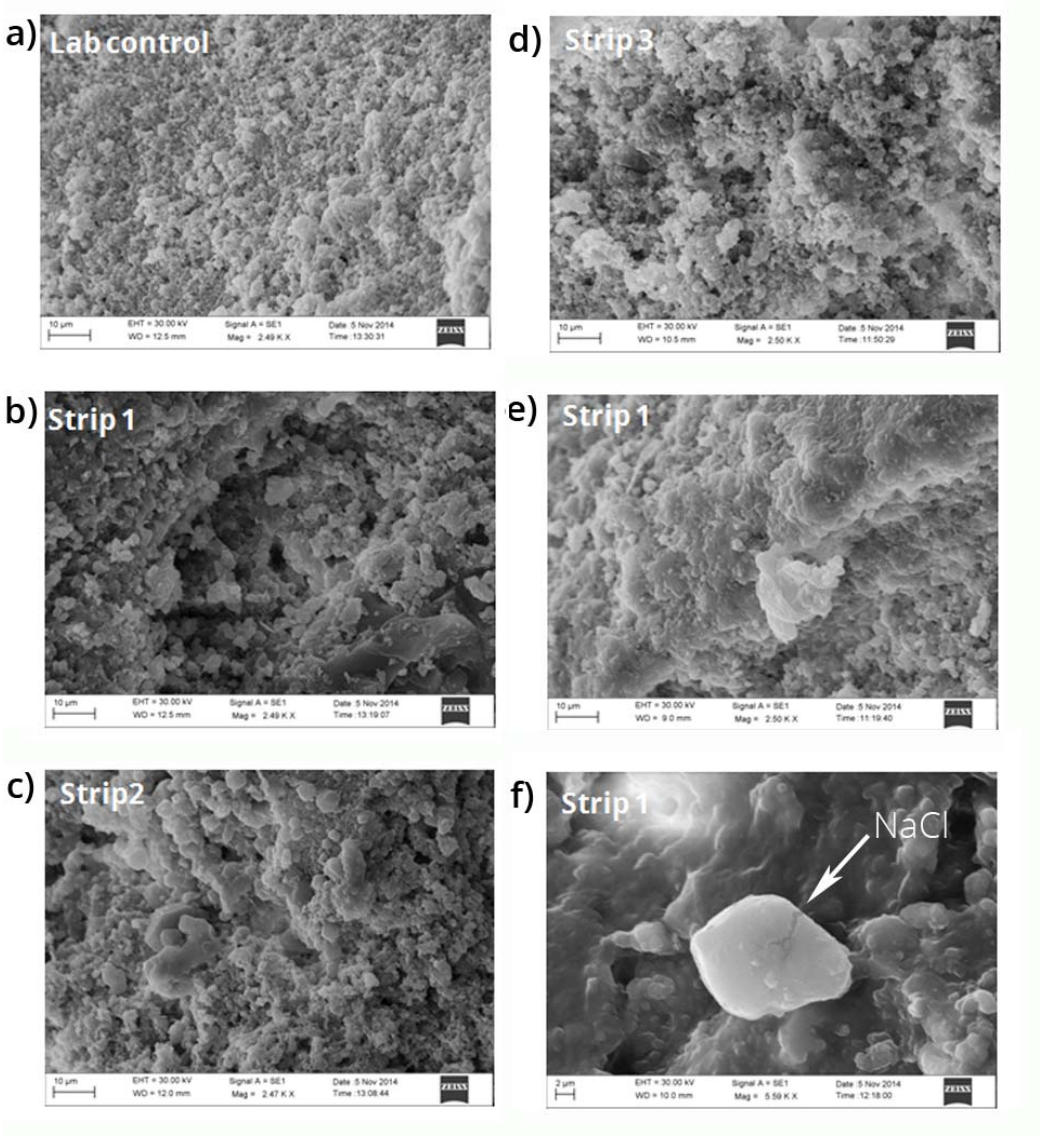

Figure 7.28. Electron microscope images taken of the Soft capping samples. a) Laboratory control sample surface. b) sample surface of strip 1, c) strip 2 and d) strip 3. e-f) amplification images of the interior of the pores of samples of strip 1.

46 S.S. Seo, S.M. Son, C.H. Lee, K. Bask. Compositional analysis of soluble salt in Bresle extraction from blocks in Newbuildings Shipyards. ISST, Osaka, 2007.

47 S.A. Nikolaus, P. Theoulakis. C. Pitinis. Dry deposition effect of marine aerosol to the building stone of the medieval city of Rhodes, Greece. Built. Environ.; 2009; 44; 260-270.

48 J.J. McAlister, B.J. Smith, A. Török. Element partitioning and potential mobility within surface dusts on buildings in a polluted urban environment. Atmos. Environ.; 2006; 40; 6780-6790.

7.4.3.9. Raman analysis

The Raman study of the samples exposed to the open air identified gypsum (Raman band at 1008 cm^{-1}), nitrocalcite (Raman band at 1050 and 712 cm^{-1}) and thenardite (Na_2SO_4, assigned by its characteristic band at 992 cm^{-1}) as degradation compounds, evidencing the atmospheric pollutants attack and the deposition of sodium particles from the marine aerosol. However, in the soft capping samples, only gypsum (Raman band at 1008 cm^{-1}) was detected as decaying compound (Fig. 7.29), although, niter (KNO_3, Raman bands at 1049 and 715 cm^{-1}) was identified also not as a transformation product of the original material, but rather as a result from deposition of the salts contained in the soil.

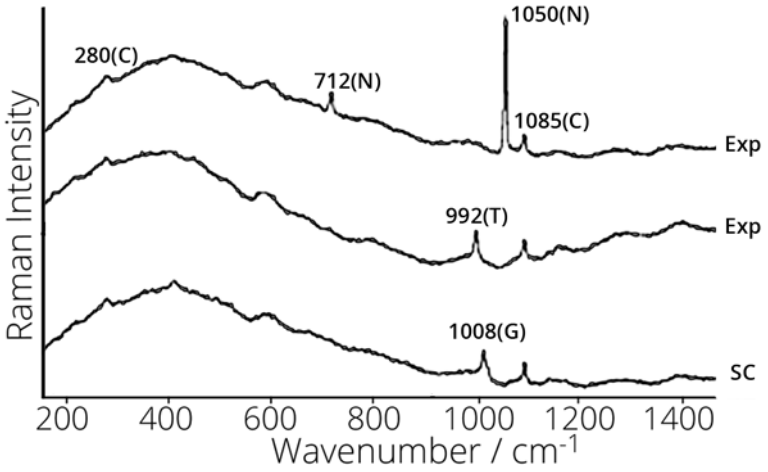

Figure 7.29. Raman spectra obtained of open air samples (Exp) and soft capping samples (SC), where calcite (C), nitrocalcite (N), thenardite (T) and gypsum (G) were found.

As it was mentioned in previous chapters, thernardite is one of the most hazardous salts due to its fast equilibrium with its decahidrated form[49]. It is usually realated with disintegrations phatologies in monumental stone[50]. However, in this case, due to the petrographic characteristicis[51] of this kind of limestone, its action could be more severe since the crystallisation tests showed its special vulnerability to this salt. Therefore, in order to preserve this stone, sulphate content of the soil as well as the efect of the vegetation over this parameter should be taken into account to increase its resistance to weathering process.

49 M. Steiger , S. Asmussen. Crystallization of sodium sulfate phases in porous materials: The phase diagram Na2SO4-H2O and the generation of stress. Geochim. Cosmochim. Ac.; 2008; 72: 4291-4306.

50 N. Tsui, R. J. Flatt, G. W. Scherer. Crystallization damage by sodium sulfate. J. Cult. Herit.; 2003; 4 : 109-115.

51 Building Research Establishment (BRE), (2014), Costwold Hill Stone (Bed 1): http://projects.bre.co.uk/ConDiv/stonelist/stonelist.html.

7.4.3.10. IC analysis and Chemometric study

The ion chromatography analysis was conclusive since the samples exposed to the open air presented higher values than any soft capping sample with the exception of sulphate, which was higher in them (Table 7.2).

Table 7.2. Concentration values in mg Kg^{-1} of ion obtained by ion chromatography from the surface of the samples.

Sample	Na^{+}	K^{+}	Mg^{2+}	Ca^{+2}	Cl^{-}	NO_3^{-}	SO_4^{-2}
Strip 1 (GS)	92	285	72	6110	232	91	1349
Strip 2 (GSS)	63	208	51	4713	177	88	1388
Strip 3 (SS)	35	215	33	3594	117	55	450
Open air (Exp)	319	383	58	5564	543	125	195
Laboratory Control (LC)	87	360	47	2544	178	47	186

*RSD: 7-22%

** Sampling surface 3.5x1.5x0.1xcm

The multivariate analysis of the data was used to obtain further information on the correlation of quantitative analysis (more information about the treatment of data can be consulted in chapter 3, section 3.3). In this way, the obtained Principal Component Analysis (PCA) explained 81% of the variance, using 3 PCAs to simplify the system (Fig 7.30).

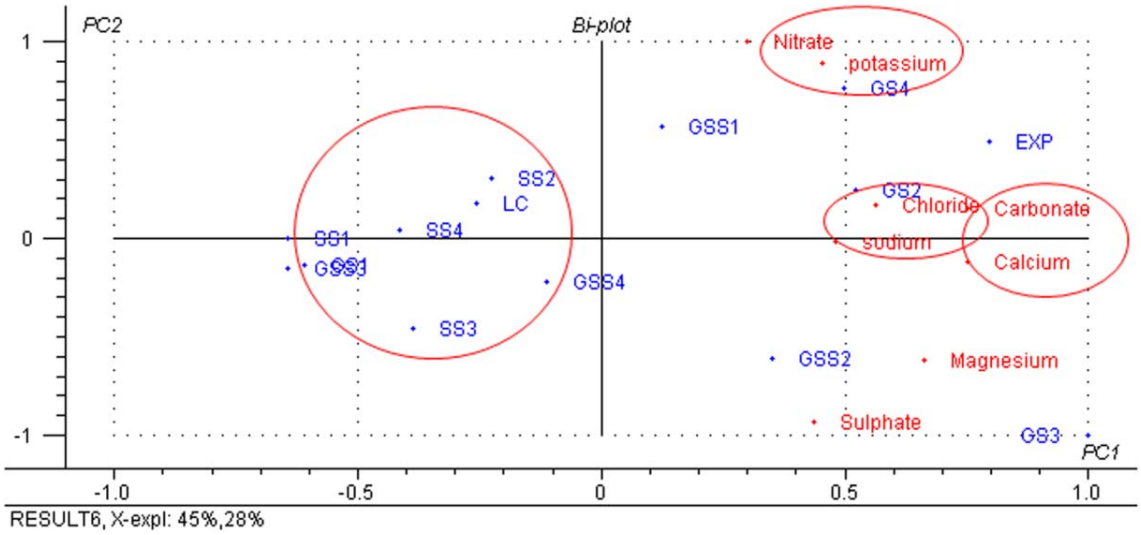

Figure 7.30. Representation of PCAs carried out by The Unscrambler. The image shows the soluble content results obtained by ion chromatography. The groups formed according to the PC1 vs PC2 are highlighted: nitrates, sulphates and chlorides.

According to the results, some salts formation were suggested with the grouping of three clusters; calcium and carbonate, potassium and nitrate, and sodium and chloride, corroborating the spectroscopic analysis.

The sample exposed to the open air (Exp) during only 9 months seemed to be related to all salts groups and the samples corresponding to the most deteriorated strip (GS) also. However, the samples belonging to the best preserved strip (SS) were displayed close to the laboratory control sample (LC), forming a group. Therefore, the quantitative data corroborated the previous results, showing the Strip 3 (sedum mat) as the most suitable composition to avoid the degradation of this kind of limestone.

7.4.3.11. Discussion

Although, in principle, a similar behavior to calcite samples was expected, the petrographic characteristics such as its porosity and the composition difference (1-2%, quartz) were determinant and, as a consequence the soft caps based on sedum mat achieved a better preservation of limestone materials.

According to the spectroscopic results and given that the main degradation compound was related with the sulphate attack, selected soils with low concentration of this anion and sedum mat species that minimize its content are recommended. Besides, in the same way, chloride content should be taking into account also since, in accordance with the SEM analysis, it seems to be related to the loss of material observed.

7.4.4. Conclusions

As main conclusion, this chapter demonstrated that Soft Capping plays a useful role in the conservation of ruined monuments and provides effective protection from weathering agents, reducing the chemical degradation.

The general requirements were established, resulting the soft caps composed by a mixture of grass and sedum plugs (Supurium tricolour) very convenient to preserve calcite materials. Besides, the soft caps based on sedum mat of the same specie demonstrated to be the best option to avoid the degradation of gypsum and limestone (at least 98% of calcite) materials. For future researches, studying the influence of similar sedum mat species on the soil is advisable since in this way, the influential parameters in the chemical deterioration (pH, ion soluble content, etc) of each material could be optimized, improving even more their conservation.

Finally, the in situ analytical methodology (pictures, spectrophotometer, 3D scanner and Raman spectroscopy) used in this work allowed monitoring real conservation treatments. Its portability as well as its non destructive application of all the techniques used really makes it a suitable tool to study the weathering occurred in

the conservation treatments. Although in this case, the resolution of the laser scanner technique was not enough to determine graphically the loss of material produced, it usefulness have to be highlighted since it could be an important technique to monitor it and in this way, quantify the changes in bigger surfaces with time. Therefore, in combination with the other portable techniques used in this work, it can provide meaningful insights into the factors that control salt weathering.

CHAPTER 8: FINAL CONCLUSION

The goals proposed to this PhD work were successfully achieved. In this manner, non destructive analytical methodologies were developed for the in situ diagnosis study of the urban built heritage, mainly affected by environmental factors. Thanks to their evaluation, through the operational cases, the characterization, classification and prediction of damage mechanisms occurred in building materials were assessed. Moreover, the usefulness of the pilot conservation method to provide an effective protection of ruined monuments was also tested.

In addition, the results of the non destructive methodologies performed were duly validated by means of micro destructive analytical techniques. In this way, its usefulness was corroborated, completing the information obtained by chemometric and thermodynamic studies. Therefore, a working protocol for a suitable diagnosis of our built heritage was provided along this work, contributing to its preservation and maintenance.

In this manner, firstly, the viability of the in-situ analysis based on Raman spectroscopy was demonstrated, evidencing its usefulness to diagnose the conservation state of building materials such as mortars, bricks, limestones and sandstones. Furthermore, the possibility offered by this technique to obtain good quality in situ results was highlighted, in compliance with the premise of preserving the total integrity of the samples. Besides, its advantages to distinguish different types of molecules, made possible to establish the chemical deterioration processes caused by atmospheric pollution, infiltration waters and biodeterioration.

Once confirmed the validity of Raman spectroscopy in the field of built heritage, the benefit offered by its combination with X-ray fluorescence (XRF) was evidenced, through the operational case of Basozabal Palace. In this way, the facilities given by this elemental technique to choose the interesting sampling areas, to make the

spectral interpretation easier, as well as its profitability to avoid further destructive laboratory analysis was demonstrated. Thanks to its joint use, the preliminary diagnosis of the conservation state was correctly carried out, in a fast and economical way, making the proposal of the chemical mechanism involved in the pathologies possible. In this manner, the first step to perform a complete suitable methodology to assist in the decision making of restoration actions was achieved.

Subsequently, the validity of the in-situ results was successfully corroborated and completed in the laboratory by means of other spectroscopic instrumentation. Besides, thanks to the ion chromatography (IC), the severity of the soluble salt damage was quantified, allowing us comparing it with the existing legislation. The treatment of the results using chemometric and thermodynamic tools allow us establishing the specific degradation chemical process that takes place in the materials, pointing out the importance of understanding the chemistry behind the damage.

Additionally, the conclusion obtained as well as the advantages and disadvantages presented between non destructive and micro-destructive techniques were compared. In this sense, the IC analysis and its chemometric study were included, as a highly recommended step, in the protocol work. Since, thanks to them, pathologies that could be overlooked as well as ionic compounds, which cannot be detected by Raman spectroscopy, were identified, assuring the maintenance of the Basozabal Palace. For these reasons, the combination of both methodologies was really advised.

On the other hand, the handicaps observed in the field analysis as the fluorescence effect caused by compounds inherent to these kind of matrix were well reduced by the implementation of diffuse reflectance infrared spectroscopy (DRIFT), as secondary technique in the field analysis. The operational study carried out in Guevara Palace demonstrated the advantages offered by this technique to identify high number of compounds as well as to help to interpret the Raman spectra, making a corroboration of the results possible, at the same time of the in situ analysis.

Apart from that, due to the influence of the external factors in the DRIFT in situ analysis, guidelines to minimize the distortions caused by the Resthralen effect were proposed, demonstrating its usefulness to collect good spectra.

In addition, given the needed of carrying out previously tested quantitative studies, the validity of a non invasive sampling method, based on paper pulp poultices, was established and thanks to it, the sampling phase was reduced and even eliminated.

With the purpose of improving the proposed work protocol, through the operational case of the Fishermen's Association, the utility presented by cross section analysis, based on mapping laboratory techniques such as μ-XRF and scanning electron microscopy with energy-dispersive X-ray spectroscopy (SEM-EDX), was manifested, determining the penetration capacity of the pollutants inside the porous matrix and their internal distribution, even for undetectable compounds to Raman spectroscopy.

Thanks to that, pathologies derived from the physical stresses and the material thickness affected were identified, providing of valuable information to select the most suitable cleaning and consolidant requirements.

Moreover, the shown necessity of monitoring the environmental influence in the damage suffered by building materials was successfully solved thanks to the application of a thermodynamic experimental chemical model, evidencing its utility to indicate the best time to perform in situ campaigns, as well as to advise the best restoration materials and consolidant products, avoiding the progression or aggravation of the existing pathologies.

In this way, the final work protocol was completed (Fig.9.1), showing its usefulness to carry out correct scientific studies to contribute in the rehabilitation and preservation of our built heritage. Besides, the inter-disciplinarity between the different professionals was promoted in order to avoid the application of erroneous interventions, demonstrating the little economic impact that this work protocol involves in a real restoration project and, in fact, the amount of money that it could save.

Finally, due to the importance of testing the response of new conservation methods before its implementation, a variation of the work protocol designed in this thesis was used. In this way, its combination with physical analysis as colour or hardness as well as 3D scanner techniques was shown through the study of different soft capping pilot applications. Thank to its use, the utility of the conservation method was evaluated demonstrating its capacity to reduce the chemical weathering of common materials such as calcite, sandstone and gypsum. Furthermore, the general requirements for obtaining its best response for each material were established, showing the versatility of the proposed work protocol.

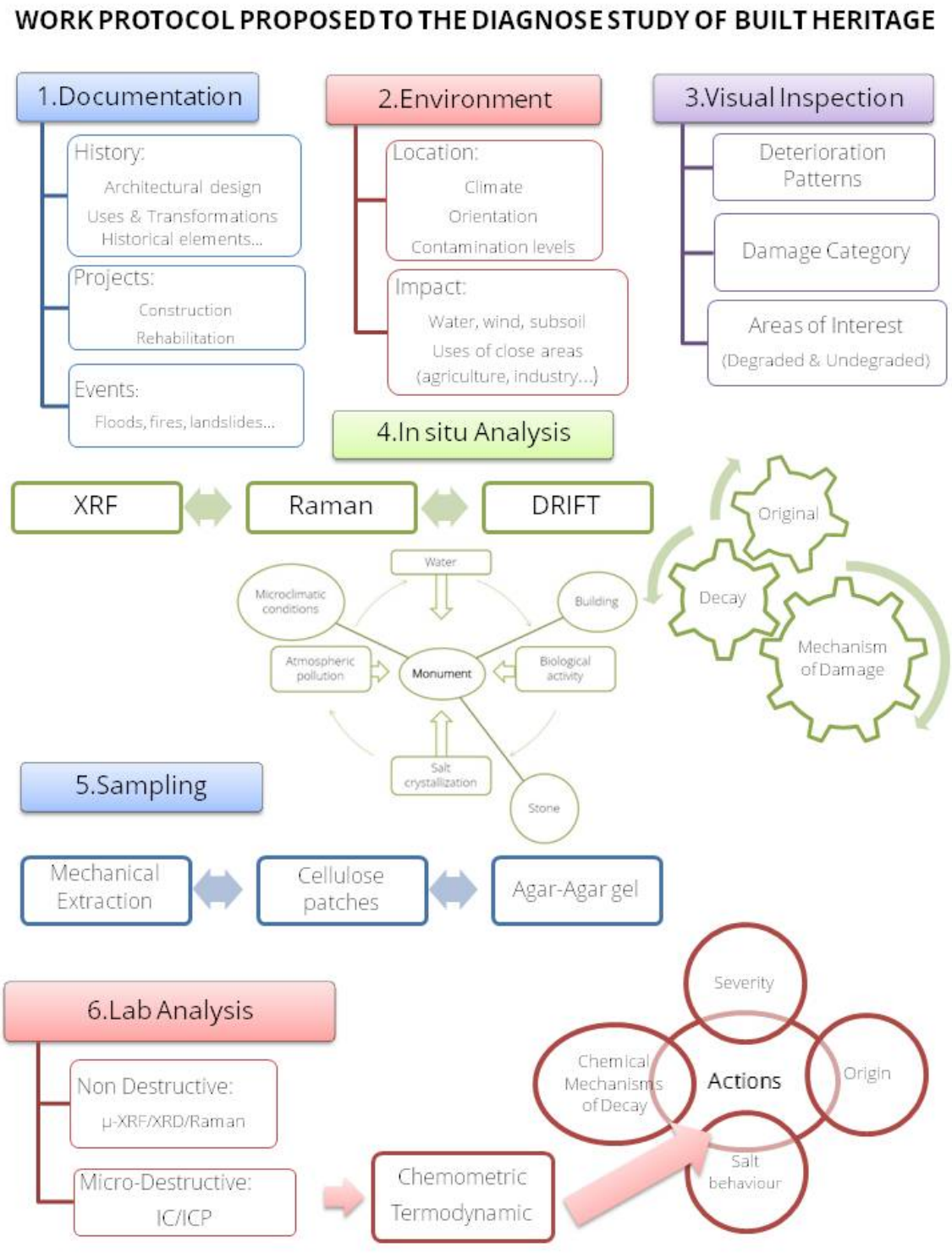

Figure 9.1. Scheme of the work protocol proposed to the diagnose study of built heritage, mainly affected by environmental factors, for an effective maintenance, preservation and revitalization.

CHAPTER 9: FUTURE WORKS

In order to solve out some of the issues found along this thesis, in future works, the following lines of research could be developed:

Given the successful methodology obtained by the combination of XRF and Raman spectroscopic for the preliminary diagnosis of the conservation state of building materials, it is advisable to implement the use of other elemental techniques to take another step forward in the characterization of materials. In this regard, laser-induced breakdown spectroscopy (LIBS) seems to be a versatile technique to be used in the field of the environmental monitoring.

According to the results obtained in chapters 5 and 6, the usefulness of DRIFT in the field analysis could be improved much better, if the existing databases include a bigger number of standards. In this way, the identification of more compounds such as silicates could be possible during the in situ analysis. Therefore, it would be recommended to expand this database in accordance to the most common original compounds that can be found in building materials.

In addition to this, the utility showed by the non-invasive method, based on paper pulp poultice, for the extraction of soluble salts used in chapter 6 could be improved. Hence, an optimization of the protocol (solvent, size and time) is recommended in order to find the most suitable option for each case.

On the other hand, taking into account the diagnosis study carried out in the Association of Fishermen along chapter 6, a pilot study of several consolidant applications is highly advisable to assess their suitability.

Finally, according to the results of soft capping work obtained in chapter 7, studying the influence of similar sedum mat species on the soil is advisable. In this way, the influential parameters in the chemical deterioration (pH, ion soluble content, etc) of each material could be optimized, improving even more their conservation. Furthermore, the application of resin in the base of the wall could be tested to avoid the ascension of water from the subsoil.

CHAPTER 10: GLOSSARY

10.1. Mineral phases

10.1.1. Oxides

Quartz α-SiO_2

Hematite Fe_2O_3

Magnetite Fe_3O_4

Goethite α-FeO(OH)

Oxyhydroxide $FeO_x(OH)_{3-2x}$

Rutile TiO_2

Limonite $FeO(OH)\cdot nH_2O$

Maghemite γ- Fe_2O_3

Lepidocrocite γ-FeOOH

10.1.2. Carbonates

Calcite $CaCO_3$

Termonatrite $Na_2CO_3\cdot H_2O$

Trona $Na_3(HCO_3)(CO_3)\cdot 2H_2O$

Natrite Na_2CO_3

Siderite $FeCO_3$

Gaylussite $Na_2Ca(CO_3)_2\cdot 5H_2O$

10.1.3. Sulphates

Anhydrite $CaSO_4$

Bassanite $CaSO_4 \cdot 0.5H_2O$

Gypsum $CaSO_4 \cdot 2H_2O$

Thenardite Na_2SO_4

Mirabilite $Na_2SO_4 \cdot 10H_2O$

Epsomite $MgSO_4 \cdot 7H_2O$

Coquimbite $Fe_2(SO_4)_3 \cdot 9H_2O$

10.1.4. Nitrates

Nitratine $NaNO_3$

Niter KNO_3

Nitromagnesite $Mg(NO_3)_2 \cdot 6H_2O$

Nitrocalcite $Ca(NO_3)_2 \cdot 4H_2O$

10.1.5. Silicates

Calcium silicate Ca_3SiO_5

Orthoclase $KAlSi_3O_8$

Kaolinite $Al_2Si_2O_5(OH)_4$

Muscovite $KAl_2(Si_3Al)O_{10}(OH)_2$

Albite $NaAlSi_3O_8$

10.1.6. Organic compounds

Whewellite $CaC_2O_4 \cdot H_2O$

Weddellite $CaC_2O_4 \cdot 2H_2O$

Scytonemin $C_{36}H_{20}N_2O_4$

Chlorophyll a $C_{55}H_{72}O_5N_4Mg$

Astaxanthin $C_{40}H_{52}O_4$

Zeaxanthin $C_{40}H_{56}O_2$

β-carotene $C_{40}H_{56}$

CHAPTER 11: ANNEXES

11.1. Scientific Publications

11.1.1. Articles

O. Gómez-Laserna, M. A. Olazabal, H. Morillas, N. Prieto-Taboada, I. Martinez-Arkarazo, G. Arana and J. M. Madariaga. In-situ spectroscopic assessment of the conservation state of building materials from a Palace house affected by infiltration water. J. Raman Spectrosc.; 2013; 44: 1277-1284.

O. Gómez-Laserna, N. Prieto-Taboada, H. Morillas, I. Arrizabalaga, M. A. Olazabal and J.M. Madariaga. Analytical study to evaluate the origin and severity of damage caused by salt weathering in a Historical Palace House: The attack of infiltration water. Anal. Methods; 2015: DOI: 10.1039/C4AY02632B.

O. Gómez-Laserna, I. Arrizabalaga, N. Prieto-Taboada, M. A. Olazabal, G. Arana and J. M. Madariaga. In situ DRIFT, Raman, and XRF implementation in a multianalytical methodology to diagnose the impact suffered by built heritage in urban atmospheres. Anal. Bioanal. Chem.; 2015: DOI 10.1007/s00216-015-8738-7.

11.1.2. Book Chapters

O. Gómez-Laserna, N. Prieto-Taboada, I. Ibarrondo, I. Martínez-Arkarazo, M. A. Olazabal and J. M. Madariaga. Raman Spectroscopic Characterization of Brick and Mortars: The Non-Destructive and in situ Analysis. Brick and Mortar Research (ISBN: 978-1-61942-927-7). NovaPublisher; 2012: 195-213.

O. Gómez-Laserna, H. Morillas, N. Prieto, I. Ibarrondo, I. Martínez, M. A. Olazabal and J. M. Madariaga. Raman spectroscopy study of a salt weathering process in

mortars of a Historical Palace House. ISMEC 2011, XXII International Symposium on Metal Complexes (ISBN: 2239-2459). ISMEC Group Series; 2011: 125-126.

O. Gómez-Laserna, I. Arrizabalaga, N. Prieto-Taboada, M. A. Olazabal, G. Arana and J. M. Madariaga. The evaluation of the water infiltration attack in building materials by spectroscopic techniques: Raman & DRIFT. ISMEC 2012, XXIII International Symposium on Metal Complexes (ISBN: 2239-2459). ISMEC Group Series; 2012: 185-186.

11.1.3. Congresses

11.1.3.1. International Congress Oral communications

O. Gómez-Laserna, N. Prieto-Taboada, H. Morillas, M. A. Olazabal and J. M. Madariaga. Multianalytical measurements to assess the impacts of acidic infiltration waters and atmospheric pollution. EMEC 12, European Meeting on Environmental Chemistry. Clermont-Ferrand, France: 2011.

O. Gómez-Laserna, H. Viles, J. Meneely, N. Prieto-Taboada, M. Olazabal, G. Arana and J. M. Madariaga. Soft wall capping: a better way of conserving ruins? Investigating the use of soil and other plants to protect ruined wall heads. EMEC 15, European Meeting on Environmental Chemistry. Brno, Czech Republic: 2014.

11.1.3.2. International Congress Posters

O. Gómez-Laserna, H. Morillas, N. Prieto-Taboada, I. Ibarrondo, I. Martínez, M. A. Olazabal and J. M. Madariaga. Raman spectroscopy study of a salt weathering process in mortars of a Historical Palace House. ISMEC 11, XXII International Symposium on Metal Complexes. Giardine Naxos, Italy: 2011.

O. Gómez-Laserna, I. Arrizabalaga, N. Prieto-Taboada, M. A. Olazabal, G. Arana and J.M. Madariaga. The evaluation of the water infiltration chemical attack in building materials by spectroscopic techniques: Raman & DRIFT. ISMEC 12, XXIII International Symposium on Metal Complexes. Lisboa, Portugal: 2012.

Our built heritage is mainly made by stone and thus, it is prone to decay by natural and irreversible processes. Moreover, materials are also exposed to an anthropogenic environment, in which there are many factors that can accelerate its deterioration. Due to this fact, before proposing any solutions to its maintenance, preservation or revitalization, the study of building materials requires a wide knowledge of the factors that have an influence in their decay.

Therefore, nowadays, the development of new diagnostic methodologies has gained importance in the field of material characterization. Moreover, given the intrinsic value of the samples, the usefulness of non-invasive methods that can be used in-situ preserving the integrity of materials is highlighted.

In this sense, this thesis is focused on developing non destructive analytical methodologies for the in-situ diagnosis of the urban built heritage, affected mainly by environmental factors. In this manner, along this work, the characterization, interpretation, classification and severity of damage suffered by building materials are assessed in real cases. Paying special attention to establishing the origin and the chemical process involved in the pathologies, as well as to study the response of previous interventions in order to contribute to its suitable preservation and maintenance. In addition to this, due to test the behavior of pilot conservation methods is widely recommended, the monitoring of a green conservation method to preserve ruins wall head is performed, through a multianalytical approach, evaluating its capacity to enhance or reduce chemical weathering of common stone materials and determining the best requirements for its implementation.

The proposed goals have been achieved thanks to the development and improvement of different combined methodologies, highlighting the usefulness presented by Raman spectroscopy in real conservation works. Moreover, the handicaps resulting from field analysis have been successfully reduced thanks to the implementation of DRIFT, providing a new path for the in-situ research of built heritage. Furthermore, micro destructive methods have been proposed to detect the penetration capacity of the weathering agents as well as to quantify the severity of salt damage, in accordance with existing legislation. Besides, the bases for reducing the sampling required for the quantification process have been established, thorough a non invasive method based on cellulose patch application. Finally, given the differences observed caused by seasonal changes, a monitoring of the salts content, in a real intervention process, has been carried out in order to select the most suitable actions to prevent the progress of existing pathologies.

The operational cases analyzed along this thesis demonstrate the aggressive attack suffered by our built heritage, evidencing the suitability of the methodologies proposed as indispensable tool to perform a correct scientific study, that allows us performing fast scientific diagnosis, helpful for the restoration or conservation procedures and thanks to them, the need to take decisions only in terms of the expertise of the conservators could be avoided.